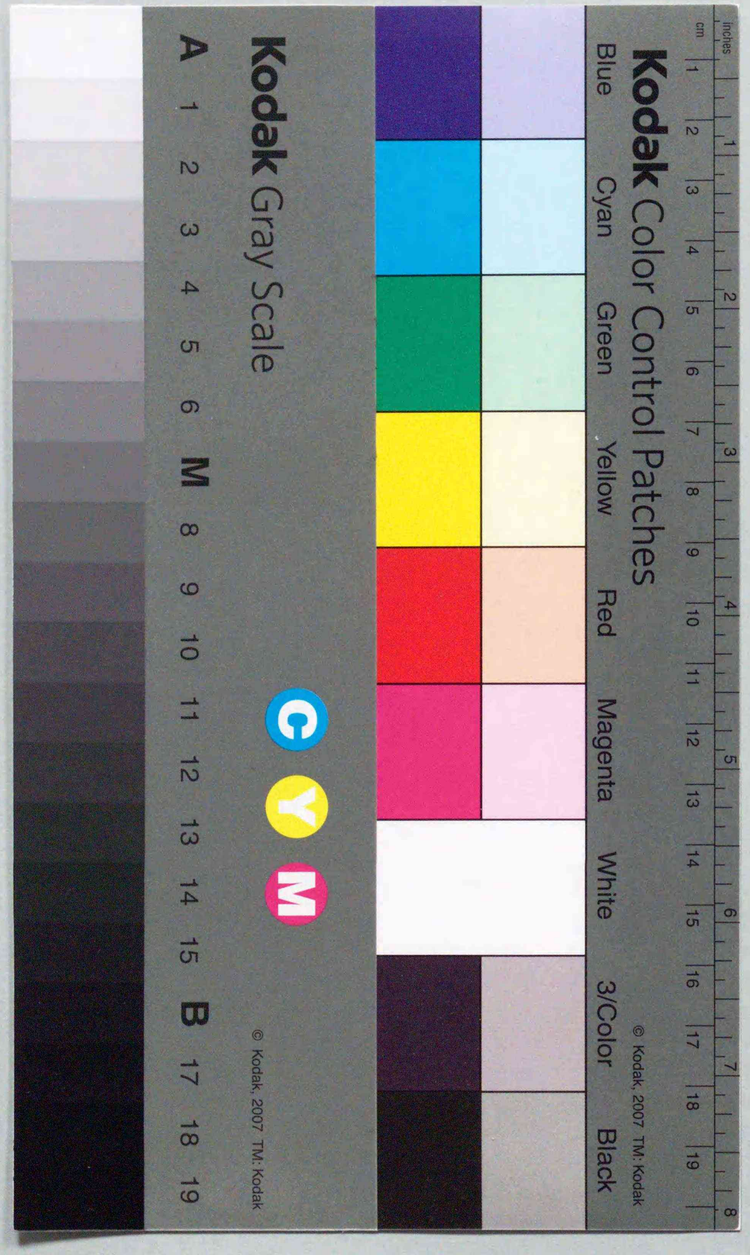

Spectroscopic Study on the Secondary Structure Formation and the Conformational Flexibility of Small Peptides in Various Mixed Solvents

Kenji Tonan

Division of Chemistry, Graduate School of Science,
Hokkaido University

2000

Spectroscopic Study on the Secondary Structure Formation and the Conformational Flexibility of Small Peptides in Various Mixed Solvents

Kenji Tonan

Division of Chemistry, Graduate School of Science,
Hokkaido University

2000

Contents

Chapter 1

Introduction

1. Background of This Study

The protein folding pathway has been one of the most important subjects on proteins and a wide variety of studies have so far been reported.[1-2] Despite these intensive studies, the origins of protein conformational stability are not clear yet[3] and it is still largely mysterious how a polypeptide chain folds in the manner which seems to be encoded in its amino acid sequence.

There has been limited success in predicting secondary and tertiary structures from its amino acid sequence. Most of such prediction methods are derived from empirical correlations of the structures with the locations of individual amino acid residues in various proteins of which X-ray structures analyses have been solved in detail.[4-7] These prediction methods have some utility,[8-10] but they do not necessarily provide insight into the origins of the protein folding.

In order to solve this issue, it is essential to discern various noncovalent contributions from local amino acid sequences. They tend toward their individual optimum structures and also must achieve an energetic balance with all the other regions of the protein molecule and satisfy the unique three-dimensional protein structure. But it is desperately difficult to deduce the constituent interactions from a folded protein structure, because individual contributions may complete with or reinforce one another, and usually a small overall thermodynamic difference is produced between a folded and unfolded states of the protein. In this case, any of each noncovalent interaction cannot be separately related.

Making use of moderate size (20-50 residues) of polypeptides offers better opportunity for structural characterization of the folding patterns in solution.[11-13] The structural simplicity of the moderate-size peptide allows us to evaluate spectroscopically or thermodynamically weak interactions such as intramolecular hydrogen-bonding or side chain packing through hydrophobic interactions, and may give useful information about the network of noncovalent interactions that determine the folding behavior of a protein.

For a solution of the protein-folding problem, it is a key to reveal the role which surrounding solvents play through the folding pathway. A protein molecule in solution will take a wide variety of local solvent conditions, ranging from hydrophilic surface to

hydrophobic inside of the molecule, and each segment of the polypeptide chain undergoes various interactions with surrounding solvent environments, which may fluctuate among wide range of solvent polarity during the folding process of the protein. Therefore, it is important to study how the local segments of a protein molecule vary their structures with change in the solvent conditions.

For the purpose, it is useful to examine the thermodynamics of the secondary structure formation for small peptides, which can be studied in detail by spectroscopic methods.[14-15] Infrared (IR) spectra are particularly useful for detecting and characterizing the hydrogen-bonds[16-17] which are associated with the peptide secondary structures such as α-helix, β-turn, and so on. Many groups have studied the structure of small peptides in solution since the 1950s.[18-19] Maraud and cowarkers[20-22] and other group[23] have studied the β-turn formation in a few organic solvents for various deputies by IR-based examinations. These results were compared with theoretical analysis and discussed in terms of β-turn forming tendency of each amino acid residue.[24] Recently Gillman and co-workers[25-30] have reported IR studies on intramolecular hydrogen bonding for series of model peptides in dichloromethane solutions. They have examined various types of hydrogen-bonded rings and quantified thermodynamic properties for a few secondary structure formations of small peptides. These results provide a useful guide to a study on a folding mechanism of polypeptides.

On the other hand, NMR spectroscopy has provided structural information about rather large polypeptides in solution. Since Wütrich and coworkers[31] first reported in 1986 a structure of tendamistat (75 amino acid residues) in solution, a data bank of protein structures determined by NMR has accumulated more and more data. In those works NOE correlations have been refined by restriction of the dihedral angles of peptide backbone, ϕ and ψ, which are related to vicinal coupling constants between amide protons and α-protons by Karplus equation.[32-34]

However, the structures of small linear peptides exhibit dynamic natures on NMR time scale. This causes some ambiguity in structural analyses, which is usually not encountered in highly rigid structures of proteins. In solutions, small peptides can adopt quite a few conformations, which interchange with one another rapidly enough on the NMR time scale. Sometimes conformational analysis of such flexible molecules has been attempted to define a single leading conformation in solution,[19] but both NOE

correlations and coupling constants must be averaged and cannot provide direct information about any of conformers. Even when the existence of some conformers has been taken into account, such studies have seldom provided quantitative information on populations of the conformers.[21, 35-36] This is because energy differences among the conformers have not been fully characterized.[37-40] Moreover, conformational equilibrium of small peptides are significantly affected by the interaction with solvent. Exact understanding of this solvent effect is essential to the study of the folding process of a polypeptide chain, because solvent condition of the local regions of the polypeptide chain may change drastically during the folding into a compact globule. In the early stage of the folding process, every local region is thought to be fully exposed to aqueous environments and has enough flexibility to fluctuate among many conformations. As the folding proceeds, the polypeptide chain gradually loses the conformational flexibility, and finally each amino acid residue adopts a unique set of dihedral angles, ϕ and ψ, depending on the type of the secondary structure concerned. Furthermore, in a protein, three-dimensional assembly and side chain packing occur through various noncovalent hydrophobic and electrostatic interactions. These processes are generally accompanied by reduction in solvent accessible surface area[41] of various local regions of the protein, which is the largest in the denatured state and the smallest for the completely buried region in the folded structure of the native protein.

2. Content of this Thesis

On these backgrounds, I have planned out the present study to elucidate the solvent effects on various structural features of small peptides, intramolecular hydrogen-bonding, *cis*-to-*trans* isomerization of the imide linkage preceding the prolyl residue (Pro), and flexibility of peptide backbone around the glycyl residue (Gly)

I have synthesized 60 kinds of small peptides with various length (di- to tetra-peptides) and different structural aspects, *e.g.*, variants of amino acid sequence of the β-turn and *N*-terminal modificants such as *N*-acetyl (Ac-), *N*-*tert*-butoxycarbonyl (Boc-), and *N*-trifluoroacetyl (Tfa-) peptides as described in Chapter 2.

Chapter 3 is devoted to IR measurements of those synthetic peptides in $CDCl_3$

solution. The observed NH stretching bands are assigned to intramolecular hydrogen-bonded (HBd) states and hydrogen-bond-free (Hbfree) states of the NH groups. On the basis of the relative band intensities, I have compared stabilities of HBd structures among the peptides and argued a contribution from each structural constituent to formation of secondary structures in $CDCl_3$, which is likely to mimic a solvent environment inside of a protein.

In Chapter 4, I have dealt with NMR measurements of solvent-dependent population changes of the *cis* and *trans* isomers about the imide bonds preceding the Pro residues, by use of five kinds of mixed solvent systems, DMSO-d_6/D_2O, $CDCl_3$/DMSO-d_6, $CDCl_3$/acetonitrile-d_3, $CDCl_3$/methanol-d_4, $CDCl_3$/acetone-d_6. I have examined how the *cis*-to-*trans* isomerization couples to the intramolecular hydrogen bonding.

In Chapter 5, I have analyzed the chemical shift changes of amide protons for the peptides in the $CDCl_3$/DMSO-d_6 mixed solvents. It has been found that the chemical shift changes provide a good measure of the extent to which an NH proton participates in intramolecular hydrogen bonding.

In Chapter 6, I have analyzed chemical shift difference between two α-protons of the Gly residue, $\Delta\delta_{\alpha/\alpha'}$. It is shown that $\Delta\delta_{\alpha/\alpha'}$ is useful for quantifying structural flexibility of peptide backbone around a Glycyl residue (Gly) in solution. Using this new index, I have estimated some thermodynamic properties for the β-turn formation of the peptides and discussed the solvent effects and contribution of each amino acid sequence.

Chapter 7 describes the conclusion of the present study. I have compared ΔG values for the β-turn formation of the peptides among results from the three kinds of spectroscopic probes described in Chapter 3 (IR) and Chapter 5 and 6 (NMR). Furthermore, I have indicated propensities of a few dipeptide sequences for the β-turn structures in solution and compared them with statistical propensity data derived from X-ray structures of proteins.[5]

Chapter 2

Peptide Synthesis

Reagents:

All the peptides (60 entries) used in the present study were synthesized by several procedures described in the following section and are listed in Chart 1. Starting compounds for the syntheses, di-*tert*-butylpyrocarbonate ($(Boc)_2O$), *N*-*tert*-butoxycarbonyl-L-amino acids (Boc-Xaa-OH: Xaa = Gly, Ala, Nle (α-*n*-butylglycyl), Leu, Ile, Tle (α-*tert*-butylglycyl), MeAla (*N*-methylalanyl), Pro, Phe, Sar (*N*-methylglycyl), condensation reagent 1-ethyl-3-(3'dimethylaminopropyl)carbodiimide (WSCI), anti-racemization reagent 1-hydroxybenzotriazole (HOBt), and 4M HCl dioxane solution used for deprotection of the Boc-peptides were purchased from Watanabe Chemical Industries, Ltd. Methyl ester or ethyl ester derivatives of the corresponding amino acids (H-Pro-OMe (HCl salt), H-Leu-OMe (HCl salt), H-Yaa-OEt (HCl salt): Yaa = Gly, Ala, Leu, Val, Phe, Sar), H-Leu-NH_2 (HCl salt), and H-Pro-Leu-Gly-NH_2 were from Sigma Chemical Co. Acetic anhydride, acetyl chloride and *S*-ethyltrifluorothioacetate were from Nacalai Tesque Co. A tetrahydrofurane solution of 40%(w/w) methylamine, a dichloromethane solution of 0.1 M *N*-trifluoroacetyl-L-prolyl chloride (Tfa-Pro-Cl) were from Aldrich Chemical Co. Solvents used for NMR and IR measurements, chloroform-*d* ($CDCl_3$), heavy water (D_2O), and dimethylsulfoxide-d_6 ($(CD_3)_2SO$) were from CEA (France), and acetone-d_6 ($(CD_3)_2CO$), acetonitrile-d_3 (CD_3CN), methanol-d_4 (CD_3OD), and carbon tetrachloride (CCl_4) were from Wako Chemical Co. All the other reagents were of the highest grade commercially available.

Synthesis:

Boc-Xaa-Yaa-OEt and Boc-Xaa-Leu-OMe. One equivalent amount (1 eq.) of Boc-Xaa-OH, H-Yaa-OEt or H-Leu-OMe (1.1 eq. As a HCl salt), and HOBt (0.7~0.9 eq.) [42-44] were dissolved in *N,N*-dimethylformamide (DMF) and the mixture was placed at 0°C. A 1.1 eq. Amount of WSCI was added in 10 portions to the mixture with stirring.[45-46] The mixture was placed at room temperature and the condensation reaction was continued for more than 16 h. After volatiles were removed with a rotary

evaporator, the slurry was suspended in ethyl acetate (about 50 mL for 10 mmol reactant) and was successively washed with 30 mL *sat*. $NaHCO_3$ aqueous solution (3 times), 25 mL 10%(w/w) citric acid aqueous solution (3 times), and 20 mL of water (2 times). After removal of residual water from the organic layer using anhydrous sodium sulfate, the resulting organic layer was evaporated and the final product was obtained (60-95% yield). NMR checked final product and any impurities were found to be negligibly small. The scheme of the reaction is indicated in Chart 2.

Boc-Yaa-Leu-NH_2. Boc-Yaa-Leu-NH_2, a precursor of each Boc-Pro-Yaa-Leu-NH_2 (Yaa = Gly, Ala, Leu, Val, Phe), was synthesized by condensation of Boc-Yaa-OH with H-Leu-NH_2 (HCl salt) and isolated in the same way as for Boc-Xaa-Yaa-OEt.

Boc-Xaa-Yaa-NHMe. Each Boc-Xaa-Yaa-NHMe was obtained by conversion of the terminal ethyl ester group of a corresponding Boc-Xaa-Yaa-OEt to the $NHCH_3$ group with excess amount (150 eq.) of methylamine in tetrahydrofuran.[47] The reaction was conducted for 18 h at room temperature and confirmed to be completed by TLC. After volatiles were removed by evaporation, the described product was isolated.

Deprotection of Boc-group. For both further elongation and *N*-terminal modification of a peptide with an acetyl (Ac-) or a trifluoroacetyl (Tfa-) groups, deprotections of the *tert*-butoxycarbonyl (Boc) groups from the *N*-termini of Boc-Xaa-Yaa-OEt, Boc-Xaa-Yaa-NHMe, and Boc-Yaa-Leu-NH_2 were carried out. Each peptide was treated with 20~30 eq. of HCl (as a 4M solution in dioxane) at 4°C.[48] After 30 min, HCl was removed from the reaction mixture with an aspirator and the volatiles were further evaporated. The resulting precipitate was washed with hexane and dried up. Final products were HCl-salts of the deprotected peptides, *e.g.*, H-Xaa-Yaa-OEt (HCl). H-Xaa-Yaa-NHMe (HCl), and H-Yaa-Leu-NH_2 (HCl). Final products were checked by NMR and any impurities were found to be negligibly small. The scheme of the reaction is indicated in Chart 3.

Boc-Pro-Leu-Gly-OEt and Boc-Pro-Yaa-Leu-NH_2. The condensation reaction of Boc-Pro-OH with a deprotected peptide was carried out in the same way as

mentioned above.

Boc-Pro-OMe. The amount of 2.1 mmol of H-Pro-OMe (HCl) was dissolved in 5 mL of dichloromethane (DCM) and 0.5 mL of triethylamine (TEA), and to this solution was added 2.1 mmol of $(Boc)_2O$ (as a solution in 2 mL DCM) at 0°C with stirring.[49-50] After 1 h, temperature was raised to 25°C and placed for 20 h. After evaporation, the resulting slurry was diluted with 40 mL of ethyl acetate and washed with 10 mL of water three times. Finally, desired product was obtained by evaporation of the ethyl acetate layer. The scheme of the reaction is indicated in Chart 4.

Ac-Yaa-OEt and Ac-Pro-OMe. 200 mmol of H-Yaa-OEt (HCl salt) or H-Pro-OMe (HCl salt) was diluted with 100 mL of DCM and 28 mL of TEA, to this solution was added a total of 210 mmol of acetyl chloride in 70 portions below -20°C with stirring. After 20 min, DCM was removed by evaporation at 4°C and the resulting slurry was suspended in 100 mL of ethyl acetate. The filtrate was left standing overnight. The supernatant was collected and evaporated to result in a white powder. It was checked by NMR that the impurities included in final product were negligibly small.

Ac-Yaa-NHMe. Ac-Yaa-NHMe was obtained by the methylamidation of Ac-Yaa-OEt. The method was the same as that for the synthesis of Boc-Xaa-Yaa-NHMe.

Ac-Pro-Leu-Gly-NH_2. 1.25 mmol of H-Pro-Leu-Gly-NH_2 was dissolved in a mixed solvent of 40 mL of DMF, 80 mL of DCM, and 4 mL of TEA. To this solution 12 mL (25 mmol) of acetic anhydride was added in 24 portions at room temperature with stirring, which was continued for 1 h. Volatiles were removed with an evaporator. The resulting slurry was washed with a total of 40 mL of anhydrous ether and the final product was obtained (69% yield). Final product was checked by NMR and any impurities were negligibly small.

Ac-Pro-Gly-OEt, Ac-Pro-Gly-NHMe, and Ac-Pro-Gly-Leu-NH_2. Each of the

HCl-salts of deprotected peptides, H-Pro-Gly-OEt, H-Pro-Gly-NHMe, and H-Pro-Gly-Leu-NH_2, was dissolved in enough volume of the mixed solvent mentioned above. To this solution was added a total of 20-60 eq. amount of acetic anhydride in 25 portions at room temperature with stirring, which was continued for 45 min. After removal of volatiles and washing of the resulting slurry with anhydrous ether, an equivalent amount of silver acetate aqueous solution was added to the slurry so that the salt form of triethylammonium is changed from a nonvolatile chloride-salt to a volatile acetate-salt. An accomplishment of the silver titration was checked with K_2CrO_4. After filtration, the volume of water was reduced to be less than 4 mL by evaporation, and the resulting *N*-acetylated peptide was extracted into a 100 mL of ethyl acetate layer. The final product was obtained by evaporation and checked by NMR and any impurities were negligibly small. The scheme of the reaction is indicated in Chart 5.

Tfa-Pro-Leu-Gly-NH_2. 352 μmol of H-Pro-Leu-Gly-NH_2 was dissolved in 21 mL of the mixed solvent mentioned above. A total of 0.1 mL (800 μmol) of *S*-ethyl trifluorothioacetate was added in 10 portions to the solution at room temperature.[51] After 30 min, volatiles were removed with an evaporator and the residue was washed with a total of a 50 mL of ether to afford 137 mmol (39% yield) of the desired compound. Final product was checked by NMR and any impurities were negligibly small. The scheme of the reaction is indicated in Chart 6.

Tfa-Pro-Gly-OEt, Tfa-Pro-Gly-NHMe, and Tfa-Pro-Gly-Leu-NH_2. Tfa-Pro-Gly-OEt, Tfa-Pro-Gly-NHMe, and Tfa-Pro-Gly-Leu-NH_2 were synthesized using *N*-trifluoroacetyl-L-prolyl chloride (Tfa-Pro-Cl). H-Gly-OEt (HCl salt), H-Gly-NHMe (HCl salt), or H-Gly-Leu-NH_2 (HCl salt), was dissolved in 20 mL of DCM. A 2.5 eq. amount of Tfa-Pro-Cl (as a 0.1 M solution in DCM) was added at 4°C with stirring. After the solution was stirred for 30 min, volatiles were removed with an evaporator and the residue was extracted with a total of 20 mL of ethyl acetate to obtain the desired compound. Final product was checked by NMR and any impurities were negligibly small. The scheme of the reaction is indicated in Chart 7.

Notes:

All structures and concise interpretations for 60 kinds of the peptides used in the present study are listed in Chart 1. And three-letter representation of amino acid residues are as follows, respectively.

Gly = glycyl
Sar = sarcosyl (= *N*-methylglycyl)
Ala = alanyl
Nle = norleucyl (= α-*n*-butylglycyl)
Leu = leucyl
Ile = isoleucyl
Tle = tauleucyl (= α-*tert*-butylglycyl)
MeAla = *N*-methylalanyl
Pro = prolyl
Val = valyl
Phe = phenylalanyl

Chart 1 : Peptides (60 kinds):

Ac-Gly-OEt, Ac-Ala-OEt, Ac-Leu-OEt, Ac-Val-OEt, Ac-Phe-OEt

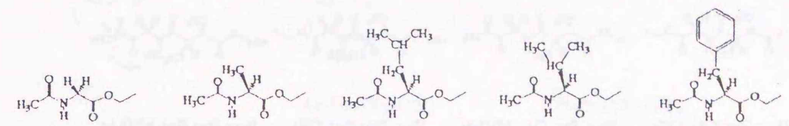

Ac-Gly-NHMe, Ac-Sar-OEt, Ac-Sar-NHMe,

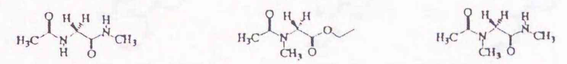

Boc-Gly-Gly-OEt, Boc-Gly-Gly-NHMe, Boc-Gly-Sar-OEt, Boc-Gly-Sar-NHMe,

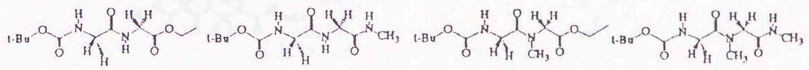

Boc-Ala-Gly-OEt, Boc-Ala-Gly-NHMe, Boc-Ala-Sar-OEt, Boc-Ala-Sar-NHMe,

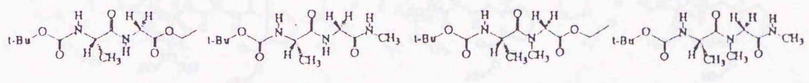

Boc-Nle-Gly-OEt, Boc-Nle-Gly-NHMe,

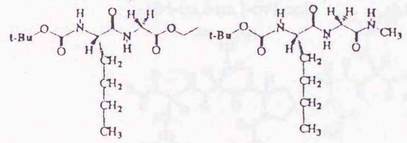

Boc-Leu-Gly-OEt, Boc-Leu-Gly-NHMe, Boc-Leu-Sar-OEt, Boc-Leu-Sar-NHMe,

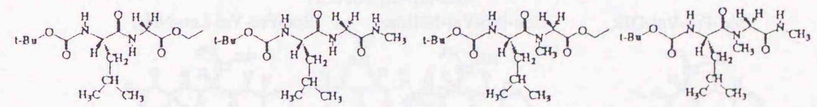

Boc-Ile-Gly-OEt, Boc-Ile-Gly-NHMe,

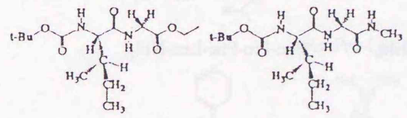

Boc-Tle-Gly-OEt, Boc-Tle-Gly-NHMe,

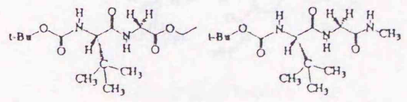

Boc-MeAla-Gly-OEt, Boc-MeAla-Gly-NHMe, Boc-MeAla-Sar-OEt, Boc-MeAla-Sar-NHMe,

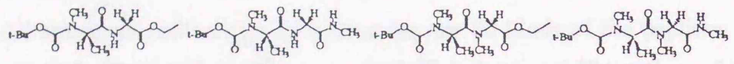

Boc-Pro-Gly-OEt, Boc-Pro-Gly-NHMe, Boc-Pro-Sar-OEt, Boc-Pro-Sar-NHMe,

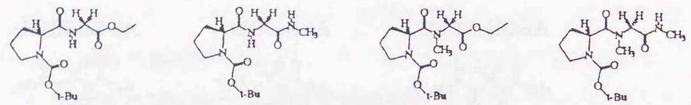

Boc-Sar-Sar-NHMe,

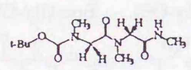

Boc-Pro-Ala-OEt, Boc-Pro-Ala-NHMe, Boc-Pro-Ala-Leu-NH_2,

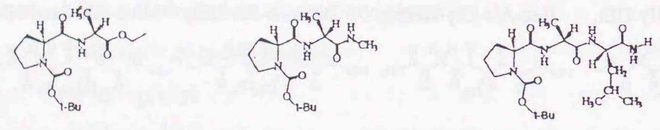

Boc-Pro-Leu-OEt, Boc-Pro-Leu-NHMe, Boc-Pro-Leu-Leu-NH_2,

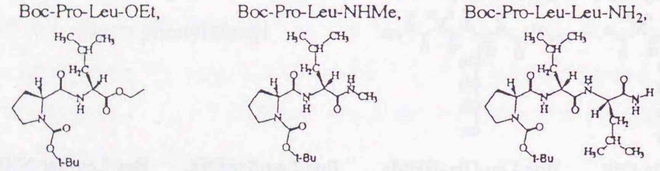

Boc-Pro-Val-OEt, Boc-Pro-Val-NHMe, Boc-Pro-Val-Leu-NH_2,

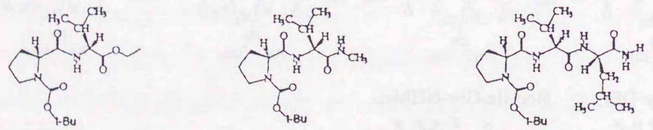

Boc-Pro-Phe-OEt, Boc-Pro-Phe-NHMe, Boc-Pro-Phe-Leu-NH_2,

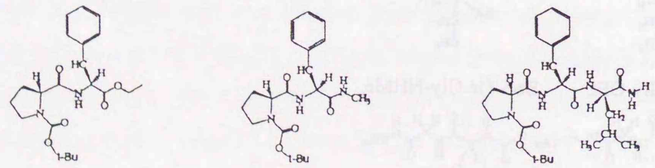

Boc-Pro-OMe,

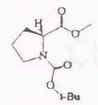

Ac-Pro-OMe

Ac-Pro-Gly-OEt,

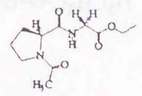

Tfa-Pro-Gly-OEt,

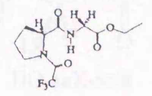

Ac-Pro-Gly-NHMe,

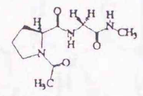

Tfa-Pro-Gly-NHMe,

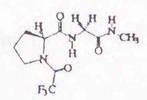

Boc-Pro-Gly-Leu-NH_2,

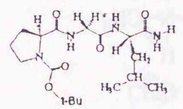

Ac-Pro-Gly-Leu-NH_2,

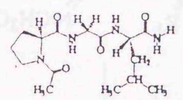

Tfa-Pro-Gly-Leu-NH_2,

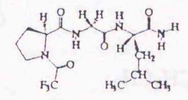

Ac-Pro-Leu-OMe,

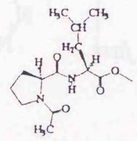

Ac-Pro-Leu-Gly-OEt,

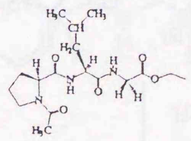

Ac-Pro-Leu-Gly-NH_2,

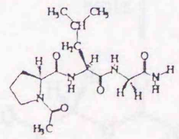

Tfa-Pro-Leu-Gly-NH_2,

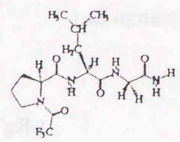

Chart 2: Condensation reaction

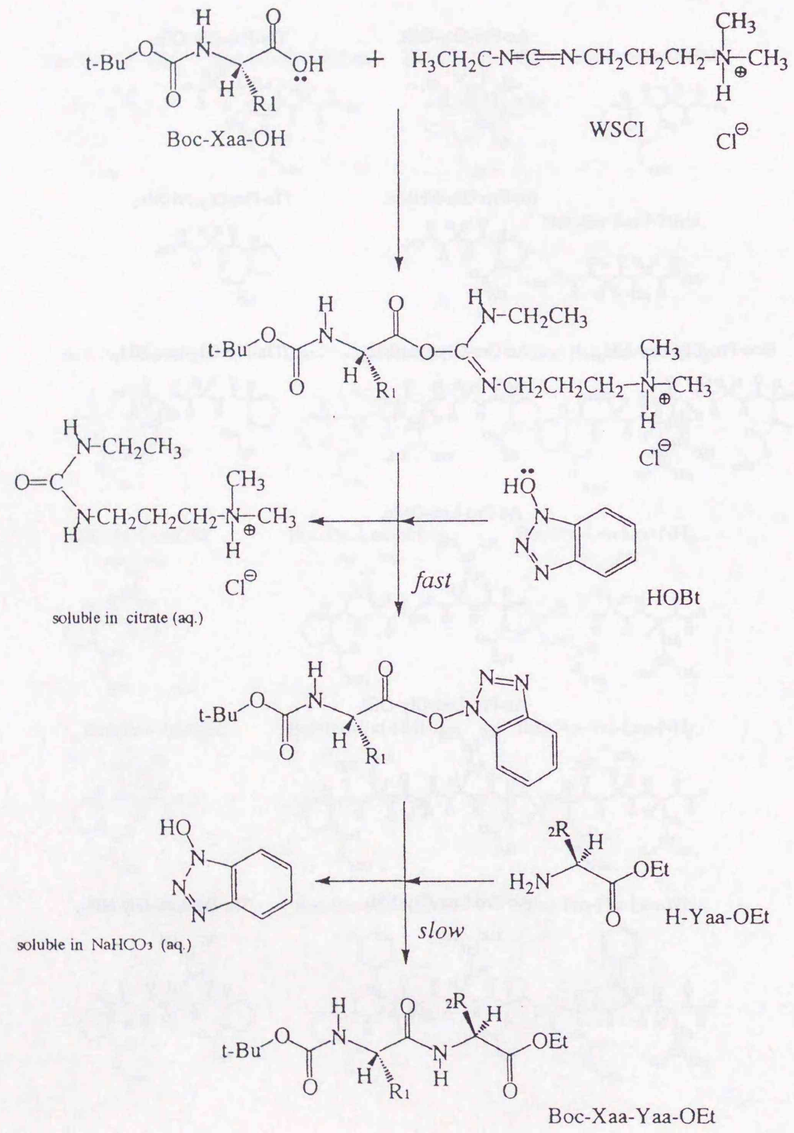

Chart 3: Deprotection of Boc-group

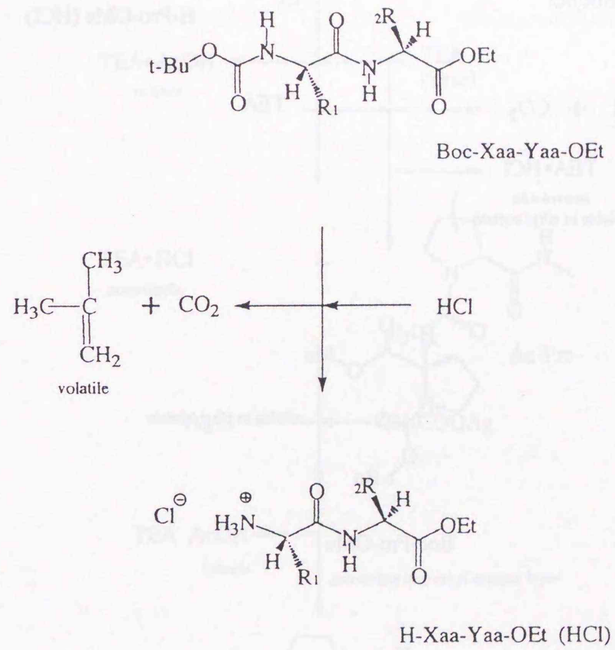

Chart 4: Synthesis of Boc-Pro-OMe

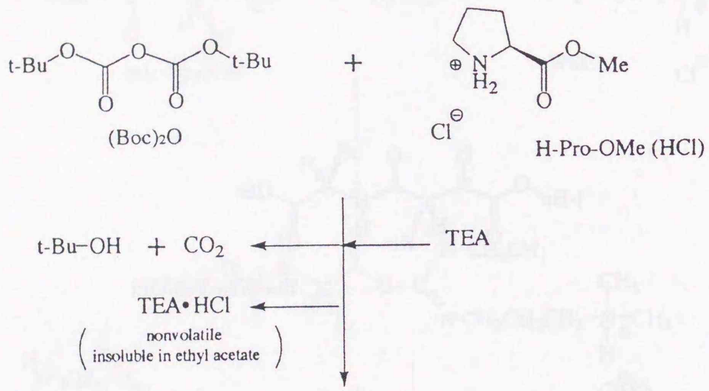

Boc-Pro-OMe

Chart 5: *N*-Acetylation of peptide (HCl salt)

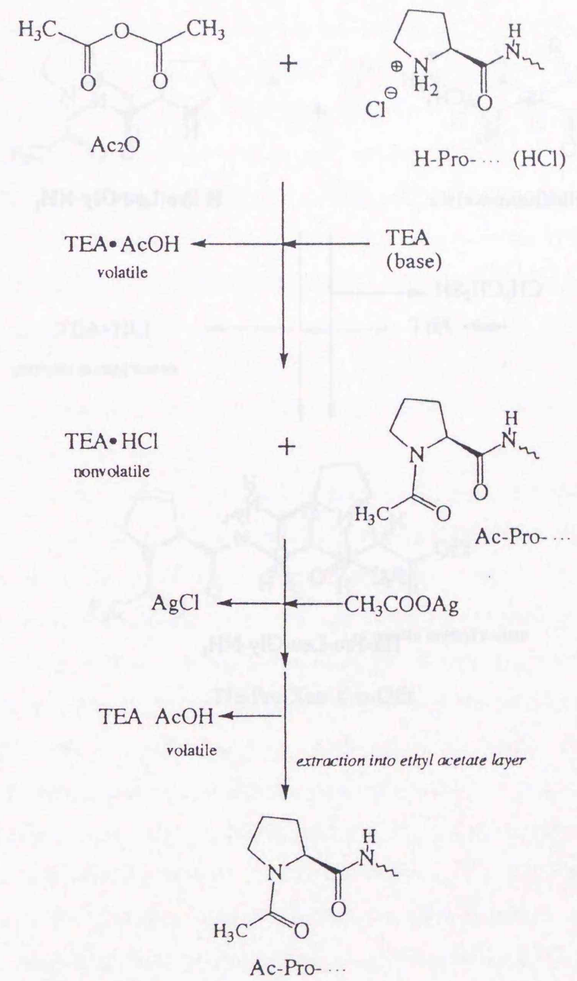

Chart 6: Synthesis of Tfa-Pro-Leu-Gly-NH_2

S-Ethyltrifluoroacetate

H-Pro-Leu-Gly-NH_2

CH_3CH_2SH

volatile

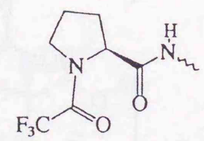

Tfa-Pro-Leu-Gly-NH_2

Chart 7: Synthesis of Tfa-peptide

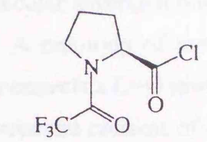

Tfa-Pro-Cl

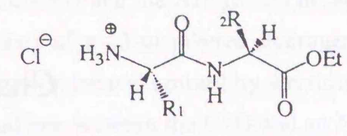

H-Xaa-Yaa-OEt (HCl)

TEA•HCl

insoluble in ethyl acetate

TEA

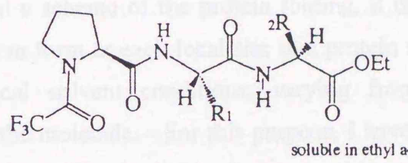

soluble in ethyl acetate

Tfa-Pro-Xaa-Yaa-OEt

Chapter 3

FTIR Study on Intramolecular Hydrogen Bonding of Small Peptides in Chloroform

Introduction:

For a long polypeptide chain to fold into a compact globule of a protein structure, formation of secondary structures in local regions of the polypeptide chain, such as α-helix, β-turn, γ-turn, and so on, is essential. These secondary structures are formed by intramolecular hydrogen bonds between the C=O and the NH groups in the peptide backbone. A one-loop of the α-helix consists of a 13-membered hydrogen-bonded ring which connects a C=O group with a NH group located upward by 4 residues, while the β-turn structure consists of a 10-membered one between the C=O and an NH group located upward by 3 residues.[52-55] The α-helix shortens the overall length of the polypeptide chain and the β-turn reverses the direction of the chain, respectively. Both secondary structures perform as frameworks equipped with further structuring interaction such as packing of side chains which belong to far separated amino acid residues in the sequence of a protein. On the other hand, a 7-membered hydrogen-bonded structure, the γ-turn,[19] is thought as a transient intermediate structure during the protein folding pathway.

In order to reveal a scheme of the protein folding, it is important to know which secondary structure can form at each local site in a protein molecule which prepares a wide variety of local solvent conditions, varying from hydrophilic surface to hydrophobic core of the molecule. For this purpose, I have used many kinds of small peptides which represent different structural aspects of local regions of the polypeptide chain, *e.g.*, ability of hydrogen-bonding or flexibility of the backbone dihedral angles. Comparison of intrinsic propensity of each local sequence for forming regular secondary structures in various environments should provide insight into the origins of the protein folding patterns. In this chapter, I have concentrated on infrared (IR) results measured in $CDCl_3$ solutions for those peptides. IR spectrum is one of the most direct indicators for detecting and characterizing the hydrogen bond[16-17] which are related to the α-helix, β-turn, γ-turn, and so on. Since NH stretching absorptions are observed distinctly for equilibrating hydrogen-bonded and hydrogen-bond-free states, it is possible to inspect the stability of hydrogen-bonded structures of peptides. In addition, a low-polarity solvent such as chloroform is thought to mimic the solvent condition inside of a folded protein molecule, where segments of the polypeptide are

embedded in hydrophobic atmospheres.

Experimental:

IR Measurements. Infrared spectra of all the peptides were measured with a BOMEM DA3 or a Perkin-Elmer System 2000 Fourier-transform spectrometers. Windows of a sample cell used were optically polished CaF_2 discs and sample pathlength was fixed at 6 mm. Chloroform-*d* ($CDCl_3$) was used as solvent after being dried over molecular sieves 4A for more than 24 h. Each sample, 1.25 mM $CDCl_3$ solution of peptide was prepared by dissolving a few milligram of peptide in 10 mL of the solvent, where uncertainty in weighting was less than 10%. The concentrations were dilute enough to neglect self-association of the peptides.

In order to get rid of spectral obstruction such as moisture and carbon dioxide in air, the main compartment of the BOMEM DA3 spectrometer was also evacuated so as to avoid interference of residual H_2O vapor in a spectral region of antisymmetric N-H stretchings of 2 cm^{-1} Absorbance of samples was obtained by subtracting the pure solvent spectrum measured under the same condition.

Decomposition of IR Spectra into Component Bands. Overlapping bands which consists of more than one or two NH stretching modes were resolved by least-square fitting with a computer. The baseline of the spectrum was taken to be a flat line estimated from a higher-frequency region which is free from the solute absorption. A Lorentzian function was used for representing each of the bands assigned to the hydrogen-bond-free (HBfree) NH groups, in view of the fact that HBfree NH bands of *N*-alkyl derivatives of acetamide are well reproduced by a Lorentzian function. Each of the bands assigned to intramolecular hydrogen-bonded (HBd) NH groups, on the other hand, was represented by a Gaussian function which is adequate to reproduce an inhomogeneously broadened band, such as the HBd bands. In general, it should be noted that curve-fitting involves some arbitrariness for the spectra in which quite a few component bands are overlapped with one another in a narrow frequency region. Under this circumstance, there might be uncertainty in estimation of band

parameters of the component bands. However, if more than two bands overlap but their peaks or shoulders are distinctly observed, relative intensities of these component bands could be estimated with a significant precision. In order to estimate the precisions of curve fittings for some spectra, I have obtained standard deviations of calculations for relative intensity of the HBd and Hbfree bands for a few peptides through independent six trials of the curve fittings. As a result, the standard deviations were found to be 4-15% for the estimation of the HBd/HBfree band intensity ratios.

Results:

Ac-Gly-NHMe and Ac-Sar-NHMe.

Figure 3.1 and 3.2 show IR spectra of 1.25 mM $CDCl_3$ solutions of Ac-Gly-NHMe and Ac-Sar-NHMe, respectively. Distinct peaks at frequencies higher than 3400 cm^{-1} are assigned to hydrogen-bond-free (HBfree) stretchings of NH groups. Of these HBfree NH bands, the band around 3450 cm^{-1} is observed for both Ac-Gly-NHMe and Ac-Sar-NHMe. Therefore, it can be assigned to the C-terminal $NHCH_3$ group for both compounds. In addition, the 3419 cm^{-1}-band of Ac-Gly-NHMe is assigned to the Gly-NH group in an HBfree state. These assignments are thought to be reasonable by the fact that an HBfree stretching for the Gly-NH of Ac-Gly-OEt (3437 cm^{-1}) has a lower frequency than that for $NHCH_3$ of N-methylacetamide (3469 cm^{-1}) in dilute solutions in $CDCl_3$.

On the other hand, broad band at 3370 cm^{-1} for Ac-Sar-NHMe is assigned to the C-terminal $NHCH_3$ group which takes part in intramolecular hydrogen bond with the acetyl C=O group to form a 7-membered HBd ring.

Boc-Xaa-Gly-OEt (Xaa = Gly, Ala, Nle, Leu, Ile, Tle, MeAla, Pro).

In Figures 3.3 to 3.8, IR spectra for Boc-Xaa-Gly-OEt (Xaa = Gly, Ala, Nle, Leu, Ile, Tle) are shown with results of curve-fitting. For these peptides, bands to be assigned to hydrogen bonds are not appreciable except for a minor swelling in the lower frequency region. Therefore, both the Xaa-NH and the Gly-NH groups of these peptides do not participate in formation of the 7-membered HBd rings.

However, for Boc-MeAla-Gly-OEt and Boc-Pro-Gly-OEt shown in Figure 3.9 and Figure 3.10, the 7-membered HBd structures are thought to be more stable than the other kinds of Boc-Xaa-Gly-OEt peptides. For these two peptides, it is also indicated that HBfree bands of the Gly-NH groups are composed of two distinct components. As will be discussed in Chapter 4, Boc-Pro-Gly-OEt and Boc-MeAla-Gly-OEt take two different configurations, *cis* and *trans* isomers about the peptide bonds preceding the Pro and the MeAla residues. The NMR study in Chapter 4 show that the *cis/trans* ratios in $CDCl_3$ solution are 29 : 71 for Boc-MeAla-Gly-OEt and 33 : 67 for Boc-Pro-Gly-OEt, respectively.

Boc-Pro-Yaa-OEt (Yaa = Ala, Leu, Val, Phe).

As shown in Figures 3.11 to 3.14, the 7-membered HBd structures are appreciable for peptides with a sequence of Boc-Pro-Yaa-OEt (Yaa = Ala, Leu, Val, Phe) in $CDCl_3$. From comparison of relative intensities of the HBd bands of these peptides listed in Table 1, it is found that the stabilities of the 7-membered HBd structures are in the following order: Val > Leu > Gly > Phe ≧ Ala for the Yaa residue in Boc-Pro-Yaa-OEt

Ac-Pro-Gly-OEt and Tfa-Pro-Gly-OEt.

For a comparison, the IR spectra of *N*-terminus modificants of Boc-Pro-Gly-OEt, Ac-Pro-Gly-OEt and Tfa-Pro-Gly-OEt, are shown in Figure 3.15 and 3.16. Relative intensities of the 7-membered HBd bands are in the following order: Ac-Pro-Gly-OEt > Tfa-Pro-Gly-OEt > Boc-Pro-Gly-OEt (Table 1).

Boc-Xaa-Sar-NHMe (Xaa = Gly, Ala, Leu, MeAla, Pro).

Each peptide with a sequence of Boc-Xaa-Sar-NHMe can form a 10-membered HBd ring, in which the C-terminal $NHCH_3$ group is linked with the Boc C=O group. In addition to the 10-membered HBd ring, a 7-membered HBd structure which is the same as that of Ac-Sar-NHMe would be possible. But, as shown in Figures 3.17 to 3.21 and Table 2, both frequencies and relative intensities of the HBd bands are dependent on the Xaa residues. These facts suggest that the 10-membered HBd structure in which the Xaa residue takes part is more probable than the 7-membered counterpart. Structural features specific to each Xaa residue, such as restriction of

backbone dihedral angles or steric hindrance by its side chain, will be more critical for the 10-membered structure than for the 7-membered one.

Comparison of the relative intensities of the HBd bands indicates that the stabilities of the 10-membered HBd structures are in the following order: Pro > Leu ≧ MeAla ≧ Ala > Gly for Xaa of Boc-Xaa-Sar-NHMe. This order is in agreement with a decreasing order in stretching frequencies of HBd bands among all the peptides studied as discussed later.

Boc-Xaa-Gly-NHMe (Xaa = Gly, Ala, Nle, Leu, Ile, Tle, MeAla, Pro).

As shown in IR spectra of Boc-Xaa-Gly-NHMe in Figures 3.22 to 3.29, the frequency of the HBd band of each peptide is similar to that of the 10-membered HBd band of the corresponding Boc-Xaa-Sar-NHMe peptide. On the other hand, the frequency for Boc-Pro-Gly-NHMe, 3355 cm^{-1}, is significantly different from that for the 7-membered HBd band of Boc-Pro-Gly-OEt, 3321 cm^{-1}. From these facts, the HBd structure of Boc-Xaa-Gly-NHMe has a 10-membered ring as that of Boc-Xaa-Sar-NHMe. As indicated in Table 3, the frequencies and relative intensities of the HBd bands are dependent on the Xaa residues. The order of Xaa stabilizing these 10-membered HBd structures is as follows: Pro ≧ Ile ≧ Ala ≧ Tle ≧ Nle ≧ Leu > Gly ≧ MeAla for Xaa of Boc-Xaa-Gly-NHMe. A decreasing order of frequencies of the HBd bands assigned to the C-terminal $NHCH_3$ groups is found to be Pro > MeAla > Tle > Ile > Nle > Leu = Ala > Gly.

Boc-Pro-Yaa-NHMe (Yaa = Ala, Leu, Val, Phe).

As shown in Figures 3.30 to 3.33 peptides with a sequence of Boc-Pro-Yaa-NHMe have HBd bands of which peak frequencies are similar to that of the 10-membered HBd structure of Boc-Pro-Gly-NHMe. The curve fitting results suggest that another lower frequency HBd band is needed to reproduce the spectra. Relative intensities of the HBd bands are compared in Table 4. Stabilities of the 10-membered HBd structures are suggested to be in the following order: Gly ≧ Phe ≧ Ala ≧ Leu ≧ Val for Yaa of Boc-Pro-Yaa NHMe, while those of the 7-membered structures for the same peptide series are in the opposite order: Val > Leu > Ala >> Phe ≧ Gly.

Ac-Pro-Gly-NHMe and Tfa-Pro-Gly-NHMe.

For comparison, IR spectra of *N*-terminus modificants of Boc-Pro-Gly-NHMe, Ac-Pro-Gly-NHMe and Tfa-Pro-Gly-NHMe, are shown in Figures 3.34 and 3.35. For both peptides, the HBd bands are assigned to the 10-membered structures. Figure 3.35 suggests that the Gly-NH group of Tfa-Pro-Gly-NHMe is also engaged in another type of HBd structure, a 7-membered one. From comparison of relative intensities of the HBd bands listed in Table 4, the formation of the 10-membered HBd structure is in the following order: Ac-Pro-Gly-NHMe > Boc-Pro-Gly-NHMe > Tfa-Pro-Gly-NHMe. On the other hand, stabilities of the 7-membered structures are in the following order: Tfa-Pro-Gly-NHMe > Ac-Pro-Gly-NHMe > Boc-Pro-Gly-NHMe.

Boc-Pro-Yaa-Leu-NH_2 (Yaa = Gly, Ala, Leu, Val, Phe).

Figure 3.36 to 3.40 show IR spectra of 1.25 mM solutions of peptides with a sequence of Boc-Pro-Yaa-Leu-NH_2. In these spectra, a few HBd bands overlap with one another and make it difficult to classify the NH groups into different types of HBd structures. Thus, although differences in spectral shape are apparent among these peptides, I could only say that more than one kinds of HBd structures co-exist for Boc-Pro-Yaa-Leu-NH_2 peptides. In spite of this limitation, it is meaningful to examine another couple of discrete bonds, each of which is assigned to one of the HBfree stretchings of the C-terminal NH_2. In general, the antisymmetric and symmetric NH stretching vibrations, ν_a and ν_s of the carboxamide NH_2 group, exhibit a large frequency splitting due to coupling of the two N-H bond stretchings. For example, the ν_a and ν_s bands of acetamide in a chloroform solution have been observed at 3534 and 3416 cm^{-1}. In an IR spectrum of Boc-Pro-Gly-Leu-NH_2, corresponding two bands are found at 3522 and 3410 cm^{-1}, respectively. In addition, a band around 3488 cm^{-1}, observed for all of the investigated peptides with C-terminal NH_2 group, is reasonably assigned to a HBfree NH stretching of the NH_2 group the other NH of which is hydrogen-bonded. Therefore, the intensity ratio of the band at around 3490 cm^{-1} to the band at around 3525 cm^{-1}, will be a good index of degree to which the C-terminal NH_2 group is concerned with the intramolecular hydrogen bonding.

Estimated intensity ratios of the two bands resolved by curve fittings are compared and listed in Table 5. The degree to which the C-terminal NH_2 group participates in

the HBd structure formation is in the following order: Phe > Ala ≧ Val > Leu > Gly for Yaa of Boc-Pro-Yaa-Leu-NH_2.

Ac-Pro-Gly-Leu-NH_2 and Tfa-Pro-Gly-Leu-NH_2.

For comparison, IR spectra of *N*-terminus modificants of Boc-Pro-Gly-Leu-NH_2, Ac-Pro-Gly-Leu-NH_2 and Tfa-Pro-Gly-Leu-NH_2, are shown in Figure 3.41 and 3.42, respectively. Remarkable difference in spectral shape can be seen among these three peptides. This means that these peptides take such HBd structures that are perturbed by changes in electronic or steric conditions at the *N*-termini. These HBd structures are probably 13-membered ring connecting the *N*-terminal C=O to the C-terminal NH_2 group.

Ac-Pro-Leu-Gly-NH_2 and Tfa-Pro-Leu-Gly-NH_2.

Difference in IR spectra is apparent between Ac-Pro-Gly-Leu-NH_2 and Ac-Pro-Leu-Gly-NH_2 shown in Figures 3.41 and 3.43, respectively, and between Tfa-Pro-Gly-Leu-NH_2 and Tfa-Pro-Leu-Gly-NH_2 in Figures 3.42 and 3.44, respectively. This means that a replacement of amino acid positions in the sequence influences the types or stabilities of HBd structures.

Ac-Pro-Leu-Gly-OEt.

Figure 3.45 shows a spectrum of Ac-Pro-Leu-Gly-OEt in $CDCl_3$. A distinct peak at 3423 cm^{-1} and a shoulder 3447 cm^{-1} are assigned to two different HBfree NH groups. Referring to spectra of Ac-Gly-OEt and Ac-Pro-Leu-OMe, the higher 3447 cm^{-1} band is assigned to the Gly-NH and the lower 3423 cm^{-1} band to the Leu-NH, respectively. On the other hand, broad bands around 3350 cm^{-1} and 3288 cm^{-1} are assigned to the NH stretchings of two different types of HBd structures, 10-membered and 7-membered rings, respectively.

Discussion:

Frequencies of HBd bands.

Figure 3.46 shows a relationship between HBd NH stretching frequencies of the $NHCH_3$ groups and intensity ratios of the HBd bands to the corresponding HBfree bands. The plots are divided into some categories by taking into account of structural constitutions of the peptides. Results for Boc-Xaa-Sar-NHMe, Boc-Xaa-Gly-NHMe, and X-Pro-Yaa-NHMe are shown in Figures 3.47 to 3.49, respectively. Correlation given by *R* for these plots were improved by such categorization. This means that comparison of HBd frequencies is useful to assess HBd structure formations which involve the same hydrogen-bond acceptor and donor. When an NH group participates in hydrogen-bonding, the NH stretching frequency shifts to a lower frequency. For a given pair of hydrogen-bond-donating and accepting groups, degree of the lower-frequency-shift will mainly depend on geometrical fit of an intervening residue which is a part of the HBd ring, and the backbone flexibility around such residue may influence strength of the HBd structure. Therefore, a linear relationship in Figure 3.48 supports that all the Boc-Xaa-Gly-NHMe peptides studied take the same type of 10-membered HBd ring.

Figure 3.50 shows a similar relationship for HBd structures which involve the C-terminal NH_2 groups. Here, it is found that degree of the lower-frequency-shift for the NH_2 group is influenced by modification of the *N*-terminus. The replacement of the Boc group with the acetyl (Ac-) or trifluoroacetyl (Tfa-) group shifts the NH stretching band to the lower or a little higher frequency.

7-membered HBd ring.

As described before, the stabilities of the 7-membered HBd rings are found to be in the following order: Ac-Pro-Gly-OEt > Tfa-Pro-Gly-OEt ≧ Boc-Pro-Val-OEt > Boc-Pro-Leu-OEt > Boc-Pro-Gly-OEt > Boc-Pro-Phe-OEt ≧ Boc-Pro-Ala-OEt.

As also mentioned before, such 7-membered HBd structures are appreciable only when the Xaa residue is Pro, as in Boc-Pro-Yaa-OEt. This is due to the unique structure of the Pro residue, the side chain of which is covalently connected to the nitrogen atom of the peptide backbone and one of the dihedral angles, $\phi_{(Pro)}$, is fixed at around –65(±10°).[56] Another dihedral angle, $\psi_{(Pro)}$, is also substantially constrained within the narrow ranges from -70° to -20° and from +60° to +160°.[56] It is known that the γ-turn structure, the most probable candidate of the 7-membered HBd ring, can form

when the two dihedral angles, $\phi_{(Pro)}$ and $\psi_{(Pro)}$, adopt -70° and +65°, respectively.[19] Because dihedral angles for any other residue are thought to be freer, other Boc-Xaa-Gly-OEt peptides except one with Xaa = MeAla cannot form the γ-turn structure to a significant degree in $CDCl_3$. In addition, some bulkier residues such as Val and Leu occupying the Yaa position of Boc-Pro-Yaa-OEt render the γ-turn structures more stable, probably because the $\psi_{(Pro)}$ angles are further constrained by steric hindrance of the bulkier side chains.

Furthermore, stability of the γ-turn is likely to be dependent on hydrogen-bond-accepting abilities of C=O groups in peptides. The γ-turn structure of Ac-Pro-Gly-OEt is more stable than that of Tfa-Pro-Gly-OEt, and much more stable than that of Boc-Pro-Gly-OEt. Trifluorination of the acetyl group will reduce the proton-accepting ability of its carbonyl oxygen owing to the considerable electron-withdrawing property of the trifluoromethyl group. Therefore, the hydrogen bond is weaker in Tfa-Pro-Gly-OEt than in Ac-Pro-Gly-OEt. On the other hand, destabilization of the γ-turn for Boc-Pro-Gly-OEt is thought to be attributed to steric hindrance by a large *tert*-butyl moiety of the Boc-group, which would spoil favorable interactions when the peptide takes the γ-turn structure.

10-membered HBd ring.

Stabilities of the 10-membered HBd structures are found to be in the following order: Boc-Pro-Sar-NHMe >> Boc-Leu-Sar-NHMe ≧ Boc-MeAla-Sar-NHMe ≧ Boc-Ala-Sar-NHMe > Boc-Gly-Sar-NHMe for the Sar-containing peptides, Boc-Pro-Gly-NHMe ≧ Boc-Ile-Gly-NHMe ≧ Boc-Ala-Gly-NHMe ≧ Boc-Tle-Gly-NHMe ≧ Boc-Nle-Gly-NHMe ≧ Boc-Leu-Gly-NHMe > Boc-Gly-Gly-NHMe ≧ Boc-MeAla-Gly-NHMe for the Gly-containing peptides, and Boc-Pro-Sar-NHMe >> Ac-Pro-Gly-NHMe > Boc-Pro-Gly-NHMe ≧ Boc-Pro-Phe-NHMe ≧ Boc-Pro-Ala-NHMe > Boc-Pro-Leu-NHMe ≧ Tfa-Pro-Gly-NHMe > Boc-Pro-Val NHMe for the Pro-containing peptides, respectively.

The Pro residue occupying the Xaa position in Boc-Xaa-Sar-NHMe is more suitable for formation of the 10-membered HBd ring than any other residue at the same position. This superiority of the Pro residue is remarkable for a series of the Sar-containing peptides but less remarkable for a series of the Gly-containing peptides.

The dihedral angles of the Pro residue, $\phi_{(Pro)}$ and $\psi_{(Pro)}$, can also fit to the β-turn structure which is the most probable candidate of the 10-membered HBd ring for such peptides. Either dihedral angle set, (-60°, -30°, -90°, 0°) for ($\phi_{(i+1)}$, $\psi_{(i+2)}$, $\phi_{(i+2)}$, $\psi_{(i+2)}$) of the type-I β-turn or , (-60°, +120°, +80°, 0°) for ($\phi_{(i+1)}$, $\psi_{(i+2)}$, $\phi_{(i+2)}$, $\psi_{(i+2)}$) of the type-II β-turn can be taken by Boc-Pro-Yaa-NHMe peptides.[19] The Sar residue at the Yaa position is definitely superior to the Gly residue in further stabilization of the β-turn structure, probably owing to the fact that the dihedral angles of the Sar residue are more constrained than those of the Gly residue. But such advantage in the Sar residue becomes unappreciable when Pro at the (i + 1)-th position is replaced by other residues. Therefore, the Sar residue at the (i + 2)-th position facilitates the β-turn formation in concert with the precedent Pro residue.

13-membered HBd ring.

Extents to which the terminal NH_2 groups are implicated in the intramolecular hydrogen-bonding are suggested to be in the following order: Boc-Pro-Phe-Leu-NH_2 > Boc-Pro-Ala-Leu-NH_2 > Boc-Pro-Val-Leu-NH_2 > Ac-Pro-Gly-Leu-NH_2 > Boc-Pro-Leu-Leu-NH_2 > Tfa-Pro-Gly-Leu-NH_2 ≧ Boc-Pro-Gly-Leu-NH_2 for a series of -Pro-Yaa-Leu-NH_2 peptides, and Ac-Pro-Gly-Leu-NH_2 > Ac-Pro-Leu-Gly-NH_2 > Tfa-Pro-Gly-Leu-NH_2 > Tfa-Pro-Leu-Gly-NH_2.

Again due to conformational rigidity, the Pro residue is fit to the starting position of the α-helix which has the 13-membered HBd rings, as well as for the β-turn (10-membered) and γ-turn (7-membered) structures. The backbone dihedral angles of every residue in the regular α-helix are ϕ = -57° and ψ = -47°, respectively.[19] These angles are possible for the Pro residue. Therefore, the above-mentioned order is thought to be an order for ability of forming α-helical structures. Of the two different types of β-turn, the type-I and type-II structures, would be possible for these peptides. The type-II structure is thought to be possible only when the (i + 2)-th position is occupied by the Gly residue, which lacks a side chain and is free from the steric repulsion with the carbonyl oxygen of the (i + 1)-th residue when the backbone takes the type-II β-turn (see Figure 3.51). Therefore, it is suggested that the type-II β-turn competes with the α-helix in Boc-Pro-Gly-Leu-NH_2, while the other type-I β-turn does in other Boc-Pro-Yaa-Leu-NH_2 (Yaa = Ala, Leu, Val, Phe).

Comparison of stability among different HBd structures.

As indicated in this chapter, IR spectroscopy has provided direct evidence of formation of various types of HBd structures for small peptides. Some peptides can take more than one type of HBd structures. From comparison of relative intensities among the 7-, 10-, and 13-membered HBd structures in $CDCl_3$ solutions, it is found that the α-helical (13-membered) and β-turn (10-membered) structures are more stable than the γ-turn (7-membered) in general.

The stability of these HBd structures will influence the *cis*-to-*trans* isomerization of the peptide bonds preceding the Pro residue as shown in the next chapter.

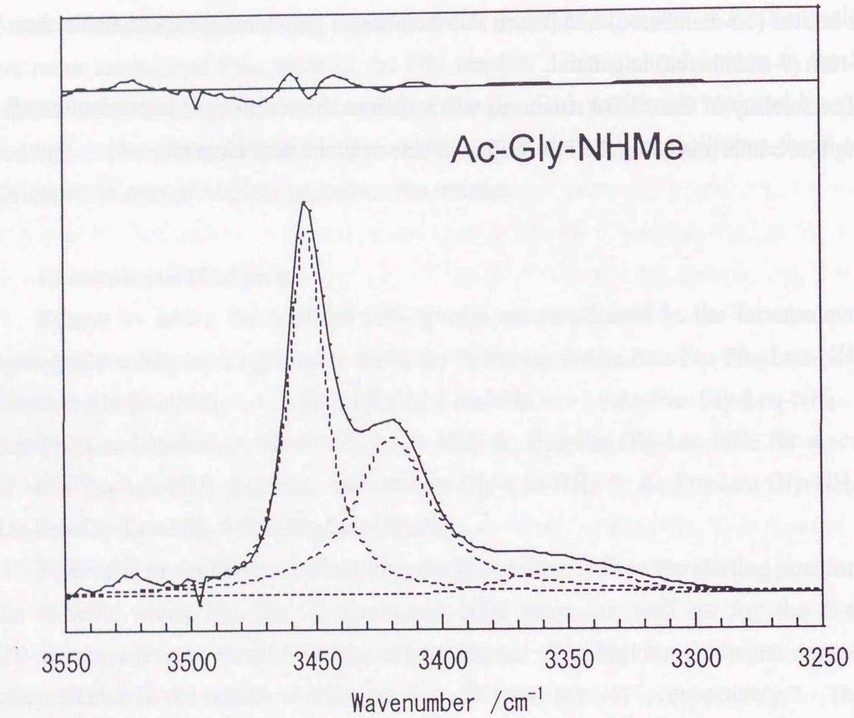

Figure 3.1. Infrared spectrum of 1.25 mM Ac-Gly-NHMe in $CDCl_3$ at 25˚C: Observed spectrum (solid line), calculated components (dotted line), and difference between the observed and calculated spectra (upper shifted solid line).

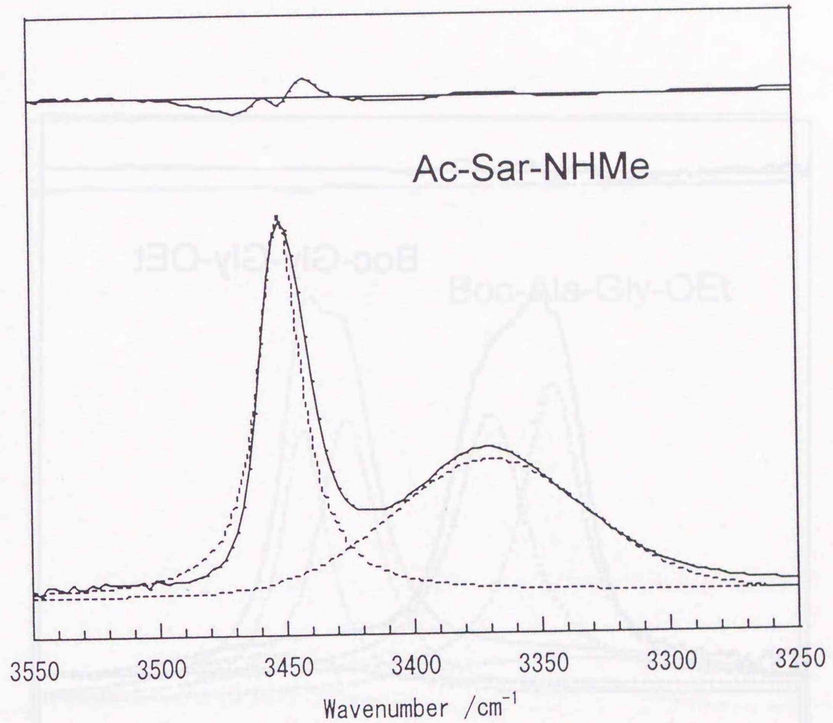

Figure 3.2. Infrared spectrum of 1.25 mM Ac-Sar-NHMe in $CDCl_3$ at 25˚C: Observed spectrum (solid line), calculated components (dotted line), and difference between the observed and calculated spectra (upper shifted solid line).

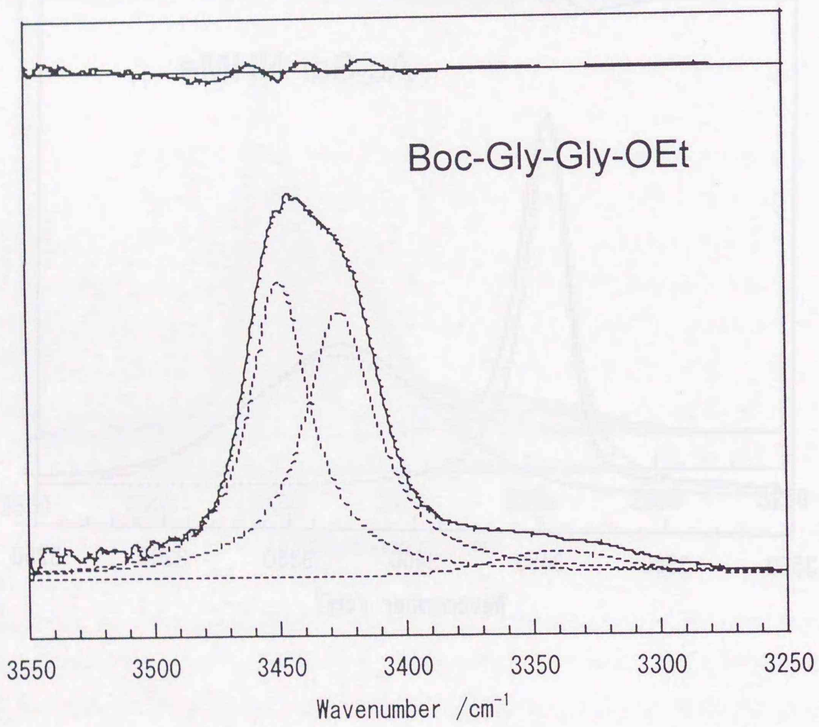

Figure 3.3. Infrared spectrum of 1.25 mM Boc-Gly-Gly-OEt in $CDCl_3$ at 25˚C: Observed spectrum (solid line), calculated components (dotted line), and difference between the observed and calculated spectra (upper shifted solid line).

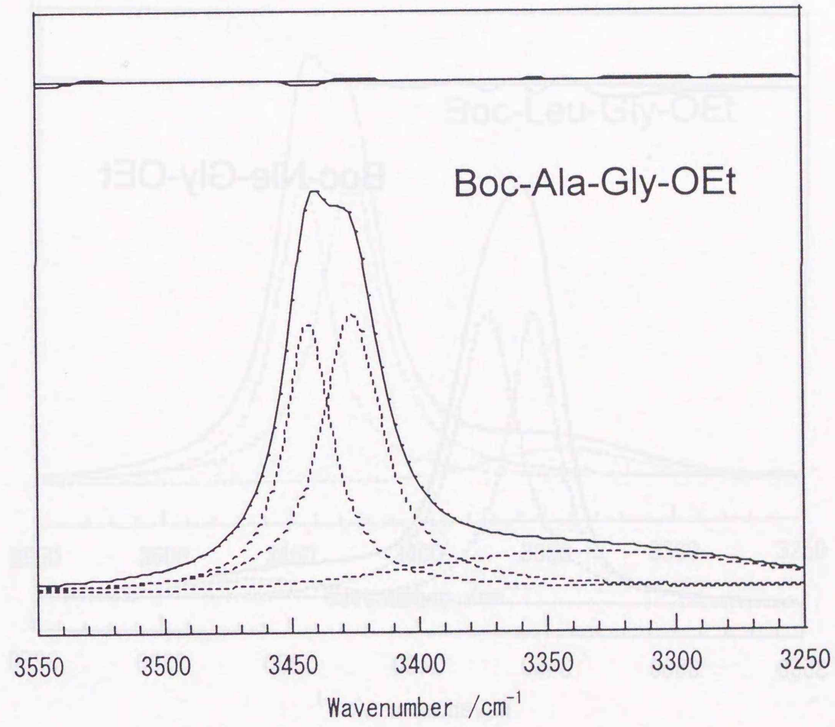

Figure 3.4. Infrared spectrum of 1.25 mM Boc-Ala-Gly-OEt in $CDCl_3$ at 25˚C: Observed spectrum (solid line), calculated components (dotted line), and difference between the observed and calculated spectra (upper shifted solid line).

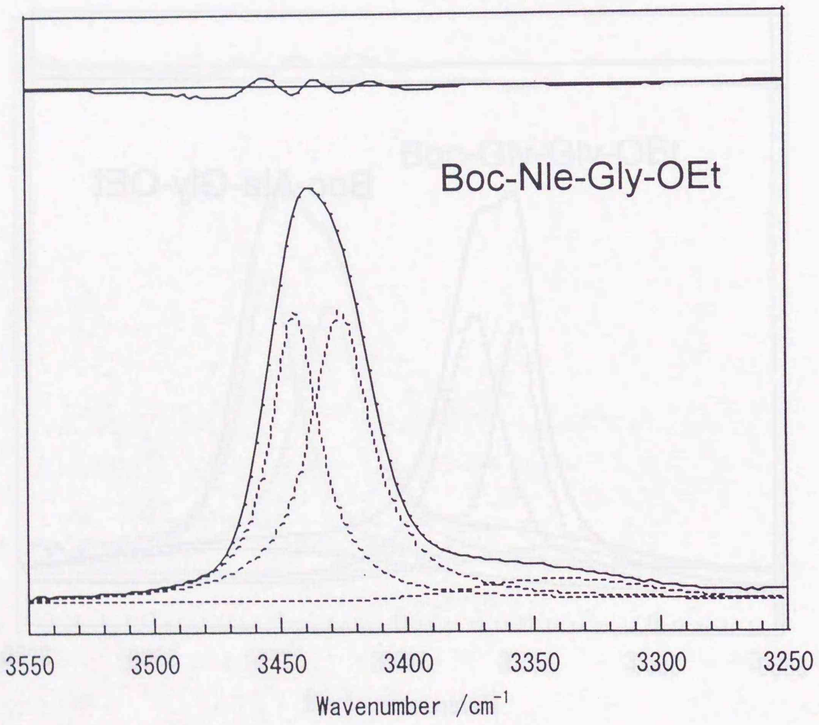

Figure 3.5. Infrared spectrum of 1.25 mM Boc-Nle-Gly-OEt in $CDCl_3$ at 25˚C: Observed spectrum (solid line), calculated components (dotted line), and difference between the observed and calculated spectra (upper shifted solid line).

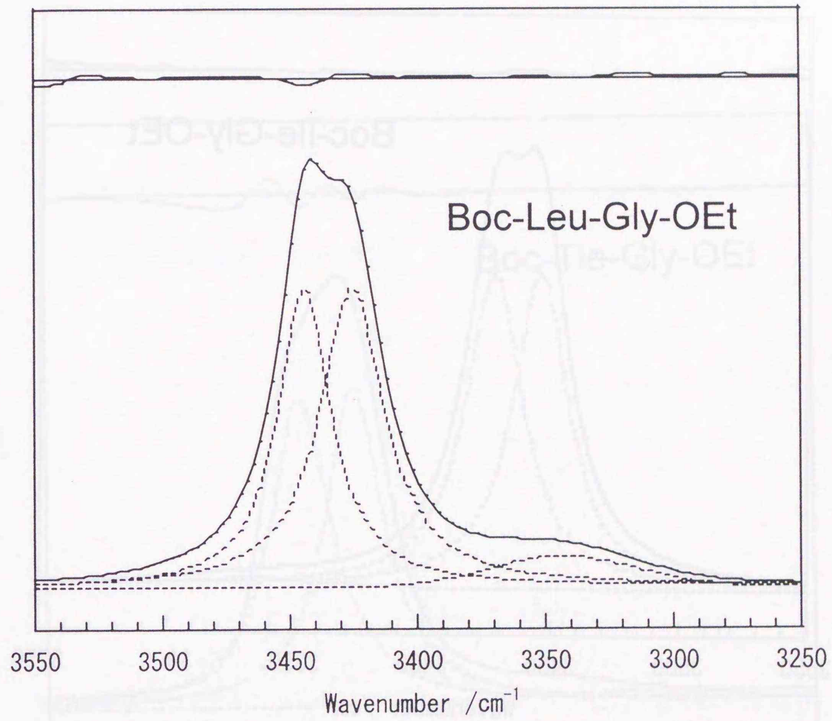

Figure 3.6. Infrared spectrum of 1.25 mM Boc-Leu-Gly-OEt in $CDCl_3$ at 25˚C: Observed spectrum (solid line), calculated components (dotted line), and difference between the observed and calculated spectra (upper shifted solid line).

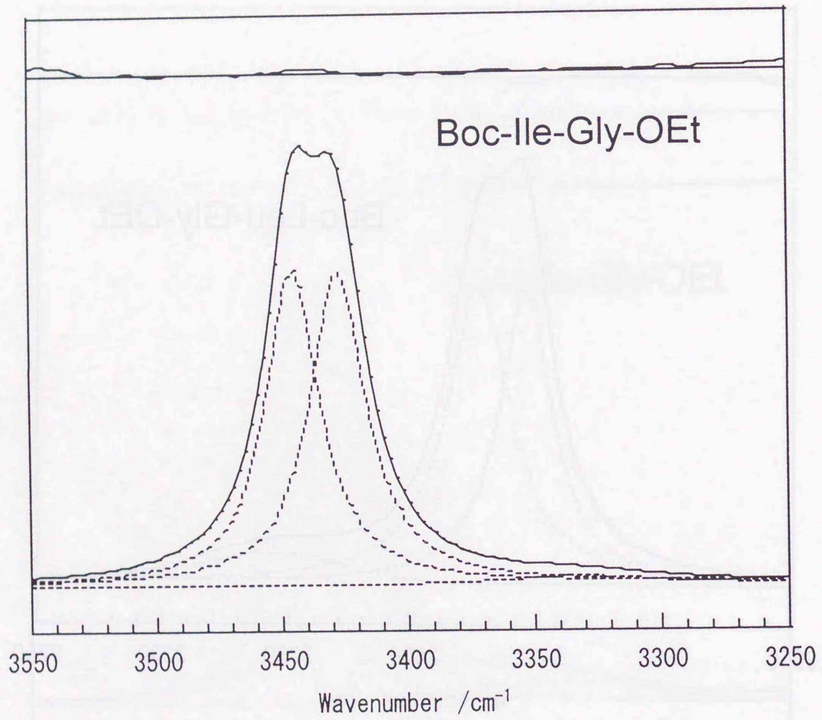

Figure 3.7. Infrared spectrum of 1.25 mM Boc-Ile-Gly-OEt in $CDCl_3$ at 25°C: Observed spectrum (solid line), calculated components (dotted line), and difference between the observed and calculated spectra (upper shifted solid line).

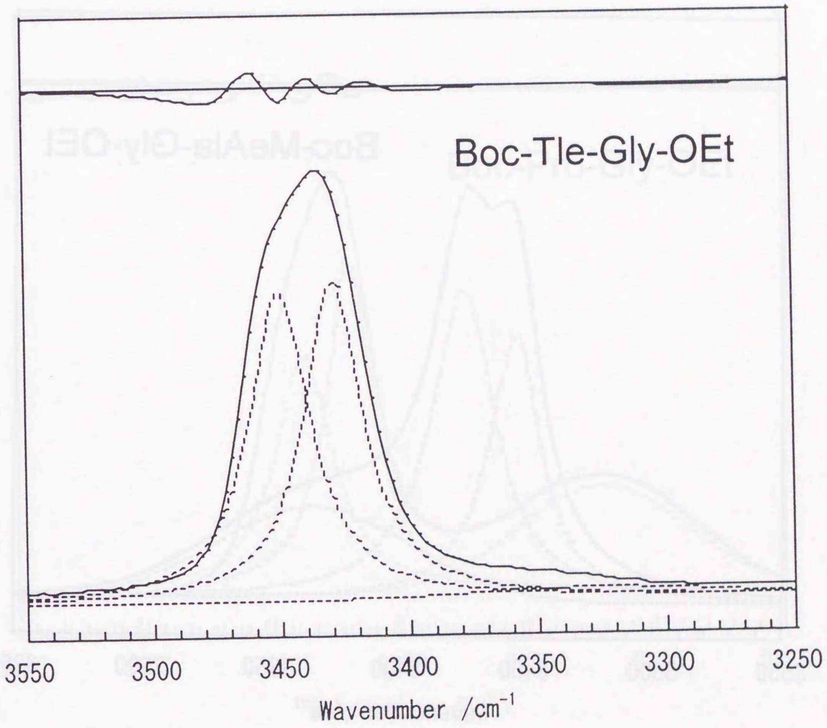

Figure 3.8. Infrared spectrum of 1.25 mM Boc-Tle-Gly-OEt in $CDCl_3$ at 25°C: Observed spectrum (solid line), calculated components (dotted line), and difference between the observed and calculated spectra (upper shifted solid line).

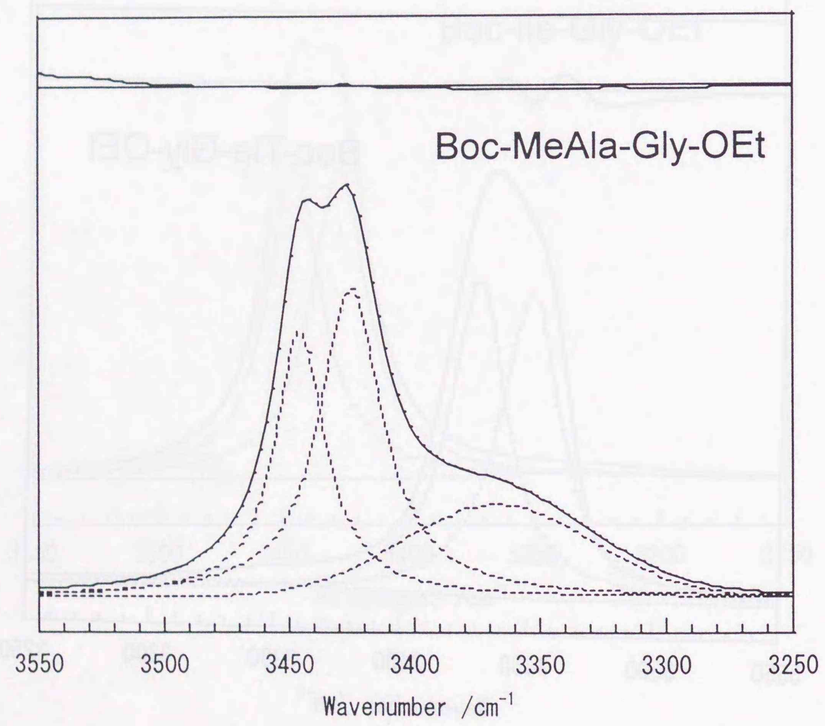

Figure 3.9. Infrared spectrum of 1.25 mM Boc-MeAla-Gly-OEt in $CDCl_3$ at 25˚C: Observed spectrum (solid line), calculated components (dotted line), and difference between the observed and calculated spectra (upper shifted solid line).

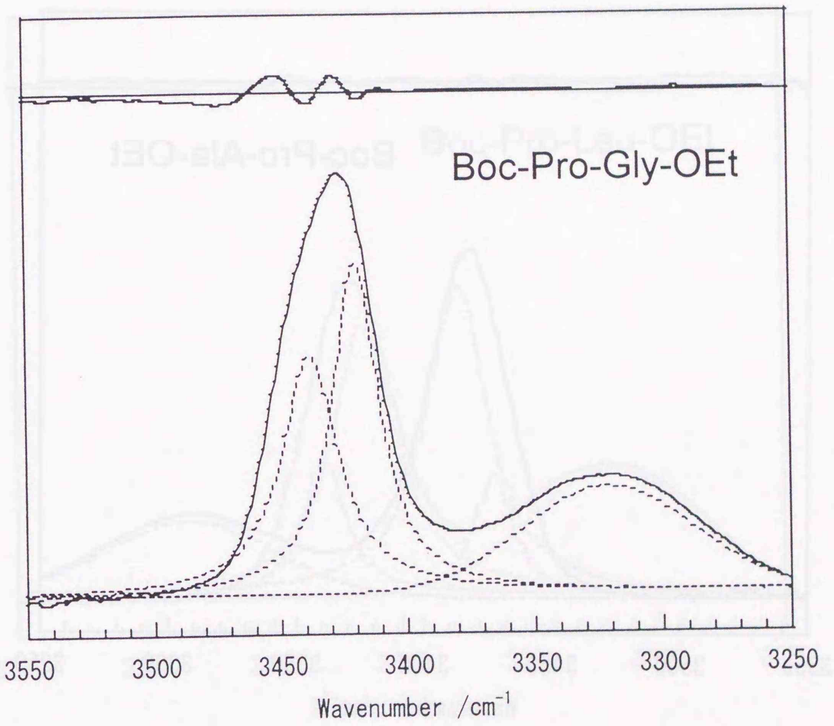

Figure 3.10. Infrared spectrum of 1.25 mM Boc-Pro-Gly-OEt in $CDCl_3$ at 25˚C: Observed spectrum (solid line), calculated components (dotted line), and difference between the observed and calculated spectra (upper shifted solid line).

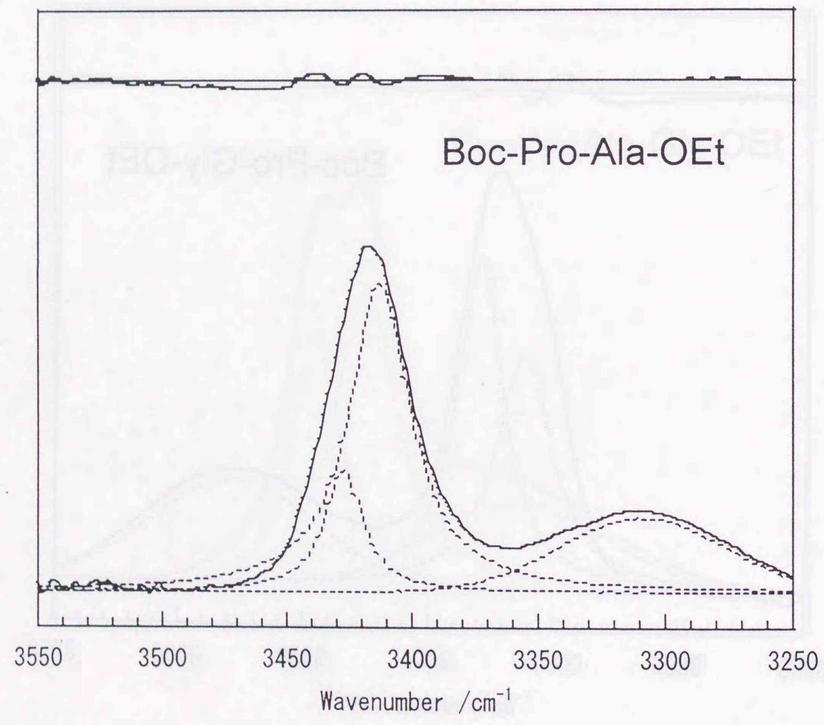

Figure 3.11. Infrared spectrum of 1.25 mM Boc-Pro-Ala-OEt in $CDCl_3$ at 25˚C: Observed spectrum (solid line), calculated components (dotted line), and difference between the observed and calculated spectra (upper shifted solid line).

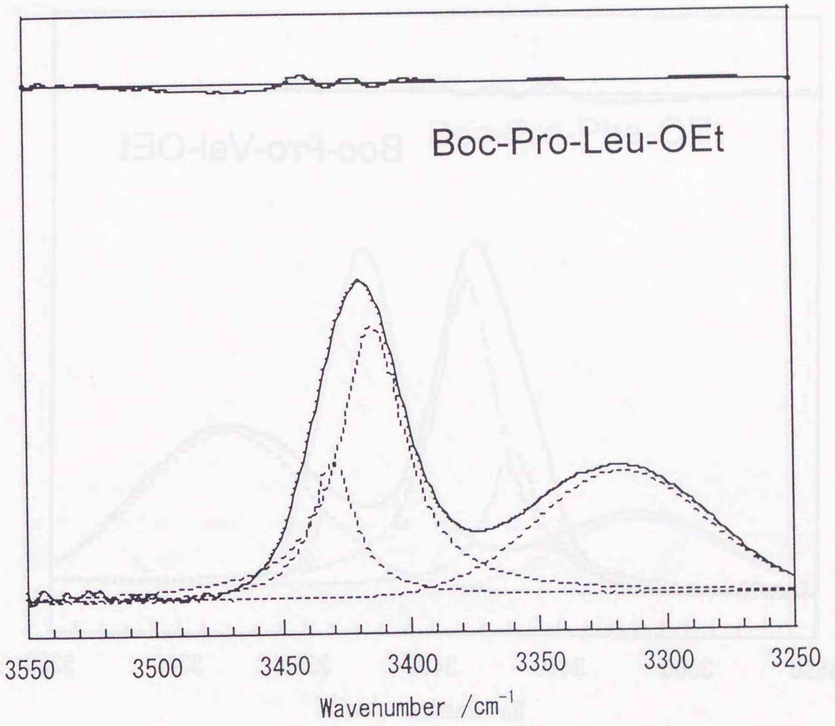

Figure 3.12. Infrared spectrum of 1.25 mM Boc-Pro-Leu-OEt in $CDCl_3$ at 25˚C: Observed spectrum (solid line), calculated components (dotted line), and difference between the observed and calculated spectra (upper shifted solid line).

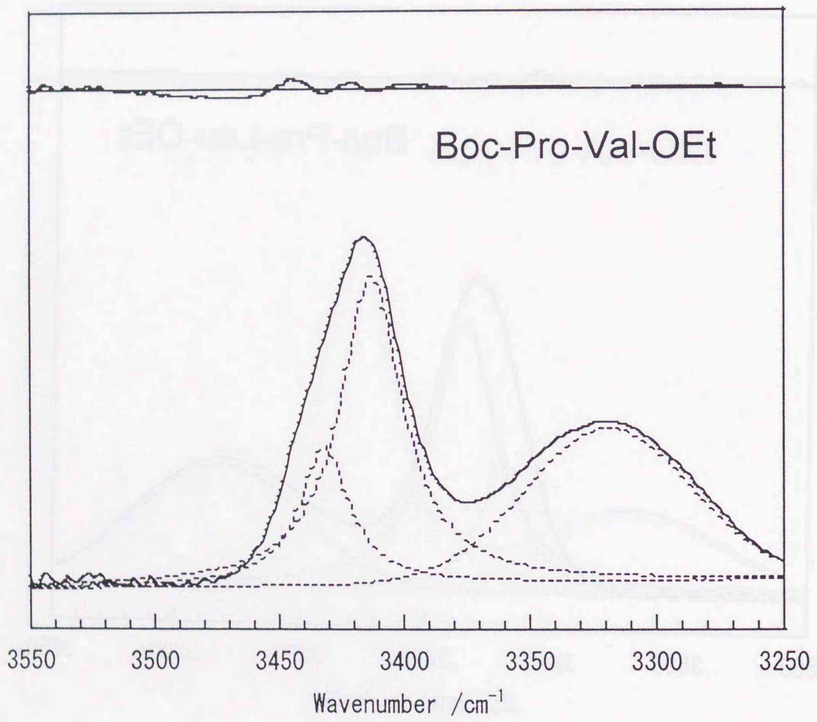

Figure 3.13. Infrared spectrum of 1.25 mM Boc-Pro-Val-OEt in $CDCl_3$ at 25˚C: Observed spectrum (solid line), calculated components (dotted line), and difference between the observed and calculated spectra (upper shifted solid line).

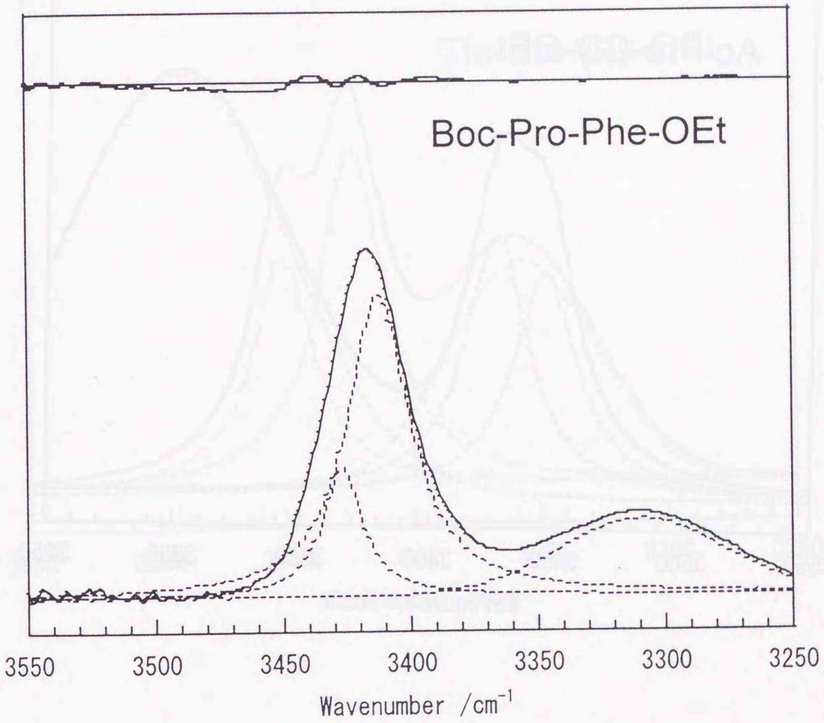

Figure 3.14. Infrared spectrum of 1.25 mM Boc-Pro-Phe-OEt in $CDCl_3$ at 25˚C: Observed spectrum (solid line), calculated components (dotted line), and difference between the observed and calculated spectra (upper shifted solid line).

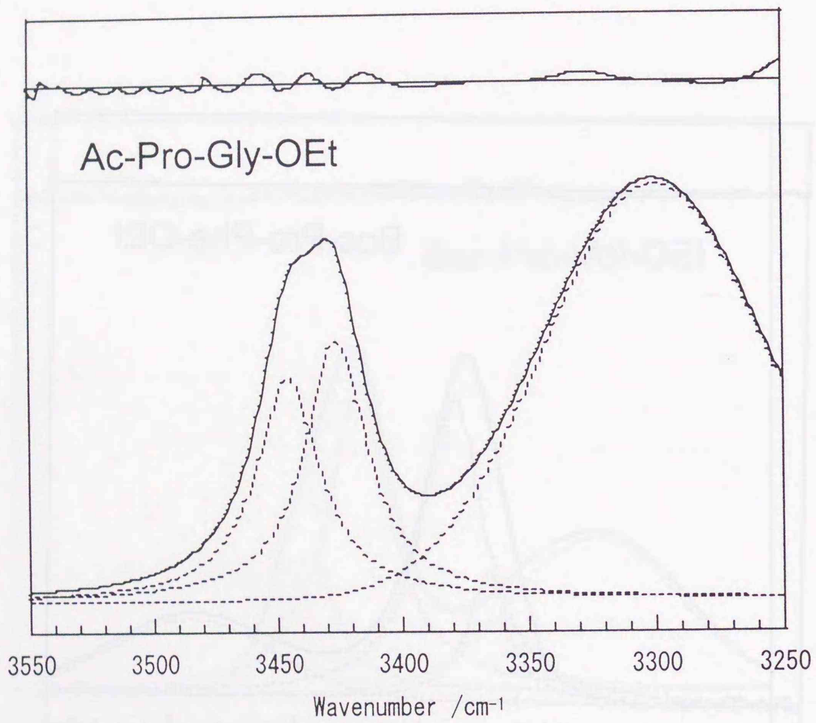

Figure 3.15. Infrared spectrum of 1.25 mM Ac-Pro-Gly-OEt in $CDCl_3$ at 25˚C: Observed spectrum (solid line), calculated components (dotted line), and difference between the observed and calculated spectra (upper shifted solid line).

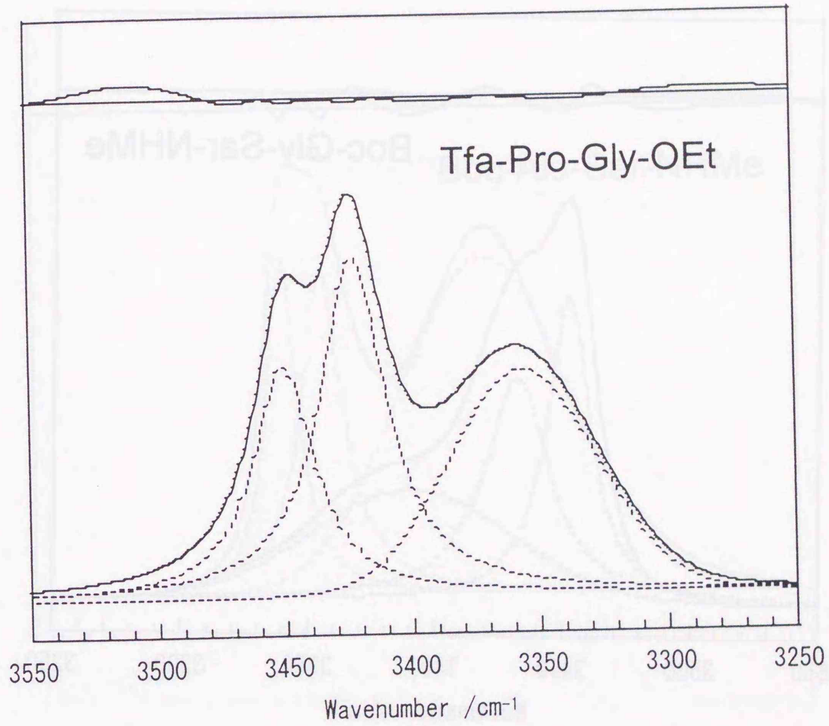

Figure 3.16. Infrared spectrum of 1.25 mM Tfa-Pro-Gly-OEt in $CDCl_3$ at 25˚C: Observed spectrum (solid line), calculated components (dotted line), and difference between the observed and calculated spectra (upper shifted solid line).

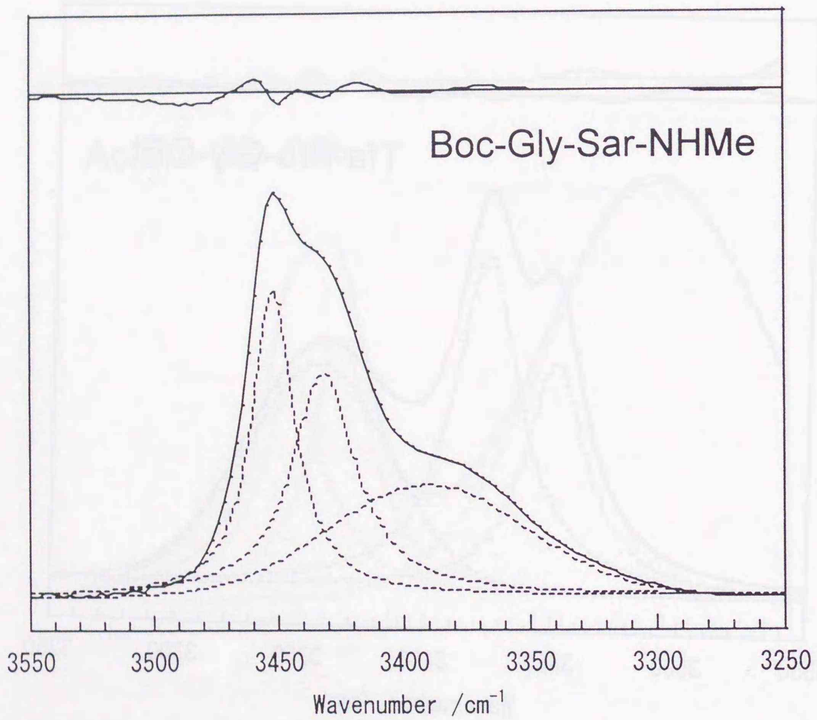

Figure 3.17. Infrared spectrum of 1.25 mM Boc-Gly-Sar-NHMe in $CDCl_3$ at 25˚C: Observed spectrum (solid line), calculated components (dotted line), and difference between the observed and calculated spectra (upper shifted solid line).

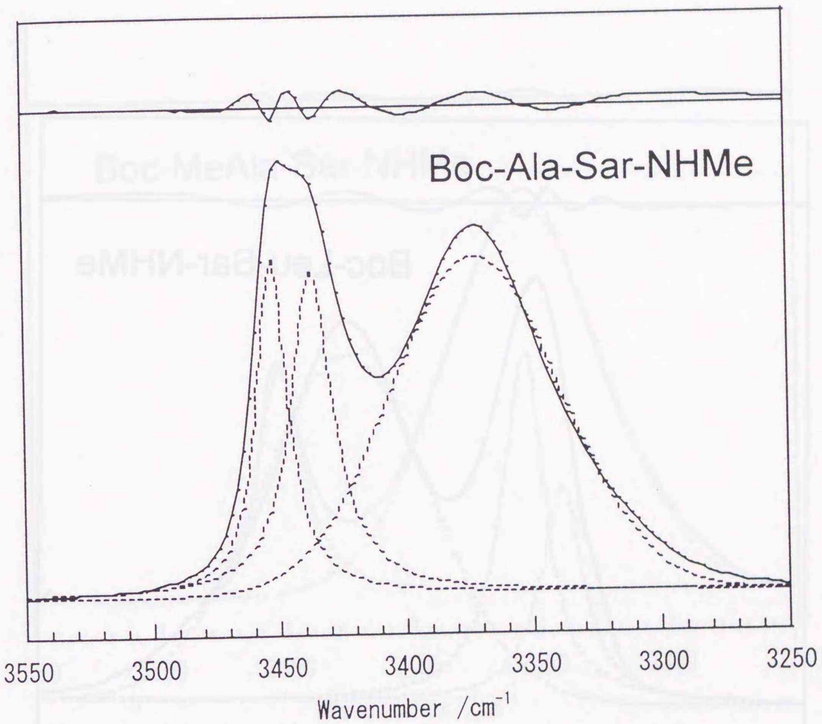

Figure 3.18. Infrared spectrum of 1.25 mM Boc-Ala-Sar-NHMe in $CDCl_3$ at 25˚C: Observed spectrum (solid line), calculated components (dotted line), and difference between the observed and calculated spectra (upper shifted solid line).

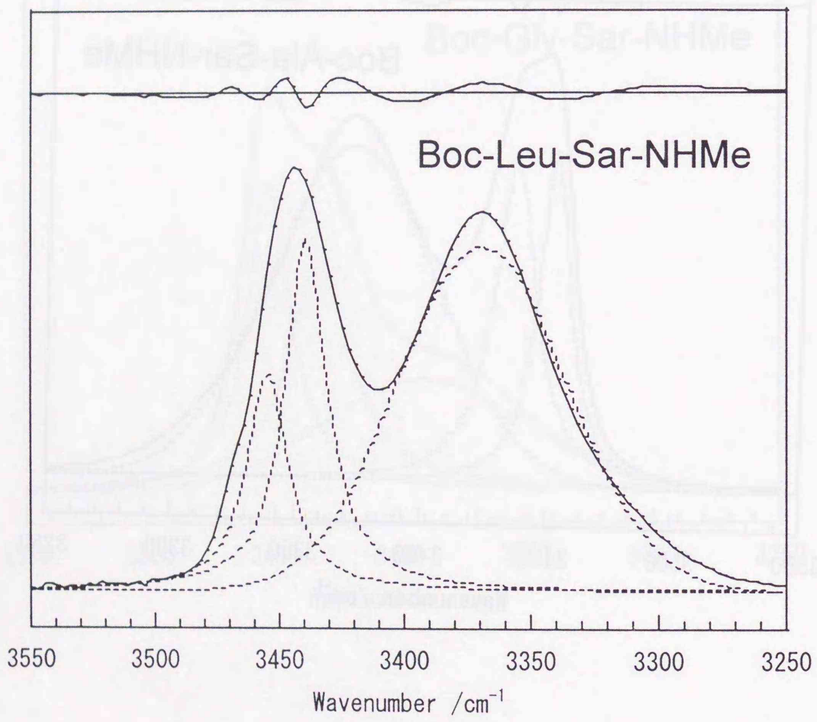

Figure 3.19. Infrared spectrum of 1.25 mM Boc-Leu-Sar-NHMe in $CDCl_3$ at 25˚C: Observed spectrum (solid line), calculated components (dotted line), and difference between the observed and calculated spectra (upper shifted solid line).

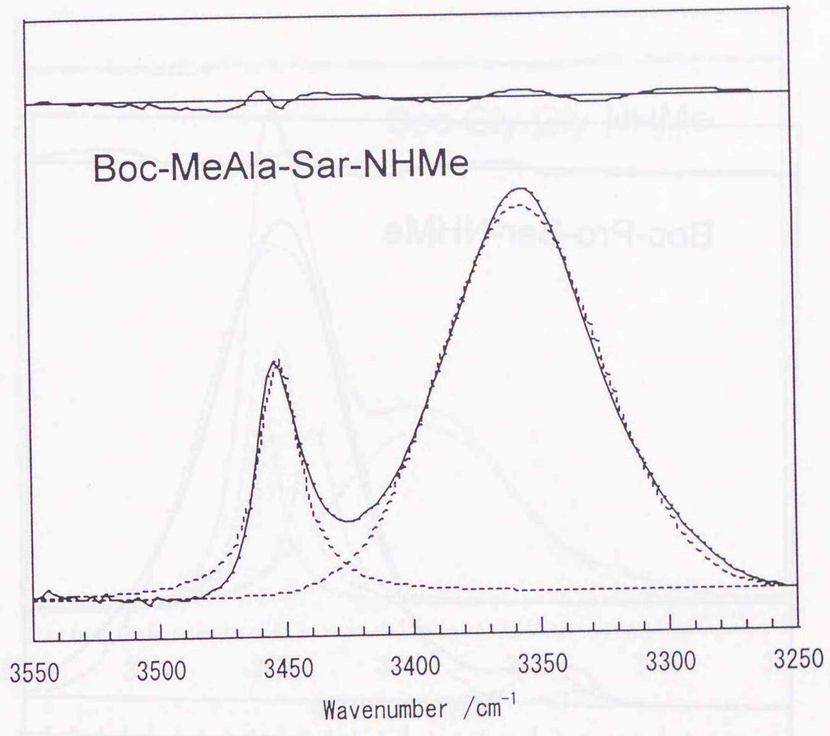

Figure 3.20. Infrared spectrum of 1.25 mM Boc-MeAla-Sar-NHMe in $CDCl_3$ at 25˚C: Observed spectrum (solid line), calculated components (dotted line), and difference between the observed and calculated spectra (upper shifted solid line).

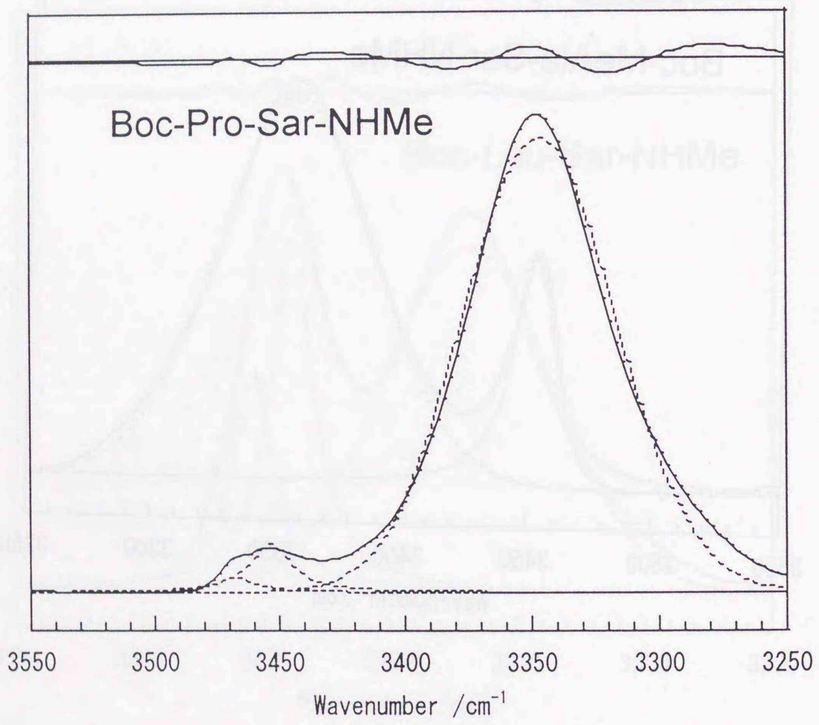

Figure 3.21. Infrared spectrum of 1.25 mM Boc-Pro-Sar-NHMe in $CDCl_3$ at 25˚C: Observed spectrum (solid line), calculated components (dotted line), and difference between the observed and calculated spectra (upper shifted solid line).

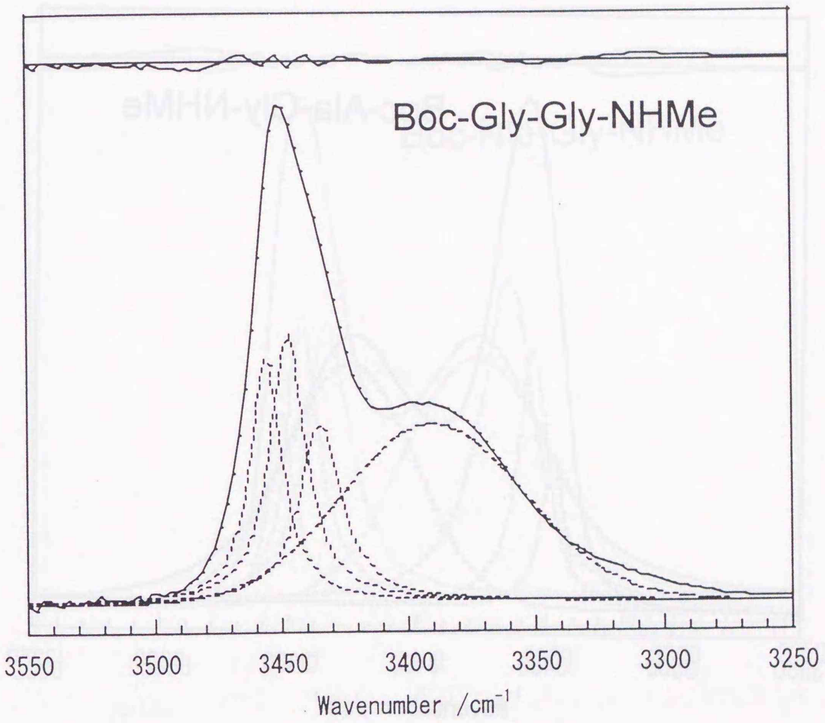

Figure 3.22. Infrared spectrum of 1.25 mM Boc-Gly-Gly-NHMe in $CDCl_3$ at 25˚C: Observed spectrum (solid line), calculated components (dotted line), and difference between the observed and calculated spectra (upper shifted solid line).

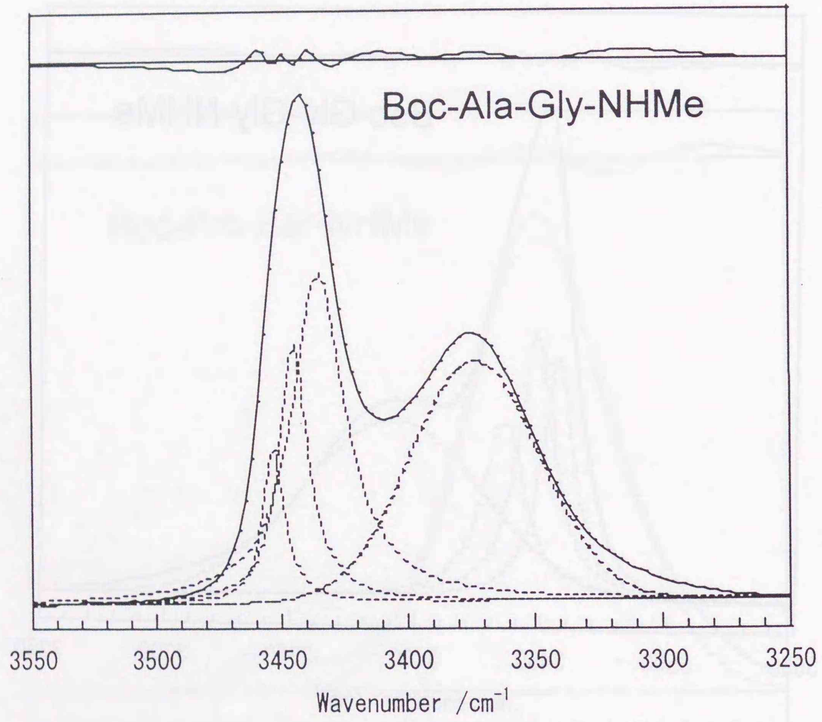

Figure 3.23. Infrared spectrum of 1.25 mM Boc-Ala-Gly-NHMe in $CDCl_3$ at 25˚C: Observed spectrum (solid line), calculated components (dotted line), and difference between the observed and calculated spectra (upper shifted solid line).

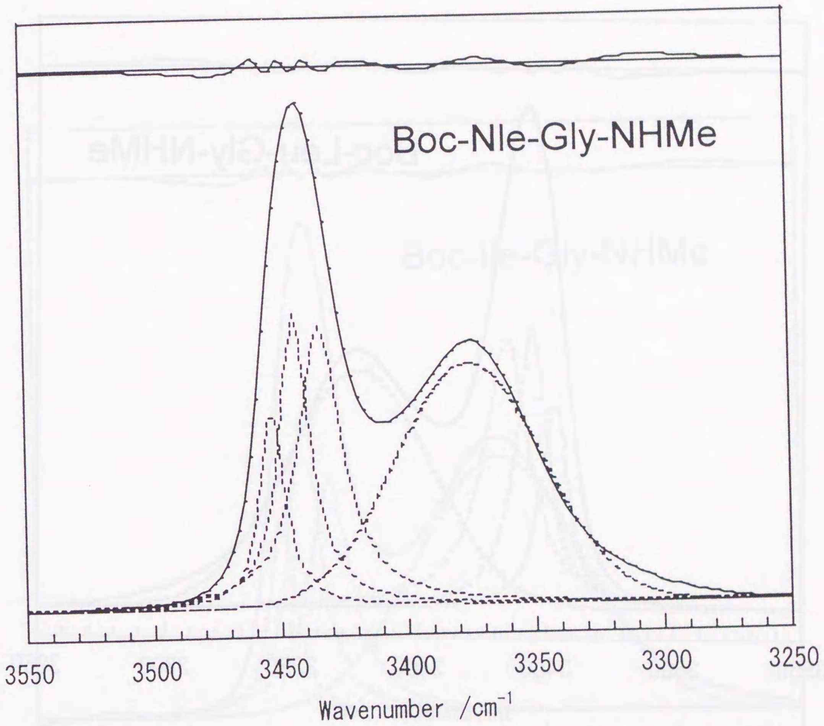

Figure 3.24. Infrared spectrum of 1.25 mM Boc-Nle-Gly-NHMe in $CDCl_3$ at 25˚C: Observed spectrum (solid line), calculated components (dotted line), and difference between the observed and calculated spectra (upper shifted solid line).

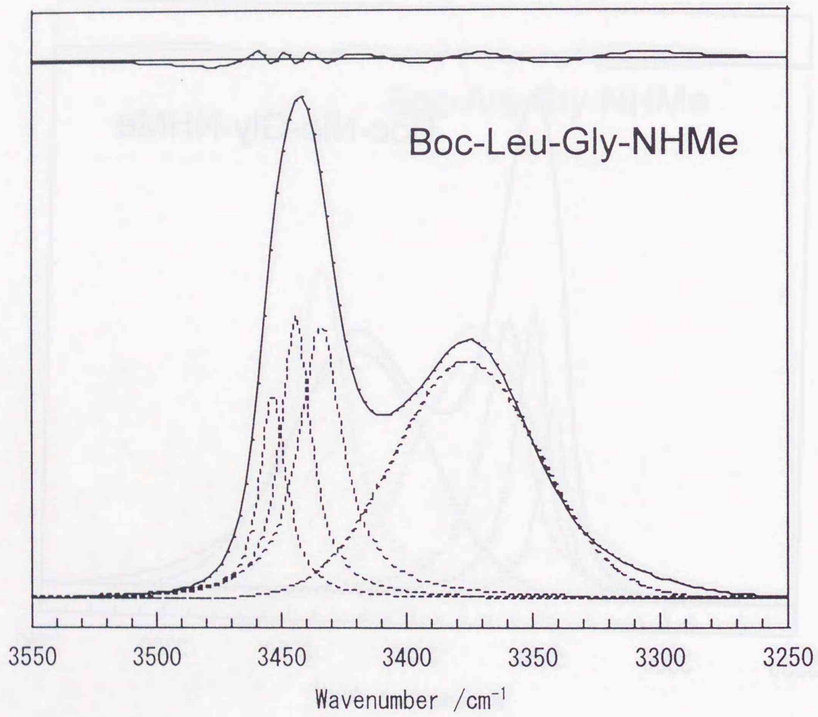

Figure 3.25. Infrared spectrum of 1.25 mM Boc-Leu-Gly-NHMe in $CDCl_3$ at 25˚C: Observed spectrum (solid line), calculated components (dotted line), and difference between the observed and calculated spectra (upper shifted solid line).

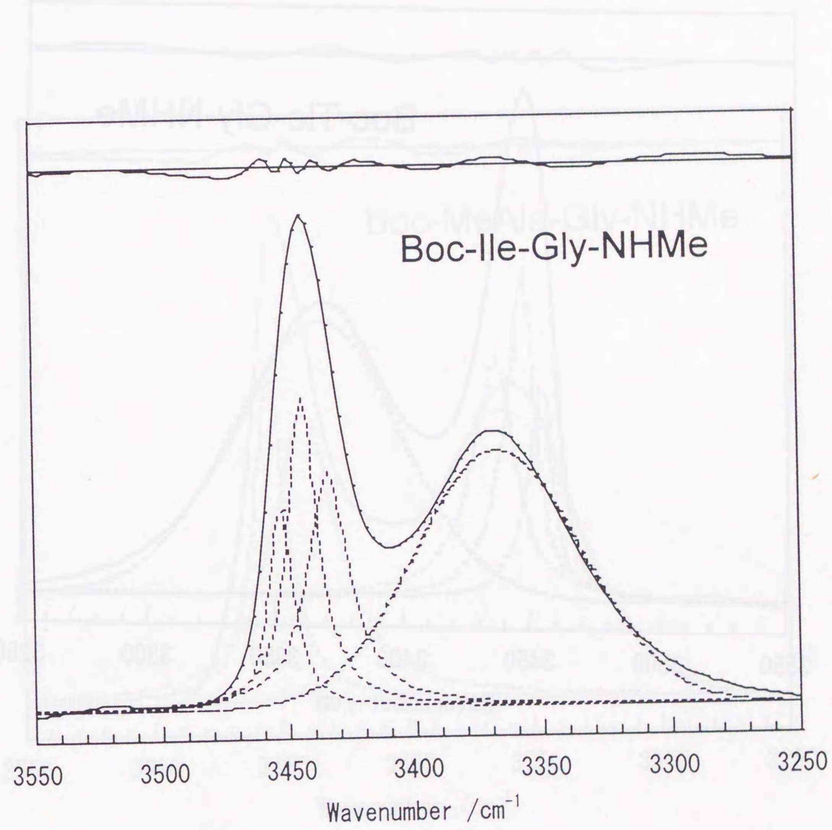

Figure 3.26. Infrared spectrum of 1.25 mM Boc-Ile-Gly-NHMe in $CDCl_3$ at 25˚C: Observed spectrum (solid line), calculated components (dotted line), and difference between the observed and calculated spectra (upper shifted solid line).

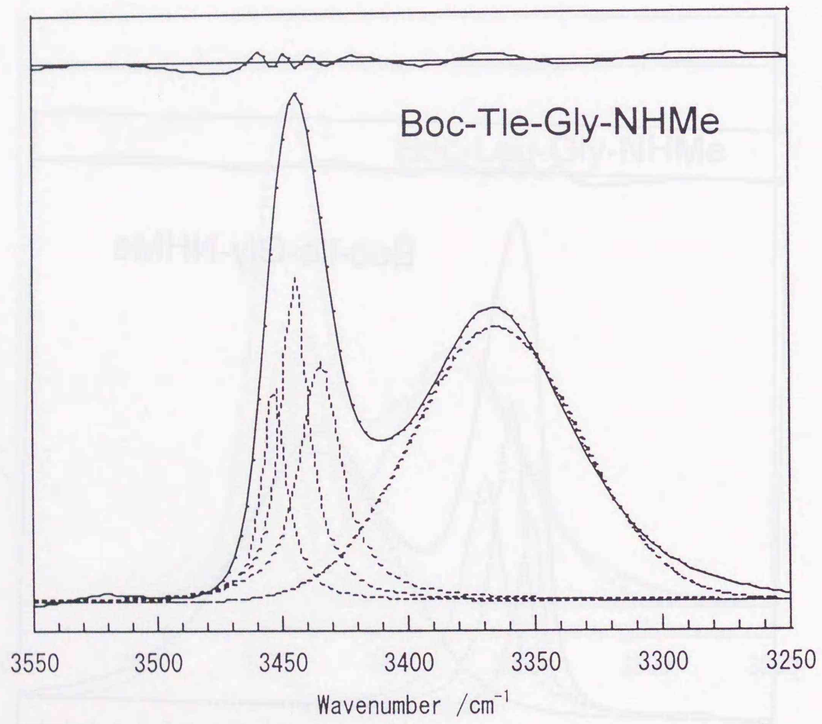

Figure 3.27. Infrared spectrum of 1.25 mM Boc-Tle-Gly-NHMe in $CDCl_3$ at 25°C: Observed spectrum (solid line), calculated components (dotted line), and difference between the observed and calculated spectra (upper shifted solid line).

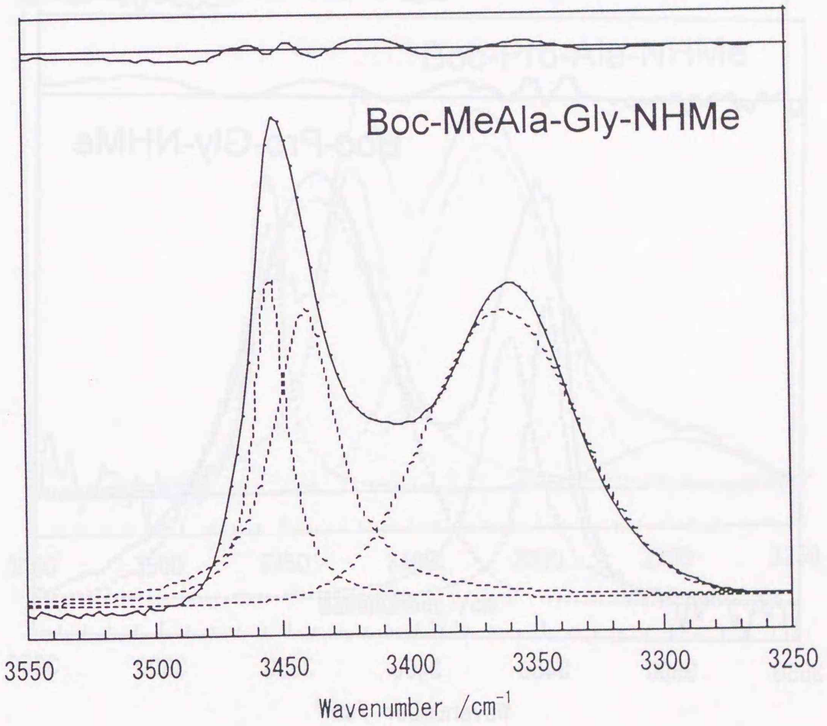

Figure 3.28. Infrared spectrum of 1.25 mM Boc-MeAla-Gly-NHMe in $CDCl_3$ at 25° C: Observed spectrum (solid line), calculated components (dotted line), and difference between the observed and calculated spectra (upper shifted solid line).

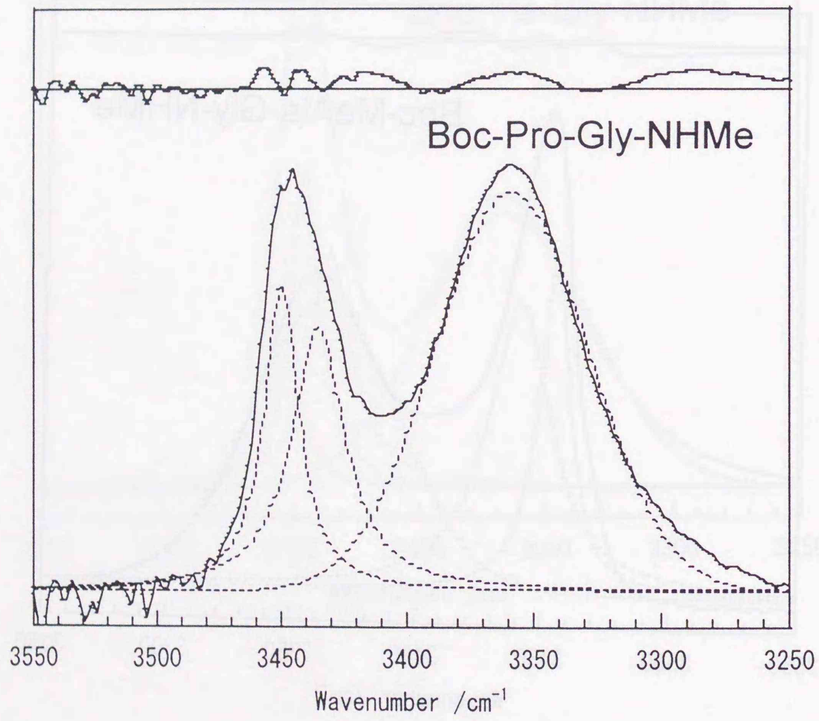

Figure 3.29. Infrared spectrum of 1.25 mM Boc-Pro-Gly-NHMe in $CDCl_3$ at 25˚C: Observed spectrum (solid line), calculated components (dotted line), and difference between the observed and calculated spectra (upper shifted solid line).

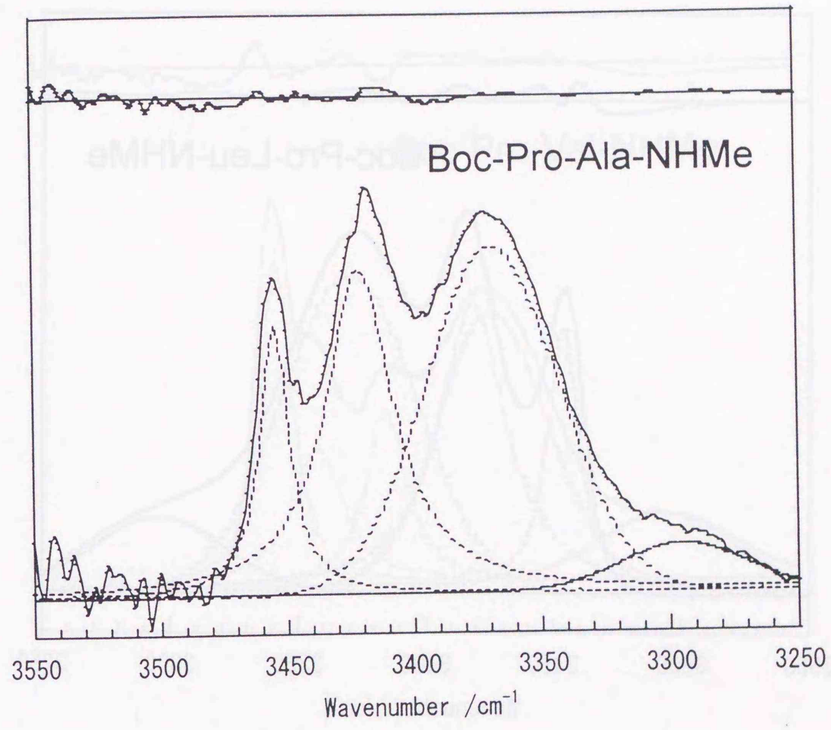

Figure 3.30. Infrared spectrum of 1.25 mM Boc-Pro-Ala-NHMe in $CDCl_3$ at 25˚C: Observed spectrum (solid line), calculated components (dotted line), and difference between the observed and calculated spectra (upper shifted solid line).

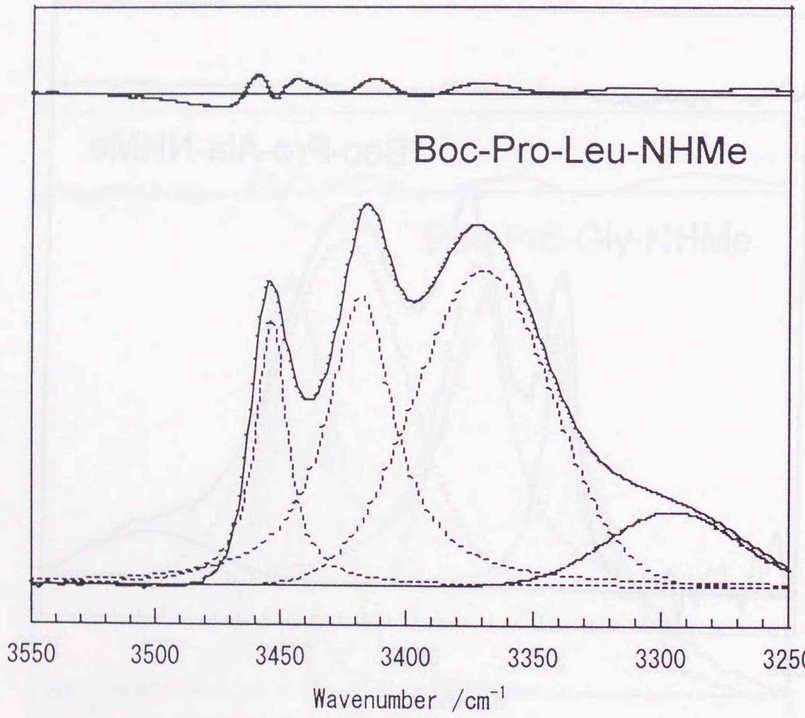

Figure 3.31. Infrared spectrum of 1.25 mM Boc-Pro-Leu-NHMe in $CDCl_3$ at 25˚C: Observed spectrum (solid line), calculated components (dotted line), and difference between the observed and calculated spectra (upper shifted solid line).

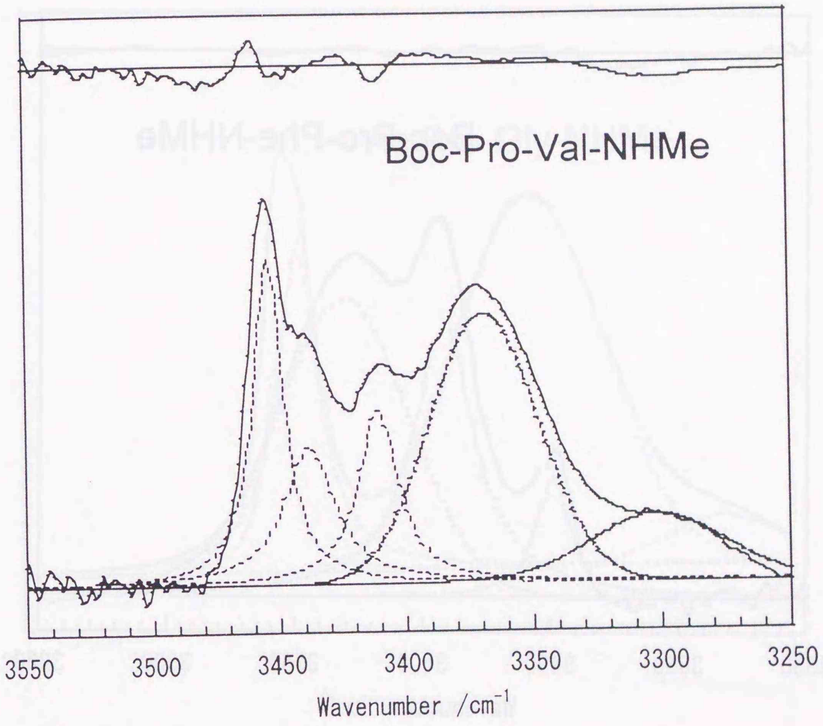

Figure 3.32. Infrared spectrum of 1.25 mM Boc-Pro-Val-NHMe in $CDCl_3$ at 25˚C: Observed spectrum (solid line), calculated components (dotted line), and difference between the observed and calculated spectra (upper shifted solid line).

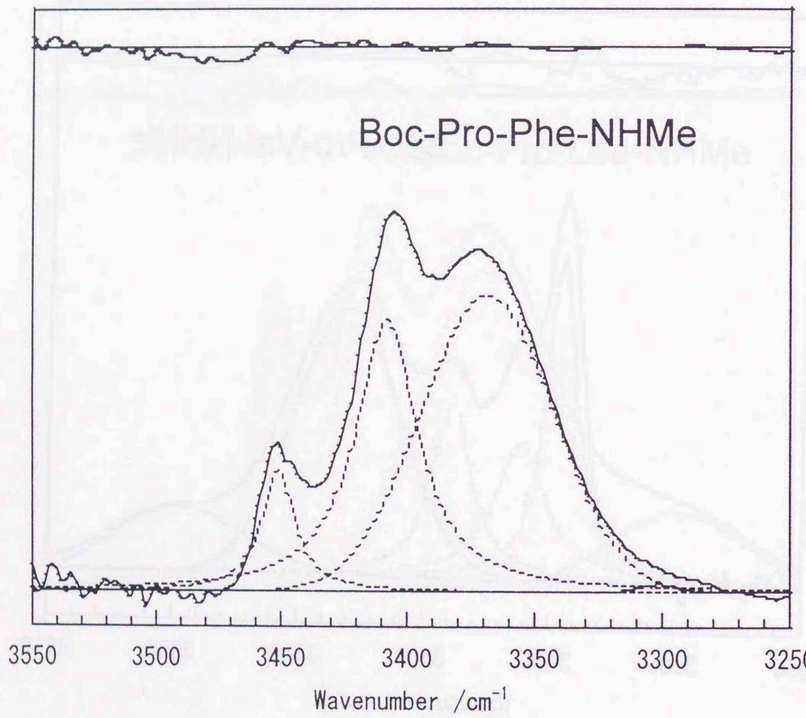

Figure 3.33. Infrared spectrum of 1.25 mM Boc-Pro-Phe-NHMe in $CDCl_3$ at 25˚C: Observed spectrum (solid line), calculated components (dotted line), and difference between the observed and calculated spectra (upper shifted solid line).

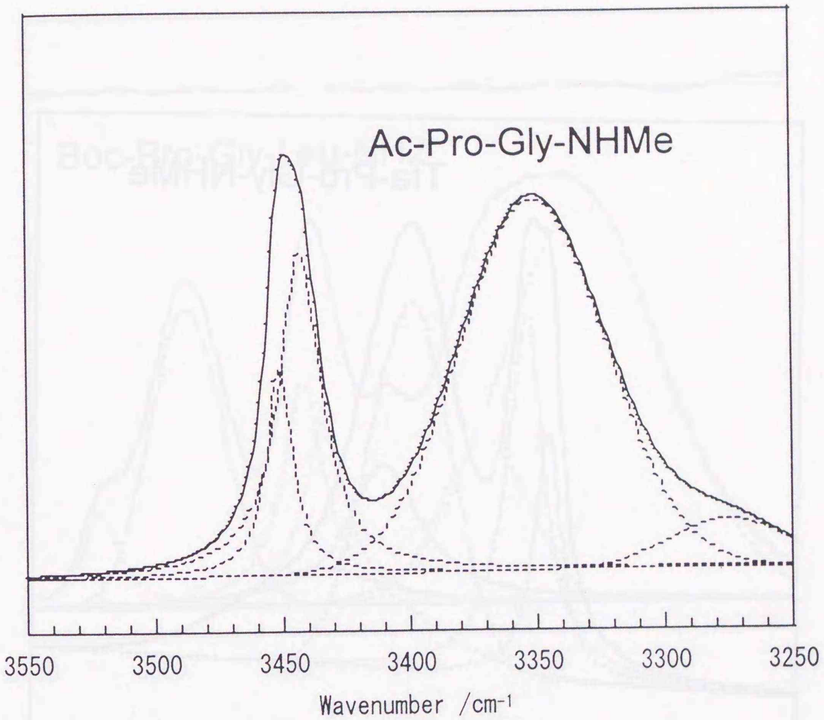

Figure 3.34. Infrared spectrum of 1.25 mM Ac-Pro-Gly-NHMe in $CDCl_3$ at 25˚C: Observed spectrum (solid line) and calculated components (dotted lone).

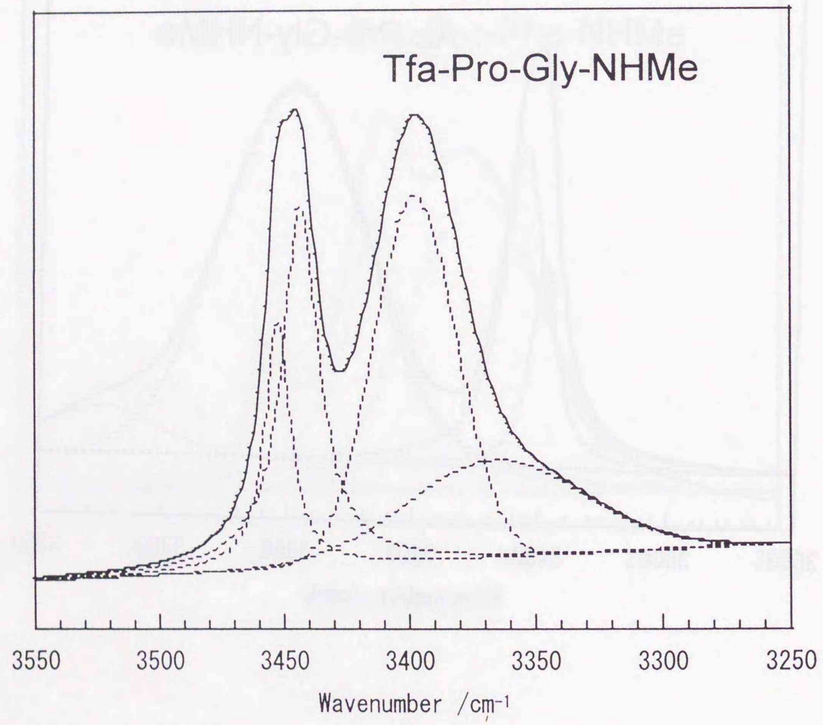

Figure 3.35. Infrared spectrum of 1.25 mM Tfa-Pro-Gly-NHMe in $CDCl_3$ at 25˚C: Observed spectrum (solid line) and calculated components (dotted lone).

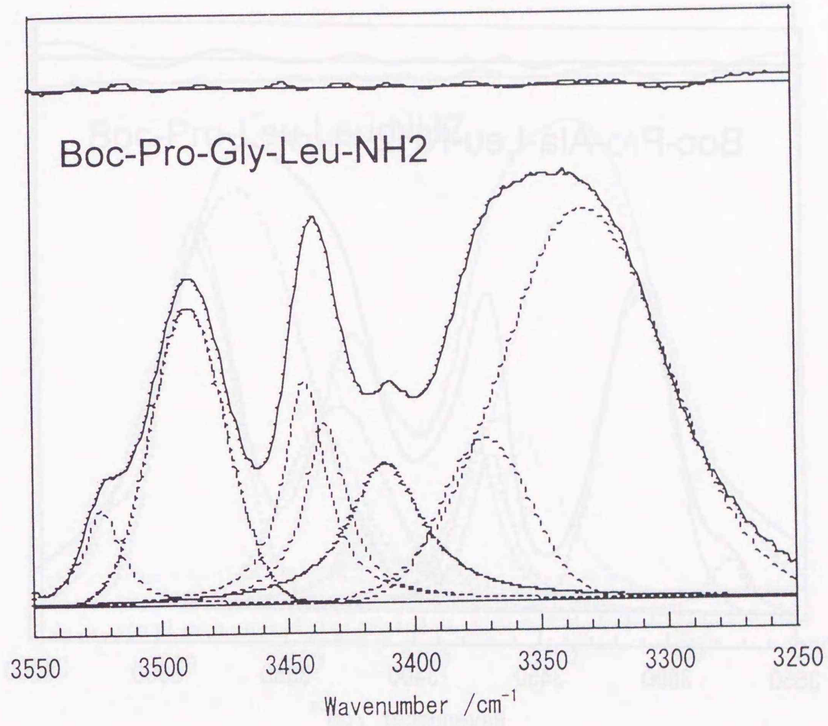

Figure 3.36. Infrared spectrum of 1.25 mM Boc-Pro-Gly-Leu-NH_2 in $CDCl_3$ at 25˚ C: Observed spectrum (solid line), calculated components (dotted line), and difference between the observed and calculated spectra (upper shifted solid line).

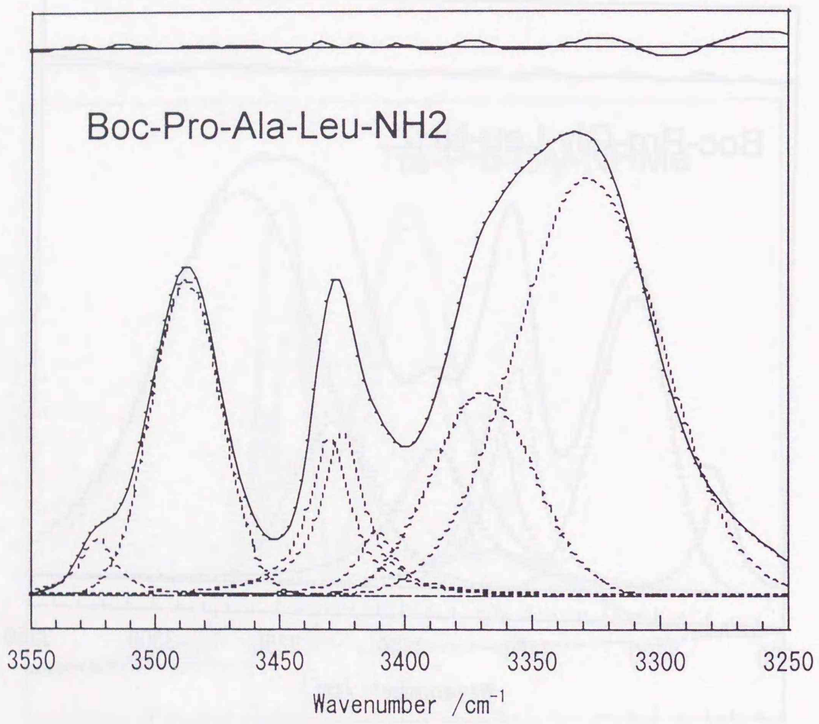

Figure 3.37. Infrared spectrum of 1.25 mM Boc-Pro-Ala-Leu-NH_2 in $CDCl_3$ at 25° C: Observed spectrum (solid line), calculated components (dotted line), and difference between the observed and calculated spectra (upper shifted solid line).

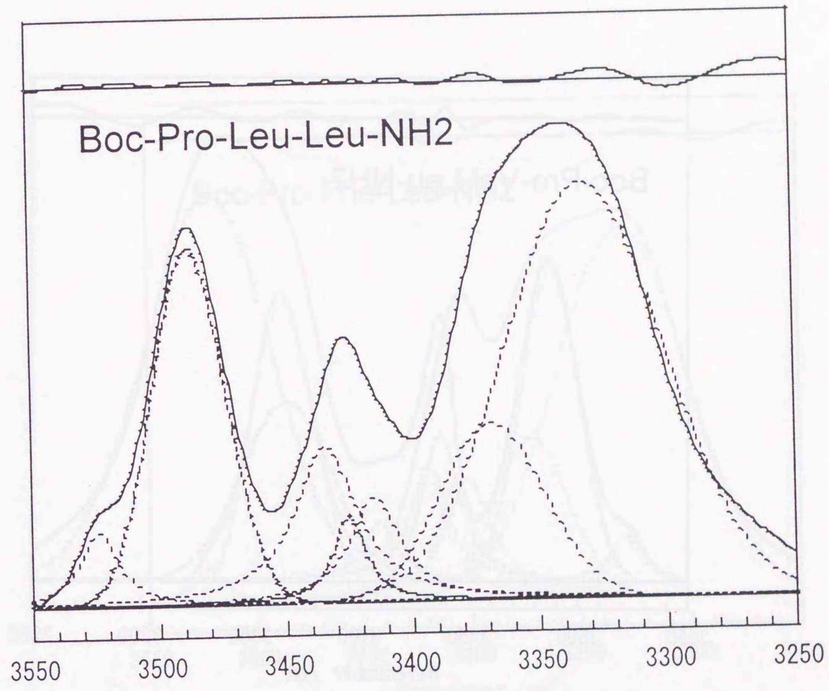

Figure 3.38. Infrared spectrum of 1.25 mM Boc-Pro-Leu-Leu-NH_2 in $CDCl_3$ at 25° C: Observed spectrum (solid line), calculated components (dotted line), and difference between the observed and calculated spectra (upper shifted solid line).

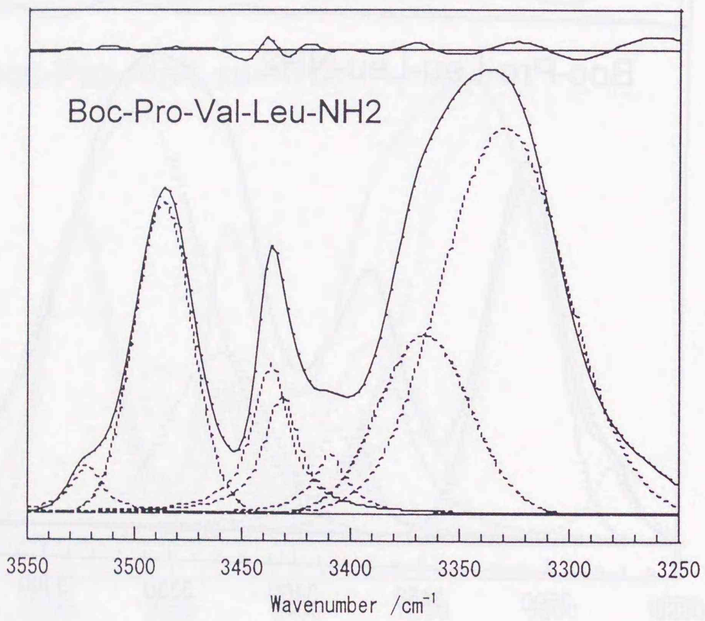

Figure 3.39. Infrared spectrum of 1.25 mM Boc-Pro-Val-Leu-NH_2 in $CDCl_3$ at 25° C: Observed spectrum (solid line), calculated components (dotted line), and difference between the observed and calculated spectra (upper shifted solid line).

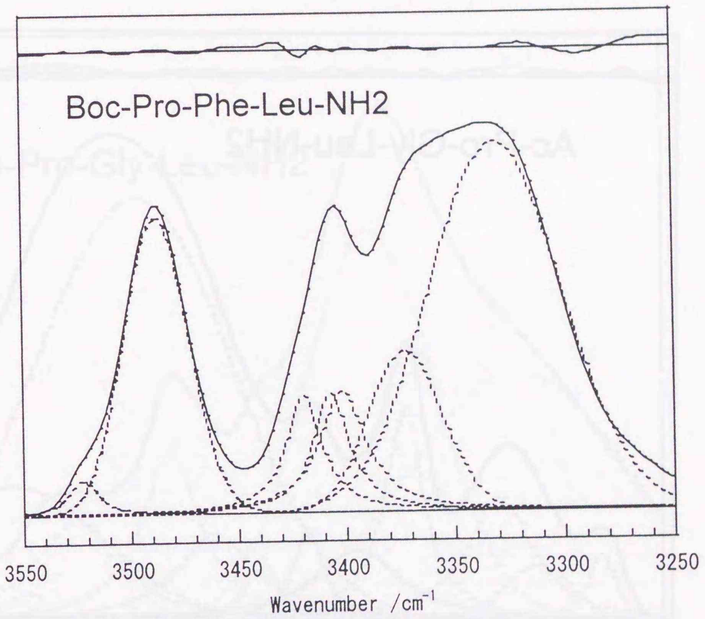

Figure 3.40. Infrared spectrum of 1.25 mM Boc-Pro-Phe-Leu-NH_2 in $CDCl_3$ at 25° C: Observed spectrum (solid line), calculated components (dotted line), and difference between the observed and calculated spectra (upper shifted solid line).

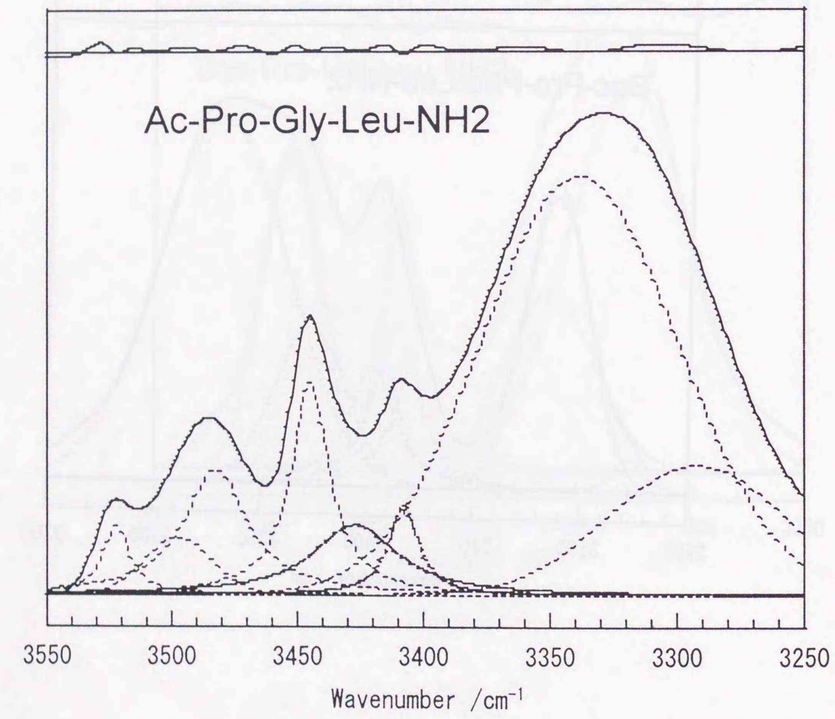

Figure 3.41. Infrared spectrum of 1.25 mM Ac-Pro-Gly-Leu-NH_2 in $CDCl_3$ at 25˚C: Observed spectrum (solid line), calculated components (dotted line), and difference between the observed and calculated spectra (upper shifted solid line).

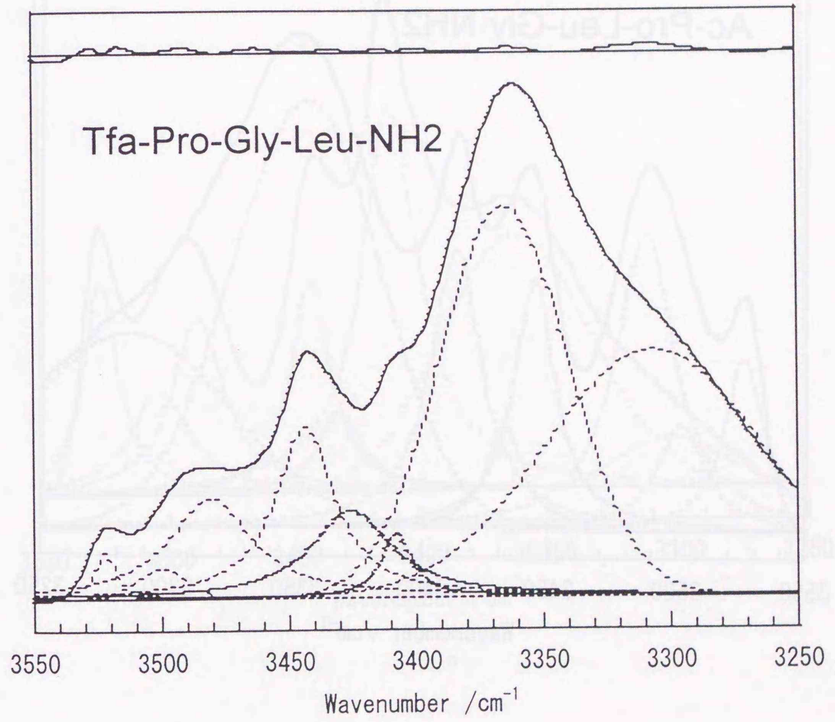

Figure 3.42. Infrared spectrum of 1.25 mM Tfa-Pro-Gly-Leu-NH_2 in $CDCl_3$ at 25˚C: Observed spectrum (solid line), calculated components (dotted line), and difference between the observed and calculated spectra (upper shifted solid line).

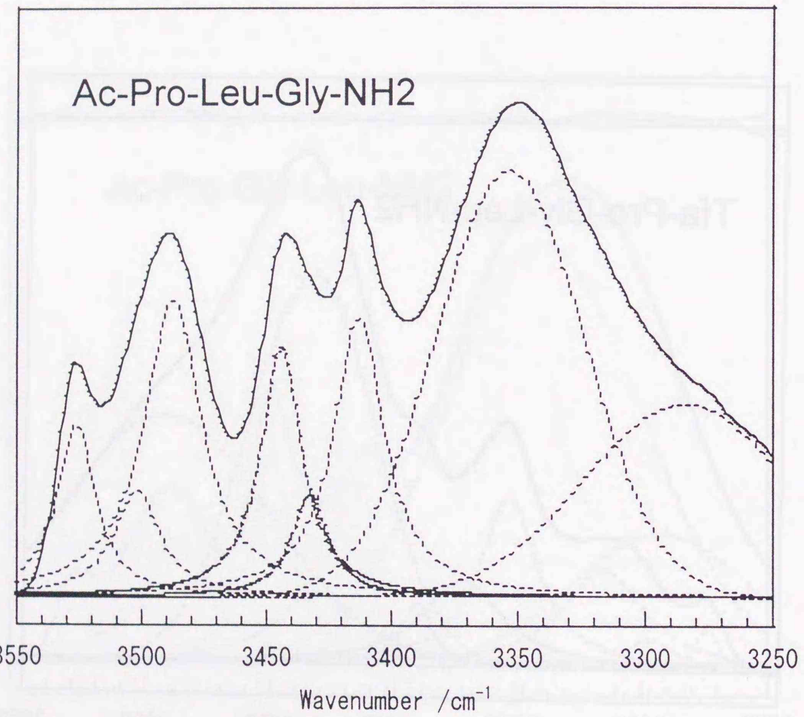

Figure 3.43. Infrared spectrum of 1.25 mM Ac-Pro-Leu-Gly-NH_2 in $CDCl_3$ at 25˚C: Observed spectrum (solid line), and calculated components (dotted line).

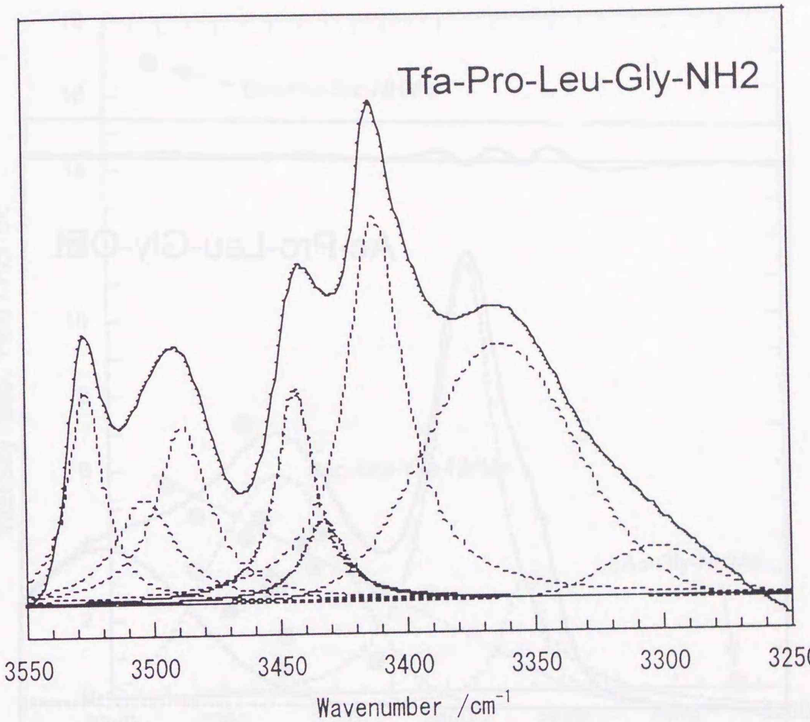

Figure 3.44. Infrared spectrum of 1.25 mM Tfa-Pro-Leu-Gly-NH_2 in $CDCl_3$ at 25˚C: Observed spectrum (solid line), and calculated components (dotted line).

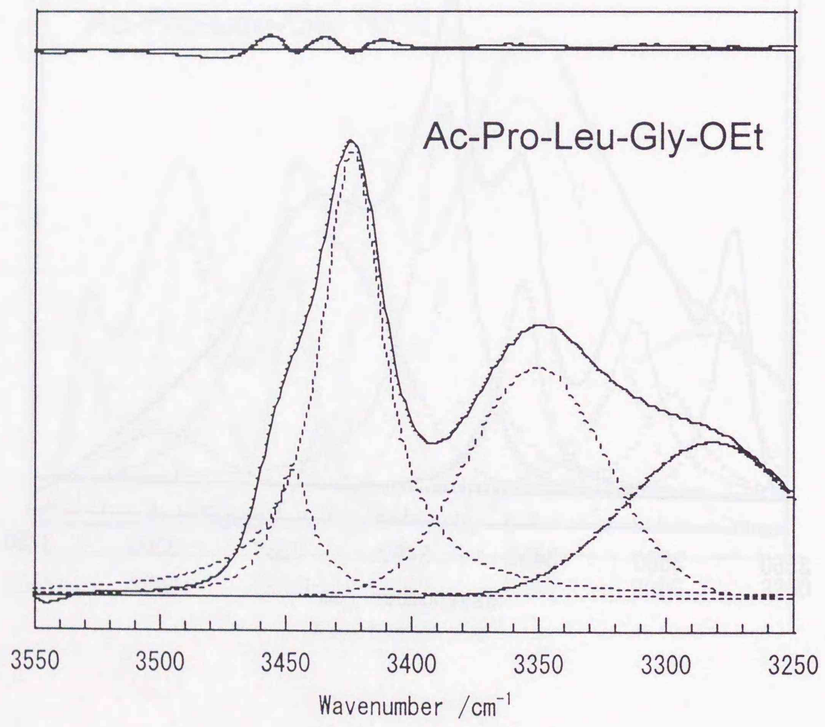

Figure 3.45. Infrared spectrum of 1.25 mM Ac-Pro-Leu-Gly-OEt in $CDCl_3$ at 25˚C: Observed spectrum (solid line), calculated components (dotted line), and difference between the observed and calculated spectra (upper shifted solid line).

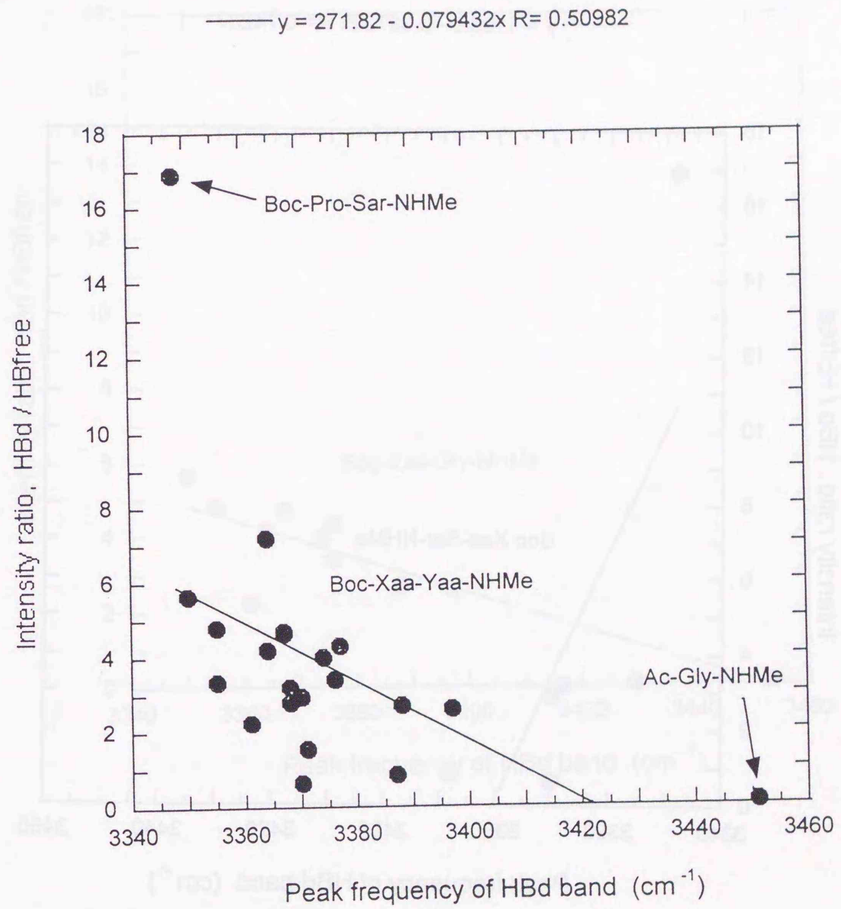

Figure 3.46. Relationships between peak frequencies of the HBd bands and intensity ratios of the HBd to the HBfree bands assigned to the NH stretchings of the C-terminal $NHCH_3$ groups. Data for all the Boc-Xaa-Yaa-NHMe sequences and Ac-Yaa-NHMe.

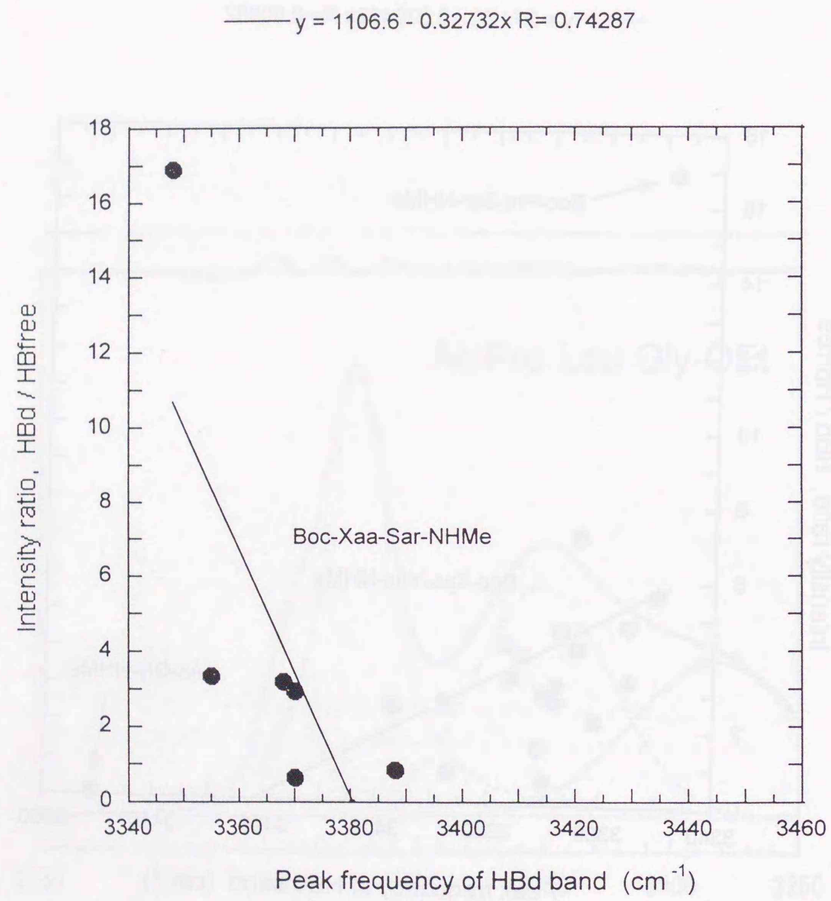

Figure 3.47. Relationships between peak frequencies of the HBd bands and intensity ratios of the HBd to the HBfree bands assigned to the NH stretchings of the C-terminal $NHCH_3$ groups for Boc-Xaa-Sar-NHMe.

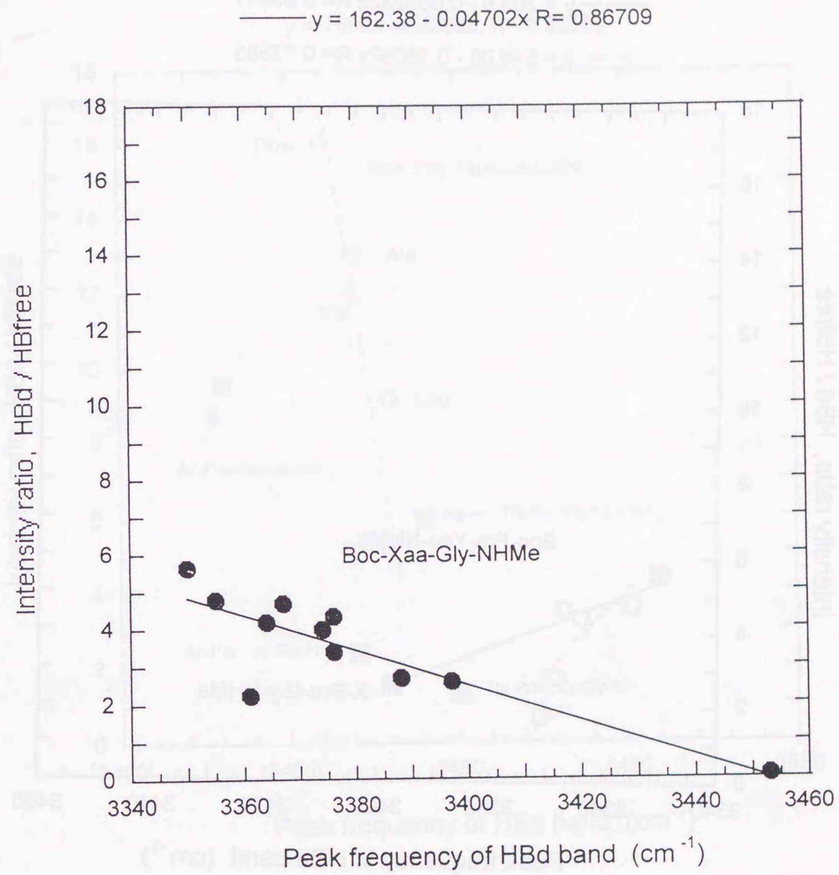

Figure 3.48. Relationships between peak frequencies of the HBd bands and intensity ratios of the HBd to the HBfree bands assigned to the NH stretchings of the C-terminal $NHCH_3$ groups for Boc-Xaa-Gly-NHMe.

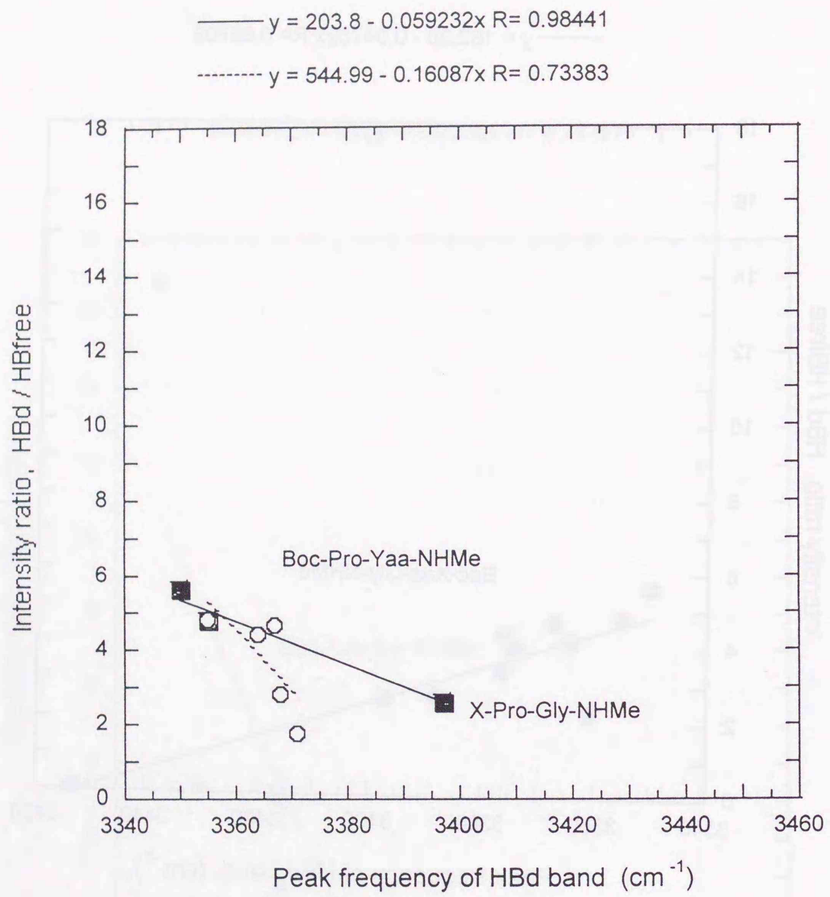

Figure 3.49. Relationships between peak frequencies of the HBd bands and intensity ratios of the HBd to the HBfree bands assigned to the NH stretchings of the C-terminal $NHCH_3$ groups for Boc-Pro-Yaa-NHMe and X-Pro-Gly-NHMe (X = Ac, Boc, Tfa).

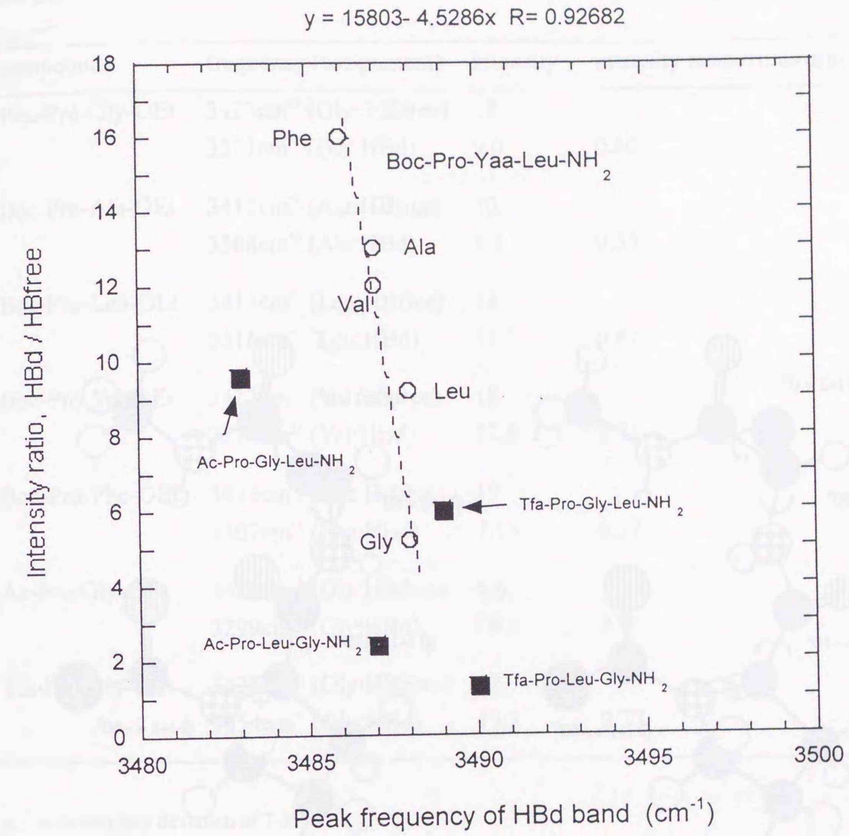

Figure 3.50. Relationships between peak frequencies of the HBd bands and intensity ratios of the HBd to the HBfree bands assigned to one of the NH stretchings of the NH_2 groups. Data for all the Boc-Pro-Yaa-Leu-NH_2 and X-Pro-Yaa-Zaa-NH_2 (X = Ac, Boc, Tfa) sequences.

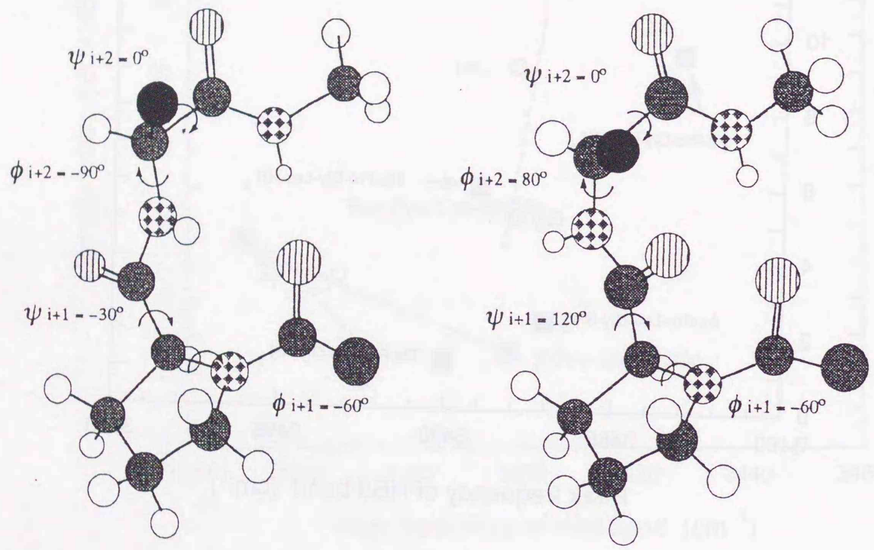

typeI β-turn typeII β-turn

Figure 3.51. Backbone structures for the type-I and type-II β-turn structures of Ac-Pro-Yaa-NHMe. Dihedral angles of the (i + 1)-th and (i + 2)-th residues are indicated.

Table 1. Frequencies and intensities of NH stretching bands which are related with formation of the 7-membered HBd structure, obtained by curve fitting for IR spectra of the peptides in 1.25 mM $CDCl_3$ solution at 25˚C.

compounds	frequency (assignment)	intensity	intensity ratio (HBd/HBfree)[a]
Boc-Pro-Gly-OEt	3423cm^{-1} (Gly: HBfree)	18	
	3321cm^{-1} (Gly:HBd)	9.0	0.50
Boc-Pro-Ala-OEt	3412cm^{-1} (Ala:HBfree)	20	
	3308cm^{-1} (Ala:HBd)	7.1	0.35
Boc-Pro-Leu-OEt	3413cm^{-1} (Leu:HBfree)	18	
	3316cm^{-1} (Leu:HBd)	11.3	0.62
Boc-Pro-Val-OEt	3413cm^{-1} (Val:HBfree)	18	
	3317cm^{-1} (Val:HBd)	12.8	0.71
Boc-Pro-Phe-OEt	3413cm^{-1} (Phe:HBfree)	19	
	3307cm^{-1} (Phe:HBd)	7.14	0.37
Ac-Pro-Gly-OEt	3426cm^{-1} (Gly:HBfree)	6.6	
	3299cm^{-1} (Gly:HBd)	19.0	2.9
Tfa-Pro-Gly-OEt	3423cm^{-1} (Gly:HBFree)	12	
	3354cm^{-1} (Gly:HBd)	15.2	0.77

a. with standard deviation of 7-9%

Table 2. Frequencies and intensities of NH stretching bands which are related with formation of the 10-membered HBd structure, obtained by curve fitting for IR spectra of the peptides in 1.25 mM $CDCl_3$ solution at 25˚C.

compounds	frequency (assignment)	intensity	intensity ratio (HBd/HBfree)[a]
Ac-Sar-NHMe	3452cm^{-1}(NHMe: HBfree)	11	
	3370cm^{-1}(NHMe: HBd)	7.0	0.65
Boc-Gly-Sar-NHMe	3453cm^{-1}(NHMe: HBfree)	14	
	3387cm^{-1}(NHMe: 10-m.HBd)	12.3	0.87
Boc-Ala-Sar-NHMe	3453cm^{-1}(NHMe: HBfree)	9.7	
	3370cm^{-1}(NHMe: 10.mHBd)	28.4	2.9
Boc-Leu-Sar-NHMe	3452cm^{-1}(NHMe: HBfree)	9.1	
	3368cm^{-1}(NHMe: 10-m.HBd)	29.1	3.4
Boc-MeAla-Sar-NHMe	3451cm^{-1}(NHMe: HBfree)	9.2	
	3355cm^{-1}(NHMe: 10-m.HBd)	30.6	3.3
Boc-Pro-Sar-NHMe	3451cm^{-1}(NHMe: HBfree)	2.2	
	3348cm^{-1}(NHMe: 10-m.HBd)	36.6	17

a. with standard deviation of 4-11%

Table 3. Frequencies and intensities of NH stretching bands which are related with formation of the 10-membered HBd structure, obtained by curve fitting for IR spectra of the peptides in 1.25 mM $CDCl_3$ solution at 25˚C.

compounds	frequency (assignment)	intensity	intensity ratio (HBd/HBfree)[a]
Boc-Gly-Gly-NHMe	3456cm^{-1}(NHMe: HBfree)	8.1	
	3388cm^{-1}(NHMe: 10-m.HBd)	21.8	2.7
Boc-Ala-Gly-NHMe	3453cm^{-1}(NHMe: HBfree)	5.0	
	3376cm^{-1}(NHMe: 10-m.HBd)	21.4	4.4
Boc-Nle-Gly-NHMe	3453cm^{-1}(NHMe: HBfree)	6.0	
	3374cm^{-1}(NHMe: 10-m.HBd)	23.8	4.0
Boc-Leu-Gly-NHMe	3453cm^{-1}(NHMe: HBfree)	6.9	
	3376cm^{-1}(NHMe: 10-m.HBd)	23.3	3.4
Boc-Ile-Gly-NHMe	3454cm^{-1}(NHMe: HBfree)	6.1	
	3367cm^{-1}(NHMe: 10-m.HBd)	28.7	4.7
Boc-Tle-Gly-NHMe	3453cm^{-1}(NHMe: HBfree)	6.2	
	3364cm^{-1}(NHMe: 10-m.HBd)	26.2	4.2
Boc-MeAla-Gly-NHMe	3453cm^{-1}(NHMe: HBfree)	12	
	3361cm^{-1}(NHMe: 10-m.HBd)	26.1	2.3
Boc-Pro-Gly-NHMe	3451cm^{-1}(NHMe: HBfree)	6.2	
	3355cm^{-1}(NHMe: 10-m.HBd)	29.5	4.8

a. with standard deviation of 6-15%

Table 4. Frequencies and intensities of NH stretching bands which are related with formation of the 7-membered or the 10-membered HBd structures, obtained by curve fitting for IR spectra of the peptides in 1.25 mM $CDCl_3$ solution at 25°C.

compounds	frequency (assignment)	intensity	intensity ratio (HBd/HBfree)[a]
Boc-Pro-Gly-NHMe	3451cm^{-1}(NHMe: HBfree)	6.2	
	3355cm^{-1}(NHMe: 10-m.HBd)	30	4.8
Boc-Pro-Ala-NHMe	3454cm^{-1}(NHMe: HBfree)	5.2	
	3364cm^{-1}(NHMe: 10-m.HBd)	23	4.4
	3421cm^{-1}(Ala: Hbfree)	20	
	3292cm^{-1}(Ala: 7-m.Hbfree)	2.3	0.1
Boc-Pro-Leu-NHMe	3453cm^{-1}(NHMe: HBfree)	7.7	
	3368cm^{-1}(NHMe: 10-m.HBd)	22	2.8
	3418cm^{-1}(Leu: HBfree)	18	
	3293cm^{-1}(Leu: 7-m.HBd)	1	0.6
Boc-Pro-Val-NHMe	3454cm^{-1}(NHMe: HBfree)	7.4	
	3371cm^{-1}(NHMe: 10-m.HBd)	11	1.6
	3411cm^{-1}(Val: HBfree)	—	—
	3299cm^{-1}(Val: 7-m.HBd)	3.8	—
Boc-Pro-Phe-NHMe	3452cm^{-1}(NHMe: HBfree)	4.4	
	3367cm^{-1}(NHMe: 10-m.HBd)	20.5	4.7
Ac-Pro-Gly-NHMe	3451cm^{-1}(NHMe: HBfree)	4.9	
	3350cm^{-1}(NHMe: 10-m.HBd)	27	5.6
	3443cm^{-1}(Gly: HBfree)	11	
	3276cm^{-1}(Gly: 7-m.HBd)	2.4	0.2
Tfa-Pro-Gly-NHMe	3452cm^{-1}(NHMe: HBfree)	6.2	
	3397cm^{-1}(NHMe: 10-m.HBd)	16	2.6
	3443cm^{-1}(Gly: HBfree)	8.9	
	3363cm^{-1}(Glyl: 7-m.HBd)	9.2	1.0

a. with standard deviation of 6-15%

Table 5. Frequencies and intensities of antisymmetric stretching bands of the C-terminal NH_2 groups which are related with HBd structures, obtained by curve fitting for IR spectra of the peptides in 1.25 mM $CDCl_3$ solution at 25°C.

compounds	frequency (assignment)	intensity	intensity ratio (HBd/HBfree)[a]
Boc-Pro-Gly-Leu-NH_2	3522cm^{-1}(NH_2(anti): HBfree)	2.7	
	3488cm^{-1}(NH_2(anti): HBd)	14.1	5.2
Boc-Pro-Ala- Leu-NH_2	3523cm^{-1}(NH_2(anti): HBfree)	1.3	
	3487cm^{-1}(NH_2(anti): HBd)	17.0	13
Boc-Pro-Leu- Leu-NH_2	3524cm^{-1}(NH_2(anti): HBfree)	1.8	
	3488cm^{-1}(NH_2(anti): HBd)	16.6	9.2
Boc-Pro-Val- Leu-NH_2	3523cm^{-1}(NH_2(anti): HBfree)	1.4	
	3487cm^{-1}(NH_2(anti): HBd)	16.7	12
Boc-Pro-Phe- Leu-NH_2	3523cm^{-1}(NH_2(anti): HBfree)	1.1	
	3486cm^{-1}(NH_2(anti): HBd)	17.9	16
Ac-Pro-Gly- Leu-NH_2	3523cm^{-1}(NH_2(anti): HBfree)	1.2	
	3483cm^{-1}(NH_2(anti): HBd)	11.9	9.6
	3498cm^{-1}		
Tfa-Pro-Gly- Leu-NH_2	3523cm^{-1}(NH_2(anti): HBfree)	1.7	
	3480cm^{-1}(NH_2(anti): HBd)	10.1	6.0
	3498cm^{-1}		
Ac-Pro-Leu-Gly-NH_2	3524cm^{-1}(NH_2(anti): HBfree)	5.4	
	3487cm^{-1}(NH_2(anti): HBd)	13.2	2.4
	3501cm^{-1}		
Tfa-Pro-Llleu-Gly-NH_2	3526cm^{-1}(NH_2(anti): HBd)	8.6	
	3490cm^{-1}(NH_2(anti): HBd)	11.1	1.3
	3503cm^{-1}		

a. with standard deviation of 6-15%

Chapter 4

NMR Study on *Cis-Trans* Isomerization of a Proline Imide Bond of Small Peptides in Chloroform-DMSO Mixed Solvents

Introduction:

Among all the peptide bonds in proteins, only the peptide bonds preceding prolyl residues, usually called proline imide bonds, can adopt *cis* as well as *trans* forms.[57-63] This is due to the unique structure of proline in which the side chain covalently connects with the nitrogen atom of the peptide backbone, forming a pyrrolidine ring. A steric hindrance between the δ-CH_2 group of the ring and the α-CH_2 group of a preceding residue is thought to destabilize the *trans* form to a considerable degree and, as a result, reduce significantly the difference in stability between the *trans* and *cis* forms. Therefore, the proline imide bonds can take both the *cis* and *trans* forms comparably.[1]

In native proteins, however, the proline imide bonds take mostly the *trans* forms, while both isomers exist comparably in unstructured polypeptides.[64] Thus, the *cis*-to-*trans* isomerization of the proline imide bond is thought as an important process in the course of protein folding. In an earlier stage of the folding pathway, every segment of the peptide chain is thought to be fully exposed to surrounding aqueous environments and have enough flexibility to fluctuate among various conformations. Under this circumstance, the proline imide bond also will not be restricted to the *trans* form. As the folding proceeds, the chain gradually loses the conformational flexibility and adopts some regular secondary structures, which have some intramolecular hydrogen bonds. Formation of these secondary structures is sometimes accompanied with the *cis*-to-*trans* conversion of the proline imide bonds. Then, it is thought that some interaction or solvent condition favorable for a specific intramolecular hydrogen-bonded structure may also drive a polypeptide chain to take the right configurations of the proline imide bonds during the protein folding process. Therefore, it is important to investigate a relationship between the hydrogen-bonding and the *cis*-to-*trans* isomerization of the proline imide bond in various solutions.

In Chapter 3, I have characterized a few types of intramolecular hydrogen-bonded (HBd) structures for various proline-containing short peptides in $CDCl_3$ solutions using FTIR spectroscopy. For instance, Boc-Pro-Gly-OEt forms a 7-membered HBd ring with the Boc C=O group linking to the Gly-NH, while Boc-Pro-Gly-NHMe forms a 10-membered HBd structure, in which the C-terminal $NHCH_3$ group takes part.

The present chapter is devoted to analysis of proton NMR spectra of several

proline-containing peptides which I have measured in mixed solvents of $CDCl_3$ and DMSO-d_6 at various mixing ratios. I examine how the *cis/trans* ratios of the proline imide bonds vary with change in solvent environments and discuss how the *cis*-to-*trans* isomerization couples to formations of various types of HBd structures which have been identified in the preceding IR study.

Experimental:

Sample Preparations. Both $CDCl_3$ and DMSO-d_6 solvents were dried over molecular sieves 4A for more than 24 h before sample preparations. Each of the peptide solutions: Boc-Pro-Sar-Zaa and Boc-Pro-Gly-Zaa (2.5-10 mM), and Ac-Pro-Leu-Zaa (1.25-2.5 mM), was prepared by dissolving the solute in the two pure solvents, and then the two solutions were mixed at various ratios in NMR sample tubes. All the concentrations were dilute enough to neglect self-association of the peptides. Residual H_2O contents of all samples were less than 5 mM.

NMR Measurements. One-dimensional proton NMR spectra of peptide solutions were measured with a JEOL EX400 Fourier-transform NMR spectrometer at room temperature. A 45° sampling pulse with a total repetition of 5.0 sec was applied. Data size collected with 16 or 32 scans was 16384 points, and the spectrum was Fourier transformed without a window function. Chemical shifts of peptide amide protons in the mixed solvents were standardized by a residual DMSO proton signal (2.49 ppm) for both solutions in the $CDCl_3$/DMSO-d_6 and those in the DMSO-d_6/D_2O, a residual $CHCl_3$ proton signal (7.24 ppm) for solutions in pure $CDCl_3$, and a residual HDO signal (4.63 ppm) for solutions in pure D_2O. For other kinds of mixed solvents, proton signals of a residual CH_3CN (1.93 ppm) in $CDCl_3$/acetonitrile-d_3, a residual CH_3OD (4.78 ppm) in $CDCl_3$/methanol-d_4, and a residual $(CH_3)_2CO$ (2.04 ppm) in $CDCl_3$/acetone-d_6 were used, respectively.

In order to assign all resonances of the peptides and classify them into signals of a few isomers, COSY (two-dimensional correlated spectroscopy) and NOESY (two-dimensional nuclear Oberhouser enhancement-exchange spectroscopy) spectra

were measured with a JEOL EX400 or a Bruker AM600 spectrometer at room temperature. The matrix size of each data collected with 8 scans was 256 x 2048 and the spectrum was obtained by Fourier transformation in both dimensions with a sine bell window function (COSY) or a squared sine bell window function (NOESY). In NOESY measurements, 300-750 msec of mixing time and a decay of 1 sec were taken between successive scans.

Analysis of *Cis/Trans* Ratio. All the NMR spectra measured were analyzed with an NMR analysis software, Alice 2 for Windows. Clearly separated signal pairs, which are assigned to the *cis* and *trans* forms of the proline imide bonds, were integrated to obtain the population ratios of the *cis* and *trans* isomers. For every peptide with a sequence of Boc-Pro-Gly-Zaa (Zaa = OEt, NHMe, Leu-NH_2), for example, the signal pairs of methyl protons of the Boc group (Boc-CH_3) and α-proton of the Pro residue (Pro-α) were used to estimate the *cis/trans* ratios, where the results from the two signal pairs agreed with each other within a few percent. Similarly, for every Ac-Pro-Leu-Zaa (Zaa = OMe, Gly-OEt, Gly-NH_2), the signal pairs of methyl protons of the acetyl groups (Ac-CH_3) and the Pro-α were used. On the other hand, each of Boc-Pro-Sar-Zaa peptides (Zaa = OEt, NHMe) has four distinct imide-bond isomers, because each of the two imide bonds preceding the Pro and Sar residues takes the *cis* and *trans* forms. In order to estimate the relative populations of these four isomers, the signal sets of the *N*-methyl protons of the Sar residue (Sar-(*N*)CH_3) and Boc-CH_3 were used.

Results:

Assignments of NMR spectra of Ac-Pro-Leu-Gly-NH_2 and related peptides.

Figure 4.1 shows a 400 MHz proton NMR spectrum of 2.5 mM Ac-Pro-Leu-Gly-NH_2 in DMSO-d_6 at 25°C. In this solution, two different signals are assigned to each proton of Ac-Pro-Leu-Gly-NH_2. This fact indicates that Ac-Pro-Leu-Gly-NH_2 in DMSO-d_6 takes two different configurations whose rate of change to each other is slow enough on NMR time scale. All the resonance lines were

assigned by a COSY spectrum, shown in Figure 4.2 and 4.3. Cross-peaks between amide protons and α-protons of every residue (Figure 4.3) are classified into a major and a minor configurations according to their relative signal intensities. All the other cross peaks can also be classified in the same manner. The two configurations are reasonably assigned to the *trans* and the *cis* isomers related to the proline imide bond. It is well known that the *cis*-to-*trans* conversion of the proline imide bond is slow enough even on the NMR time scale. Therefore, the *trans* and the *cis* isomers will give different sets of signals for each proton resonance, as observed in the NMR spectrum in Figure 4.1. This assignment to the two isomers is confirmed by NOESY. Figure 4.4 and 4.5 show NOESY spectra of Ac-Pro-Leu-Gly-NH_2 in DMSO-d_6, where both cross peaks of NOE (in positive phase, marked by "N") and exchanging pairs (negative phase) are observed. NOE cross peaks between the acetyl group and the prolyl protons are good indices of the *cis/trans* isomers. In the *cis* isomer, a prolyl α-proton (Pro-α) and the acetyl methyl protons (Ac-CH_3) of the acetyl group are put spatially close to each other within distance of 3 Å, while the distance between the prolyl δ-protons (Pro-δ) and the Ac-CH_3 protons is far apart. The reverse is true for the *trans* isomer.[65] The major configuration of Ac-Pro-Leu-Gly-NH_2 in DMSO-d_6 provides NOE cross peaks between the Ac-CH_3 and two Pro-δ protons, therefore, it is assigned to the *trans* isomer. On the other hand, the minor configuration is assigned to the *cis* isomer because an NOE belonging to the Ac-CH_3 is observed with the Pro-α proton.

Figure 4.6 shows an NMR spectrum of 1.25 mM Ac-Pro-Leu-Gly-NH_2 in $CDCl_3$ at 25°C. All the resonance lines were assigned by a COSY spectrum. In the $CDCl_3$ solution each proton shows only one signal, which is assigned to the *trans* isomer by NOESY. Two singlet signals at 5.23 ppm and 6.62 ppm are assigned to two amide protons of the C-terminal NH_2 group. The 5.23-ppm peak is assigned to a *syn* amide proton of the NH_2 group, because its chemical shift is close to that of a *syn* amide proton of acetamide in $CDCl_3$, 5.25 ppm. The 6.62-ppm peak, which is assigned to the *anti* amide proton of the NH_2 group, is at a remarkably lower-field than the corresponding *anti* amide proton of acetamide in $CDCl_3$, 5.40 ppm. These results indicate that only the *anti* amide proton in the C-terminal NH_2 group participates in the hydrogen-bonding.

Assignments of NMR spectra of Boc-Pro-Sar-NHMe and related peptides.

Figure 4.7 shows a 400 MHz proton NMR spectrum of 2.5 mM Boc-Pro-Sar-NHMe in DMSO-d_6 at 25°C. As mentioned in the experimental section, Boc-Pro-Sar-NHMe can take four distinct configurational isomers which have different *cis/trans* configurations about two imide linkages at Boc-Pro and Pro-Sar. In order to classify all the signals into the four isomers, NOE correlations are analyzed for the four distinct signals of the Sar-(*N*)CH_3 (marked by No.1-4). From the observation that No.1 and No.2 signals have NOE cross peaks with the Pro-α proton (4.57 ppm) while neither No.3 nor No.4 does, both signals of No.1 and No.2 are assigned to the *trans* isomers about the Pro-Sar linkage. On the other hand, two different signals of the Boc-CH_3 protons, at 1.32 and 1.38 ppm, are classified into the *cis* and *trans* isomers about the Boc-Pro linkage, respectively, by referring to NMR spectra of related peptides with the Boc group. From analysis of relative populations of the four isomers by both the Boc-CH_3 and the Sar-(*N*)CH_3 signal intensities, the following assignments are obtained: No.1; *trans*+*trans*, No.2; *cis*+*trans*, No.3; *trans*+*cis*, and No.4; *cis*+*cis* isomers.

The *cis/trans* ratios of Ac-Pro-Leu-Zaa in $CDCl_3$/DMSO-d_6 mixed solvents.

Figure 4.8 shows changes in relative signal intensities of the *trans* isomer of Ac-Pro-Leu-Gly-NH_2 with solvent mixing ratios in $CDCl_3$/DMSO-d_6 mixed solvents. Different results obtained from signal pairs of the Ac-CH_3, Pro-α, Gly-NH, and Leu-NH protons agree with one another within a few percent.

Figure 4.9 shows changes in population of the *trans* isomer with solvent mixing ratios in the two kinds of mixed solvents, D_2O/DMSO-d_6 and $CDCl_3$/DMSO-d_6, for peptides with an Ac-Pro-Leu- sequence. In the D_2O/DMSO-d_6 mixed solvents, the *cis/trans* ratios for all the three compounds are almost independent of the solvent mixing ratios. In the $CDCl_3$/DMSO-d_6 mixed solvents, however, the *trans* isomers of the three compounds increase with increasing $CDCl_3$ fraction in the mixed solvent. Their ratios of the *trans* isomer in pure $CDCl_3$ solutions are different from one another. These results indicate that chloroform as a solvent more or less facilitates *cis*-to-*trans* isomerizations of the proline imide bonds of Ac-Pro-Leu-OMe, Ac-Pro-Leu-Gly-OEt,

and Ac-Pro-Leu-Gly-NH_2. The IR studies in the preceding chapter have shown that these peptides form some intramolecular hydrogen-bonded (HBd) structures in $CDCl_3$ solutions. Among all the possible HBd rings, particularly important are what involve the carbonyl group preceding the prolyl residue. These HBd rings are considered to be closely related to the *cis*-to-*trans* isomerization of the proline imide bond. Ac-Pro-Leu-OMe can take a 7-membered HBd ring, and Ac-Pro-leu-Gly-NH_2 is likely to form a 13-membered HBd ring in addition to the 10- or 7-membered rings. Formation of these HBd rings has been confirmed by IR spectra as shown in Chapter 3.

Four isomers of Boc-Pro-Sar-NHMe in $CDCl_3$/DMSO-d_6 mixed solvents.

Figure 4.10 shows changes in relative signal intensities of the four isomers of Boc-Pro-Sar-NHMe with solvent mixing ratios in the two kinds of mixed solvents, DMSO-d_6/D_2O and $CDCl_3$/DMSO-d_6. With decrease in solvent polarity, the *trans+trans* isomer becomes dominant, while the *cis+trans* isomer decays gradually.

A similar relationship among the four isomers of Boc-Sar-Sar-NHMe is shown in Figure 4.11. As compared with he case of Boc-Pro-Sar-NHMe, the *trans+trans* isomer of Boc-Sar-Sar-NHMe is not so dominant and dependence on the solvent polarity is less marked. The IR results have indicated that Boc-Pro-Sar-NHMe takes the 10-membered HBd structure more abundantly than Boc-Sar-Sar-NHMe in $CDCl_3$. Therefore, the *cis*-to-*trans* isomerization of both the Boc-pro and Pro-Sar linkages, are facilitated by forming 10-membered HBd structure in solutions of lower solvent polarity.

Solvent effects on the *cis*-to-*trans* isomerization.

In Figure 4.12, 4.13, and 4.14 show the similar plots of Boc-Pro-Sar-NHMe in other mixed solvents, $CDCl_3$/acetonitrile-d_3, $CDCl_3$/methanol-d_4, $CDCl_3$/acetone-d_6, respectively. In Figure 4.15, the populations of the *trans+trans* isomer of this peptide are plotted against molar fractions of $CDCl_3$, $x_{(CDCl_3)}$, in the different mixed solvents. Since only the *trans+trans* isomer is compatible with the 10-membered HBd structure of Boc-Pro-Sar-NHMe, it is suggested that the degree of decrease in population of the *trans+trans* isomer at a given $x_{(CDCl_3)}$ is related to the ability of the solvents to break the intramolecular HBd structure. Furthermore, if the same *trans+trans* percentage is

plotted against the dielectric constants of the mixed solvents, ε, which are calculated from the dielectric constants of the component solvents, some solvent specificity is reversed as in Figure 4.16. That is the solvent ability to form a hydrogen bond with the peptide by breaking the intramolecular HBd structure. Regardless of the high dielectric constant and large dipole moment, acetonitrile is the weakest hydrogen-bond acceptor among the five polar solvents. On the contrary, DMSO and acetone are powerful breakers of intramolecular hydrogen-bond of a peptide. Methanol is thought to act as both a strong hydrogen-bond-acceptor and a donor. However, its effect is mild at its low fractions in the $CDCl_3$/methanol-d_4 mixed solvent. This fact suggests that methanol prefers a self-association to a hydrogen-bonding with the peptide in the chloroform-rich solutions.

The *cis*-to-*trans* ratios of Boc-Pro-Yaa-Zaa in various solvents.

Figure 4.17 shows changes in the population of the *trans+trans* isomers with the solvent mixing ratios of the $CDCl_3$/DMSO-d_6 mixed solvents for peptides with a Boc-Pro- sequence in common. Similarly to the results for peptides with an Ac-Pro- sequence shown in Figure 4.9, the way of increase in population of the *trans+trans* isomer is clearly related with types of HBd structures which the peptides can take. For Boc-Pro-OMe and Boc-Pro-Sar-OEt with no possibility of HBd structure, populations of the *trans* configurations at the Boc-Pro linkages are independent of the solvent mixing ratios. For Boc-Pro-Gly-OEt with an only possibility of the 7-membered HBd structure, the *trans* isomer increases only to a small extent with increasing fractions of $CDCl_3$ up to 100%(v/v). The increase is much more great for Boc-Pro-Sar-NHMe and Boc-Pro-Gly-NHMe both of which form the 10-membered HBd ring. These facts are consistent with the present IR result that the 7-membered HBd structure of Boc-Pro-Gly-OEt is less stable than the 10-membered HBd structures of Boc-Pro-Gly-NHMe and Boc-Pro-Sar-NHMe as shown in Chapter 3. Further, Boc-Pro-Gly-Leu-NH_2 which forms a 13-membered HBd ring is also directed to the *trans* isomer as the $CDCl_3$ fraction increases.

Discussion:

As mentioned above, the population of the *trans* configuration of the proline imide bond increases with increasing fraction of $CDCl_3$ in $CDCl_3$/DMSO-d_6 and other $CDCl_3$-containing mixed solvents. In addition, to what percentage the *trans* isomer is attainable is dependent on the type of HBd structure which the peptide forms in a $CDCl_3$ solution. From the combining analysis with IR results, it is indicated that the stable 13- and 10-membered HBd structures facilitate the *cis*-to-*trans* isomerization of the proline imide bonds more effectively than the 7-membered HBd structure as shown in Table 6. These 7-, 10, and 13-membered HBd rings are considered to be similar to the secondary structures of a peptide segment, γ-turn, β-turn, and α-helix, respectively. These secondary structures require the proline imide bond to adopt the *trans* configurations. Therefore, the efficiency to facilitate the *cis*-to-*trans* isomerization of the proline imide bond is in the following order: α-helix ≧ β-turn > γ-turn.

Mixed solvents used in the present experiments, $CDCl_3$/DMSO-d_6 and DMSO-d_6/D_2O, cover quite a wide range of dielectric constants, 4.9-78.3. Moreover, chloroform, DMSO, and water are significantly different in ability as a hydrogen-bond acceptor or as a donor. It is well-known and also confirmed in this work that water and DMSO act as a powerful breaker of the intramolecular hydrogen-bond of the peptides. Therefore, it is thought that any intramolecular HBd structures of small peptides are destabilized under DMSO-rich solvent conditions, but it is difficult to obtain direct evidence for this by IR studies because DMSO itself has a strong absorption in the frequency regions of N-H stretching of the peptides. Compared with water and DMSO, chloroform is much more mild in perturbing the HBd structures of the peptide, owing to a lack of a hydrogen-bond-accepting group and to the weakness of its hydrogen-bond donating ability. Therefore, the $CDCl_3$/DMSO-d_6 and DMSO-d_6/D_2O mixed solvents are thought to be useful in mimicking solvent environments of local segments of a polypeptide chain, where the solvent conditions will change variously during the protein folding process.

In the following chapter, I will show that the chemical shift changes of amide protons in such mixed solvents are useful for evaluating extents to which the NH protons of peptides are related with the intramolecular hydrogen bonding.

Ac-Pro-Leu-Gly-NH_2

(400 MHz)

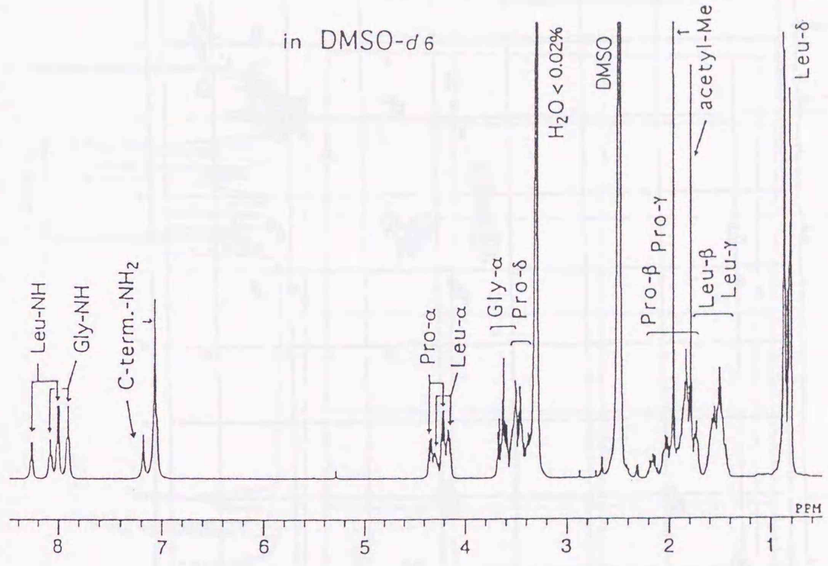

Figure 4.1. 400 MHz ^{1}H-NMR spectrum of Ac-Pro-Leu-Gly-NH_2 at 2.5 mM in DMSO-d_6 at 25°C.

COSY
(600 MHz)

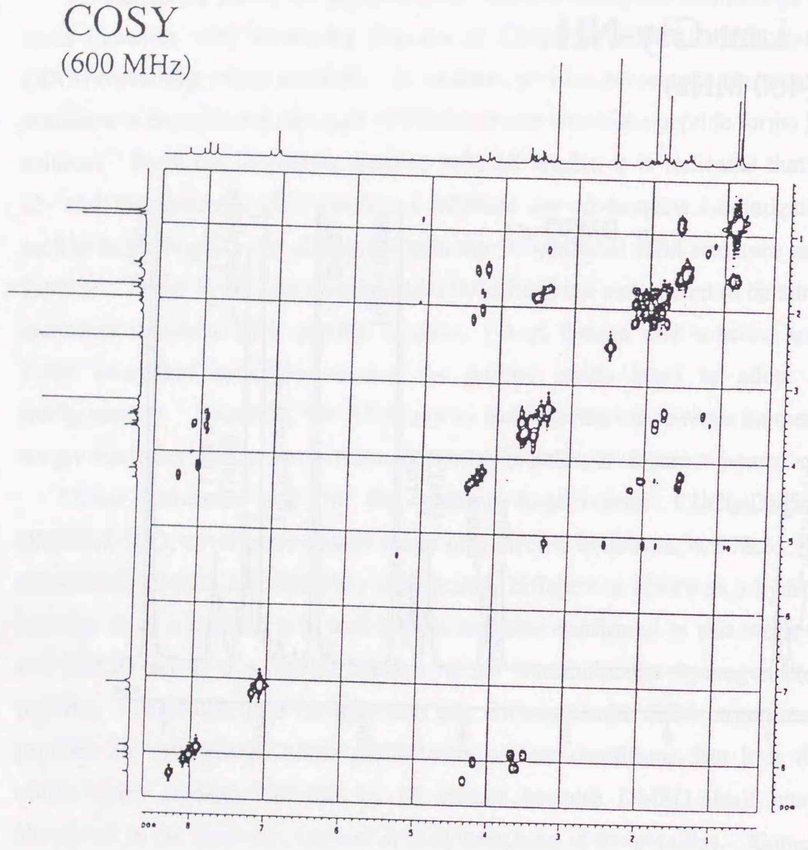

Figure 4.2. 600 MHz ^{1}H-COSY spectrum of Ac-Pro-Leu-Gly-NH_2 at 2.5 mM in DMSO-d_6 at 25°C.

COSY
(600 MHz)

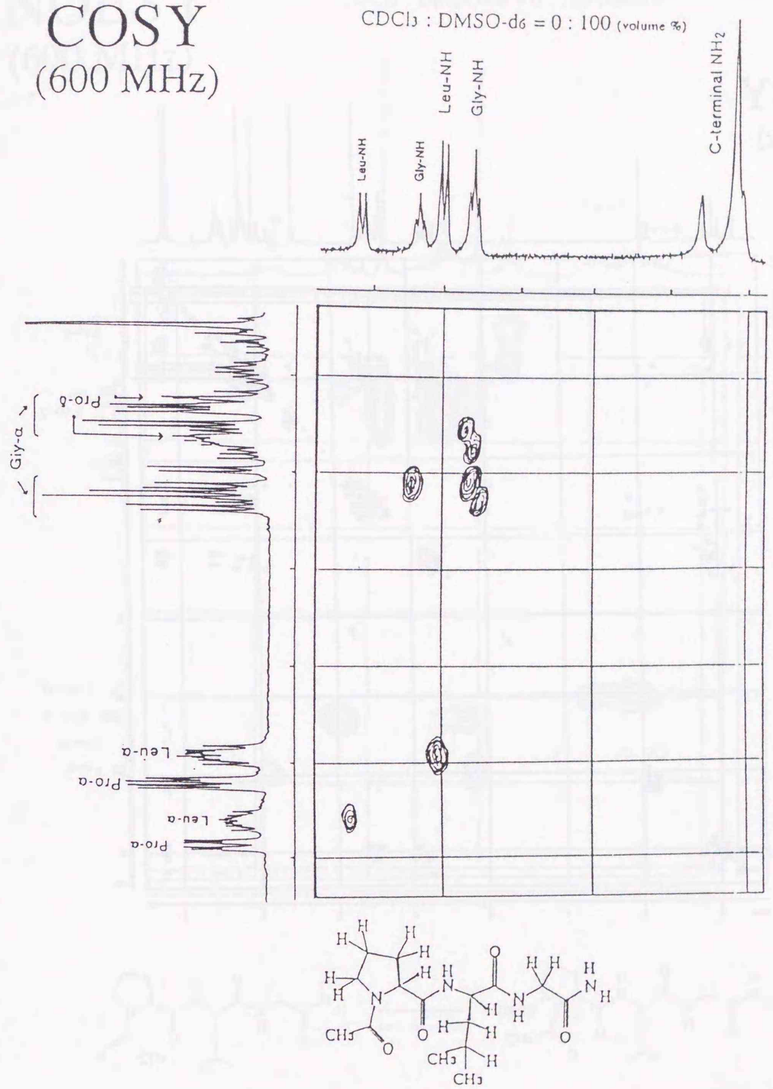

Figure 4.3. An expanded region of the 600 MHz ^{1}H-COSY spectrum of Ac-Pro-Leu-Gly-NH_2 at 2.5 mM in DMSO-d_6 at 25°C. Discrimination between assignments to the *trans* and *cis* configuration isomers is shown by the size of letters: the larger is for the *trans* isomer and the smaller is to the *cis* isomer.

NOESY
(600 MHz)

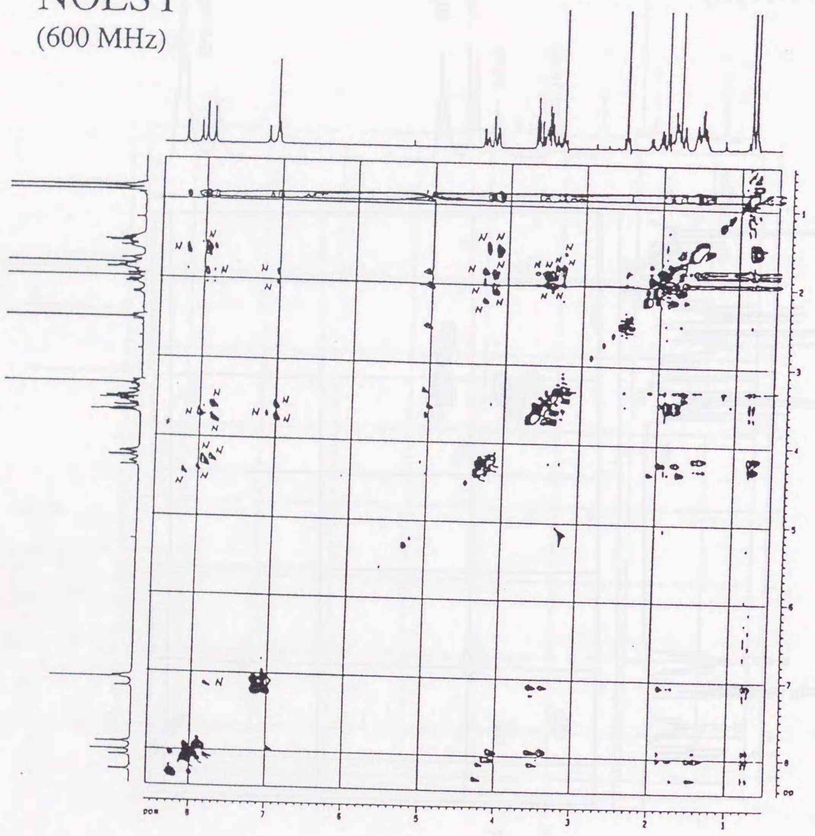

Figure 4.4. 600 MHz ^{1}H-NOESY spectrum of Ac-Pro-Leu-Gly-NH_2 at 2.5 mM in DMSO-d_6 at 25°C.

NOESY
(600 MHz)

CDCl$_3$: DMSO-d_6 = 0 : 100 (volume %)

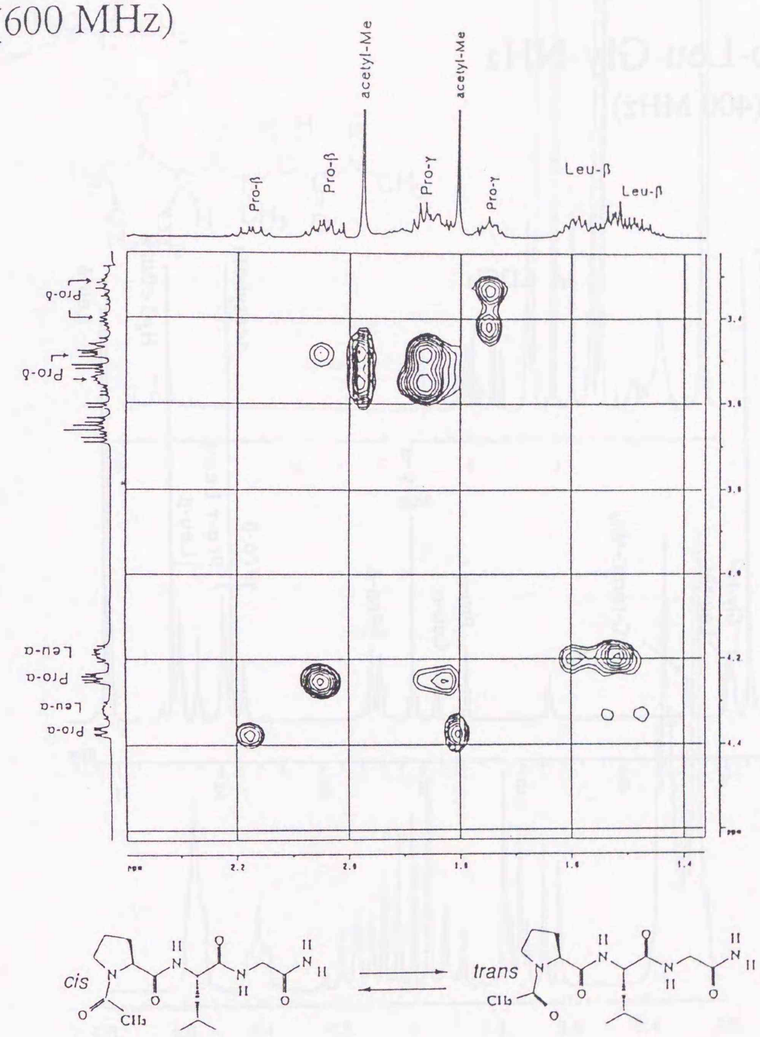

Figure 4.5. A fingerprint region of the 600 MHz ^{1}H-COSY spectrum of Ac-Pro-Leu-Gly-NH_2 at 2.5 mM in DMSO-d_6 at 25°C. Discrimination between assignments to the trans and cis configuration isomers is shown by the size of letters: the larger is to the *trans* isomer and the smaller is to the *cis* isomer.

Ac-Pro-Leu-Gly-NH_2

(400 MHz)

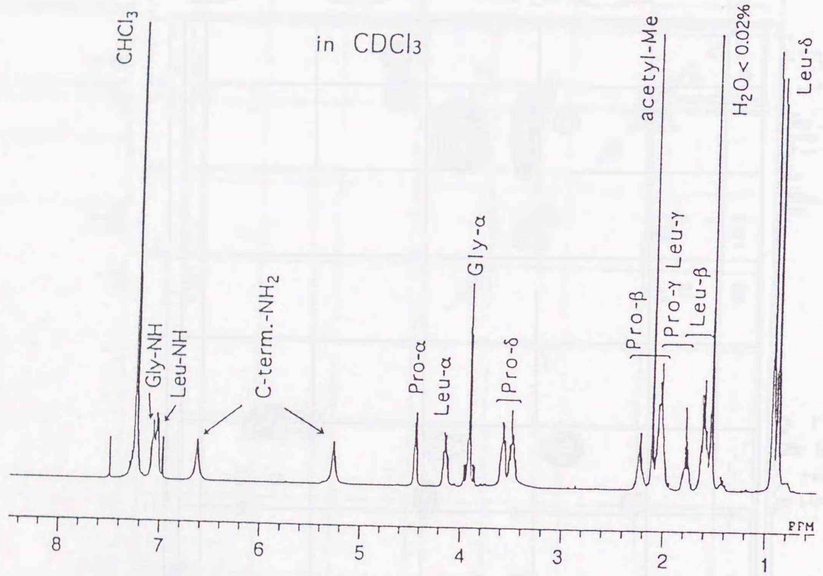

Figure 4.6. 400 MHz 1H-NMR spectrum of Ac-Pro-Leu-Gly-NH_2 at 1.25 mM in $CDCl_3$ at 25°C.

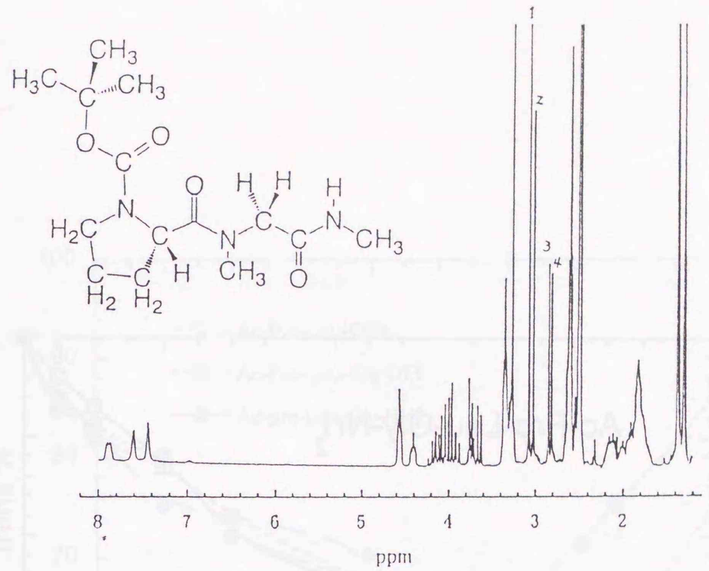

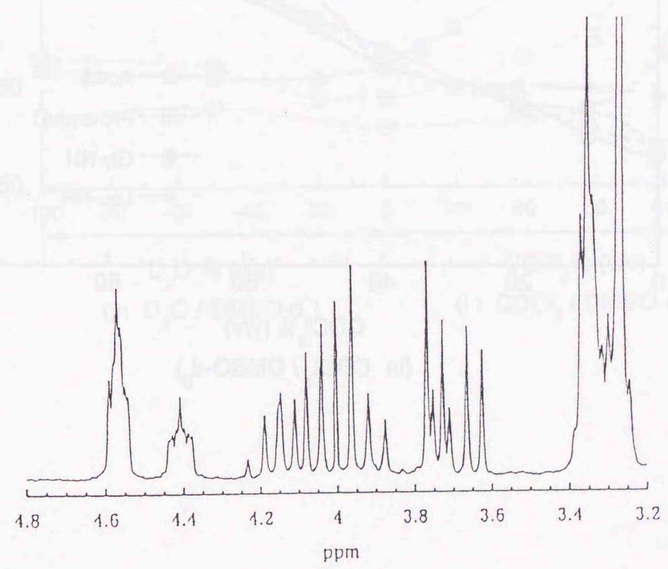

Figure 4.7. 400 MHz 1H-NMR spectrum of Boc-Pro-Sar-NHMe at 2.5 mM in DMSO-d_6 at 25°C. The number attached to signals around 2.8-3.1 ppm, the four Sar-(*N*)CH_3 signals for different four isomers (see text).

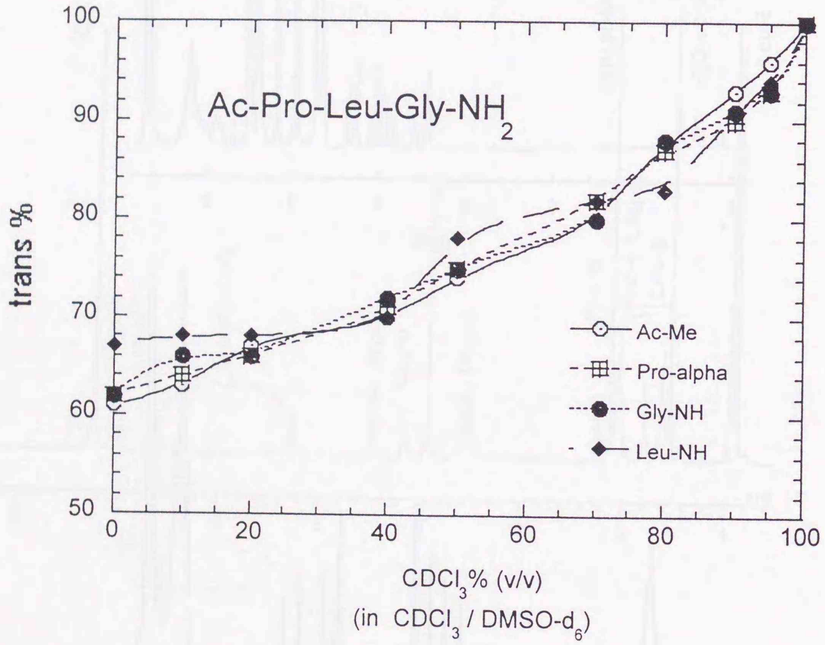

Figure 4.8. Plots of *trans* % of Ac-Pro-Leu-Gly-NH_2 against $CDCl_3$%(v/v) of the $CDCl_3$/DMSO-d_6 mixed solvent. Each set of the plots is obtained from the integrated intensities of the *cis* and the *trans* signals for each of the indicated protons.

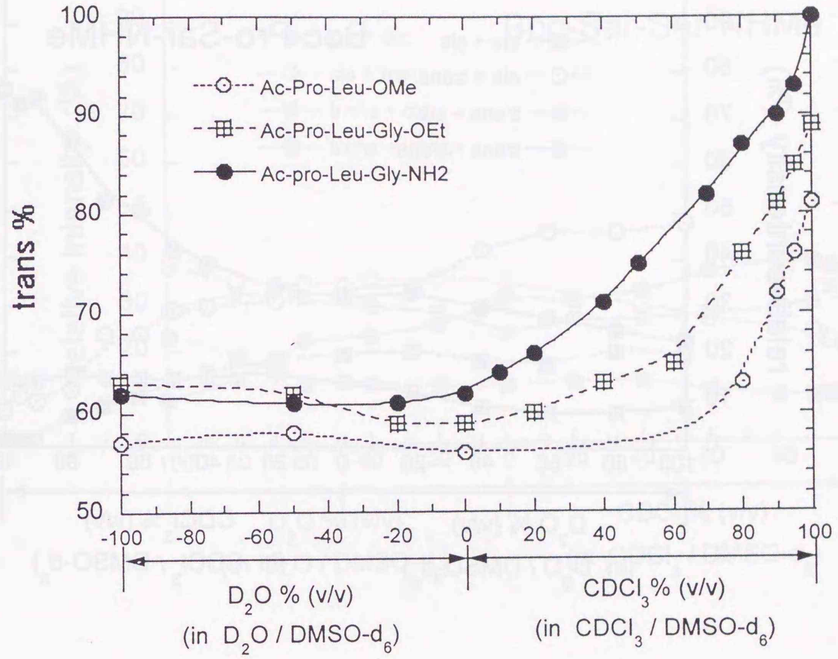

Figure 4.9. Plots of *trans* % of Ac-compounds against mixing ratios of DMSO-d_6/D_2O and $CDCl_3$/DMSO-d_6 mixed solvent. The percentages are obtained from the integrated intensities of the signal pair for the Pro-α proton of the peptides.

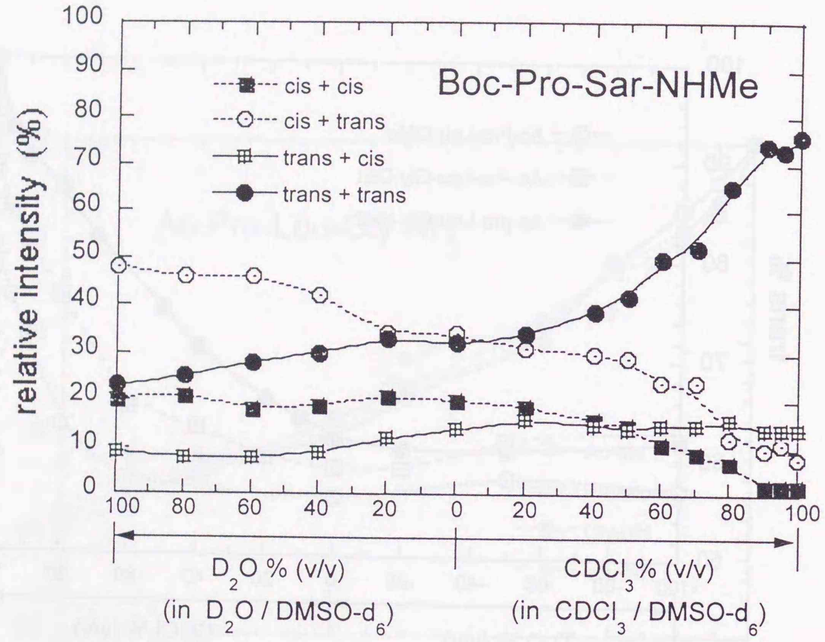

Figure 4.10. Relative populations of the four isomers about imide linkages at Boc-Pro and Pro-Sar of Boc-Pro-Sar-NHMe in mixed solvents of DMSO-d_6/D_2O and $CDCl_3$/DMSO-d_6 at various mixing ratios at 25°C.

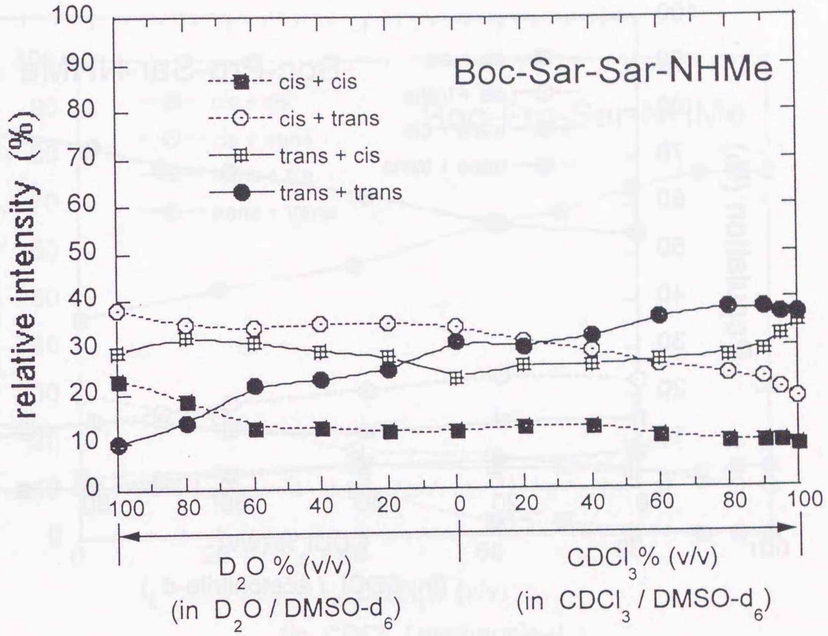

Figure 4.11. Relative populations the four isomers about imide linkages at Boc-Sar and Sar-Sar of Boc-Sar-Sar-NHMe in mixed solvents of DMSO-d_6/D_2O and $CDCl_3$/DMSO-d_6 at various mixing ratios at 25°C.

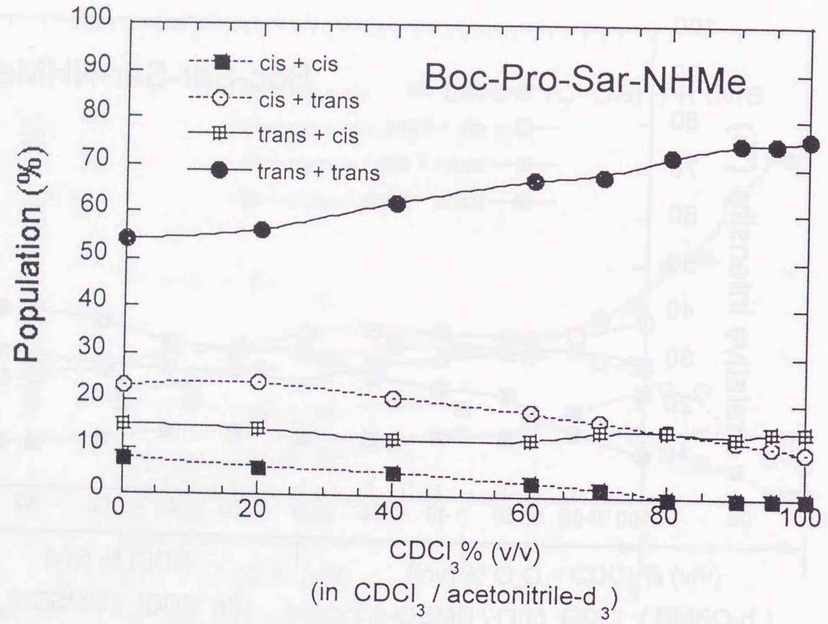

Figure 4.12. Plots of relative populations of four isomers about imide linkages at Boc-Pro and Pro-Sar of Boc-Pro-Sar-NHMe in mixed solvents of $CDCl_3$/acetonitrile-d_3 at various mixing ratios at 25°C.

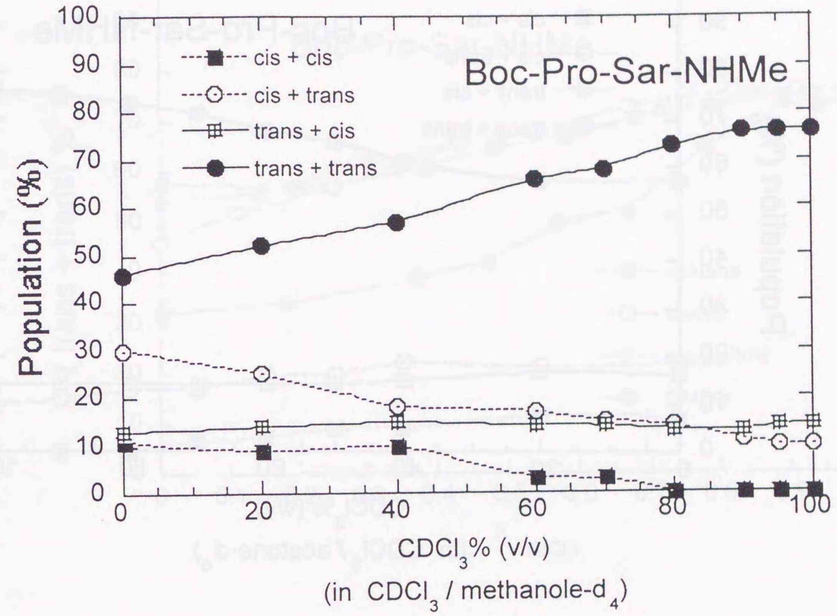

Figure 4.13. Plots of relative populations of four isomers about imide linkages at Boc-Pro and Pro-Sar of Boc-Pro-Sar-NHMe in mixed solvents of $CDCl_3$/methanol-d_4 at various mixing ratios at 25°C.

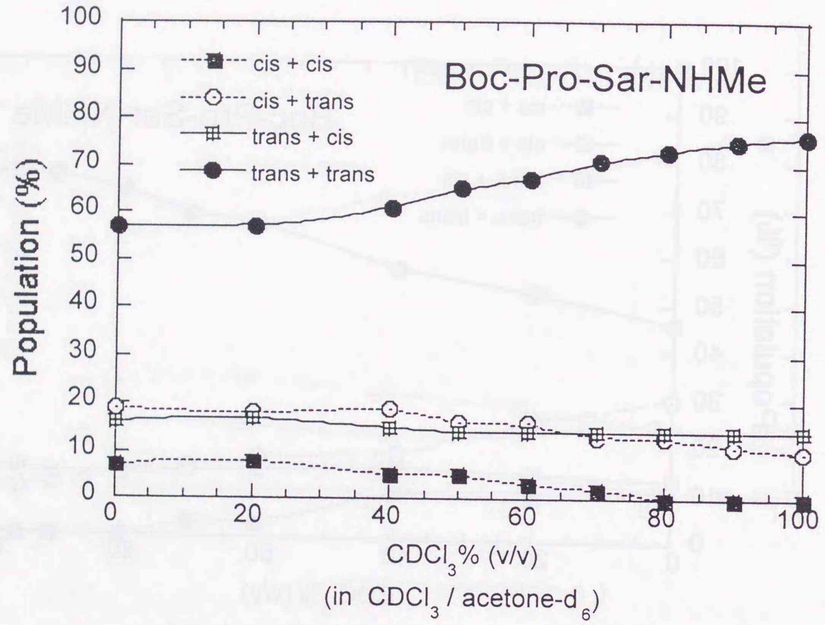

Figure 4.14. Plots of relative populations of four isomers about imide linkages at Boc-Pro and Pro-Sar of Boc-Pro-Sar-NHMe in mixed solvents of $CDCl_3$/acetone-d_6 at various mixing ratios at 25°C.

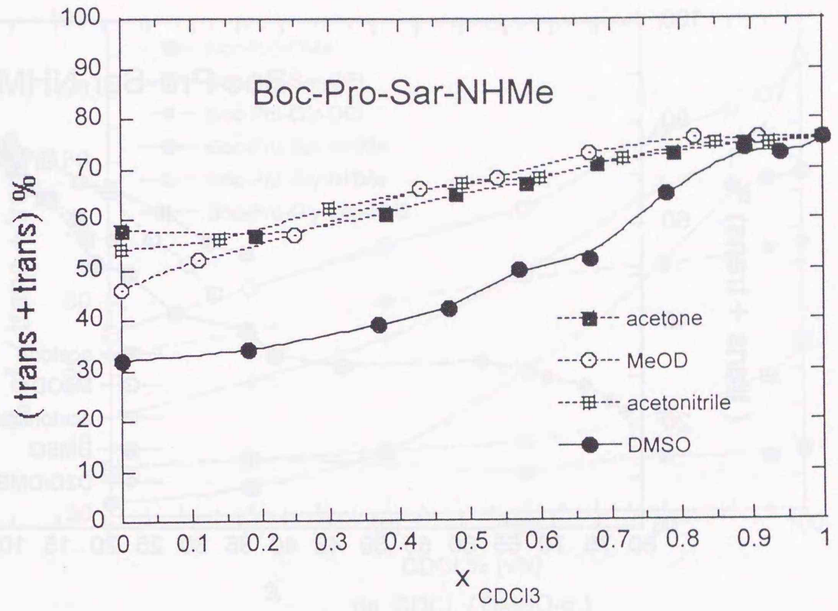

Figure 4.15. Plots of relative populations of the (*trans*+*trans*) isomer of Boc-Pro-Sar-NHMe against molar fraction of $CDCl_3$, x_{CDCl_3}, in four kinds of mixed solvents, $CDCl_3$/acetone-d_6, $CDCl_3$/methanol-d_4, $CDCl_3$/acetonitrile-d_3, and $CDCl_3$/DMSO-d_6 at 25°C.

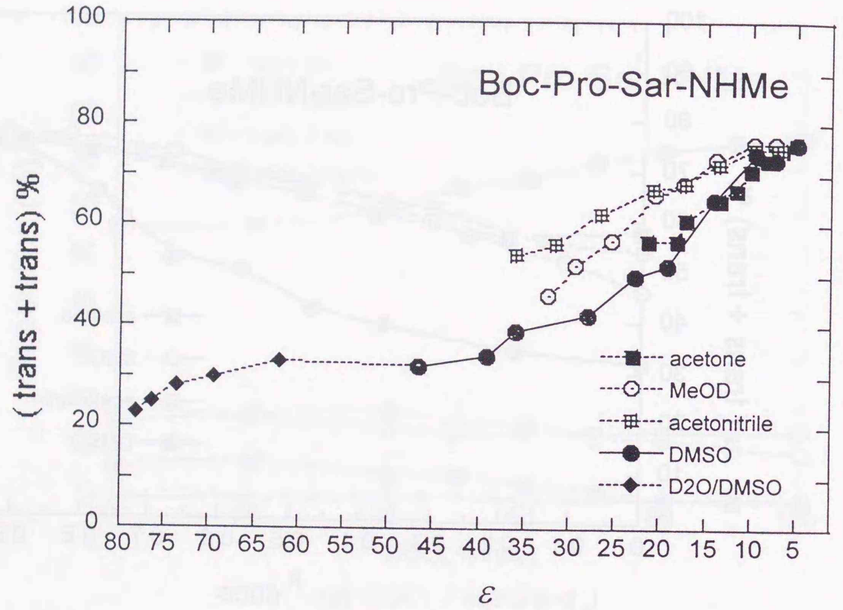

Figure 4.16. Plots of relative populations of the (*trans*+*trans*) isomer of Boc-Pro-Sar-NHMe against solvent dielectric constants of five kinds of mixed solvents, $CDCl_3$/acetone-d_6, $CDCl_3$/methanol-d_4, $CDCl_3$/acetonitrile-d_3, and $CDCl_3$/DMSO-d_6, and DMSO-d_6/D_2O at 25°C.

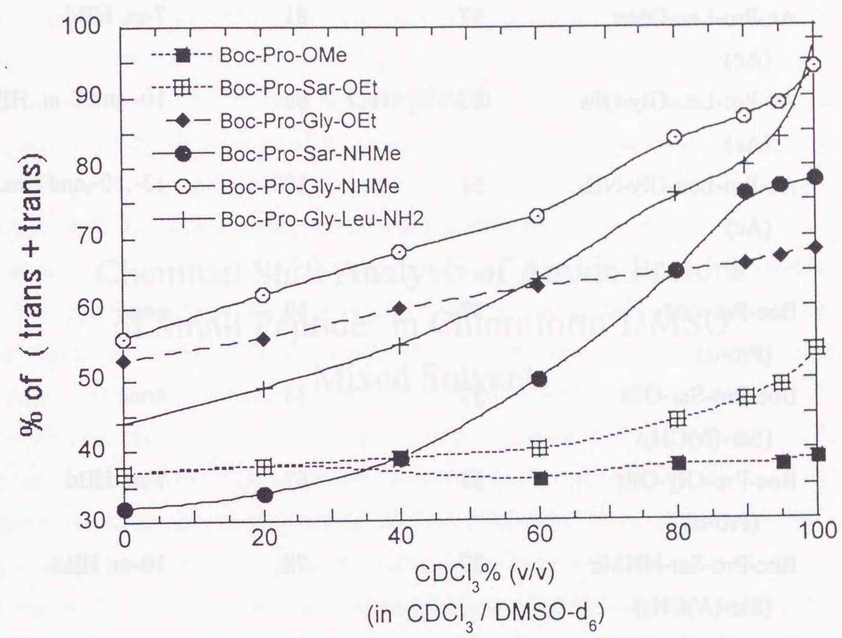

Figure 4.17. Plots of (*trans*+*trans*) % of Boc-compounds against $CDCl_3$%(v/v) of the $CDCl_3$/DMSO-d_6 mixed solvent at 25°C. The percentages are obtained from integrated intensities of the signal pairs of the Pro-α protons for Boc-Pro-OMe and Gly-containing peptides and from the intensities of the Sar-(N)CH_3 proton signals of Sar-containing peptides.

Table 6. Relative populations of the *trans* (*trans*+*trans*) isomers about proline imide bonds of various peptides, obtained from NMR signal intensities of the peptides in 1.25 mM solutions at 25°C.[a]

compounds (signal)	% in DMSO-d_6	% in $CDCl_3$	Type of HBd
Ac-Pro-Leu-OMe (Ac)	57	81	7-m. HBd
Ac-Pro-Leu-Gly-OEt (Ac)	63	89	10- and 7-m. HBd
Ac-Pro-Leu-Gly-NH_2 (Ac)	61	100	13-,10-,and 7-m. HBd
Boc-Pro-OMe (Pro-α)	37	39	none
Boc-Pro-Sar-OEt (Sar-(*N*)CH_3)	37	54	none
Boc-Pro-Gly-OEt (Pro-α)	53	67	7-m. HBd
Boc-Pro-Sar-NHMe (Sar-(*N*)CH_3)	32	78	10-m. HBd
Boc-Pro-Gly-NHMe (Pro-α)	56	94	10- and 7-m. HBd
Boc-Pro-Gly-Leu-NH_2 (Pro-α)	44	98	13-,10-,and 7-m. HBd

a. Dispersion among the results from different NMR signals is less than 5%.

Chapter 5

Chemical Shift Analysis of Amide Protons of Small Peptides in Chloroform-DMSO Mixed Solvents

Introduction:

In Chapter 3, I have identified the structures with intramolecular hydrogen-bond (HBd) of various short peptides in $CDCl_3$ solutions by IR spectroscopy. And the NMR study in Chapter 4 has shown that populations of the *trans* isomer of the proline imide bond of the peptides increase with increasing $CDCl_3$ fraction in the $CDCl_3$/DMSO-d_6 mixed solvent. These results strongly suggest that formation of the HBd structures facilitates the conversion of the proline imide bond from the *cis* form to the *trans* form, so as to yield the regular secondary structures which can be formed in hydrophobic atmospheres such as mimicked by the chloroform-rich solutions.

In those studies, the *cis/trans* ratios in various solvents were measured by NMR, while the direct evidence of the hydrogen-bonding was provided by IR measurements in $CDCl_3$ solutions. Comparison of the IR and NMR data for the amide proton would provide straightforward information on the intramolecular hydrogen bonding of small peptides in the $CDCl_3$/DMSO-d_6 mixed solvents. However, a strong absorption of DMSO itself in the NH stretching frequency region does not permit IR measurements in the mixed solvents, giving no information about HBd structures of the peptides in the mixed solvents. Therefore, it is required to utilize some NMR index which can be coupled to IR observations in $CDCl_3$ for characterizing HBd characters of the peptides in the mixed solvents. The chemical shift of the amide proton is measurable in solution in the $CDCl_3$/DMSO-d_6 mixed solvent with any mixing ratio and is sensitive to hydrogen bonding. It is well known that DMSO acts as a strong hydrogen-bond acceptor while $CDCl_3$ does not, and therefore, change in the chemical shift of the amide proton of the peptide with the solvent mixing ratio is considered to be caused by change in hydrogen-bonding between the peptide and DMSO solvents, and to be dependent on the extent to which the NH proton is involved in the intramolecular hydrogen-bonding.

In this chapter, I have analyzed the chemical shifts of amide protons for the same peptides as investigated in the preceding chapters. The IR spectra of these peptides in $CDCl_3$ solutions are used as direct evidence of formation of the HBd structures and provide support for the arguments based on the NMR chemical shifts of the amide protons.

Experimental:

Experimental details of the NMR measurements have been described in Chapter 4. The observed chemical shifts are standardized by using a signal of the residual DMSO proton (2.49 ppm) for solutions in the $CDCl_3$/DMSO-d_6 mixed solvents and a residual $CHCl_3$ proton signal (7.24 ppm) for solutions in pure $CDCl_3$.

Results:

Chemical shift changes with solvent mixing ratios.

Figure 5.1 shows how the chemical shifts of the NH protons of Ac-Gly-OEt (Gly-NH), Ac-Gly-NHMe (Gly-NH and -$NHCH_3$), Ac-Sar-NHMe (-$NHCH_3$), and *N*-methylacetamide (-$NHCH_3$) vary with the $CDCl_3$ fractions in the $CDCl_3$/DMSO-d_6 mixed solvents. Large variations of the chemical shifts are observed for the Gly-NH of Ac-Gly-OEt and for the $NHCH_3$ of *N*-methylacetamide. These results can be interpreted as follows. Since DMSO is a strong hydrogen-bond acceptor, it is reasonable to assume that these amide protons are intermolecularly hydrogen-bonded to DMSO and yield higher chemical shifts in pure DMSO solvents. Then the decrease in the chemical shift with increasing fraction of $CDCl_3$ in the mixed solvent is attributed to break of the peptide-DMSO intermolecular hydrogen-bonds. Therefore, a chemical shift change given by the Gly-NH of Ac-Gly-OEt, 2.172 ppm, can be taken as a standard for the amide proton exposed to the solvents at the mid position in the amino acid sequence. A standard for the terminal amide proton is given by the $NHCH_3$ amide proton of *N*-methylacetamide, 2.374 ppm. For the $NHCH_3$ amid proton of Ac-Gly-NHMe, the chemical shift variation from pure DMSO-d_6 to pure $CDCl_3$ is slightly smaller than the standard, and the variation for the $NHCH_3$ amide proton of Ac-Sar-NHMe is further smaller than that of Ac-Gly-NHMe. The IR spectra in Chapter 3 showed that Ac-Sar-NHMe forms the 7-membered HBd structure in a $CDCl_3$ solution to a considerable degree, while Ac-Gly-NHMe takes it less appreciably.

Ala-containing peptides.

Figure 5.2 shows solvent-dependent changes of the chemical shifts of NH protons for four different Ala-containing peptides. From comparison of the chemical shift profiles for each individual NH group, remarkably small chemical shift changes are observed for $NHCH_3$ amide protons of both Boc-Ala-Gly-NHMe and Boc-Ala-Sar-NHMe. This fact suggests that the terminal $NHCH_3$ groups mainly participate in intramolecular hydrogen bonding for both peptides. These HBd structures are thought to be the β-turn-like 10-membered HBd rings. The Gly-NH protons of Boc-Ala-Gly-OEt and Boc-Ala-Gly-NHMe exhibit chemical shift change which is somewhat smaller than the standard, but they are thought to participate in intramolecular hydrogen bonding to a very little degree, compared with the $NHCH_3$ groups of Boc-Ala-Gly-NHMe and Boc-Ala-Sar-NHMe.

Peptides with Leu-related residues.

In Figures 5.3 to 5.6, similar profiles are shown for a series of peptides with different amino acid residues at their (i + 1)-th positions. The Leu and Ile are amino acid residues found in natural protein molecules, while Nle and Tle are not. As can be seen in Chart 1, these four residues are different from one another in bulkiness at the β-carbons of the side chains which are *n*-butyl (Nle), *iso*-butyl (Leu), *sec*-(+)-butyl (Ile), and *tert*-butyl (Tle) groups, respectively.

Similarly to the case of Ala-containing peptides, the terminal $NHCH_3$ groups are found to be mainly involved in 10-membered HBd formation.

MeAla-containing peptides.

Figure 5.7 shows similar profiles for the *trans* isomers of MeAla-containing peptides. For all of them, the imide bonds precedent to MeAla can take both the *cis* and *trans* configurations and usually the *trans* isomers are superior in solutions with all the mixing ratios of the mixed solvent.

Also similarly to the above-mentioned peptides, the terminal $NHCH_3$ groups of Boc-MeAla-Gly-NHMe and Boc-MeAla-Sar-NHMe take part in the formation of the 10-membered HBd structures.

Pro-containing peptides.

Figure 5.8 shows the profiles for three different Pro-containing peptides. Here, only results for the *trans* isomers about the proline imide bonds are plotted for Boc-Pro-Gly-OEt and Boc-Pro-Gly-NHMe, and results for the *trans*+*trans* isomer for Boc-Pro-Sar-NHMe.

The smallest chemical shift change is observed for the $NHCH_3$ amide proton of Boc-Pro-Sar-NHMe, thus the largest degree of 10-membered HBd formation is suggested for Boc-Pro-Sar-NHMe. This observation is consistent with the IR spectra in $CDCl_3$ solutions, which have shown that Boc-Pro-Sar-NHMe is second to none in the relative band intensity for the 10-membered HBd structure among all the peptides studied (the second largest: Boc-Pro-Gly-NHMe). In addition, for the $NHCH_3$ amide protons of Boc-Pro-Sar-NHMe and Boc-Pro-Gly-NHMe, the chemical shift profiles are very flat even in the solvent ranges with $CDCl_3$ fractions between 70%(v/v) and 90%(v/v), where other amide protons so far described exhibit distinctly sharper transitions. This is probably because the 10-membered HBd structures of these two peptides are so stable that even DMSO cannot break them completely.

Furthermore, Figure 5.8 also indicates that Boc-Pro-Gly-OEt forms a 7-membered HBd structure in $CDCl_3$. This means that the Boc C=O group is connected with the Gly-NH forming the 7-membered ring, while the Boc C=O group of Boc-Pro-Gly-NHMe prefers the terminal $NHCH_3$ to the Gly-NH as the hydrogen-bond partner and forms the 10-membered HBd ring.

X-Pro-Gly-Leu-NH_2.

Figure 5.9 shows profiles for Ac-, Boc-, and Tfa-Pro-Gly-Leu-NH_2. Among four different amide protons in their sequences, the Leu-NH and the anti amide protons of the C-terminal NH_2 groups exhibit very small chemical shift variations. Therefore, these three peptides will form both 13- and 10-membered HBd rings, in each of which the Leu-NH or the *anti*-NH_2 group is linked with the *N*-terminal C=O group. Among these three peptides, chemical shift variations for each amide proton are different from one another. This means that the extent to which each type of HBd structure is formed is different from one to another peptides. The differences are due to different abilities of accepting hydrogen-bond among three kinds of *N*-terminal C=O groups, Ac-C=O, Boc-C=O, and Tfa-C=O, respectively. For instance, it is suggested that the

13-membered HBd structure involving the *anti*-NH_2 group is the most stable in Ac-Pro-Gly-Leu-NH_2 and the least in Tfa-Pro-Gly-Leu-NH_2. This is probably due to a strong electron-withdrawing property of the trifluoromethyl group which results in deterioration of the Tfa-C=O group as a hydrogen-bond acceptor.

Ac-Pro-Leu-Gly-NH_2 and related peptides.

In Figure 5.10, solvent-dependent changes in chemical shifts of some NH protons are compared among peptides with various lengths. The Leu-NH group of Ac-Pro-Leu-OMe is indicated to be involved in a 7-membered HBd ring. For Ac-Pro-Leu-Gly-OEt, it is suggested that the 7-membered HBd ring concerned with the Leu-NH is more favorable that the 10-membered one with the Gly-NH. It is likely that the 13-membered HBd structure is mainly formed for Ac-Pro-Leu-Gly-NH_2.

Discussion:

Criterion for judging HBd formation.

The present NMR observations indicated that the chemical shift variation in the mixed solvents from pure DMSO to pure $CDCl_3$ provide a measure of the extent to which an NH proton takes part in intramolecular hydrogen bonding. The observed chemical shift variations, $\Delta\delta$, for every amide proton of all the peptides studied are listed in Table 7 to 14. Furthermore, the ratio of the chemical shift variation of each amide proton to that of a suitable standard is estimated. I have adopted several standard is estimated. I have adopted several standards, $\Delta\delta$(ref), for analysis of the different NH protons. For instance, the Yaa-NH amide protons of Ac-Yaa-OEt (Yaa = Gly, Ala, Leu, Val, Phe) are used as standards for analysis of all the corresponding Yaa-NH amide protons of all peptides with Yaa. And the $NHCH_3$ amide proton of *N*-methylacetamide and both the *syn* and *anti* NH_2 amide protons of acetamide are taken as standards for analysis of peptides with these groups, respectively. The values of one minus the resulting ratios, [1-$\Delta\delta/\Delta\delta$(ref)], are assumed to be relative ratios of being involved in the intramolecular hydrogen bonding for the amide protons and listed in the fifth column of each table.

As a criterion for judging whether an NH proton is involved in the intramolecular hydrogen bonding to a significant degree or not, I take a value of 0.5 for [1-$\Delta\delta/\Delta\delta$(ref)] for the time being. On the basis of this criterion, the possible HBd structures are depicted in Chart 8 and 9. Here the stable HBd structures, of which [1-$\Delta\delta/\Delta\delta$(ref)] values are larger than 0.7, are indicated with a bold arrow.

Boc-Pro-Yaa-OEt: 7-membered HBd.

As shown in Chart 8, all peptides with a sequence of Boc-Pro-Yaa-OEt form the 7-membered HBd rings, which are thought as the γ-turn-like structure. It is intriguing that the Val residue occupying the Yaa position significantly stabilizes this γ-turn-like structure, in contrast with little effect of other residues at the same Yaa position. Furthermore, the γ-turn-like structure is shown to be more stable in Ac-Pro-Gly-OEt than in Boc-Pro-Gly-OEt (Chart 9). This is probably due to migration in steric repulsion by replacing the *N*-terminus from a bulkier Boc-group to an Ac-group.

Boc-Pro-Yaa-NHMe: 10-membered vs 7-membered HBd.

All peptides with a sequence of Boc-Pro-Yaa-NHMe form both the 10- and the 7-membered HBd rings. Except for Boc-Pro-Val-NHMe, the 10-membered structures are found to be dominant. Figure 5.11 shows plots of the [1-$\Delta\delta/\Delta\delta$(ref)] values of the terminal $NHCH_3$ amide protons against those of the Yaa-NH protons for five kinds of Boc-Pro-Yaa-NHMe peptides. A competitive correlation can be seen between formations of the 7-membered and 10-membered HBd structures. In view of this, Boc-Pro-Gly-NHMe forms the 10-membered HBd ring most exclusively. This is probably due to fit of the Gly-residue to the (i + 2)-th position of the type-II β-turn structure. As discussed in Chapter 3, other residues occupying the same Yaa position in Boc-Pro-Yaa-NHMe would force peptides to escape from the type-II structure and to take only the type-I β-turn structure. For Boc-Pro-Val-NHMe, a bulky isopropyl group of the Val side chain is not well accommodated to the type-I structure and rather prefers the 7-membered HBd structure where the bulky side chain will be outside of the HBd ring.

Difference in the trend toward β-turn formation between Ac-Pro-Gly-NHMe and Boc-Pro-Gly-NHMe is rather small, in contrast with the fact that γ-turn formation is

somewhat inhibited in Boc-Pro-Gly-OEt but not in Ac-Pro-Gly-OEt. This could be interpreted as follows. In the γ-turn structure of Boc-Pro-Gly-OEt, a bulky *tert*-butyl moiety would be repulsive with the backbone of such small size of the HBd ring and considerably destabilize it. This steric repulsion will not be significant in the γ-turn structure of Ac-Pro-Gly-OEt and also in the β-turn structure of Boc-Pro-Gly-NHMe. Compared with the γ-turn, an elongated intervening part of the β-turn structure, which separates the terminal Boc-group by one-residue father distance from its hydrogen-bond-donor group, will allow the bulky *tert*-butyl moiety to be kept away from the most crowded region.

Boc-Pro-Yaa-Leu-NH_2: 13-membered vs 10-membered HBd.

Peptides with an additional -Leu-NH_2 sequence have possibility of a 13-membered HBd ring as well as the above-mentioned 10- and 7-membered rings. In Figure 5.12, relationships among three kinds of HBd structures are shown for Boc-Pro-Yaa-Leu-NH_2 peptides. A competitive correlation is seen between 10- and 13-membered HBd structures. For instance, the 10-membered HBd structure is the most probable for a peptide with the Gly residue at the (i + 2)-th position in the sequence, and the 13-membered structure is the least probable for the same peptide among the series of Boc-Pro-Yaa-Leu-NH_2 peptides. This is attributed also to the remarkable suitability of the Gly-residue-containing type-II β-turn structure. A comparison between a pair of sequence-exchanged peptides, Ac-Pro-Gly-Leu-NH_2 and Ac-Pro-Leu-Gly-NH_2, also shows a similar result. The former peptide with the Gly residue at the (i + 2)-th position tends to form the 10-membered HBd structure preferably to the 13-membered one, but the situation is opposite for Ac-Pro-Leu-Gly-NH_2 with the Leu residue at the (i + 2)-th position in place of Gly. In addition, it is intriguing that the 7-membered structure is appreciable for Boc-Pro-Ala-Leu-NH_2 even at the condition where both 10 and 13-membered structures are more probable.

A comparison among three kinds of *N*-terminal modificants, Boc-, Ac-, and Tfa-Pro-Gly-Leu-NH_2, indicates that trends toward the 13- and 10-membered HBd structures are found to be different from one another. This difference is represented by the ratios, $P_{13}/P_{10} = [1\text{-}\Delta\delta/\Delta\delta(\text{ref})]_{13} / [1\text{-}\Delta\delta/\Delta\delta(\text{ref})]_{10}$, which are 0.88, 0.92, and 0.80 for Boc-, Ac-, Tfa-Pro-Gly-Leu-NH_2, respectively. This means that the both types of

HBd structures can form comparably, but their stabilities are sensitive to the hydrogen-bond accepting ability of the C=O group at the N-termini of the peptides.

Comparison with IR results in $CDCl_3$ solutions of peptides.

The present chemical shift studies, concentrating on analysis of the amide proton in the $CDCl_3$/DMSO-d_6 mixed solvents, provide much information about HBd structures which the peptides adopt in low-polar solvent such as $CDCl_3$. But as mentioned before, direct evidence of the HBd formation is obtained only by IR spectra. Therefore, it is essential to compare the results of the present NMR studies with the results of the IR studies in Chapter 3.

Figure 5.13 shows a relationship between such ways of assessing HBd formation for some 7-membered HBd forming peptides. Similar plots for the 10-membered and 13-membered HBd structures are shown in Figures 5.14 an 5.15, respectively. In these plots, correlations between the NMR and IR indices can be seen.

HBd structure formation of peptides in DMSO-containing solvents.

As also mentioned before, IR measurements are very difficult in DMSO-containing solutions. On the other hand, NMR measurements are applicable to a wider variety of solvents. Some amide protons which are involved in 10- and 13-membered hydrogen-bonding exhibit somewhat flat chemical shift profiles in the solvent range of $CDCl_3$ fractions between 70%(v/v) and 90%(v/v), where the chemical shifts of other HBfree amide protons change sharply. The flat profiles at rather higher DMSO fractions suggest that the HBd structures remain significantly even in such polar solvents.

In the following chapter, I will introduce another useful NMR index, chemical shift difference between the two α-protons of the Gly residue, in order to challenge the problem of structural flexibility of the peptides in solutions.

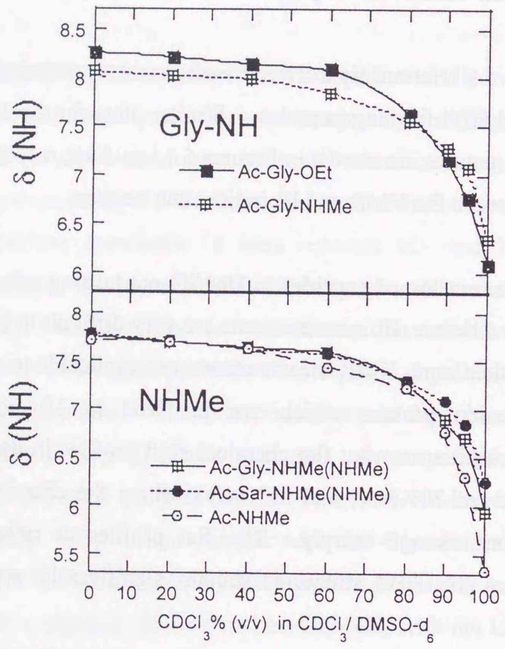

Figure 5.1. Chemical shift variations of amide protons of N-methylacetamide ($NHCH_3$), Ac-Gly-OEt (Gly-NH), Ac-Gly-NHMe (Gly-NH, $NHCH_3$), and Ac-Sar-NHMe (NHCH3) with $CDCl_3$%(v/v) in the $CDCl_3$/DMSO-d_6 mixed solvents.

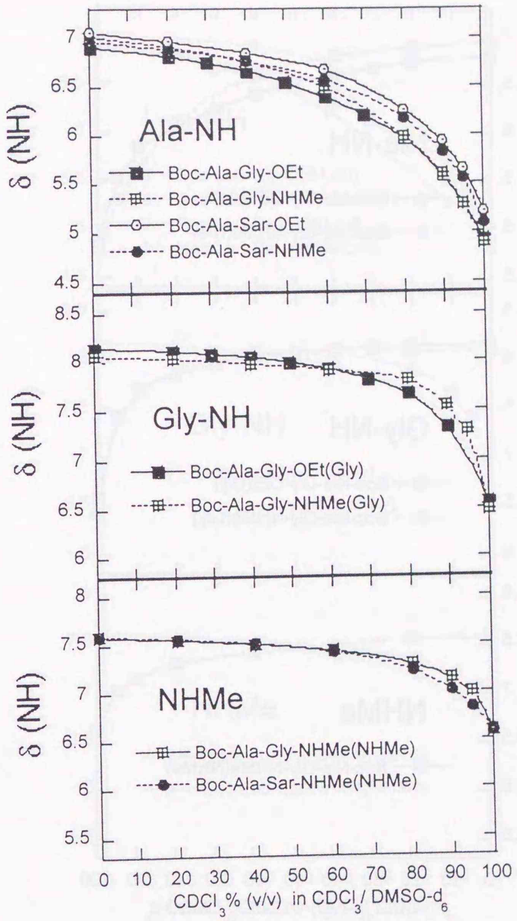

Figure 5.2. Chemical shift variations of amide protons of Boc-Ala-Gly-OEt (Ala-NH, Gly-NH), Boc-Ala-Gly-NHMe (Ala-NH, Gly-NH, $NHCH_3$), Boc-Ala-Sar-OEt (Ala-NH), and Boc-Ala-Sar-NHMe (Ala-NH, $NHCH_3$) with $CDCl_3$%(v/v) in the $CDCl_3$/DMSO-d_6 mixed solvents.

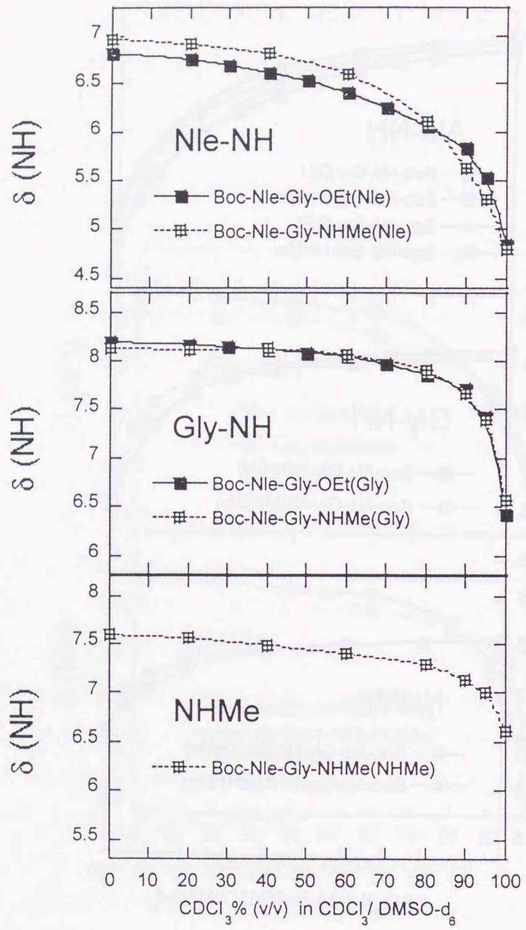

Figure 5.3. Chemical shift variations of amide protons of Boc-Nle-Gly-OEt (Nle-NH, Gly-NH), Boc-Nle-Gly-NHMe (Nle-NH, Gly-NH, $NHCH_3$) with $CDCl_3$%(v/v) in the $CDCl_3$/DMSO-d_6 mixed solvents.

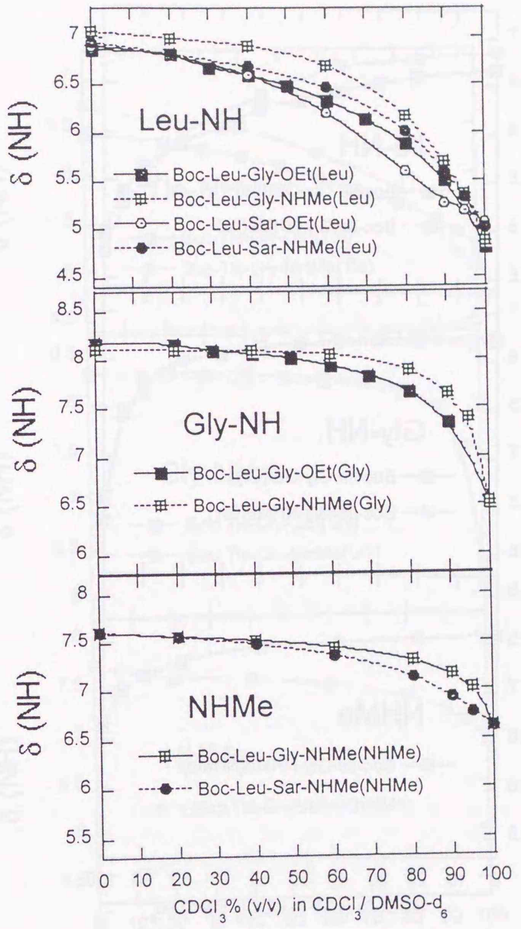

Figure 5.4. Chemical shift variations of amide protons of Boc-Leu-Gly-OEt (Leu-NH, Gly-NH), Boc-Leu-Gly-NHMe (Leu-NH, Gly-NH, $NHCH_3$), Boc-Leu-Sar-OEt (Leu-NH), and Boc-Leu-Sar-NHMe (Leu-NH, $NHCH_3$) with $CDCl_3$%(v/v) in the $CDCl_3$/DMSO-d_6 mixed solvents.

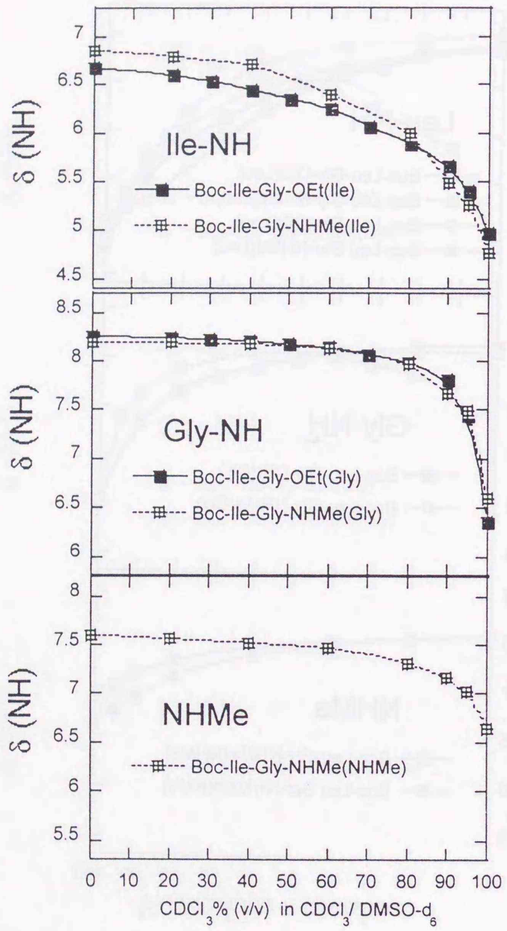

Figure 5.5. Variations of chemical shifts of amide protons of Boc-Ile-Gly-OEt (Ile-NH, Gly-NH), Boc-Ile-Gly-NHMe (Ile-NH, Gly-NH, $NHCH_3$) with $CDCl_3$%(v/v) in the $CDCl_3$/DMSO-d_6 mixed solvent.

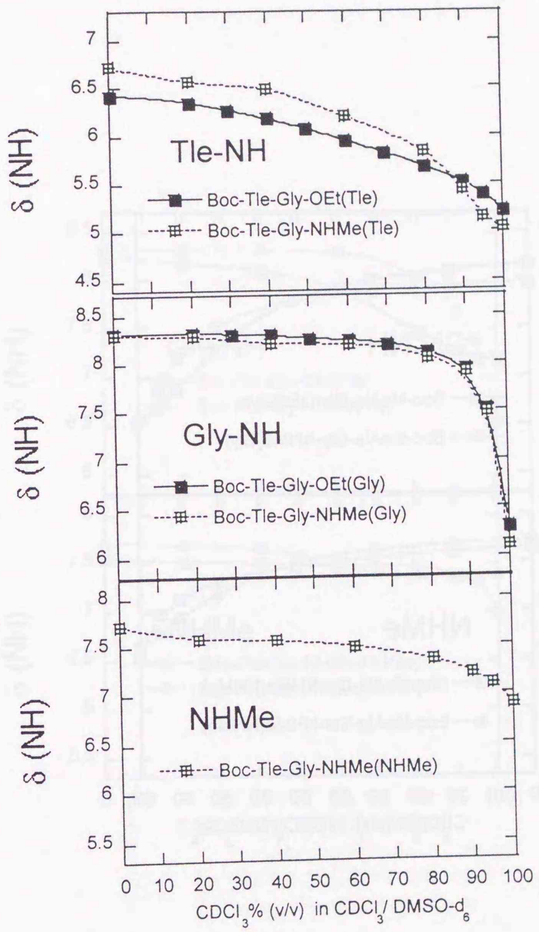

Figure 5.6. Chemical shift variations of amide protons of Boc-Tle-Gly-OEt (Nle-NH, Gly-NH), Boc-Tle-Gly-NHMe (Tle-NH, Gly-NH, $NHCH_3$) with $CDCl_3$%(v/v) in the $CDCl_3$/DMSO-d_6 mixed solvents.

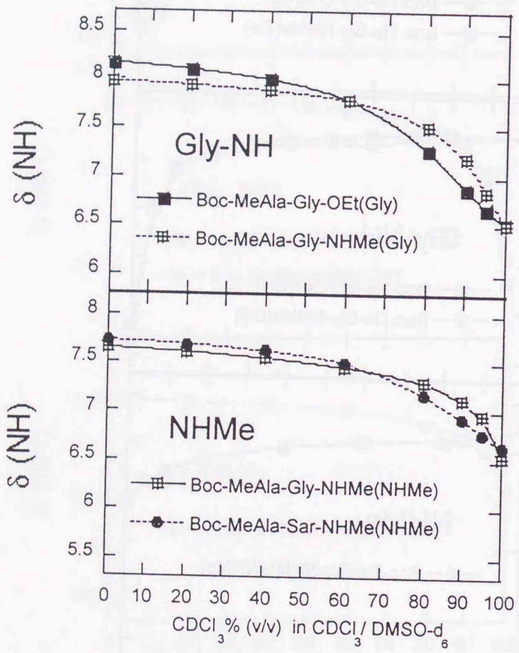

Figure 5.7. Chemical shift variations of amide protons of Boc-MeAla-Gly-OEt (Gly-NH), Boc-MeAla-Gly-NHMe (Gly-NH, $NHCH_3$), and Boc-MeAla-Sar-NHMe ($NHCH_3$) with $CDCl_3$%(v/v) in the $CDCl_3$/DMSO-d_6 mixed solvents.

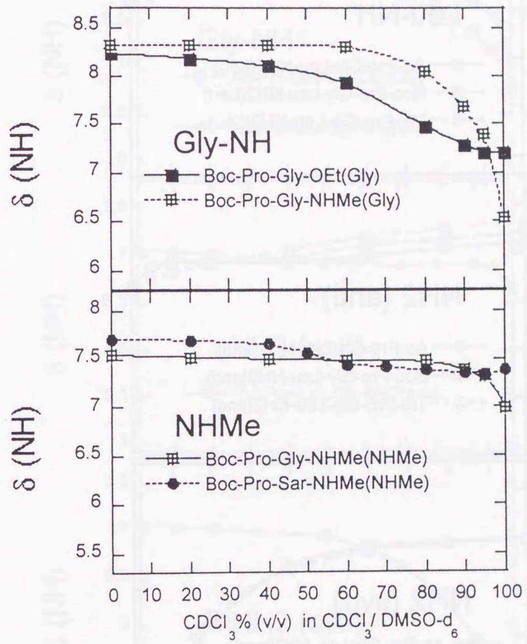

Figure 5.8. Chemical shift variations of amide protons of Boc-Pro-Gly-OEt (Gly-NH), Boc-Pro-Gly-NHMe (Gly-NH, $NHCH_3$), and Boc-Pro-Sar-NHMe ($NHCH_3$) with $CDCl_3$%(v/v) in the $CDCl_3$/DMSO-d_6 mixed solvents.

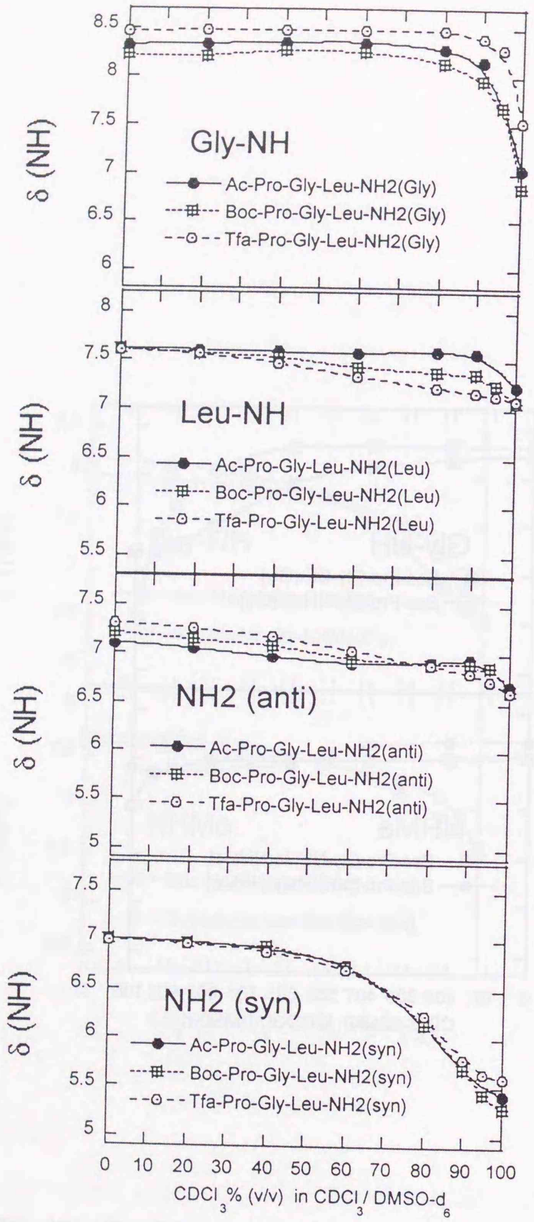

Figure 5.9. Chemical shift variations of amide protons (Gly-NH, Leu-NH, *anti*-NH_2, *syn*-NH_2) of Ac-Pro-Gly-Leu-NH_2, Boc-Pro-Gly-Leu-NH_2, and Tfa-Pro-Gly-Leu-NH_2 with $CDCl_3$%(v/v) in the $CDCl_3$/DMSO-d_6 mixed solvents.

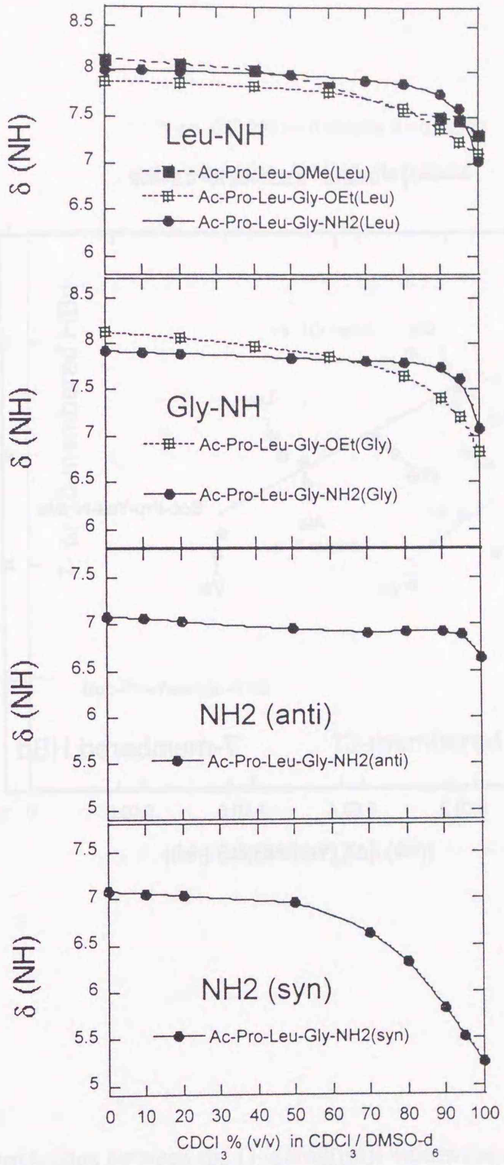

Figure 5.10. Chemical shift variations of amide protons of Ac-Pro-Leu-OMe (Leu-NH), Ac-Pro-Leu-Gly-OEt (Leu-NH, Gly-NH), and Ac-Pro-Leu-Gly-NH_2 (Leu-NH, Gly-NH, *anti*-NH_2, *syn*-NH_2) with $CDCl_3$%(v/v) in the $CDCl_3$/DMSO-d_6 mixed solvents.

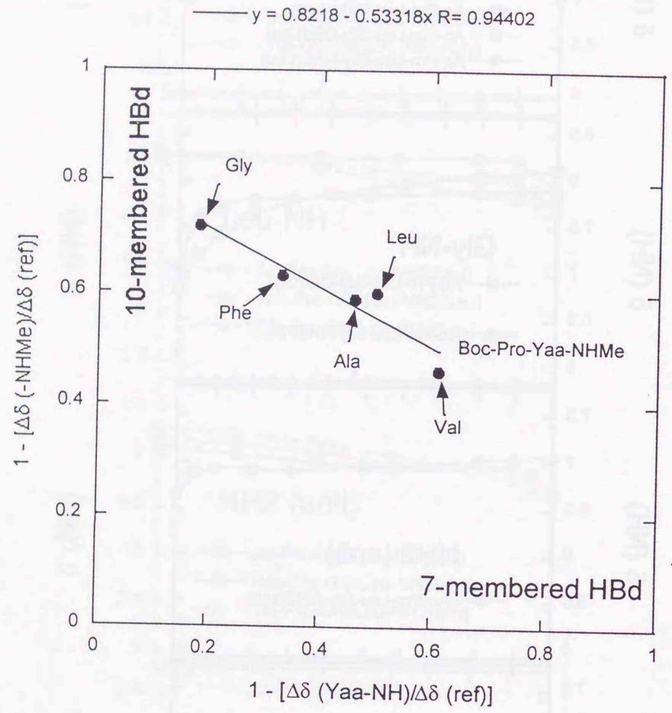

Figure 5.11. Correlations between the [1-$\Delta\delta/\Delta\delta$(ref)] values for Yaa-NH and NHCH3 amide protons of Boc-Pro-Yaa-NHMe peptides.

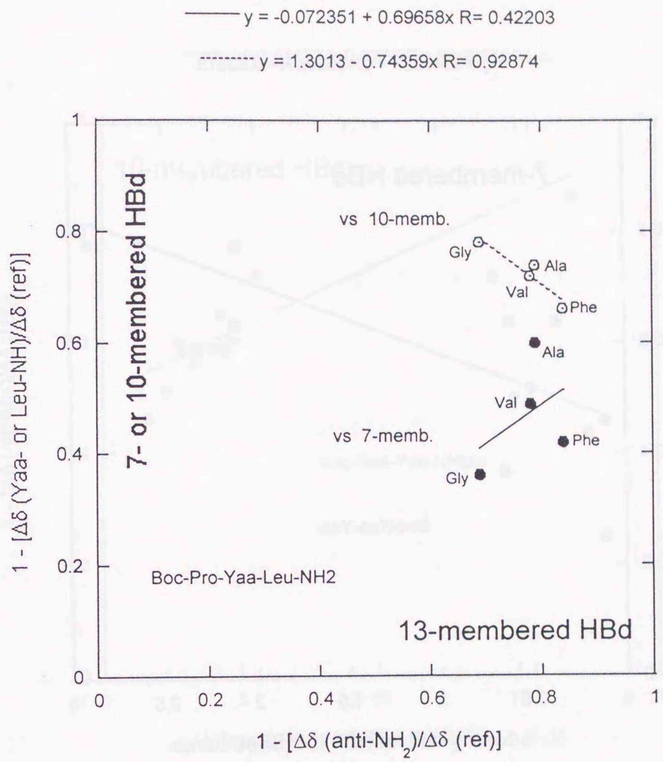

Figure 5.12. Correlations between the [1-$\Delta\delta/\Delta\delta$(ref)] values for *anti*-NH_2 and Yaa-NH amide protons (closed circle), and between those for *anti*-NH_2 and Leu-NH amide protons (open circle) of Boc-Pro-Yaa-Leu-NH_2 peptides.

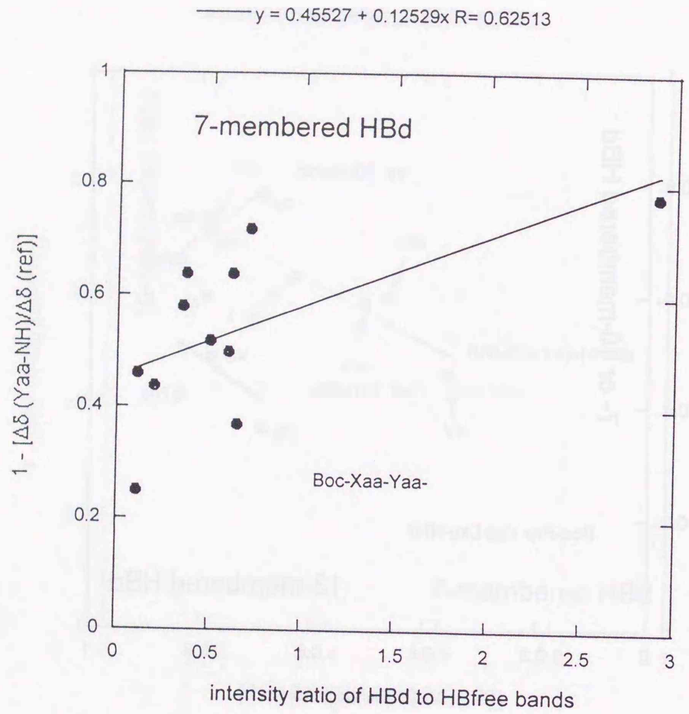

Figure 5.13. Relationships between [1-$\Delta\delta/\Delta\delta$(ref)] values and intensity ratios of the HBd bands to the HBfree bands assigned to the NH stretching of the Yaa-NH group for the peptides with sequences of the Boc-Xaa-Yaa-NHMe and Boc-Xaa-Yaa-Leu-NH_2.

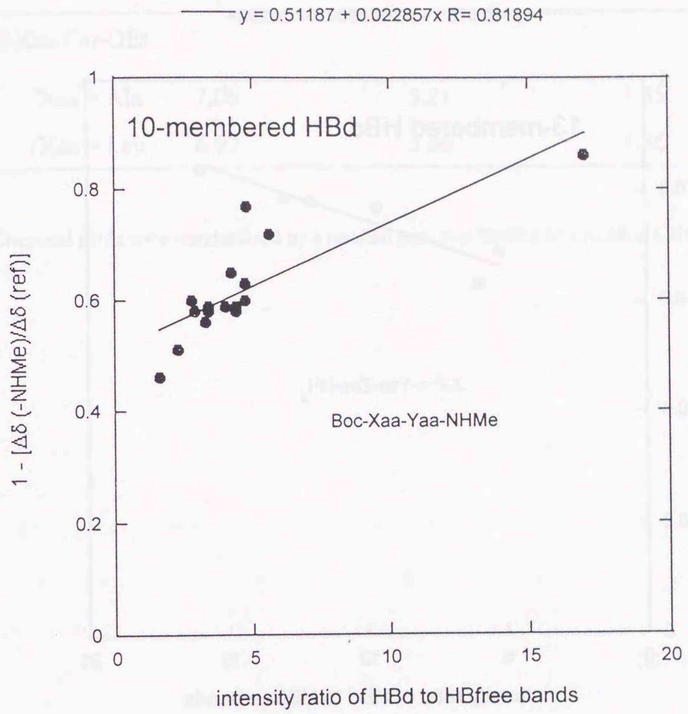

Figure 5.14. Relationships between [1-$\Delta\delta/\Delta\delta$(ref)] values and intensity ratios of the HBd bands to the HBfree bands assigned to the NH stretching of the terminal $NHCH_3$ group for the peptides with a sequence of the Boc-Xaa-Yaa-NHMe.

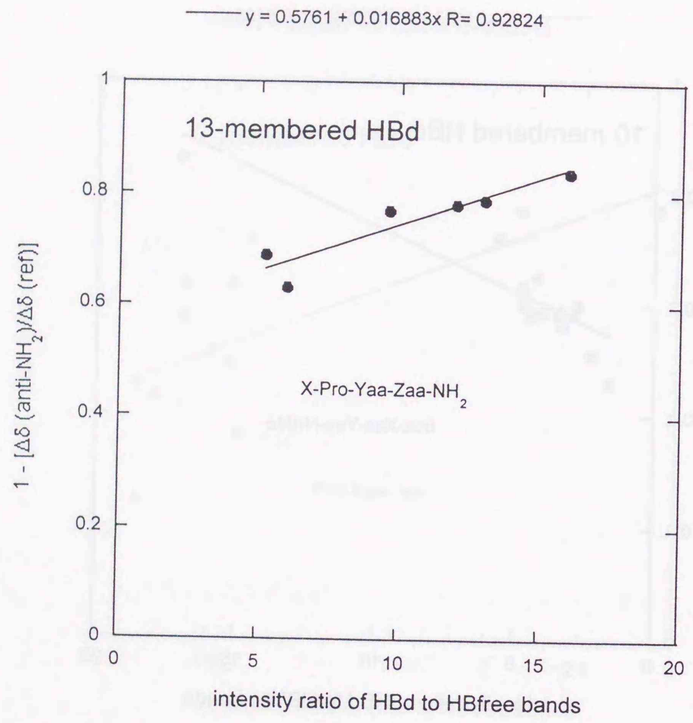

Figure 5.15. Relationships between [1-$\Delta\delta/\Delta\delta$(ref)] values of the *anti*-NH_2 amide protons and intensity ratios of the HBd bands to the HBfree bands assigned to the NH stretchings of the terminal NH_2 group for the peptides with a sequence of the X-Pro-Yaa-Zaa-NH_2.

Table 7. Chemical shifts of the amide protons of peptides.[a]

compound / proton	δ(DMSO)	$\delta(CDCl_3)$	$\Delta\delta = \delta$(DMSO) $- \delta(CDCl_3)$
Boc-Xaa-Sar-OEt			
/Xaa = Ala	7.06	5.21	1.85
/Xaa = Leu	6.92	5.06	1.86

a. Chemical shifts were standardized by a residual proton of DMSO or a residual $CHCl_3$ proton.

Table 8. Chemical shifts of the amide protons of peptides.[a]

compound / proton	δ(DMSO)	$\delta(CDCl_3)$	$\Delta\delta = \delta$(DMSO) $- \delta(CDCl_3)$	$1-(\Delta\delta/\Delta\delta ref)$
Ac-Gly-OEt				
/Gly	8.25	6.08	2.17	0
Boc-Ala-Gly-OEt				
/Ala	6.91	4.91	2.00	–
/Gly	8.15	6.56	1.59	0.27
Boc-Nle-Gly-OEt				
/Nle	6.82	4.85	1.97	–
/Gly	8.19	6.43	1.76	0.19
Boc-Leu-Gly-OEt				
/Leu	6.87	4.80	2.06	–
/Gly	8.18	6.52	1.66	0.25
Boc-Ile-Gly-OEt				
/Ile	6.67	4.98	1.70	–
/Gly	8.25	6.36	1.89	0.13
Boc-Tle-Gly-OEt				
/Tle	6.43	5.21	1.22	–
/Gly	8.32	6.29	2.03	0.06
Boc-MeAla-Gly-OEt				
/Gly	8.17	6.54	1.63	0.25
Boc-Pro-Gly-OEt				
/Gly	8.24	7.20	1.04	0.52
Ac-Pro-Gly-OEt				
/Gly	8.21	7.52	0.69	0.68

a. Chemical shifts were standardized by a residual proton of DMSO or a residual $CHCl_3$ proton.

Table 9. Chemical shifts of the amide protons of peptides.[a]

compound / proton	δ(DMSO)	$\delta(CDCl_3)$	$\Delta\delta = \delta$(DMSO) $- \delta(CDCl_3)$	$1-(\Delta\delta/\Delta\delta ref)$
Ac-NHMe				
(N-Methylacetamide)				
/NHMe	7.71	5.34	2.37	0
Ac-Sar-NHMe				
/NHMe	7.77	6.27	1.50	0.37
Boc-Ala-Sar-NHMe				
/Ala	6.97	5.09	1.87	–
/NHMe	7.60	6.59	1.01	0.58
Boc-Leu-Sar-NHMe				
/Leu	6.95	5.01	1.94	–
/NHMe	7.62	6.62	1.00	0.58
Boc-MeAla-Sar-NHMe				
/NHMe	7.72	6.66	1.06	0.56
Boc-Pro-Sar-NHMe				
/NHMe	7.72	7.38	0.33	0.86

a. Chemical shifts were standardized by a residual proton of DMSO or a residual $CHCl_3$ proton.

Table 10. Chemical shifts of the amide protons of peptides.[a]

compound / proton	δ(DMSO)	δ($CDCl_3$)	$\Delta\delta = \delta$(DMSO) $- \delta$($CDCl_3$)	$1-(\Delta\delta/\Delta\delta ref)$
Ac-NHMe				
/NHMe	7.71	5.34	2.37	0
Ac-Gly-OEt				
/Gly	8.25	6.08	2.17	0
Ac-Gly-NHMe				
/Gly	8.06	6.29	1.77	0.19
/NHMe	7.72	5.94	1.78	0.25
Boc-Ala-Gly-NHMe				
/Ala	7.01	4.89	2.12	–
/Gly	8.07	6.48	1.58	0.27
/NHMe	7.59	6.58	1.00	0.58
Boc-Nle-Gly-NHMe				
/Nle	6.97	4.80	2.17	–
/Gly	8.13	6.57	1.56	0.28
/NHMe	7.59	6.61	0.98	0.59
Boc-Leu-Gly-NHMe				
/Leu	7.06	4.87	2.19	–
/Gly	8.12	6.53	1.59	0.27
/NHMe	7.61	6.63	0.98	0.59
Boc-Ile-Gly-NHMe				
/Ile	6.86	4.76	2.10	–
/Gly	8.19	6.60	1.59	0.27
/NHMe	7.60	6.64	0.97	0.60
Boc-Tle-Gly-NHMe				
/Tle	6.72	5.04	1.69	–
/Gly	8.30	6.11	2.19	0
/NHMe	7.72	6.90	0.83	0.65
Boc-MeAla-Gly-NHMe				
/Gly	7.97	6.52	1.46	0.33
/NHME	7.72	6.56	1.16	0.51
Boc-Pro-Gly-NHMe				
/Gly	8.32	6.54	1.78	0.18
/NHMe	7.55	7.00	0.55	0.77
Ac-Pro-Gly-NHMe				
/Gly	8.21	6.99	1.22	0.44
/NHMe	7.56	6.89	0.67	0.72

a. Chemical shifts were standardized by a residual proton of DMSO or a residual $CHCl_3$ proton.

Table 11. Chemical shifts of the amide protons of peptides.[a]

compound / proton	δ(DMSO)	δ($CDCl_3$)	$\Delta\delta = \delta$(DMSO) $- \delta$($CDCl_3$)	$1-(\Delta\delta/\Delta\delta ref)$
Ac-Yaa-OEt				
/Yaa = Gly	8.25	6.08	2.17	0
/Yaa = Ala	8.23	6.02	2.21	0
/Yaa = Leu	8.17	5.78	2.40	0
/Yaa = Val	8.08	5.90	2.18	0
/Yaa = Phe	8.33	5.86	2.47	0
Boc-Pro-Yaa-OEt				
/Yaa = Gly	8.24	7.20	1.04	0.52
/Yaa = Ala	8.24	7.30	0.94	0.58
/Yaa = Leu	8.16	7.30	0.86	0.64
/Yaa = Val	8.05	7.44	0.61	0.72
/Yaa = Phe	8.19	7.30	0.89	0.64

a. Chemical shifts were standardized by a residual proton of DMSO or a residual $CHCl_3$ proton.

Table 12. Chemical shifts of the amide protons of peptides.[a]

compound / proton	δ(DMSO)	δ($CDCl_3$)	$\Delta\delta = \delta$(DMSO) $- \delta$($CDCl_3$)	$1-(\Delta\delta/\Delta\delta ref)$
Boc-Pro-Gly-NHMe				
/Gly	8.32	6.54	1.78	0.18
/NHMe	7.55	7.00	0.55	0.77
Boc-Pro-Ala-NHMe				
/Ala	7.93	6.71	1.23	0.46
/NHMe	7.63	6.66	0.96	0.59
Boc-Pro-Leu-NHMe				
/Leu	7.84	6.64	1.19	0.50
/NHMe	7.62	6.67	0.96	0.60
Boc-Pro-Val-NHMe				
/Val	7.68	6.83	0.85	0.61
/NHMe	7.83	6.55	1.29	0.46
Boc-Pro-Phe-NHMe				
/Phe	7.89	6.22	1.67	0.33
/NHMe	7.60	6.71	0.89	0.63

a. Chemical shifts were standardized by a residual proton of DMSO or a residual $CHCl_3$ proton.

Table 13. Chemical shifts of the amide protons of peptides.[a]

compound / proton	δ(DMSO)	δ($CDCl_3$)	$\Delta\delta = \delta$(DMSO) $- \delta$($CDCl_3$)	$1-(\Delta\delta/\Delta\delta ref)$
Ac-NH_2				
/NH_2 (*anti*)	7.25	5.38	1.87	0
/ NH_2 (*syn*)	6.97	5.24	1.73	0
Boc-Pro-Gly-Leu-NH_2				
/Gly	8.22	6.86	1.36	0.36
/Leu	7.61	7.08	0.53	0.78
/NH_2 (*anti*)	7.21	6.64	0.58	0.69
/NH_2 (*syn*)	7.01	5.30	1.71	0.01
Boc-Pro-Ala-Leu-NH_2				
/Ala	8.06	7.18	0.88	0.60
/Leu	7.62	7.00	0.62	0.74
/NH_2 (*anti*)	7.15	6.75	0.40	0.79
/NH_2 (*syn*)	6.98	5.19	1.79	0
Boc-Pro-Val-Leu-NH_2				
/Val	7.71	6.59	1.12	0.49
/Leu	7.77	7.10	0.67	0.72
/NH_2 (*anti*)	7.17	6.80	0.41	0.78
/NH_2 (*syn*)	6.95	5.18	1.77	0
Boc-Pro-Phe-Leu-NH_2				
/Phe	7.86	6.43	1.43	0.42
/Leu	7.78	6.96	0.82	0.66
/NH_2 (*anti*)	7.03	6.72	0.31	0.84
/NH_2 (*syn*)	6.97	5.16	1.81	0
Ac-Pro-Gly-Leu-NH_2				
/Gly	8.32	7.04	1.28	0.41
/Leu	7.62	7.24	0.38	0.84
/NH_2 (*anti*)	7.11	6.68	0.43	0.77
/NH_2 (*syn*)	7.01	5.43	1.58	0.08
Tfa-Pro-Gly-Leu-NH_2				
/Gly	8.47	7.54	0.93	0.57
/Leu	7.60	7.10	0.50	0.79
/NH_2 (*anti*)	7.31	6.62	0.69	0.63
/NH_2 (*syn*)	6.99	5.61	1.38	0.19

a. Chemical shifts were standardized by a residual proton of DMSO or a residual $CHCl_3$ proton.

Table 14. Chemical shifts of the amide protons of peptides.[a]

compound / proton	δ(DMSO)	$\delta(CDCl_3)$	$\Delta\delta = \delta$(DMSO) $- \delta(CDCl_3)$	$1-(\Delta\delta/\Delta\delta ref)$
Ac-Pro-Leu-OMe				
/Leu	8.13	7.31	0.82	0.66
Ac-Pro-Leu-Gly-OEt				
/Leu	7.89	7.11	0.78	0.67
/Gly	8.13	6.82	1.31	0.40
Ac-Pro-Leu-Gly-NH_2				
/Leu	8.02	7.03	0.99	0.59
/Gly	7.92	7.09	0.83	0.62
/NH_2 (*anti*)	7.08	6.63	0.45	0.77
/NH_2 (*syn*)	7.08	5.25	1.83	0

a. Chemical shifts were standardized by a residual proton of DMSO or a residual $CHCl_3$ proton.

Chart 8: Characterized HBd structure (1)

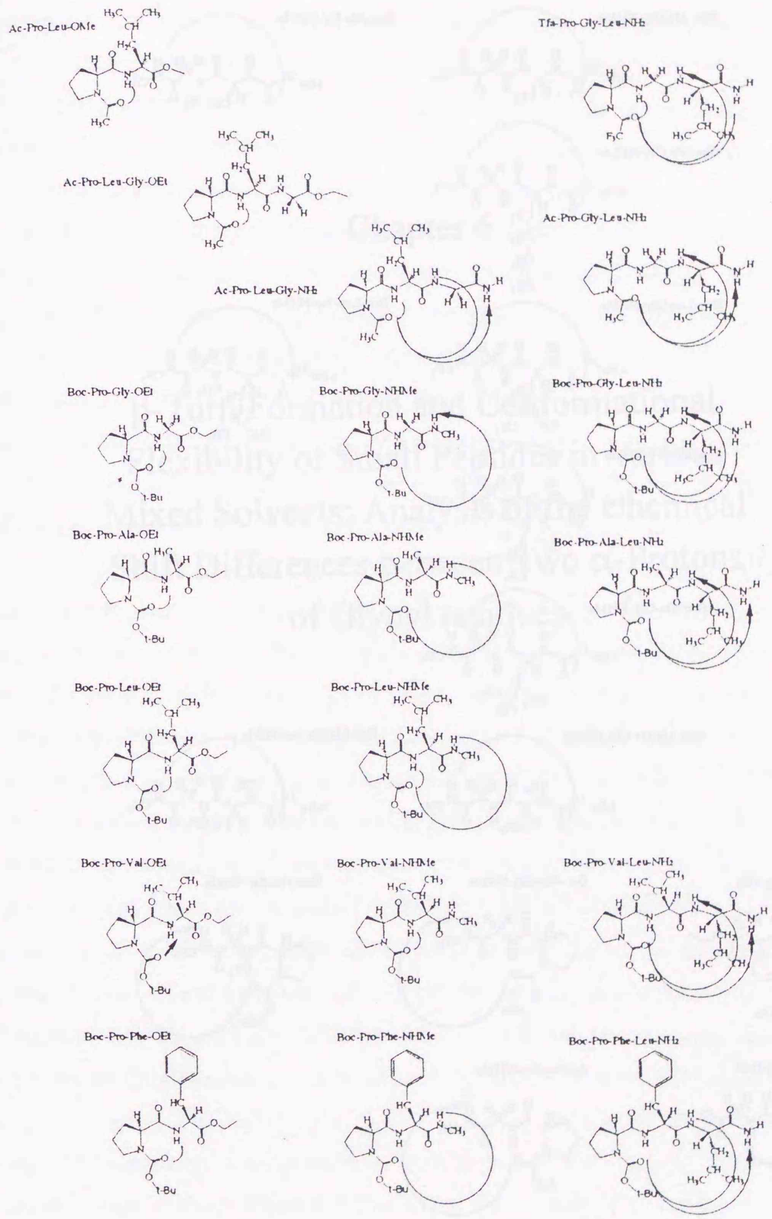

Chart 9: Characterized HBd structure (2)

Boc-Ala-Gly-NHMe

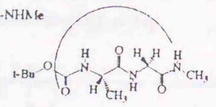

Boc-Ala-Sar-NHMe

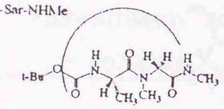

Boc-Nle-Gly-NHMe

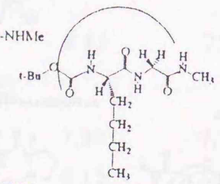

Boc-Leu-Gly-NHMe

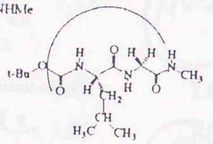

Boc-Leu-Sar-NHMe

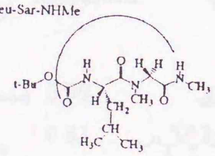

Boc-Ile-Gly-NHMe

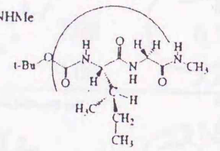

Boc-Tle-Gly-NHMe

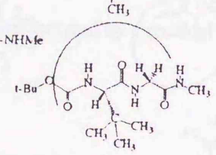

Boc-MeAla-Gly-NHMe

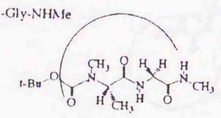

Boc-MeAla-Sar-NHMe

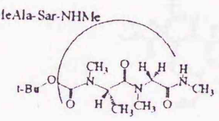

Boc-Pro-Gly-OEt

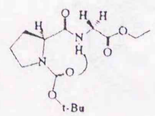

Boc-Pro-Gly-NHMe

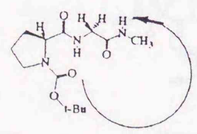

Boc-Pro-Sar-NHMe

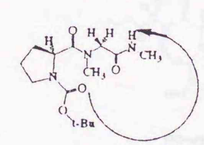

Ac-Pro-Gly-OEt

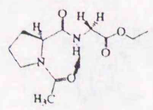

Ac-Pro-Gly-NHMe

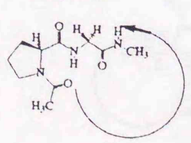

Chapter 6

β-Turn Formation and Conformational Flexibility of Small Peptides in Various Mixed Solvents: Analysis of the Chemical Shift Differences between Two α-Protons of Glycyl residues

Introduction:

So far, I have found a few types of intramolecular HBd structures for various small peptides in $CDCl_3$ in Chapter 3, and then found that the *cis*-to-*trans* isomerizations of the proline imide bonds of the peptides are facilitated by formations of the HBd structures, directing toward more stable secondary structures as written in Chapter 4. Furthermore, solvent-dependent chemical shift changes of amide protons have been analyzed using the $CDCl_3$/DMSO-d_6 mixed solvents in Chapter 5, and it has been shown that the magnitudes of the chemical shift changes are consistent with the degrees of stabilities of the HBd structures estimated from relative intensities of the IR bands.

The direct evidence of the hydrogen bonds is only given from the IR spectra, but the measurements of IR spectra were difficult for the DMSO-containing solutions. The NMR measurements, on the other hand, can be conducted with much less restrictions of solvent and provide various information about the secondary structures of the proline-containing peptides under polar solvent conditions such as in the $CDCl_3$/DMSO-d_6 mixed solvents.

In the present chapter, I will notice the glycyl two α-protons for assessing flexibility of peptide backbone around this residue by NMR. In protein molecules, the two α-protons of some Gly residues are found to have remarkably different chemical $\Delta\delta_{\alpha/\alpha'}$ shifts from each other.[66-69] The two α-protons can have such different chemical shifts if they are placed in magnetically non-identical environments sustained long enough on the NMR time scale. The different environments will be mainly caused by difference in position between the two α-protons relative to nearby C=O groups. Therefore, the chemical shift difference between the two α-protons of the Gly residue, $\Delta\delta_{\alpha/\alpha'}$, will provide useful information about flexibility of the local backbone structure around the Gly residue of a peptide. However, little attention has so far been paid to $\Delta\delta_{\alpha/\alpha'}$ except for a limited number of semi-empirical and *ab initio* calculations.[70-72] Therefore, $\Delta\delta_{\alpha/\alpha'}$ has been little utilized for analysis of conformational flexibility of small peptides to our knowledge.

In this work, proton NMR spectra of various peptides have been measured under a wide range of solvent conditions, and it is shown that magnitudes of $\Delta\delta_{\alpha/\alpha'}$ of the Gly or the N-methylglycyl (Sar) residues can be specific indices of the β-turn structure.

Using these $\Delta\delta_{\alpha/\alpha'}$ indices, some thermodynamic properties for the β-turn formation of the peptides are discussed in terms of solvent effects and contribution of each amino acid residue in a sequence.

Experimental:

NMR Measurements. Methods of NMR measurements and assignments are the same as described in Chapter 4. In short, all the chemical shifts were standardized by using a residual DMSO proton signal (2.49 ppm) for solutions in $CDCl_3$/DMSO-d_6 and in the DMSO-d_6/D_2O, a residual $CHCl_3$ proton signal (7.24 ppm) for solutions in pure $CDCl_3$, and a residual HDO signal (4.63 ppm) for solutions in pure D_2O. For other kinds of mixed solvents, a residual acetonitrile (1.93 ppm) in $CDCl_3$/acetonitrile-d_3, a residual CH_3OD (4.78 ppm) in $CDCl_3$/methanol-d_4, and a residual $(CH_3)_2CO$ (2.04 ppm) in $CDCl_3$/acetone-d_6 were used, respectively.

When a peptide has more than single configurational isomers about the imide linkages, only the result for only the *trans* isomer is discussed. Assignments of all the NMR signals have been conducted by COSY and NOESY as described in Chapter 4.

ABX spin systems. In this chapter, I will discuss chemical shifts of two glycyl α-protons (Gly-α/α') of each peptide. The Gly-α/α' protons, in general, give eight distinct lines which are characteristic of A and B protons in an ABX spin system (see Figure 6.1). These eight lines can be divided into two analogous sets, each of which is composed of four resonance lines, and are hereafter donated by subscripts, A, B, C, and D, a, b, c, and d. The resonance frequencies are given as follows:[73]

$$\nu_A = \overline{\nu} + [(+2J_{gem} + J_+ + J_-)/4] + D_l,$$
$$\nu_B = \overline{\nu} + [(-2J_{gem} + J_+ + J_-)/4] + D_l,$$
$$\nu_C = \overline{\nu} + [(+2J_{gem} + J_+ + J_-)/4] - D_l,$$
$$\nu_D = \overline{\nu} + [(-2J_{gem} + J_+ + J_-)/4] - D_l,$$
$$\nu_a = \overline{\nu} + [(+2J_{gem} - J_+ - J_-)/4] + D_i,$$
$$\nu_b = \overline{\nu} + [(-2J_{gem} - J_+ - J_-)/4] + D_i,$$
$$\nu_c = \overline{\nu} + [(+2J_{gem} - J_+ - J_-)/4] - D_i,$$

$$\nu_d = \overline{\nu} + [(-2J_{gem} - J_+ - J_-)/4] - D_i,$$

where $\overline{\nu}$ is the average of the eight frequencies.

$$\overline{\nu} = (\nu_A + \nu_B + \nu_C + \nu_D + \nu_a + \nu_b + \nu_c + \nu_d)/8,$$

J_{gem} is a geminal coupling constant between the two α-protons (Gly-α/α'), J_+ and J_- are vicinal coupling constants of the Gly-α and Gly-α', respectively, with the Gly-NH proton, D_l and D_i are given by

$$D_l = 1/2 \cdot [\{(\Delta\nu) + (\Delta J/2)\}^2 + (J_{gem})^2]^{1/2},$$

$$D_i = 1/2 \cdot [\{(\Delta\nu) - (\Delta J/2)\}^2 + (J_{gem})^2]^{1/2}.$$

Here, $\Delta\nu$ and ΔJ are the differences in chemical shift and vicinal coupling constant, respectively, between the two α-protons and given as follows:

$$\Delta\nu = 1/2 \cdot [\{(2D_l)^2 - (J_{gem})^2\}^{1/2} + \{(2D_i)^2 - (J_{gem})^2\}^{1/2}]$$

$$= 1/2 \cdot [\{(\nu_A - \nu_D)(\nu_B - \nu_C)\}^{1/2} + \{(\nu_a - \nu_d)(\nu_b - \nu_c)\}^{1/2}],$$

$$\Delta J = \{(2D_l)^2 - (J_{gem})^2\}^{1/2} - \{(2D_i)^2 - (J_{gem})^2\}^{1/2}$$

$$= \{(\nu_A - \nu_D)(\nu_B - \nu_C)\}^{1/2} - \{(\nu_a - \nu_d)(\nu_b - \nu_c)\}^{1/2}.$$

Then the chemical shifts of the two glycyl α-protons and the vicinal coupling constants are given by

$$\delta_+ = \{\overline{\nu} + (\Delta\nu/2)\}/\nu_0,$$

$$\delta_- = \{\overline{\nu} - (\Delta\nu/2)\}/\nu_0,$$

$$J_+ = [\{(\nu_A + \nu_B + \nu_C + \nu_D) - (\nu_a + \nu_b + \nu_c + \nu_d)\}/4] + (\Delta J/2),$$

$$J_- = [\{(\nu_A + \nu_B + \nu_C + \nu_D) - (\nu_a + \nu_b + \nu_c + \nu_d)\}/4] - (\Delta J/2),$$

Where ν_0 is the frequency of externally applied magnetic field, 400 MHz in the present measurements. Then the chemical shift difference between the two α-protons, $\Delta\delta$, is given from observed chemical shifts, $\delta_i = (\nu_0 - \nu_i)/\nu_0$,

$$\Delta\delta = \delta_+ - \delta_-$$

$$= 1/2 \cdot [\{(\delta_A - \delta_D)(\delta_B - \delta_C)\}^{1/2} + \{(\delta_a - \delta_d)(\delta_b - \delta_c)\}^{1/2}].$$

AB spin systems. In both cases of the Gly-α/α' in D_2O-containing solvents and of the *N*-methylglycyl residues (Sar-α/α'), two α-protons exhibit signal splitting into four distinct lines as seen in Figure 6.1. This signal splitting is characteristic of an AB spin system. The four resonance frequencies of the AB spin system, referred to as peaks 1, 2, 3, and 4 in the order of frequencies, are given as follows:[73]

$$\nu_1 = \overline{\nu} + D + (J_{gem}/2),$$

$$\nu_2 = \overline{\nu} + D - (J_{gem}/2),$$

$$\nu_3 = \overline{\nu} - D + (J_{gem}/2),$$

$$\nu_4 = \overline{\nu} - D - (J_{gem}/2),$$

where $\overline{\nu}$ is the average of the four frequencies,

$$\overline{\nu} = (\nu_1 + \nu_2 + \nu_3 + \nu_4)/4,$$

J_{gem} a geminal coupling constant between the two protons, and D is given by

$$D = 1/2 \cdot \{(J_{gem})^2 + (\Delta\nu)^2\}^{1/2}.$$

Therefore, the chemical shift difference between the two protons, $\Delta\delta$, is given from observed chemical shifts,

$$\Delta\delta = \Delta\nu/\nu_0$$

$$= \{(\nu_1 - \nu_4)(\nu_2 - \nu_3)\}^{1/2}/\nu_0$$

$$= \{(\delta_1 - \delta_4)(\delta_2 - \delta_3)\}^{1/2},$$

where δ_i is a shift of the *i*-th resonance line. Then the chemical shifts for the two protons are given by

$$\delta_+ = \{\delta_1 + \delta_2 + \delta_3 + \delta_4\}/4\} + (\Delta\delta/2),$$

$$\delta_- = \{\delta_1 + \delta_2 + \delta_3 + \delta_4\}/4\} - (\Delta\delta/2).$$

Results:

NMR spectra of peptides with an ABX or an AB spin system.

Figure 6.2 shows 400 MHz proton NMR spectra of some Gly-containing peptides and Boc-Pro-Sar-NHMe under the same solvent condition at 25°C. In the Gly-α/α' region of Ac-Gly-NHMe, a doublet signal which is split by vicinal coupling of the α-protons with the Gly-NH proton is observed with $J_+ = J_- = 6.2$ Hz. This fact indicates that the two Gly-α/α'protons of Ac-Gly-NHMe are magnetically equivalent to each other on the NMR time scale. For other three peptides, on the other hand, the signal splittings of the Gly-α/α'or Sar-α/α'protons are found to be characteristic of the ABX or AB spin systems, respectively. Spectral patterns for the two α-protons are different among the peptides. This is caused by difference in both configurational and conformational restrictions sustainable on the NMR time scale, as discussed in the following.

Boc-Xaa-Gly-OEt (Xaa = Ala, Nle, Leu, Ile, Tle, MeAla, Pro).

In Figures 6.3, chemical shift obtained for each of the two Gly-α/α' protons of Boc-Ala-Gly-OEt are plotted against solvent mixing ratios of three kinds of mixed solvents, DMSO-d_6/D_2O, $CDCl_3$/DMSO-d_6, and CCl_4/$CDCl_3$. The shift values of the two Gly-α/α' protons are different from each other under all solvent conditions investigated, but chemical shift differences between the two protons, $\Delta\delta_{\alpha/\alpha'}$, are smaller than 0.1 ppm.

The similar tendencies are observed for other related peptides, Boc-Nle-Gly-OEt, Boc-Leu-Gly-OEt, Boc-Ile-Gly-OEt, and Boc-Tle-Gly-OEt, as shown in Figures 6.4 to 6.7. The IR spectra of these peptides in $CDCl_3$ solutions, shown in Chapter 3, have indicated that Boc-Xaa-Gly-OEt peptides, except MeAla and Pro for Xaa, do not form 7-membered HBd structures to an appreciable degree. The $\Delta\delta_{\alpha/\alpha'}$ values listed in Table 15 for these peptides are different according to side chain bulkiness of the Xaa residues. For instance, a bulkier Ile residue precedent to the Gly residue makes the $\Delta\delta_{\alpha/\alpha'}$ value larger than the Nle and Leu residues. This is more obvious for the bulkiest Tle residue which yields the largest $\Delta\delta_{\alpha/\alpha'}$ value.

In Boc-MeAla-Gly-OEt (*trans* isomer), which can form a 7-membered HBd structure in $CDCl_3$, the solvent-dependent changes in chemical shift of the two Gly-α/α' protons are slightly larger (Figure 6.8), but the $\Delta\delta_{\alpha/\alpha'}$ value is at most 0.23 ppm. In addition, Boc-Pro-Gly-OEt (*trans* isomer) which is also found to take a 7-membered HBd structure in a $CDCl_3$ solution, exhibits less remarkable solvent-dependence. Therefore, the magnitude of $\Delta\delta_{\alpha/\alpha'}$ is not related with formation of the 7-membered HBd structure, which is thought to be like the γ-turn structure.

Boc-Xaa-Gly-NHMe (Xaa = Ala, Nle, Leu, Ile, Tle, MeAla, Pro).

The solvent-dependent change in chemical shifts of the two Gly-α/α' protons of Boc-Ala-Gly-NHMe shown in Figures 6.10 is larger than that of Boc-Ala-Gly-OEt shown in Figure 6.3. Other Boc-Xaa-Gly-NHMe (Xaa = Nle, Leu, Ile, Tle, MeAla, Pro) peptides show the similar solvent-dependencies, as shown in Figures 6.11 to 6.16. The $\Delta\delta_{\alpha/\alpha'}$ values of these peptides increase with increasing fraction of the lower-polarity solvent component in both the DMSO-d_6/D_2O and $CDCl_3$/DMSO-d_6

mixed solvents. Among these peptides, Boc-Pro-Gly-NHMe and Boc-Tle-Gly-NHMe have particularly remarkable solvent-dependent changes in $\Delta\delta_{\alpha/\alpha'}$ values.

The increase in $\Delta\delta_{\alpha/\alpha'}$ values in the range of lower solvent polarity is expected to be related with formation of a β-turn structure, the hydrogen bond of which is characterized by IR (Chapter 3) and NMR (Chapter 4, 5) studies. The relationship between the $\Delta\delta_{\alpha/\alpha'}$ value and the type of HBd structures is discussed later.

Boc-Xaa-Sar-OEt (Xaa = Ala, Leu, MeAla, Pro).

Similar plots for four kinds of Boc-Xaa-Sar-OEt (Xaa = Ala, Leu, MeAla, Pro) peptides are shown in Figures 6.17 to 6.20. Obviously the solvent-dependent-change of the $\Delta\delta_{\alpha/\alpha'}$ value for Boc-Pro-Sar-OEt is much more remarkable than those for other three peptides. Since Boc-Pro-Sar-OEt has no NH group which could participate in hydrogen-bonding, such change in the $\Delta\delta_{\alpha/\alpha'}$ value with lowering solvent polarity is not attributed to the intramolecular hydrogen bonding, but should be attributed to an acquisition of some regular backbone structure which is stabilized under low-polarity conditions.

Boc-Xaa-Sar-NHMe (Xaa = Ala, Leu, MeAla, Pro).

Similar plots for four kinds of Boc-Xaa-Sar-NHMe (Xaa = Ala, Leu, MeAla, Pro) peptides are shown in Figures 6.21 to 6.24. From IR (Chapter 3) and NMR (Chapter 5) studies, it is shown that these peptides from considerably stable β-turn structures in $CDCl_3$.

Solvent-dependent changes of $\Delta\delta_{\alpha/\alpha'}$ for Ala-containing peptides.

Figure 6.25 shows solvent-dependent changes in the $\Delta\delta_{\alpha/\alpha'}$ values for four kinds of Ala-containing peptides. The data are plotted against dielectric constants of three kinds of mixed solvents, DMSO-d_6/D_2O (calculated range of ε: 78.3-46.7), $CDCl_3$/DMSO-d_6 (46.7-4.9), and CCl_4/$CDCl_3$ (4.9-2.3). Except for Boc-Ala-Gly-OEt, the $\Delta\delta_{\alpha/\alpha'}$ values increase as the solvent dielectric constants decrease, and magnitudes of their changes are different from one another. For Boc-Ala-Sar-NHMe, a steep transition of the $\Delta\delta_{\alpha/\alpha'}$ values is found in the ε range of 30 to 5, and for Boc-Ala-Sar-OEt such a steep transition is seen in the lower ε range. The different

chemical shifts of the two sarcosyl α-protons are due to their different structural environments which are sustained long enough on the NMR time scale. Therefore, the $\Delta\delta_{\alpha/\alpha'}$ values will tell about how rigid the backbone dihedral angles around the Sar residue are in solutions. Thee large increase in the $\Delta\delta_{\alpha/\alpha'}$ value in the solvent with lowering polarity, observed for Boc-Ala-Sar-NHMe, indicated that the dihedral angles of the Sar residue become more restricted through formation of a certain regular secondary structure, probably the β-turn.

A large increase in $\Delta\delta_{\alpha/\alpha'}$ is also observed for Boc-Ala-Sar-OEt in spite of absence of HBd structure. The fact suggests that some interaction different from the intramolecular hydrogen bonding operate to restrict the backbone dihedral angles of the Sar residue in Boc-Ala-Sar-OEt as for Boc-Pro-Sar-OEt mentioned before.

Boc-Ala-Gly-NHMe also shows a similar solvent-dependent transition of the $\Delta\delta_{\alpha/\alpha'}$ value, but the increase in the $\Delta\delta_{\alpha/\alpha'}$ is much smaller than that of Boc-Ala-Sar-NHMe. The IR results have shown that the β-turn-like 10-membered HBd structure of Boc-Ala-Gly-NHMe is as stable as that of Boc-Ala-Sar-NHMe. However, the smaller $\Delta\delta_{\alpha/\alpha'}$ value of Boc-Ala-Gly-NHMe indicates that the backbone structure around the Gly residue of this peptide is more flexible and thus the observed $\Delta\delta_{\alpha/\alpha'}$ value is the average of the values of a wide range of conformations occurring during the observation period of NMR. As being well known, the NMR time scale is very long with a time resolution from several milliseconds to a few seconds, while the time scale for breaking and reforming of the intramolecular hydrogen-bonds in solution will be much shorter than the NMR time scale. Therefore, the $\Delta\delta_{\alpha/\alpha'}$ value provides an index of rigidity of the backbone structure, *e.g.*, an extent to which a peptide backbone is restricted to the β-turn geometry. The β-turn geometry is expected to yield a large intrinsic $\Delta\delta_{\alpha/\alpha'}$ value.

Leu-peptides series.

Figure 6.26 shows the solvent-dependent change of $\Delta\delta_{\alpha/\alpha'}$ values for a series of Leu-containing peptides. The differences in transitions of $\Delta\delta_{\alpha/\alpha'}$ values between Leu-containing peptides are similar to those for corresponding Ala-containing peptides mentioned above.

MeAla-containing peptides.

Figure 6.27 shows the similar tendencies for a series of MeAla-containing peptides. In these plots, results for the *trans* isomers about the imide bonds preceding the MeAla residues are indicated.

Pro-peptides series.

As shown in Figure 6.28, a series of Pro-containing peptides exhibit the similar tendencies as mentioned above. But a magnitude of the solvent-dependent $\Delta\delta_{\alpha/\alpha'}$ change for Boc-Pro-Sar-NHMe is considerably larger than those for other Boc-Xaa-Sar-NHMe peptides (Xaa = Ala, Leu, MeAla).

To search the most probable structural candidate for Boc-Pro-Sar-NHMe responsible for the largest $\Delta\delta_{\alpha/\alpha'}$ value in low polarity solvent, I performed Molecular Mechanics calculations (MM+).[74] The result indicates that a type-II β-turn structure is the most stable structure for Boc-Pro-Sar-NHMe (Chart 10). IR spectra support the formation of this type of 10-membered HBd structure, and have indicated that the stabilities of the β-turn structure is in the following order: Boc-Pro-Sar-NHMe >> Boc-Leu-Sar-NHMe ≧ Boc-MeAla-Sar-NHMe ≧ Boc-Ala-Sar-NHMe (Chapter 3). The chemical shift analyses of their $NHCH_3$ amide protons have also indicated the similar order for extents to which the β-turn structure is formed: Boc-Pro-Sar-NHMe >> Boc-Leu-Sar-NHMe ≧ Boc-Ala-Sar-NHMe ≧ Boc-MeAla-Sar-NHMe (Chapter 5). The superiority of the Pro to the other three residues in fitting to the $(i + 1)$-th position in the β-turn-like structure is consistent with the well-known fact that the Pro residue appear at the same position of the β-turns in proteins with the overwhelmingly highest probability.[4-5,7]

A large solvent-dependent $\Delta\delta_{\alpha/\alpha'}$ change is observed also for Boc-Pro-Sar-OEt, and this magnitude is larger than those for other Boc-Xaa-Sar-OEt peptides. It is probably because Boc-Pro-Sar-OEt can take a backbone structure, which is also like the β-turn, without help of intramolecular hydrogen-bonding but with help of some solvent-driven interaction relating to the conformations of the peptide, *e.g.*, differences in compactness and in electric properties such as dipole and quadrupole moments, between the conformations.

Although the magnitude of changes is smaller than that for Boc-Pro-Sar-NHMe,

Boc-Pro-Gly-NHMe exhibits a distinct solvent-dependency of the $\Delta\delta_{\alpha/\alpha'}$ values. For Boc-Pro-Gly-OEt, the solvent-dependent change is not appreciable.

α-Helix forming peptides.

Figures 6.29 to 6.31 show solvent-dependent $\Delta\delta_{\alpha/\alpha'}$ changes for Boc-, Tfa-, and Ac-Pro-Gly-Leu-NH_2, respectively, and Figure 6.32 compares those changes.

The result for Boc-Pro-Gly-Leu-NH_2 is similar to that for Boc-Pro-Gly-NHMe. This fact suggests that Boc-Pro-Gly-Leu-NH_2 keeps a backbone structure around its Gly residue which is similar to the β-turn structure of Boc-Pro-Gly-NHMe. The chemical shift analysis of amide protons for Boc-Pro-Gly-Leu-NH_2 has indicated that the Leu-NH is mainly concerned with intramolecular hydrogen-bonding and thus Boc-Pro-Gly-Leu-NH_2 prefers the β-turn structure to other HBd structures (Chapter 5).

Tfa-Pro-Gly-Leu-NH_2 shows a similar solvent-dependence, but the magnitude of the $\Delta\delta_{\alpha/\alpha'}$ change is a little larger than the one in Boc-Pro-Gly-Leu-NH_2. The chemical shift analysis of amide protons for Tfa-Pro-Gly-Leu-NH_2 suggested that the Leu-NH is also involved in the β-turn formation to a slightly larger extent (Chapter 5).

Being different from the other two compounds, the $\Delta\delta_{\alpha/\alpha'}$ value of Ac-Pro-Gly-Leu-NH_2 decreases in the region of the $CDCl_3$ fraction over 80%(v/v). This result is probably attributed to the fact that Ac-Pro-Gly-Leu-NH_2 takes the 13-membered HBd structure in $CDCl_3$-rich solutions rather than the β-turn structure. This is supported by a comparison of the extents to which the *anti*-NH_2 amide proton takes part in the hydrogen bonding, which indicates that Ac-Pro-Gly-Leu-NH_2 can form the most stable 13-membered HBd structure, which is thought to be the α-helix-like structure. These facts suggest that the large $\Delta\delta_{\alpha/\alpha'}$ values are characteristics of the β-turn but not of the α-helix.

Discussion:

Utility of $\Delta\delta_{\alpha/\alpha'}$ values as indices of β-turn formation.

As mentioned so far, the large $\Delta\delta_{\alpha/\alpha'}$ values for some Gly and Sar-containing peptides are due to the formation of rigid β-turn structure. When the peptides from the

type-II β-turns (Chart 11), the Gly or the Sar residues occupy the (i + 2)-th position in the turns. The unique set of the dihedral angles of the (i + 2)-th residue, $\phi = 80^\circ$ and $\psi = 0^\circ$,[19] makes different geometries of the two α-protons relative to nearby C=O groups in the sequence. Under these circumstances, the two α-protons may have very different chemical shifts mainly due to the anisotropy of the diamagnetic susceptibility of the C=O group of the preceding residue.

On the other hand, the $\Delta\delta_{\alpha/\alpha'}$ values for 13-membered HBd structure forming peptides are considerably small, and the value for Ac-Pro-Gly-Leu-NH_2 becomes smaller in $CDCl_3$ than in more polar solution such as 80%(v/v) $CDCl_3$. These small magnitudes of $\Delta\delta_{\alpha/\alpha'}$ value are thought to be caused by alternation of HBd structure from β-turn to α-helix in the lower-polarity solvent. This speculation implies that the two Gly α-protons have similar chemical shifts in the α-helical structure. This is contrary to the case of the β-turn. However, the α-helical structure also takes a unique set of dihedral angles, $\phi = -57^\circ$ and $\psi = -47^\circ$ for every residue,[19] and the two Gly α-protons will be placed at different positions relative to both the Pro C=O and Gly C=O groups. It is unknown whether these two C=O groups give diamagnetically anisotropic effects on each of the two α-protons competitively or concertedly. Another possible explanation is to attribute it to large fluctuation of the dihedral angles of the Gly residues, which would remain quite large even when the peptide takes the α-helical structure.

The combined analysis of the IR and NMR results shows that Boc-Pro-Sar-NHMe makes the strongest β-turn among the peptides measured in the present study. As mentioned before, the pyrrolidine ring of the Pro residue restricts one of the dihedral angles of this residue, ϕ_{Pro}, to about -60°, which is particularly fit for the β-turn backbone.[19,56] Moreover, the $\Delta\delta_{\alpha/\alpha'}$ values for Boc-Pro-Sar-NHMe are much larger than those for Boc-Pro-Gly-NHMe. This is because the dihedral angles of the Sar residue at the (i + 2)-th position of the turn are less flexible than those of the Gly residue at the same position, which is probably due to a steric effect of the Sar-CH_3 group.

Estimation of ΔG values for β-turn formation of some peptides.

In this section, I make use of the $\Delta\delta_{\alpha/\alpha'}$ indices for estimating the free energy, ΔG, for formation of the β-turn structures of peptides in solutions. As seen in Figure 6.28,

Boc-Pro-Sar-NHMe shows a steep transition of the $\Delta\delta_{\alpha/\alpha'}$ value as the solvent dielectric constant changes. The infrared spectra of Boc-Pro-Sar-NHMe in $CCl_4/CDCl_3$ mixed solvents have shown that the population of a HBfree conformer is very small in $CDCl_3$, and completely disappears in solutions with CCl_4 fraction of higher than 60%(v/v), where dielectric constants of solvents are lower than 3.5. In this case, the observed $\Delta\delta_{\alpha/\alpha'}$ value in CCl_4, 1.593 ppm, can be taken as the upper limit at which the Sar- and the Gly-containing peptides take completely the β-turn structures. On the other hand, the minimum $\Delta\delta_{\alpha/\alpha'}$ value observed in pure D_2O solution for each peptide is thought to provide the lower limit at which the peptide is the most flexible enough to fluctuate among various conformations within the NMR time scale. This flexibility is facilitated by a break of the intramolecular hydrogen-bond which is replaced by an intermolecular hydrogen-bond with D_2O. Such a state of peptides with the maximum degree of conformational fluctuation can be described as a random structure. Therefore, it is reasonable to assume that an intermediate $\Delta\delta_{\alpha/\alpha'}$ value is a weighted average and provides a population ratio of the β-turn structure to the random structure:

$$P(\beta\text{-turn})/P(\text{random}) = (\Delta\delta_{\alpha/\alpha'} - \Delta\delta_{\alpha/\alpha'(D2O)})/(1.593 - \Delta\delta_{\alpha/\alpha'}).$$

Then, the free energy for formation of the β-turn structure of the peptide is given by

$$\Delta G = -RT\ln[(\Delta\delta_{\alpha/\alpha'} - \Delta\delta_{\alpha/\alpha'(D2O)})/(1.593 - \Delta\delta_{\alpha/\alpha'})].$$

Figures 6.33 and 6.34 show the plots of ΔG values against dielectric constants for some Boc-Xaa-Yaa-NHMe peptides with Yaa = Gly and Yaa = Sar, respectively. The ΔG values indicate that the β-turn structure of Boc-Pro-Sar-NHMe is the most stable among those of all the peptides studied in the nonpolar to moderately polar solvent range. With somewhat higher ΔG values, other three Boc-Pro-Sar-NHMe and Boc-Pro-Gly-NHMe also form the β-turn structure to an appreciable degree in the similar solvent range.

Solvent effects on ΔG values.

Figure 6.35 compares the ΔG values measured by using five kinds of the mixed solvents for the β-turn formation of Boc-Pro-Sar-NHMe (*trans* + *trans*). The dielectric constants of mixed solvents, ε, are obtained by taking averages of dielectric constants of pure components with weights of mole fractions. Dependence of ΔG values on these solvents suggests that the solvent ability as a hydrogen-bond acceptor is in the following

order: water > DMSO > acetone > methanol > acetonitrile > chloroform.

Regardless of the high dielectric constant and large dipole moment, acetonitrile is very weak as a hydrogen-bond acceptor and thought to be harmless to the peptidyl NH group. When the $CDCl_3$/acetonitrile-d_3 mixed solvents are used, the ΔG values increase gradually with increasing solvent dielectric constants.

The ΔG values for the $CDCl_3$/DMSO-d_6 mixed solvents are definitely higher than those for $CDCl_3$/acetonitrile-d_3. This additional destabilization of the β-turn structure by DMSO is mainly attributed to the strong hydrogen-bonding ability of the sulfoxide group of DMSO. It will accept the peptidyl NH group by taking the place of the peptidyl C=O group.

It is intriguing that the effect of methanol is rather similar to that of acetonitrile at low fractions in the $CDCl_3$/methanol-d_4 mixed solvent, but becomes similar to that of DMSO at high fractions. This is probably because methanol molecules tend to associate each other in the chloroform-rich solutions and can not afford to fully perturb the intramolecular hydrogen-bond of a peptide.

Other thermodynamic properties for β-turn formation.

Figure 6.36 shows temperature-dependent $\Delta\delta_{\alpha/\alpha'}$ changes in $CDCl_3$ solutions for Boc-Ala-Gly-NHMe and Boc-Pro-Gly-NHMe. Similar measurements were conducted for Boc-Ala-Sar-NHMe and Boc-Pro-Sar-NHMe at various mixing ratios of the $CDCl_3$/DMSO-d_6 mixed solvents, and the results are shown in Figures 6.37 and 6.38, respectively. Using these $\Delta\delta_{\alpha/\alpha'}$ values, temperature-dependences of ΔG for solutions of Boc-Ala-Sar-NHMe and Boc-Pro-Sar-NHMe are estimated and shown in Figures 6.39 and 6.40. At every solvent mixing ratio, the ΔG value for β-turn formation of Boc-Ala-Sar-NHMe gradually increases with increasing temperature. In addition, the slopes of changes become less steep at high DMSO fractions in the mixed solvents. For Boc-Pro-Sar-NHMe, similar temperature dependence is seen. On the basis of thermodynamic relationship, $\Delta G = \Delta H - T\Delta S$, enthalpy and entropy changes for the β-turn formation, ΔH and ΔS, respectively, are obtained from the slope and the intercept of the plot of ΔG vs T as follows,

$$\Delta S = S_{\beta\text{-turn}} - S_{\text{random}}$$
$$= -(\partial\,\Delta G(T)/\partial\,T)$$

$= -$ [slope],

$\Delta H = H_{\beta\text{-turn}} - H_{\text{random}}$

$= \Delta G(298) + 298\Delta S$

$=$ [intercept] $- 298$[slope].

In Figure 6.41, resulting values of the three thermodynamic functions for Boc-Ala-Sar-NHMe are plotted against the mole fraction of $CDCl_3$, x_{CDCl_3}. In the range of x_{CDCl_3} higher than 0.9, the ΔG value for β-turn formation of Boc-Ala-Sar-NHMe is negative, which is due to a largely negative ΔH value. And the β-turn formation for this peptide is by 1.3 kcal/mol favorable than that for Boc-Ala-Gly-NHMe in $CDCl_3$. This increase in stability is mainly due to a reduction in magnitude of the entropic term, $T\Delta S$, yielded by replacing the Gly to the Sar residue. Negative ΔS values are thought to be caused by losing structural flexibility upon β-turn formation in which the dihedral angles of the residues concerned are fixed at optimal angles. As the DMSO fraction increases, the unfavorable entropy contribution attenuates considerably, but, instead, ΔH becomes positive so steeply that the β-turn of Boc-Ala-Sar-NHMe is destabilized further. DMSO solvent, by forming a strong intermolecular hydrogen-bond, deprives the terminal $NHCH_3$ group of its intramolecular hydrogen-bond partner, the C=O group. In this case, formation of the solvent-peptide hydrogen-bonds is expected to reduce both enthalpy and entropy to a larger extent in random structure than in the β-turn state. Therefore, resulting ΔH and ΔS values for β-turn formation in the solutions containing DMSO becomes more positive and less negative, respectively, than in $CDCl_3$.

In Figure 6.42, results of similar analysis for Boc-Pro-Sar-NHMe are plotted. Compared with Boc-Ala-Sar-NHMe, the entropic term, $T\Delta S$, is more favorable for the β-turn formation in all the solvent range of the $CDCl_3$/DMSO-d_6 mixed solvents, while the contribution of ΔH is not so different from that for Boc-Ala-Sar-NHMe. The smaller magnitude of the entropic term for Boc-Pro-Sar-NHMe can be understood by the fact that ϕ_{Pro}, one of the dihedral angles which must be restricted to their specific values in the β-turn, is always restricted around at -65° due to the stiffness of the pyrrolidine ring, and therefore ΔS for the β-turn formation is less in Boc-Pro-Sar-NHMe than in Boc-Ala-Sar-NHMe.

Correlations of the present results with chemical shift changes of amide protons.

Next, I have compared two different indices of the β-turn formation in $CDCl_3$. One is based on difference of the $\Delta\delta_{\alpha/\alpha'}$ values obtained in the present chapter and the other is based on the analysis of chemical shift changes of amide protons discussed in Chapter 5.

As seen in Figure 6.43, a certain correlation between the two indices clearly exists for the β-turn structures of Boc-Xaa-Gly-NHMe and Boc-Xaa-Sar-NHMe. The larger $\Delta\delta_{\alpha/\alpha'}$ values, which indicate the larger rigidity around the Gly or Sar residue, are observed for the peptides with the larger extent to which its terminal $NHCH_3$ group is involved in the β-turn formation.

For α-helix-forming peptides shown in Figure 6.44, on the other hand, relationship is apparent but opposite to that for the above-mentioned peptides. This fact suggests that the α-helix formation inhibits the β-turn formation occurring in the same peptide molecule.

Correlations of the present results with IR results.

Finally I have also inspected correlation between the present $\Delta\delta_{\alpha/\alpha'}$ indices with the IR results which has been discussed in Chapter 3. As shown in Figure 6.45 and 6.46, a certain similar correlation is seen between the two different indices.

In the following chapter, I will discuss contribution of each amino acid residue toward β-turn formation using these three indices.

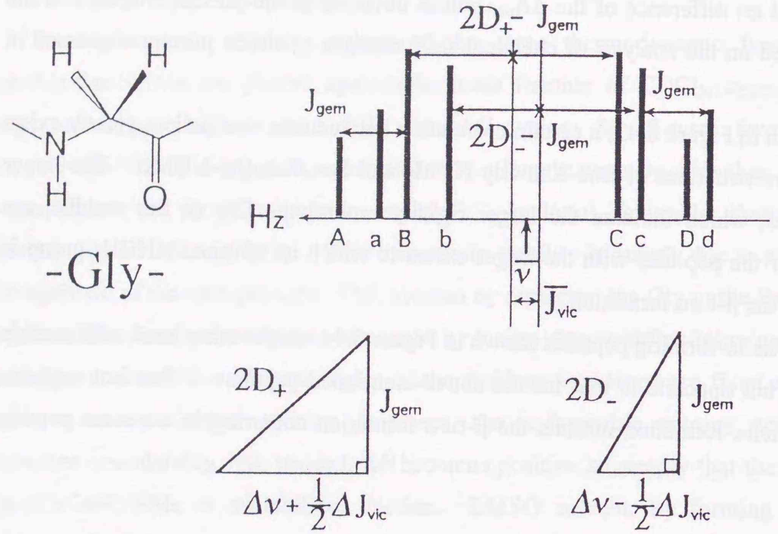

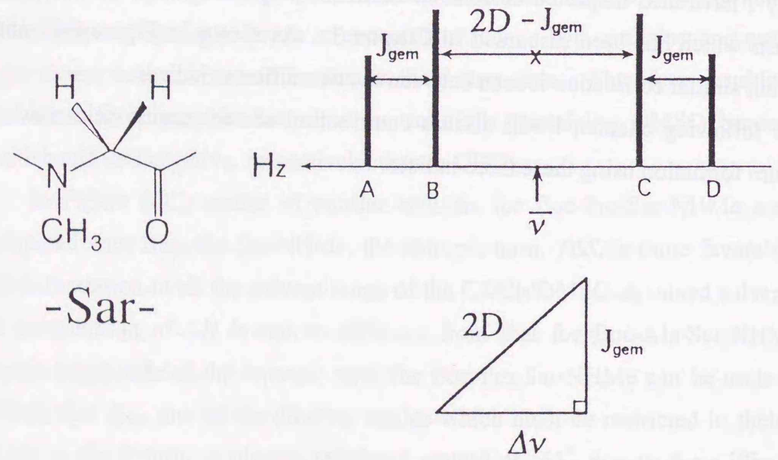

Figure 6.1. Patterns of NMR signals for A and B protons in ABX and AB spin systems.

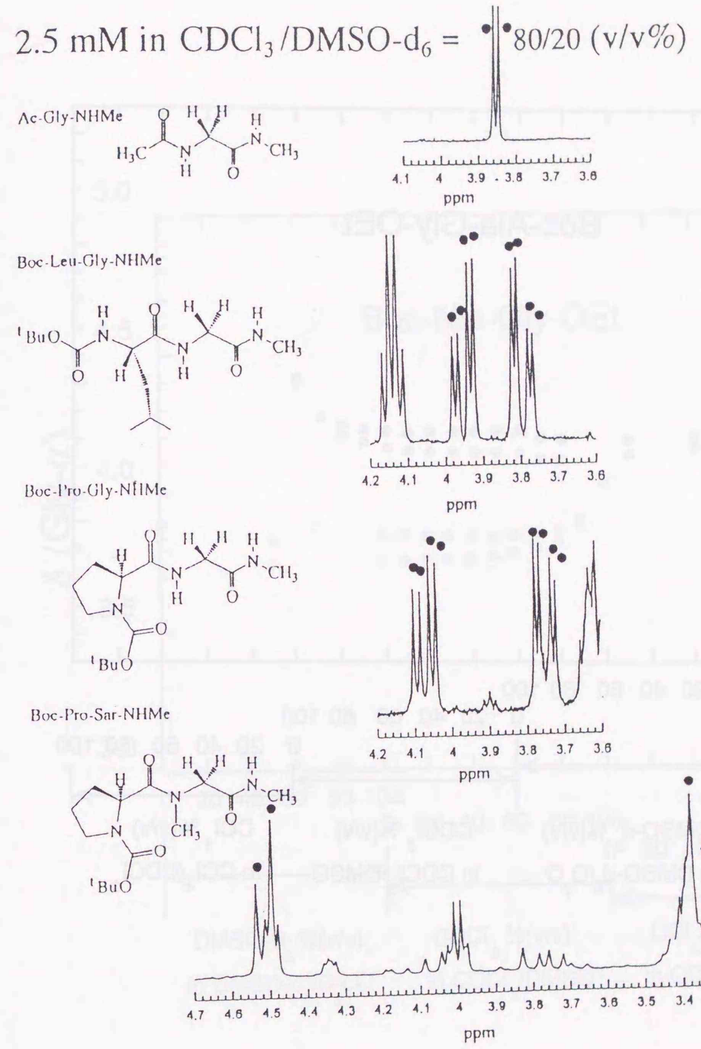

Figure 6.2. 400 MHz 1H-NMR spectra in the Gly-α/α' and Sar-α/α' proton region of Ac-Gly-NHMe, Boc-Leu-Gly-NHMe, Boc-Pro-Gly-NHMe, and Boc-Pro-Sar-NHMe in 2.5 mM solutions in the $CDCl_3$/DMSO-d_6 (80/20(v/v%)) mixed solvent at 25˚C.

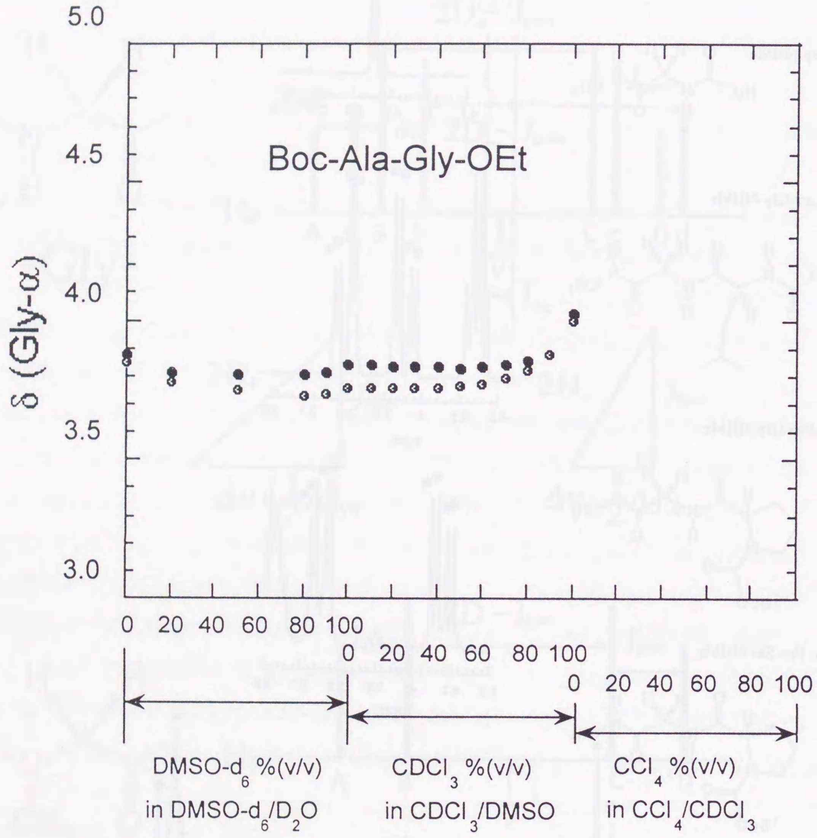

Figure 6.3. Plots of chemical shifts for the two glycyl α-protons of 2.5 mM Boc-Ala-Gly-OEt in mixed solvents of DMSO-d_6/D_2O and $CDCl_3$/DMSO-d_6 at 25˚C against solvent mixing ratios.

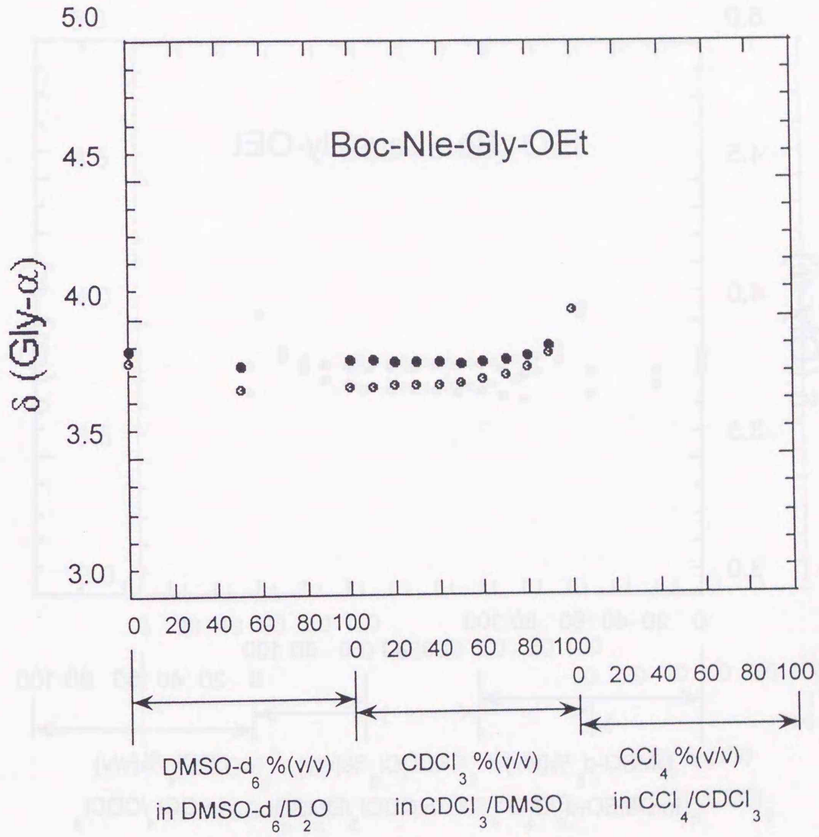

Figure 6.4. Plots of chemical shifts for the two glycyl α-protons of 2.5 mM Boc-Nle-Gly-OEt in mixed solvents of DMSO-d_6/D_2O and $CDCl_3$/DMSO-d_6 at 25˚C against solvent mixing ratios.

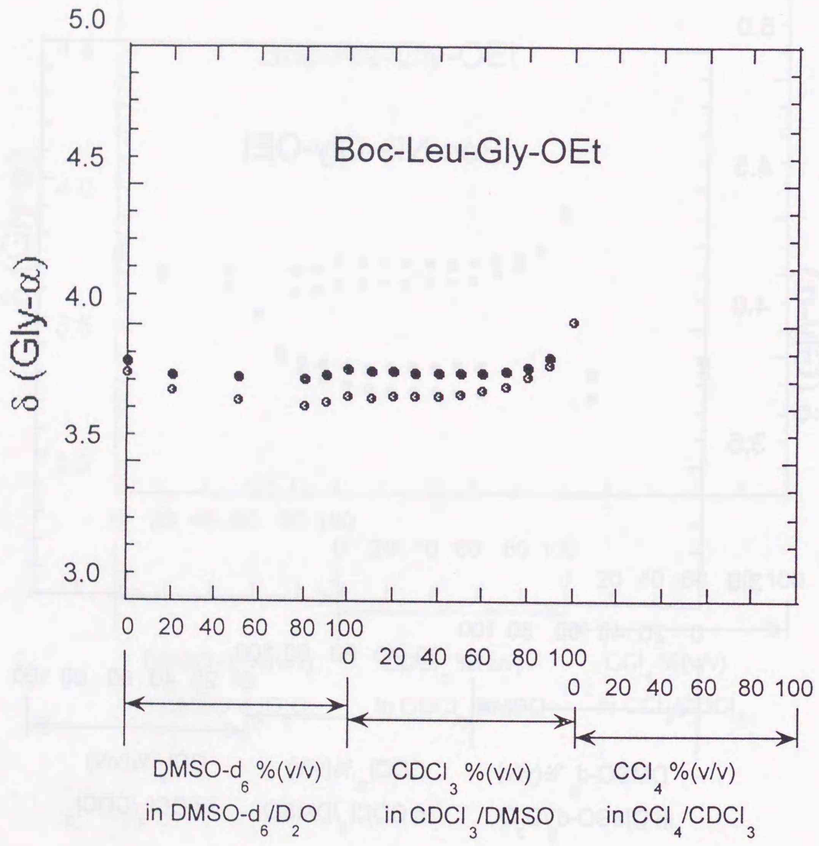

Figure 6.5. Plots of chemical shifts for the two glycyl α-protons of 2.5 mM Boc-Leu-Gly-OEt in mixed solvents of DMSO-d_6/D_2O and $CDCl_3$/DMSO-d_6 at 25˚C against solvent mixing ratios.

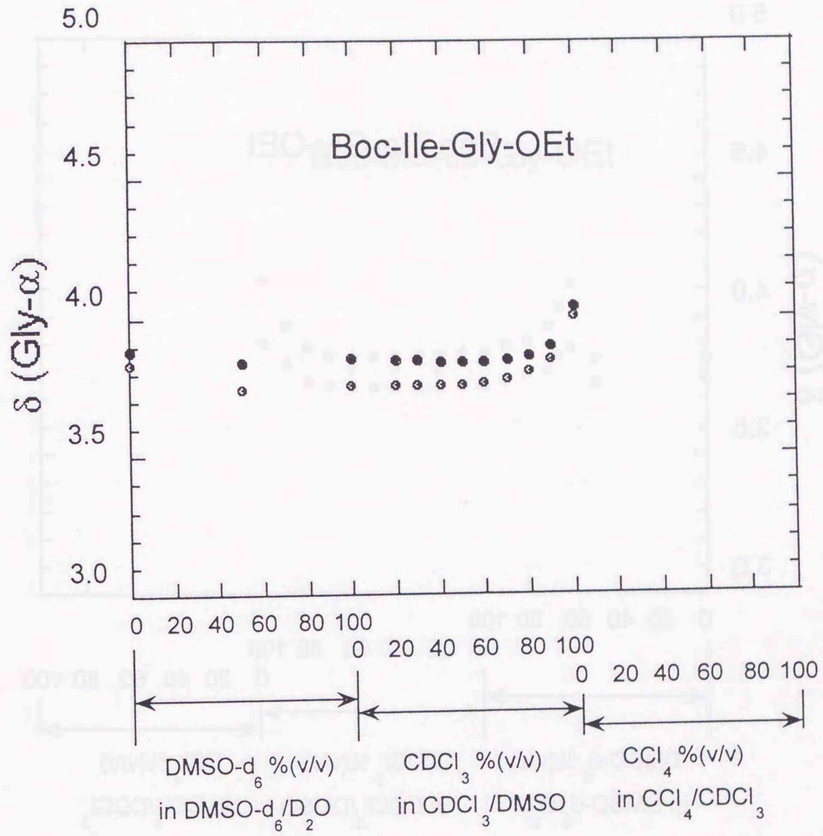

Figure 6.6. Plots of chemical shifts for the two glycyl α-protons of 2.5 mM Boc-Ile-Gly-OEt in mixed solvents of DMSO-d_6/D_2O and $CDCl_3$/DMSO-d_6 at 25˚C against solvent mixing ratios.

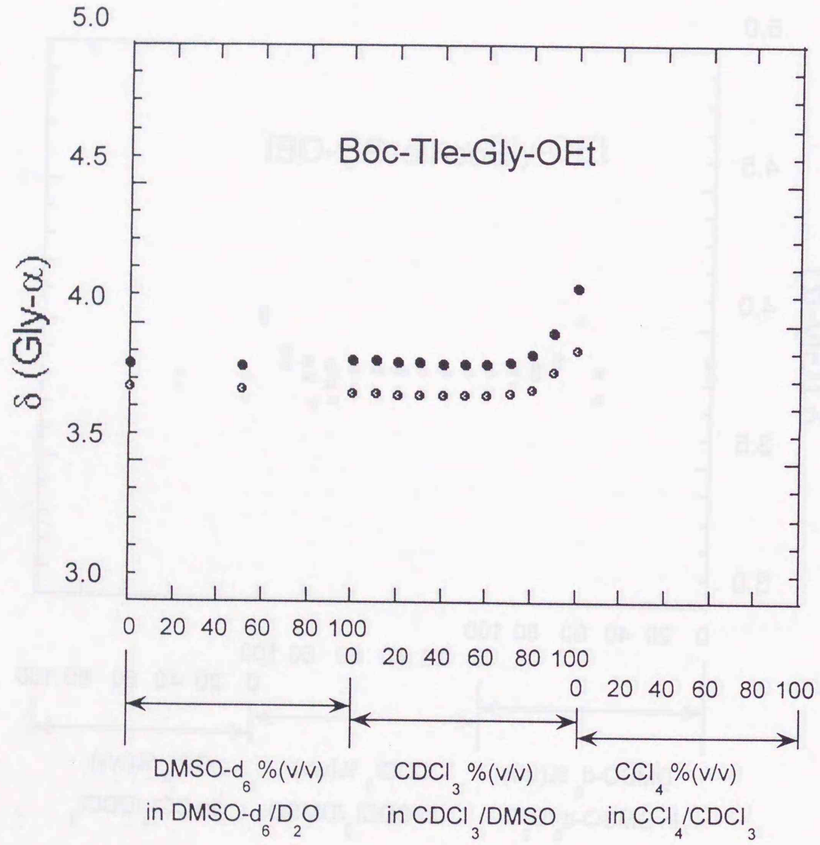

Figure 6.7. Plots of chemical shifts for the two glycyl α-protons of 2.5 mM Boc-Tle-Gly-OEt in mixed solvents of DMSO-d_6/D_2O and $CDCl_3$/DMSO-d_6 at 25˚C.

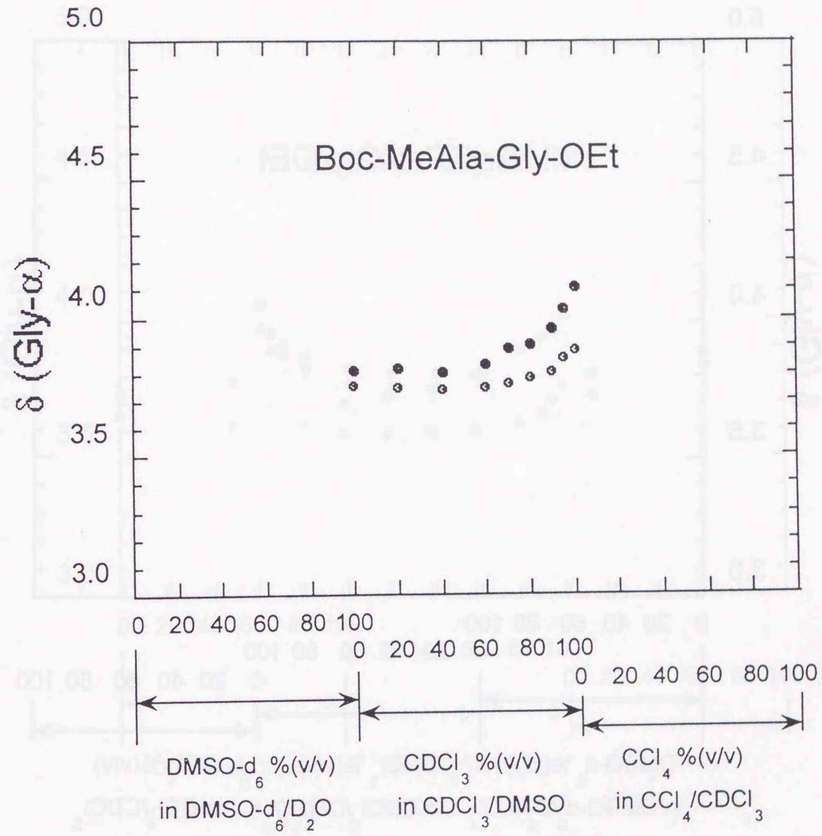

Figure 6.8. Plots of chemical shifts for the two glycyl α-protons of 2.5 mM Boc-MeAla-Gly-OEt in mixed solvent of $CDCl_3$/DMSO-d_6 at 25˚C.

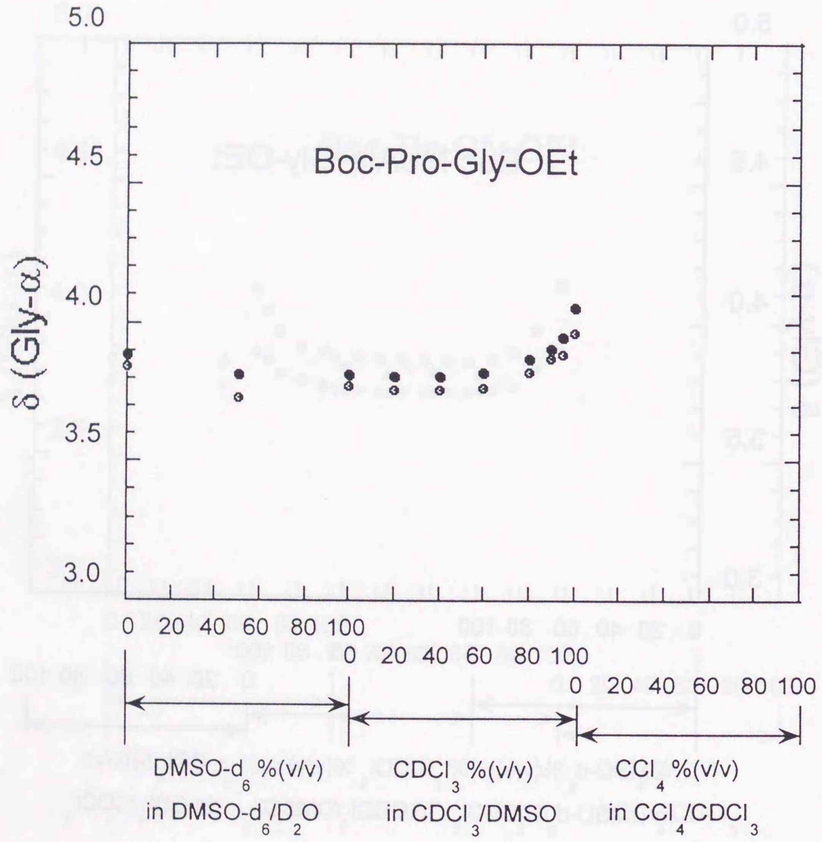

Figure 6.9. Plots of chemical shifts for the two glycyl α-protons of 2.5 mM Boc-Pro-Gly-OEt in mixed solvents of DMSO-d_6/D_2O and $CDCl_3$/DMSO-d_6 at 25˚C against solvent mixing ratios.

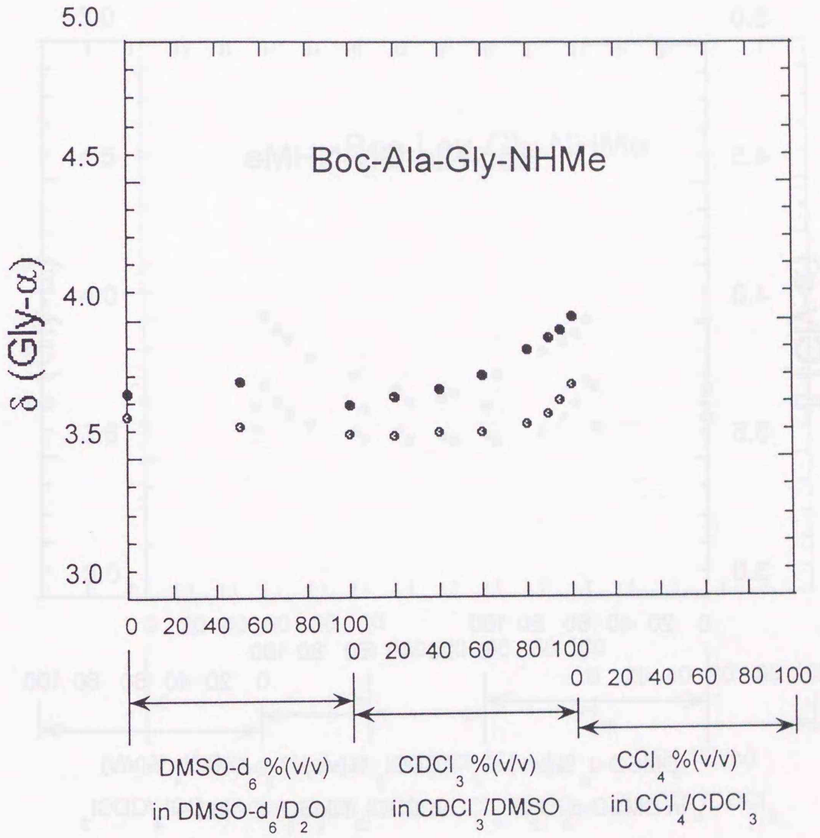

Figure 6.10. Plots of chemical shifts for the two glycyl α-protons of 2.5 mM Boc-Ala-Gly-NHMe in mixed solvents of DMSO-d_6/D_2O and $CDCl_3$/DMSO-d_6 at 25˚C against solvent mixing ratios.

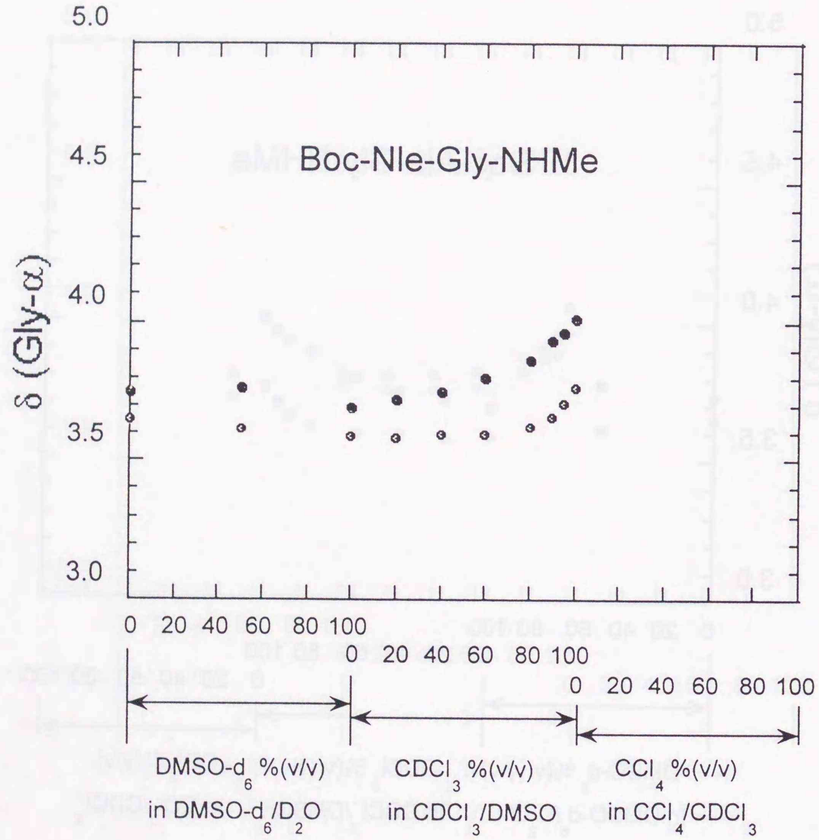

Figure 6.11. Plots of chemical shifts for the two glycyl α-protons of 2.5 mM Boc-Nle-Gly-NHMe in mixed solvents of DMSO-d_6/D_2O and $CDCl_3$/DMSO-d_6 at 25˚C against solvent mixing ratios.

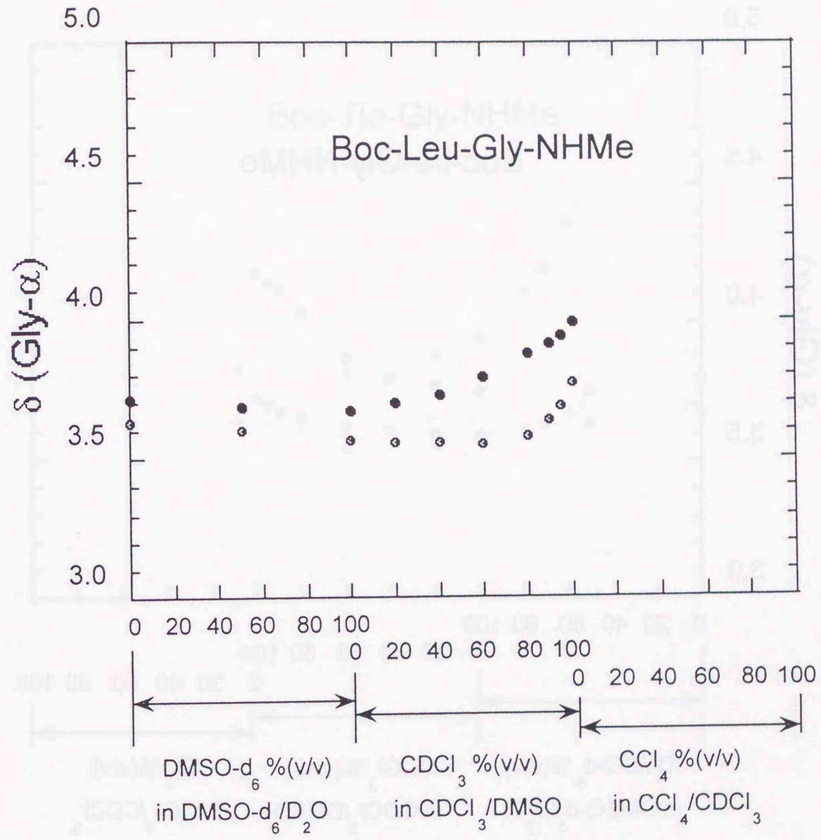

Figure 6.12. Plots of chemical shifts for the two glycyl α-protons of 2.5 mM Boc-Leu-Gly-NHMe in mixed solvents of DMSO-d_6/D_2O and $CDCl_3$/DMSO-d_6 at 25˚C against solvent mixing ratios.

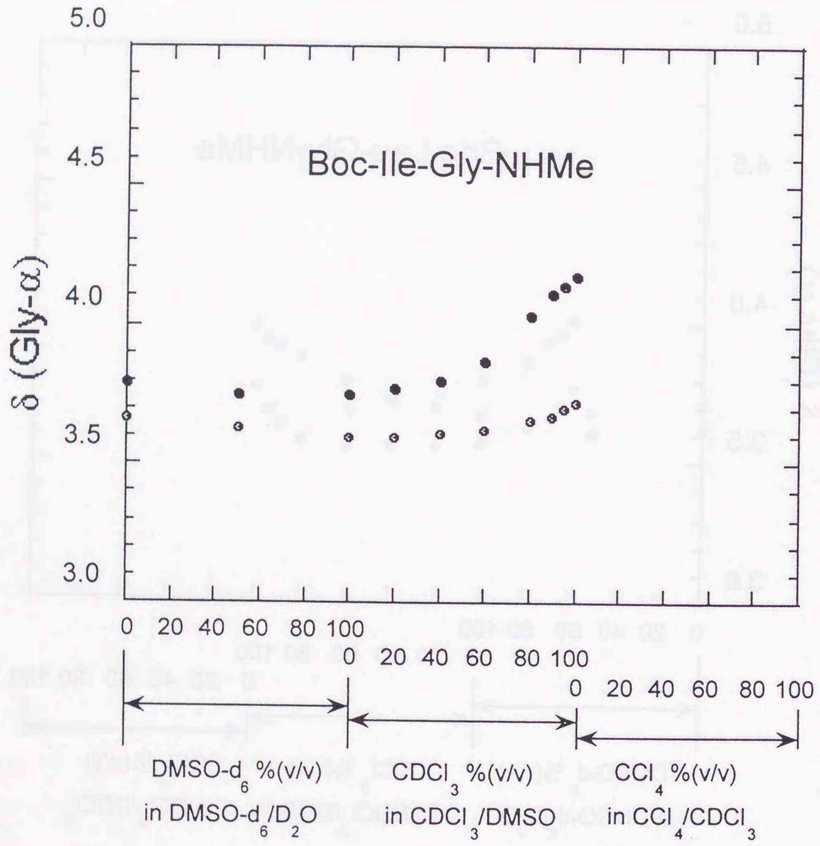

Figure 6.13. Plots of chemical shifts for the two glycyl α-protons of 2.5 mM Boc-Ile-Gly-NHMe in mixed solvents of DMSO-d_6/D_2O and $CDCl_3$/DMSO-d_6 at 25˚C against solvent mixing ratios.

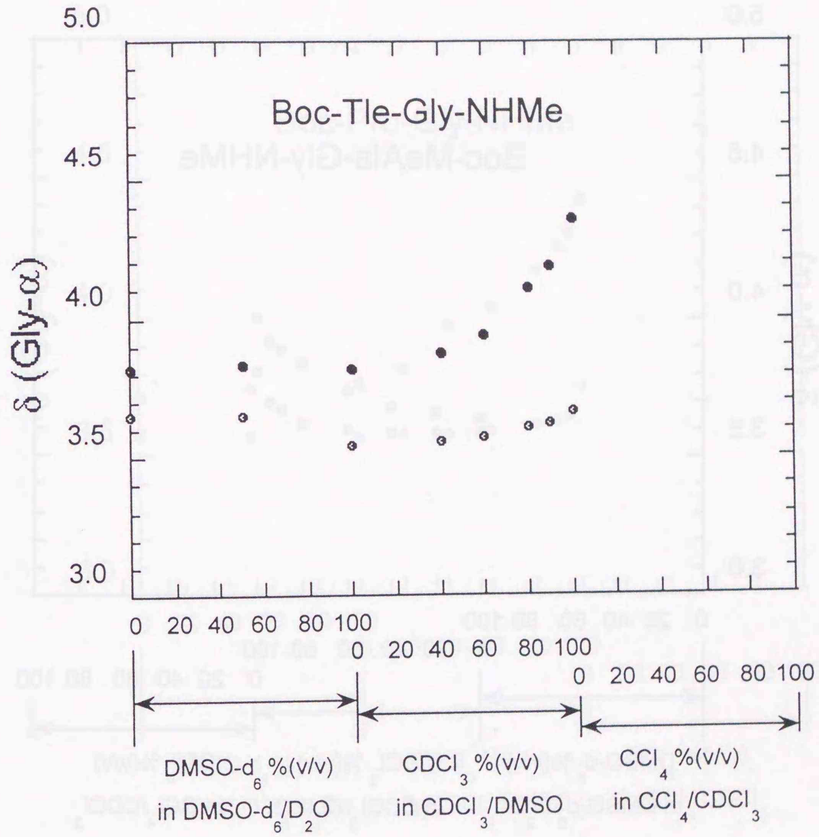

Figure 6.14. Plots of chemical shifts for the two glycyl α-protons of 2.5 mM Boc-Tle-Gly-NHMe in mixed solvents of DMSO-d_6/D_2O and $CDCl_3$/DMSO-d_6 at 25˚C against solvent mixing ratios.

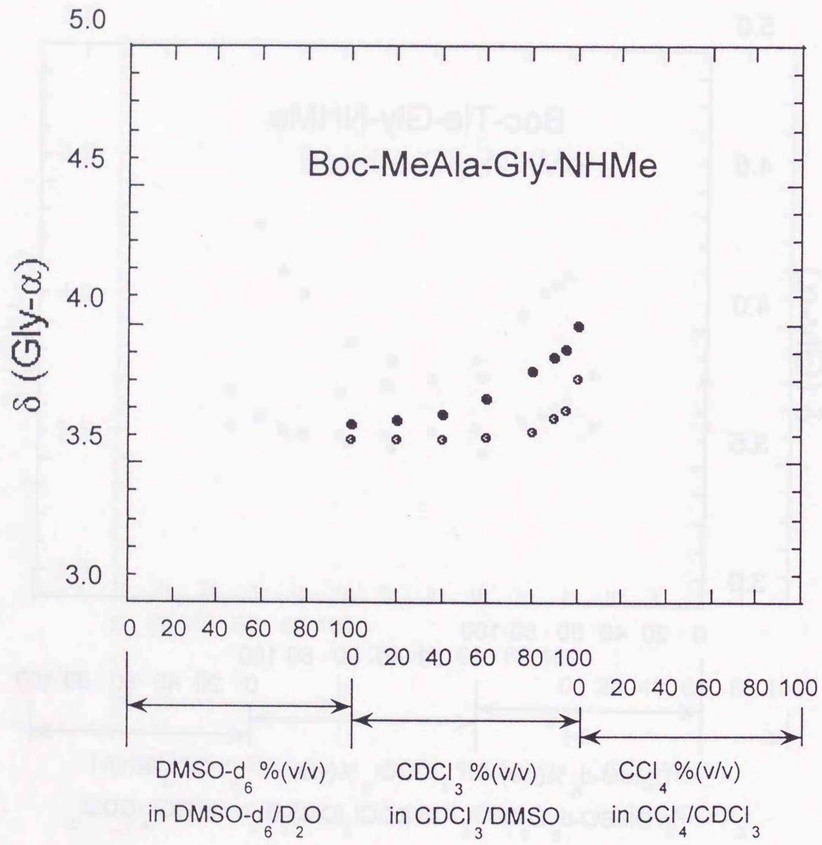

Figure 6.15. Plots of chemical shifts for the two glycyl α-protons of 2.5 mM Boc-MeAla-Gly-NHMe in mixed solvent of $CDCl_3$/DMSO-d_6 at 25˚C against solvent mixing ratios.

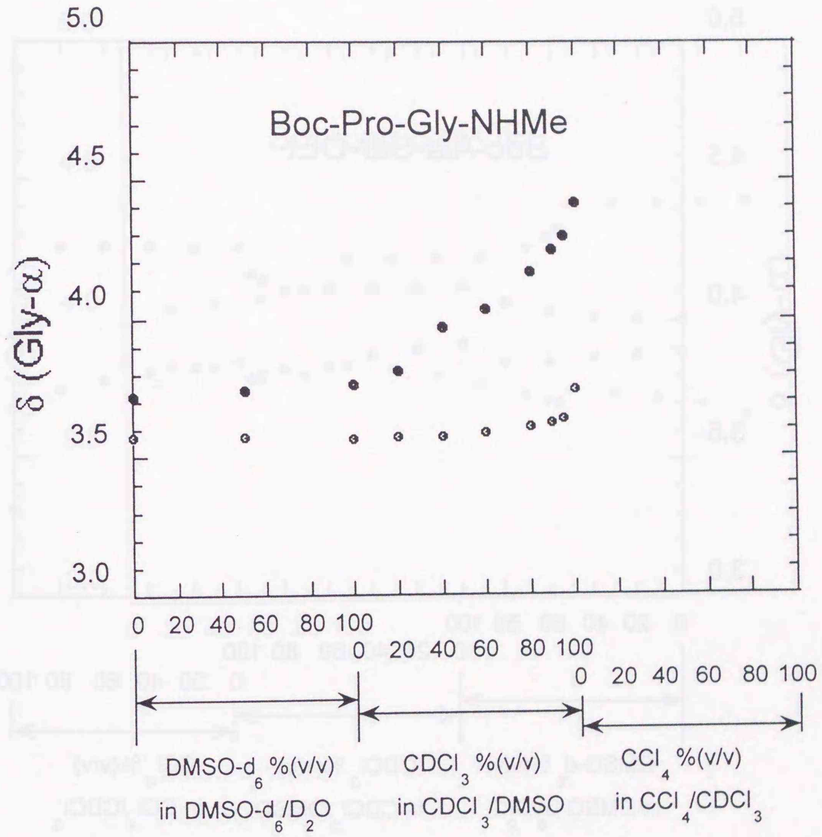

Figure 6.16. Plots of chemical shifts for the two glycyl α-protons of 2.5 mM Boc-Pro-Gly-NHMe in mixed solvents of DMSO-d_6/D_2O and $CDCl_3$/DMSO-d_6 at 25˚C against solvent mixing ratios.

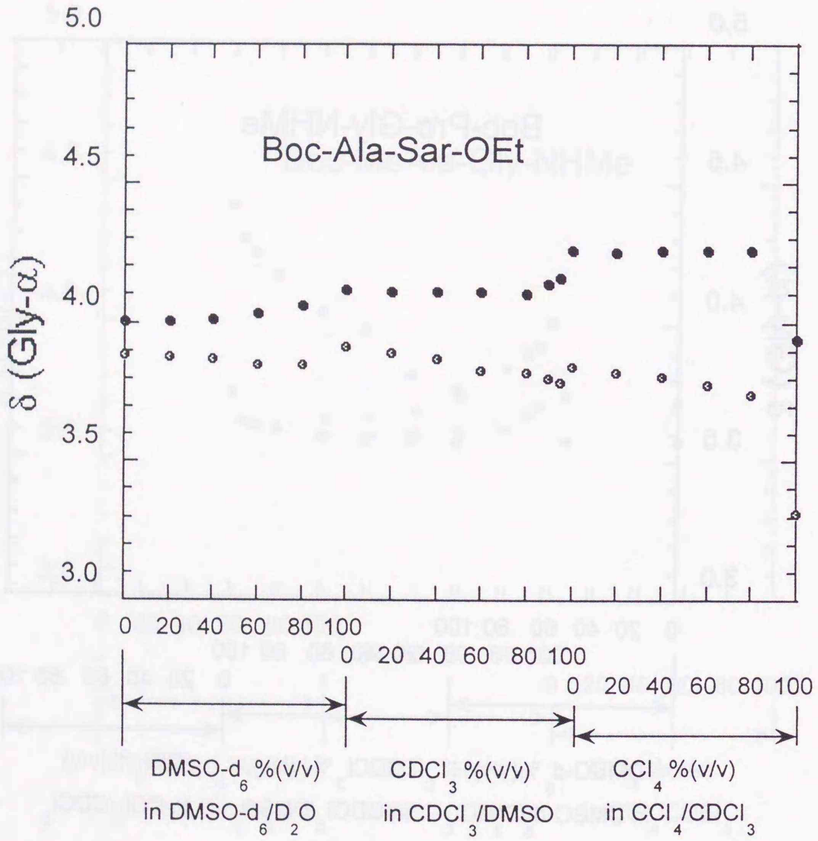

Figure 6.17. Plots of chemical shifts for the two sarcosyl α-protons of 2.5 mM Boc-Ala-Sar-OEt in mixed solvents of DMSO-d_6/D_2O, $CDCl_3$/DMSO-d_6, and CCl_4/$CDCl_3$ at 25˚C against solvent mixing ratios.

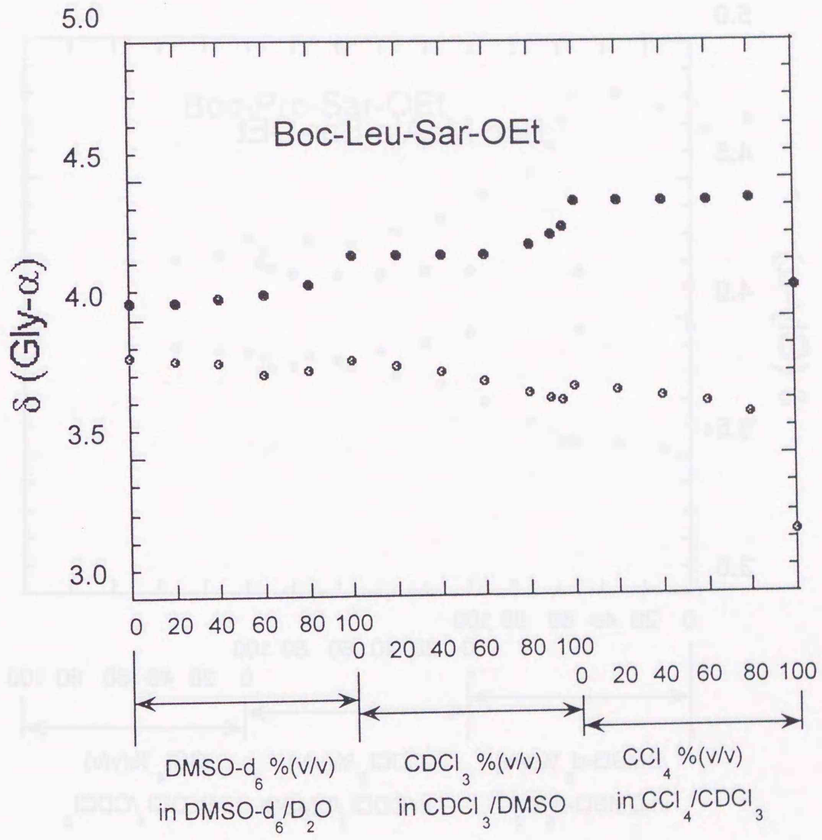

Figure 6.18. Plots of chemical shifts for the two sarcosyl α-protons of 2.5 mM Boc-Leu-Sar-OEt in mixed solvents of DMSO-d_6/D_2O, $CDCl_3$/DMSO-d_6, and CCl_4/$CDCl_3$ at 25˚C against solvent mixing ratios.

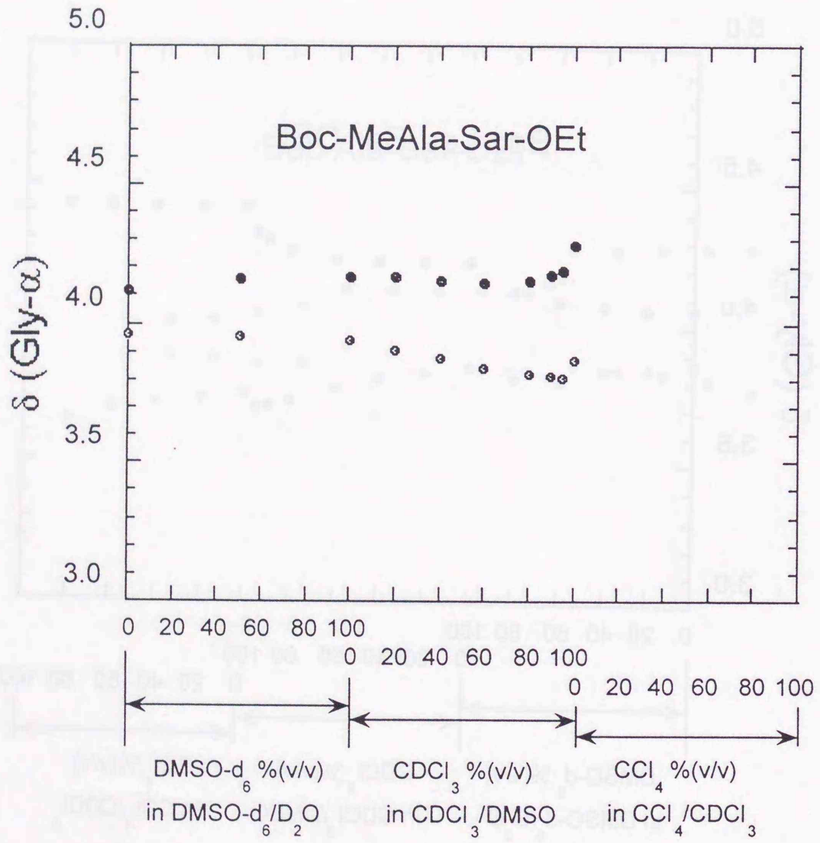

Figure 6.19. Plots of chemical shifts for the two sarcosyl α-protons of 2.5 mM Boc-MeAla-Sar-OEt in mixed solvents of DMSO-d_6/D_2O and $CDCl_3$/DMSO-d_6 at 25˚C against solvent mixing ratios.

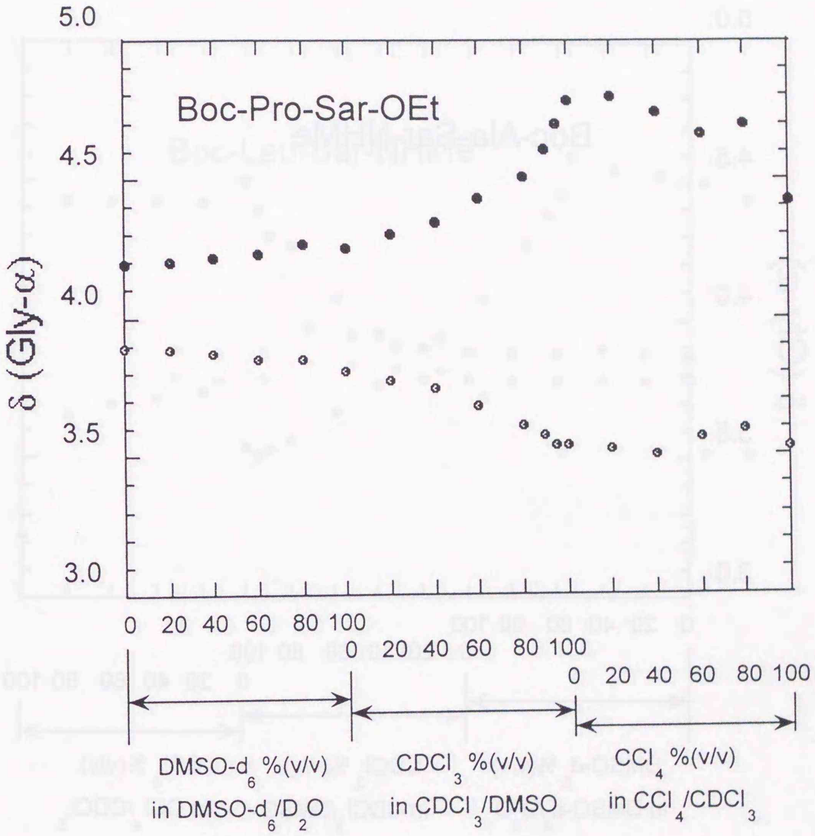

Figure 6.20. Plots of chemical shifts for the two sarcosyl α-protons of 2.5 mM Boc-Pro-Sar-OEt in mixed solvents of DMSO-d_6/D_2O, $CDCl_3$/DMSO-d_6, and CCl_4/$CDCl_3$ at 25˚C against solvent mixing ratios.

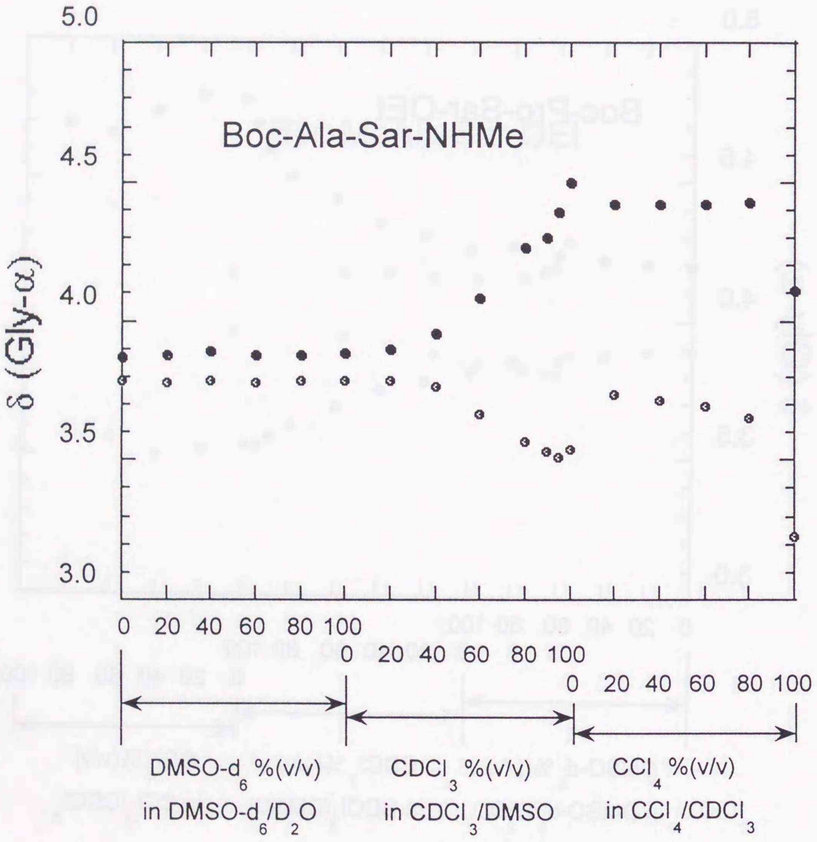

Figure 6.21. Plots of chemical shifts for the two sarcosyl α-protons of 2.5 mM Boc-Ala-Sar-NHMe in mixed solvents of DMSO-d_6/D_2O, $CDCl_3$/DMSO-d_6, and CCl_4/$CDCl_3$ at 25˚C against solvent mixing ratios.

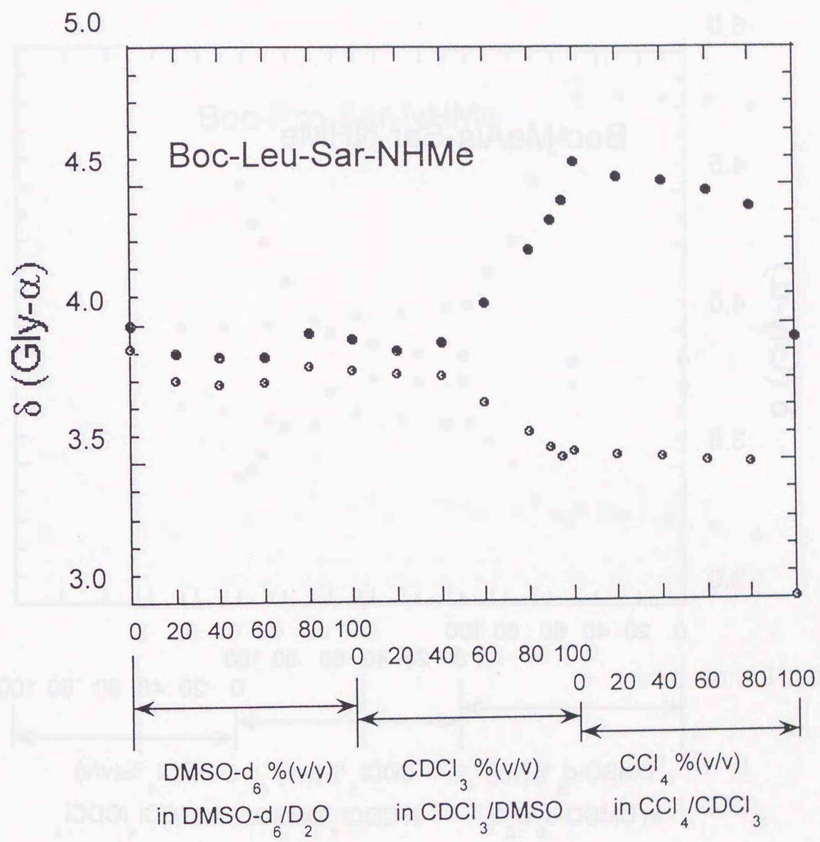

Figure 6.22. Plots of chemical shifts for the two sarcosyl α-protons of 2.5 mM Boc-Leu-Sar-NHMe in mixed solvents of DMSO-d_6/D_2O, $CDCl_3$/DMSO-d_6, and CCl_4/$CDCl_3$ at 25˚C against solvent mixing ratios.

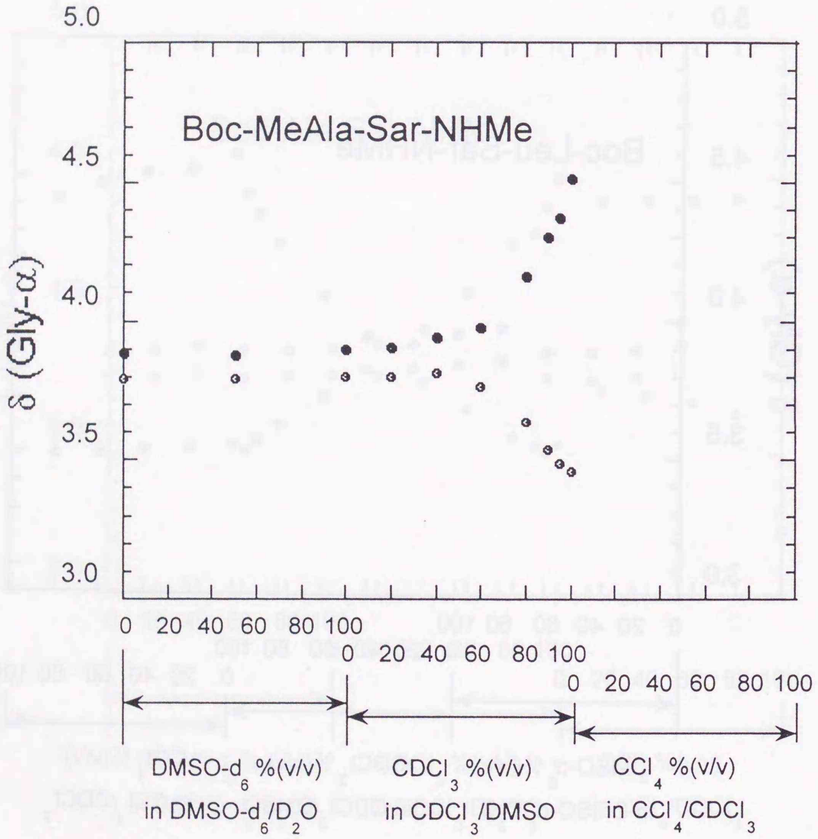

Figure 6.23. Plots of chemical shifts for the two sarcosyl α-protons of 2.5 mM Boc-MeAla-Sar-NHMe in mixed solvents of DMSO-d_6/D_2O and $CDCl_3$/DMSO-d_6 at 25 °C against solvent mixing ratios.

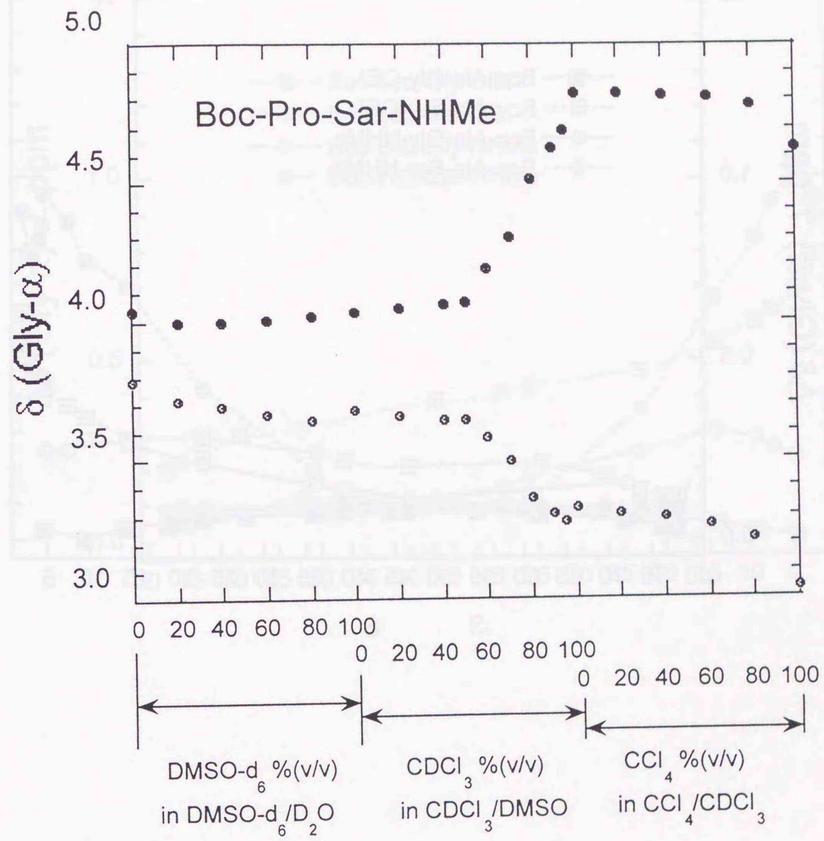

Figure 6.24. Plots of chemical shifts for the two sarcosyl α-protons of 2.5 mM Boc-Pro-Sar-NHMe in mixed solvents of DMSO-d_6/D_2O, $CDCl_3$/DMSO-d_6, and CCl_4/$CDCl_3$ at 25 °C against solvent mixing ratios.

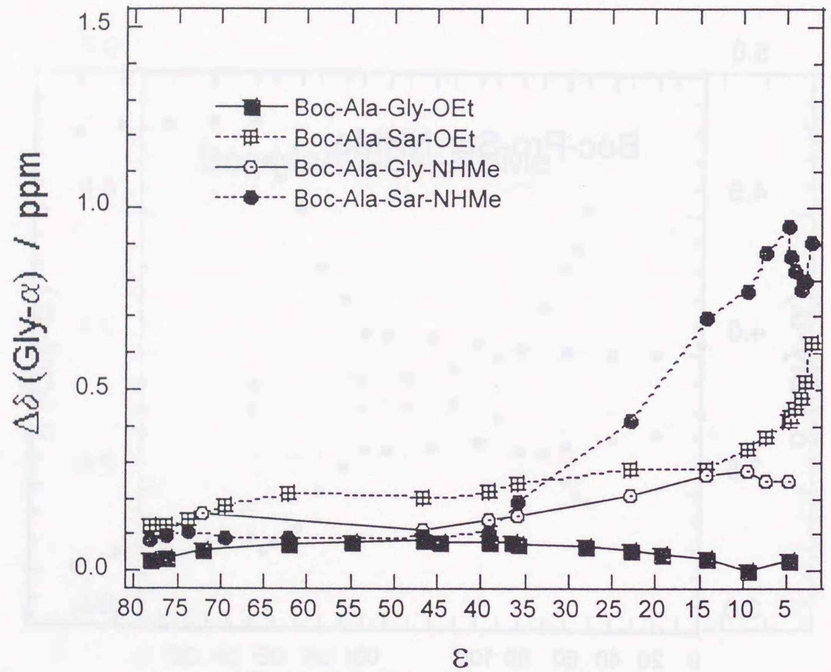

Figure 6.25. Changes of $\Delta\delta_{\alpha/\alpha'}$ values with solvent dielectric constants for 2.5 mM solutions of Boc-Ala-Gly-OEt, Boc-Ala-Sar-OEt, Boc-Ala-Gly-NHMe, and Boc-Ala-Sar-NHMe in DMSO-d_6/D_2O, $CDCl_3$/DMSO-d_6, and CCl_4/$CDCl_3$ mixed solvents at 25˚C.

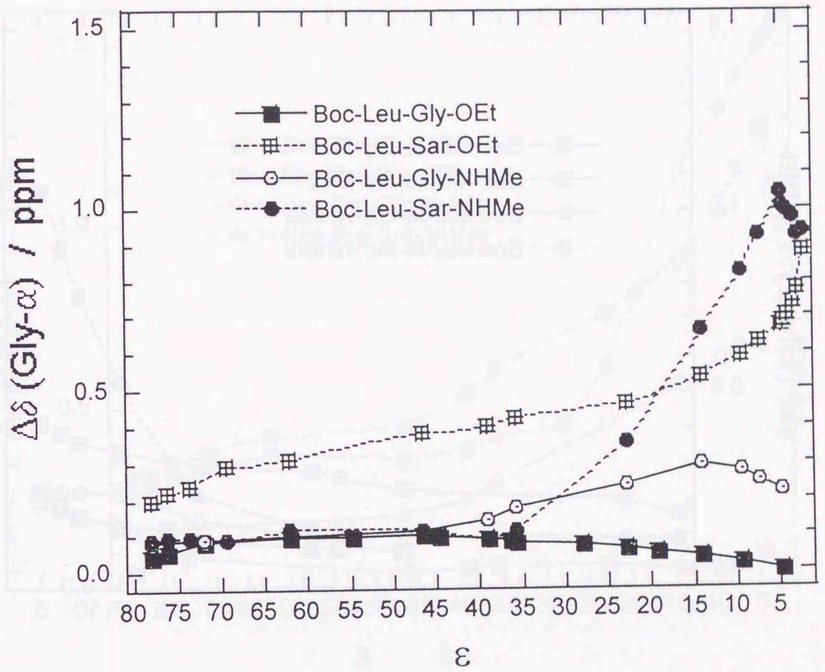

Figure 6.26. Changes of $\Delta\delta_{\alpha/\alpha'}$ values with solvent dielectric constants for 2.5 mM solutions of Boc-Leu-Gly-OEt, Boc-Leu-Sar-OEt, Boc-Leu-Gly-NHMe, and Boc-Leu-Sar-NHMe in DMSO-d_6/D_2O, $CDCl_3$/DMSO-d_6, and CCl_4/$CDCl_3$ mixed solvents at 25˚C.

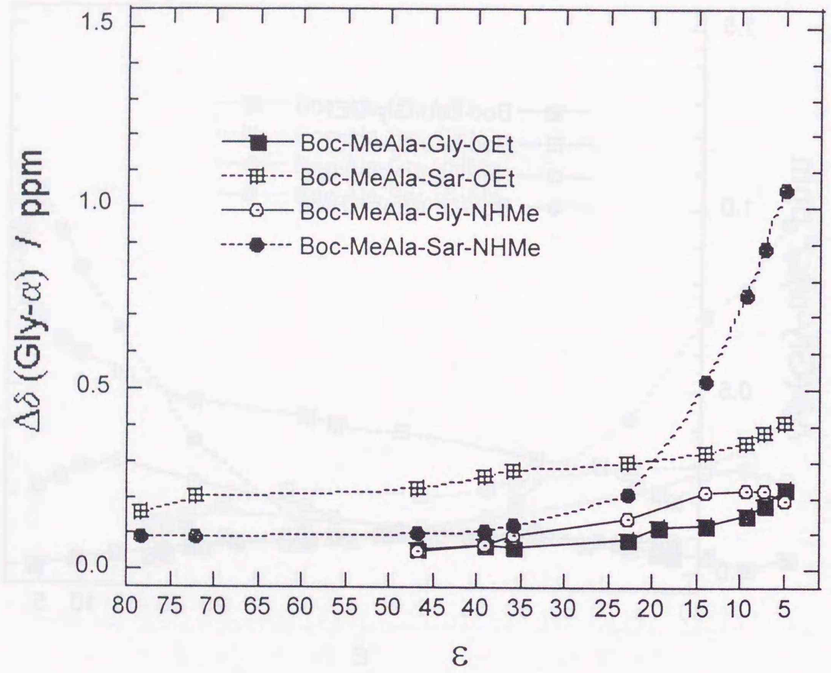

Figure 6.27. Changes of $\Delta\delta_{\alpha/\alpha'}$ values with solvent dielectric constants for 2.5 mM solutions of Boc-MeAla-Gly-OEt, Boc-MeAla-Sar-OEt, Boc-MeAla-Gly-NHMe, and Boc-MeAla-Sar-NHMe in DMSO-d_6/D_2O and $CDCl_3$/DMSO-d_6 mixed solvents at 25° C.

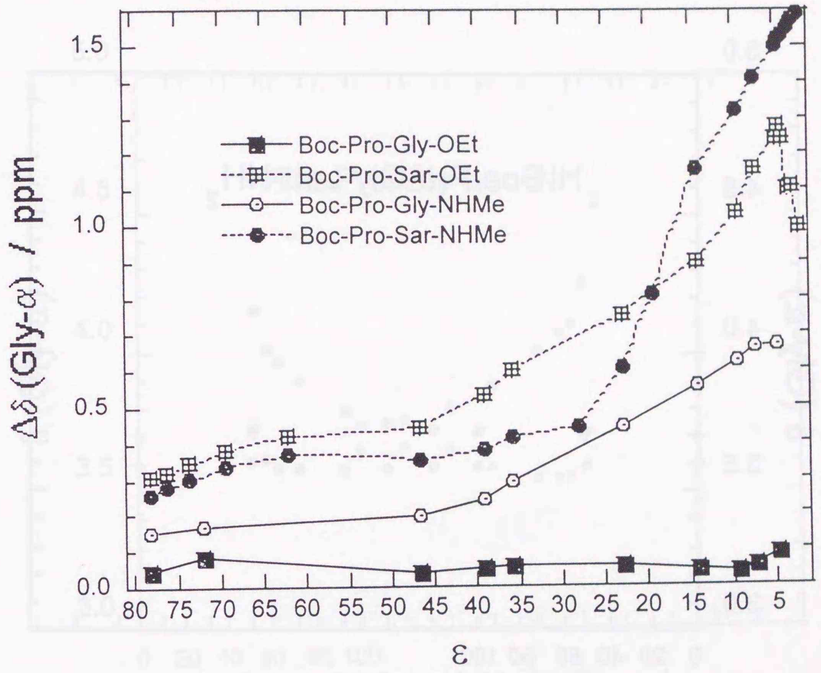

Figure 6.28. Changes of $\Delta\delta_{\alpha/\alpha'}$ values with solvent dielectric constants for 2.5 mM solutions of Boc-Pro-Gly-OEt, Boc-Pro-Sar-OEt, Boc-Pro-Gly-NHMe, and Boc-Pro-Sar-NHMe in DMSO-d_6/D_2O, $CDCl_3$/DMSO-d_6, and CCl_4/$CDCl_3$ mixed solvents at 25°C.

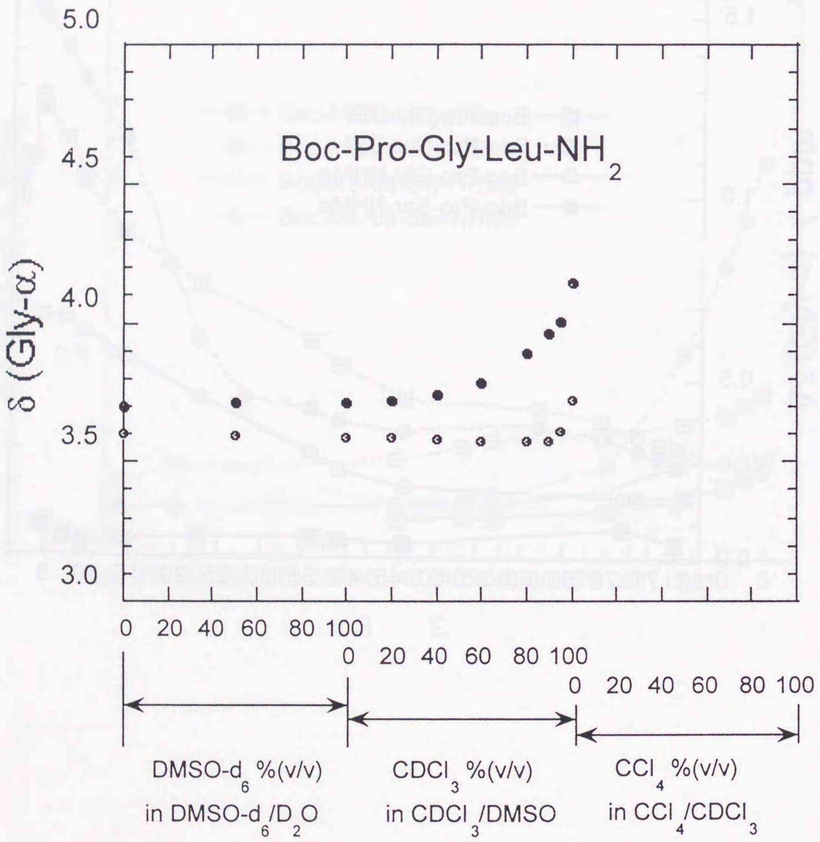

Figure 6.29. Plots of chemical shifts for the two glycyl α-protons of 2.5 mM Boc-Pro-Gly-Leu-NH_2 in mixed solvents of DMSO-d_6/D_2O and $CDCl_3$/DMSO-d_6 at 25 °C against solvent mixing ratios.

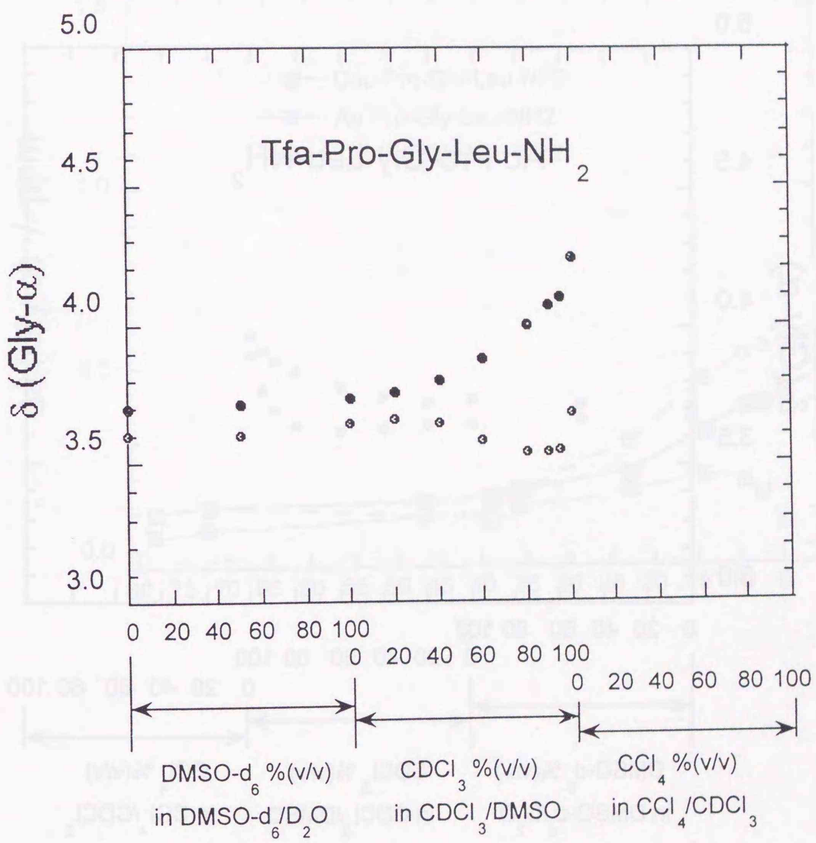

Figure 6.30. Plots of chemical shifts for the two glycyl α-protons of 2.5 mM Tfa-Pro-Gly-Leu-NH_2 in mixed solvents of DMSO-d_6/D_2O and $CDCl_3$/DMSO-d_6 at 25° C against solvent mixing ratios.

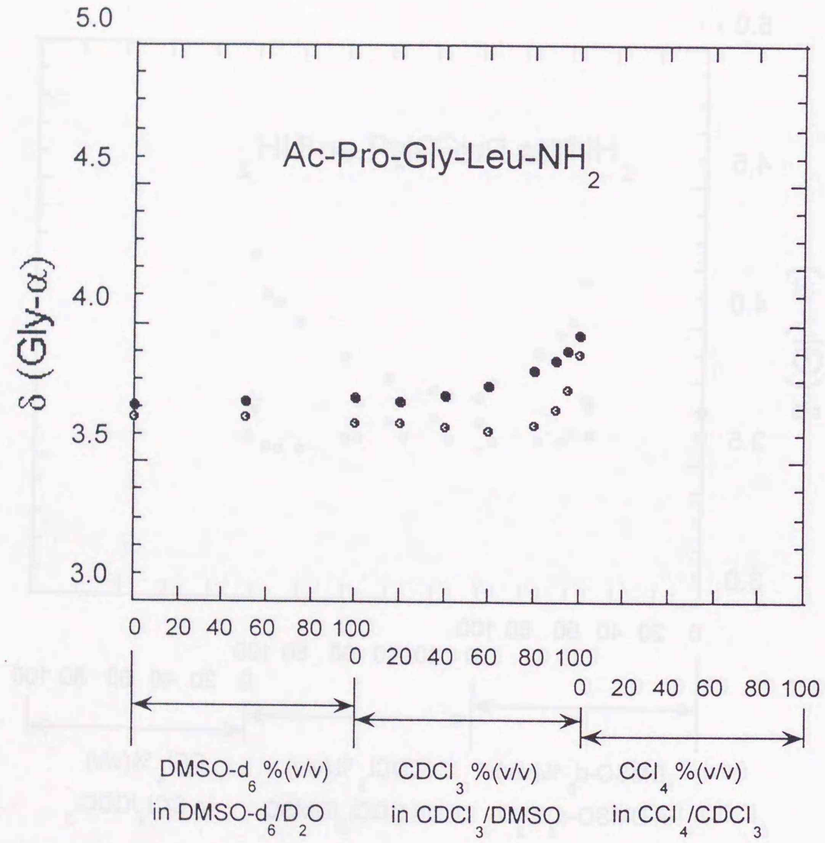

Figure 6.31. Plots of chemical shifts for the two glycyl α-protons of 2.5 mM Ac-Pro-Gly-Leu-NH_2 in mixed solvents of DMSO-d_6/D_2O and $CDCl_3$/DMSO-d_6 at 25˚C against solvent mixing ratios.

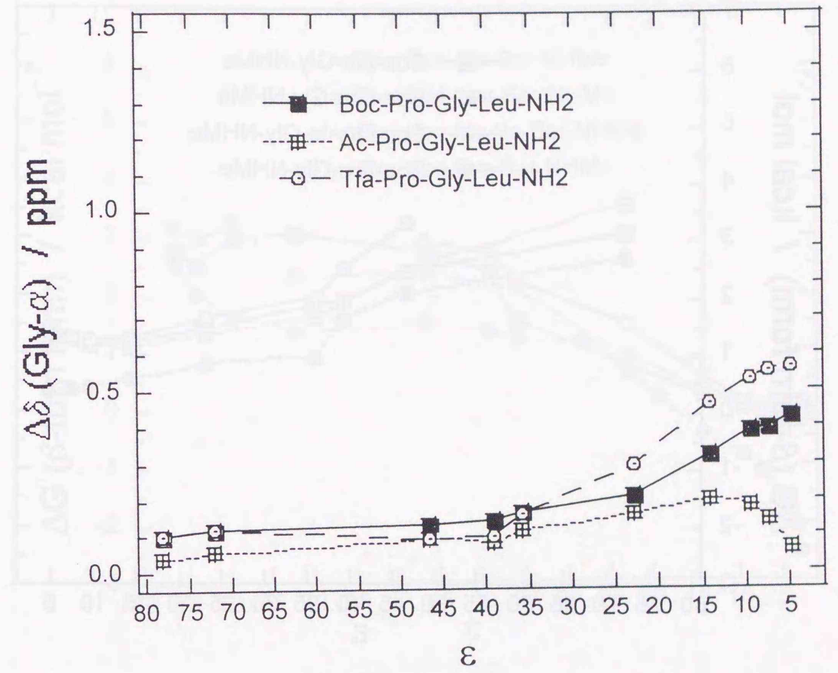

Figure 6.32. Changes of $\Delta\delta_{\alpha/\alpha'}$ values with solvent dielectric constants for 2.5 mM solutions of Boc-Pro-Gly-Leu-NH_2, Ac-Pro-Gly-Leu-NH_2, and Tfa-Pro-Gly-Leu-NH_2 in DMSO-d_6/D_2O and $CDCl_3$/DMSO-d_6 mixed solvents at 25˚C.

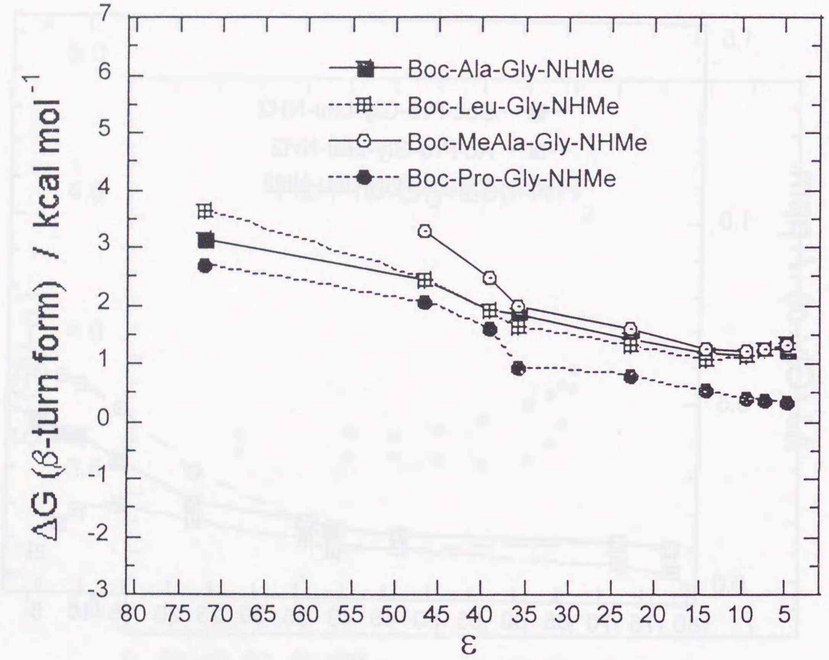

Figure 6.33. Changes of ΔG values for β-turn formations of Boc-Ala-Gly-NHMe, Boc-Leu-Gly-NHMe, Boc-MeAla-Gly-NHMe, and Boc-Pro-Gly-NHMe in DMSO-d_6/D_2O and $CDCl_3$/DMSO-d_6 mixed solvents at 25˚C with solvent dielectric constants.

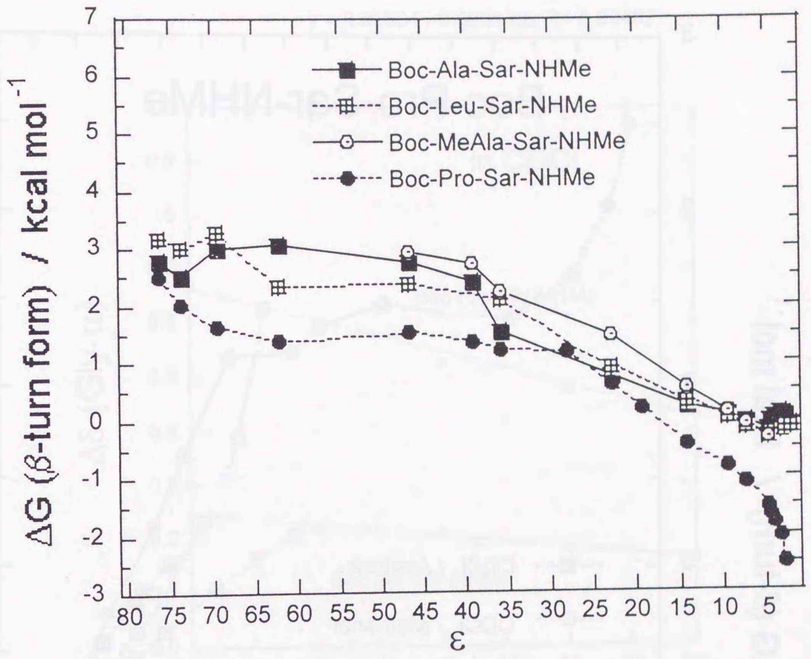

Figure 6.34. Changes of ΔG values for β-turn formations of Boc-Ala-Sar-NHMe, Boc-Leu-Sar-NHMe, Boc-MeAla-Sar-NHMe, and Boc-Pro-Sar-NHMe in DMSO-d_6/D_2O and $CDCl_3$/DMSO-d_6 mixed solvents at 25˚C with solvent dielectric constants.

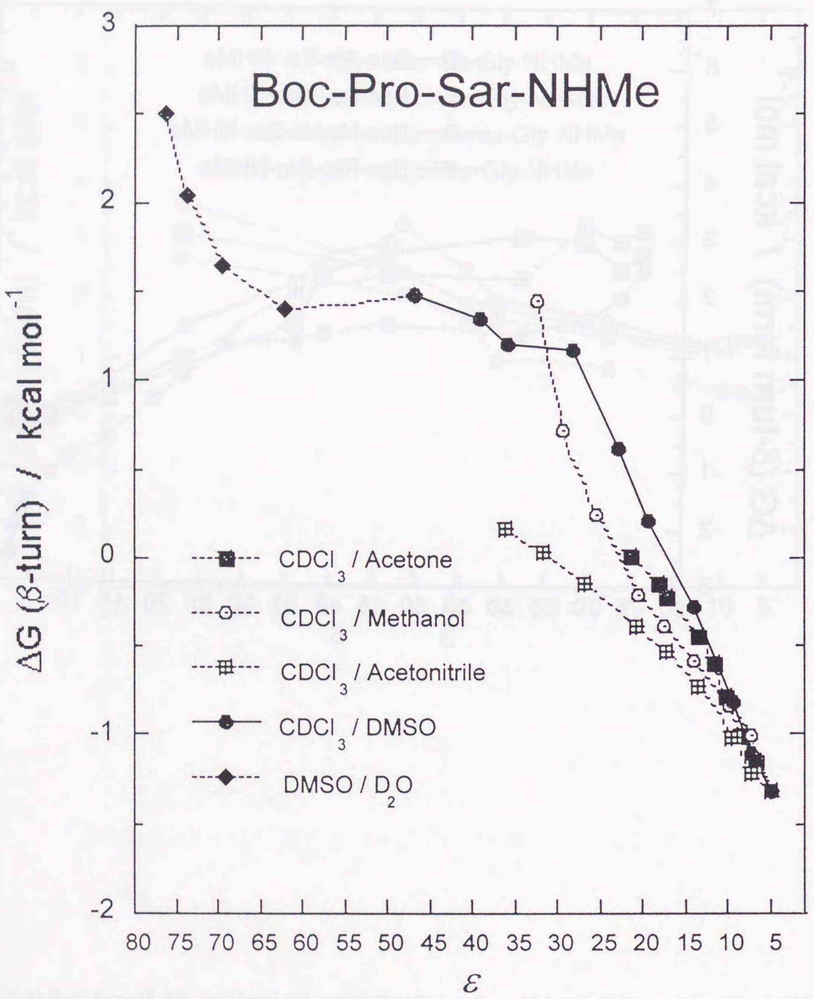

Figure 6.35. Plots of ΔG values for β-turn formation of Boc-Pro-Sar-NHMe in DMSO-d_6/D_2O, $CDCl_3$/DMSO-d_6, $CDCl_3$/acetonitrile-d_3, $CDCl_3$/methanol-d_4, $CDCl_3$/acetone-d_6 at 25˚C mixed solvents against solvent dielectric constants.

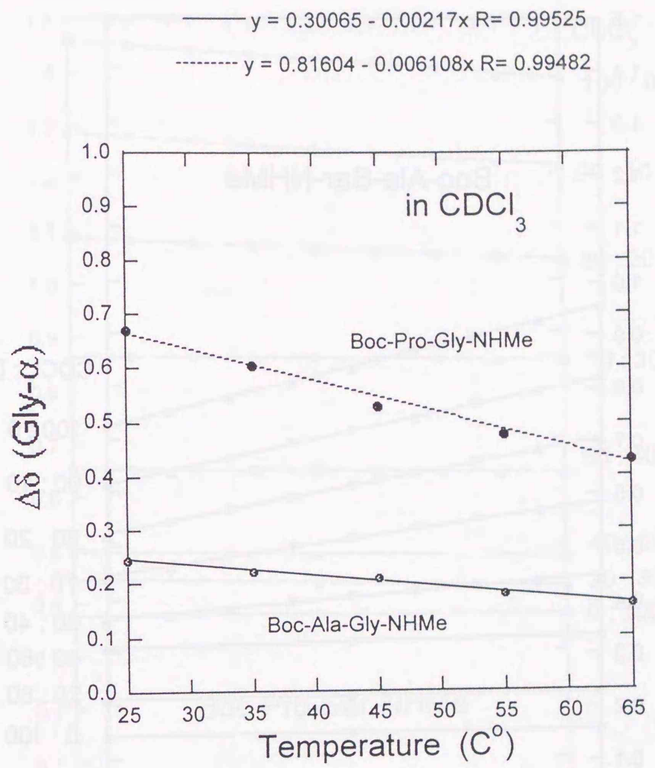

Figure 6.36. Plots of $\Delta\delta_{\alpha/\alpha'}$ values against temperatures for 2.5 mM $CDCl_3$ solutions of Boc-Ala-Gly-NHMe and Boc-Pro-Gly-NHMe.

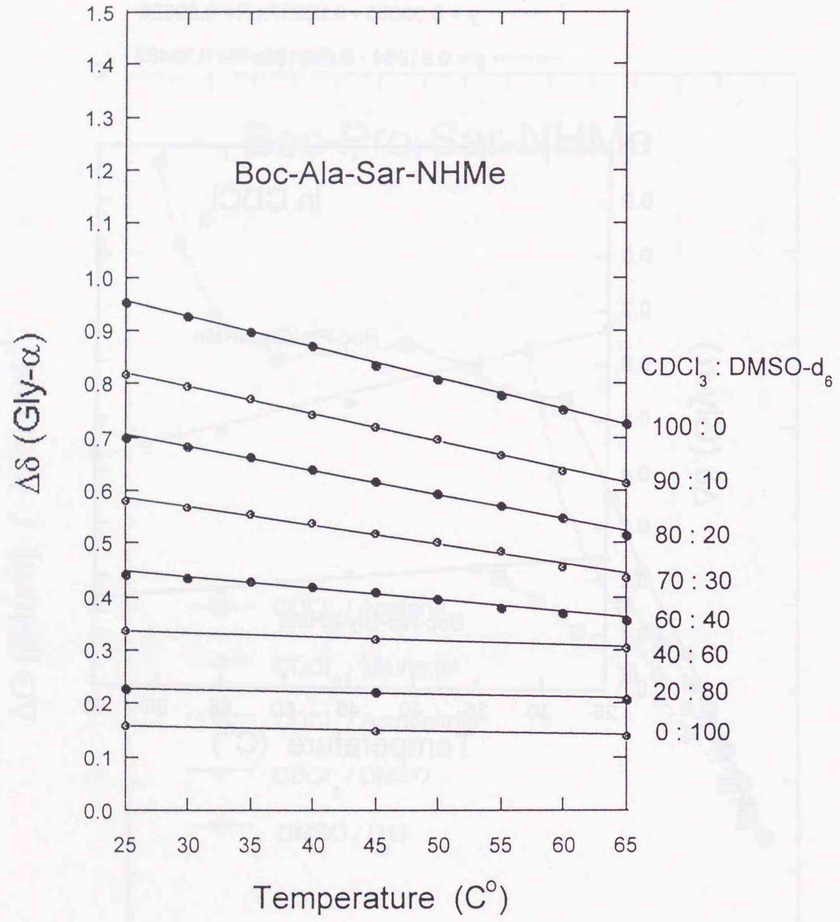

Figure 6.37. Plots of $\Delta\delta_{\alpha/\alpha'}$ values against temperatures for 2.5 mM Boc-Ala-Sar-NHMe in $CDCl_3$/DMSO-d_6 mixed solvents at various mixing ratios (v/v%).

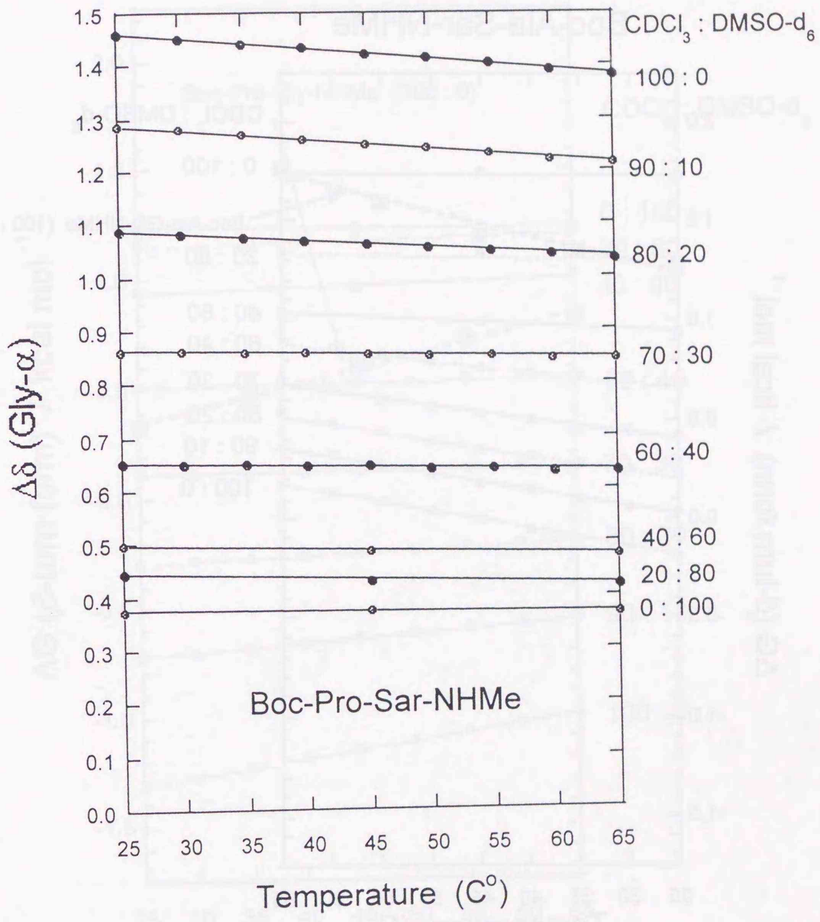

Figure 6.38. Plots of $\Delta\delta_{\alpha/\alpha'}$ values against solution temperature for 2.5 mM Boc-Pro-Sar-NHMe in $CDCl_3$/DMSO-d_6 mixed solvents at various mixing ratios (v/v%).

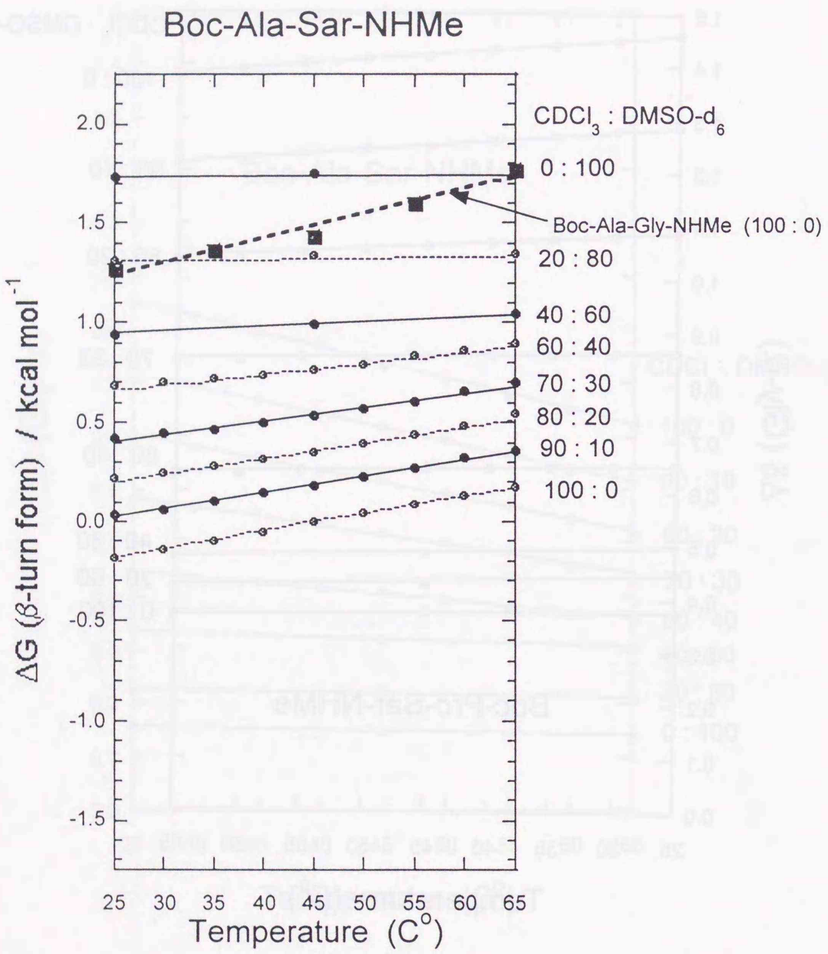

Figure 6.39. Plots of ΔG values for β-turn formation solution temperatures for 2.5 mM Boc-Ala-Sar-NHMe in $CDCl_3$/DMSO-d_6 mixed solvents at various mixing ratios (v/v%). Plots for 2.5 mM Boc-Ala-Gly-NHMe in $CDCl_3$ are included for comparison.

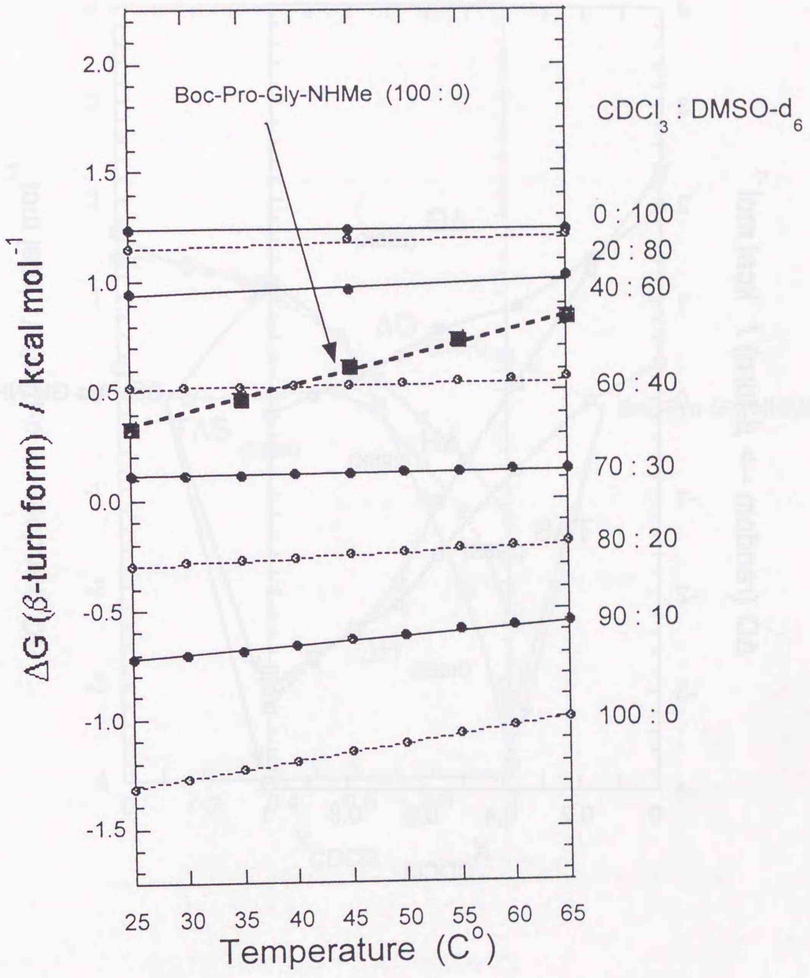

Figure 6.40. Plots of ΔG values for β–turn formation against solution temperatures for 2.5 mM Boc-Pro-Sar-NHMe in $CDCl_3$ DMSO-d_6 mixed solvents at various mixing ratios (v/v%). Plots for 2.5 mM Boc-Pro-Gly-NHMe in $CDCl_3$ are included for comparison.

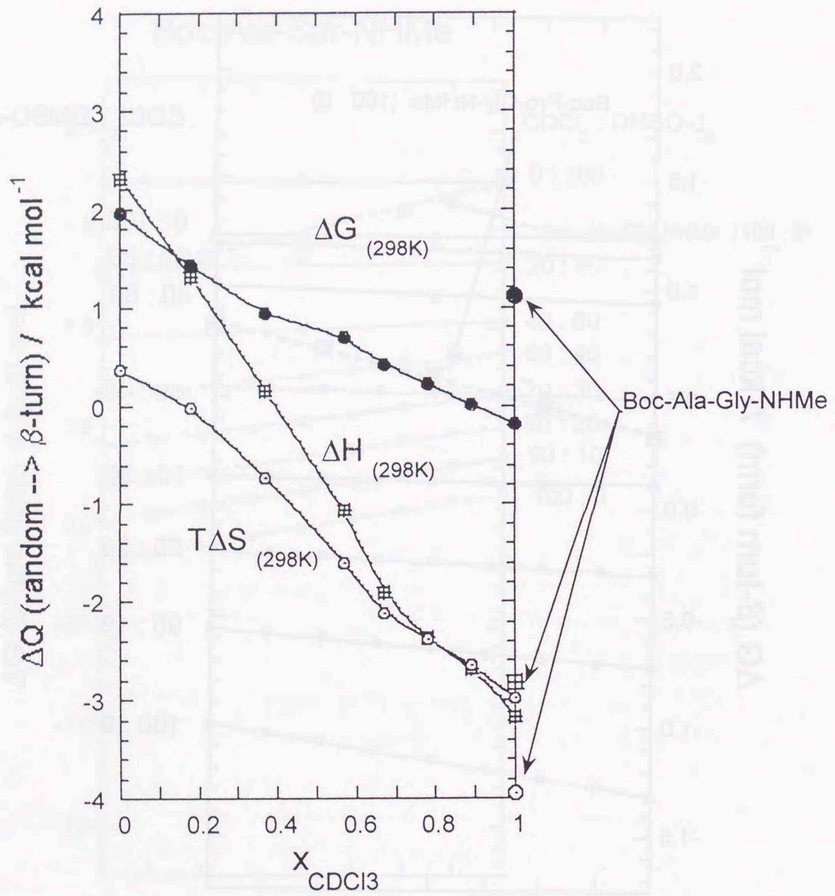

Figure 6.41. Plots of the thermodynamic properties, ΔG, ΔH, $T\Delta S$, for β–turn formation of Boc-Ala-Sar-NHMe against molar fraction of $CDCl_3$, x_{CDCl3}, in the $CDCl_3$/DMSO-d_6 mixed solvents at 25˚C. Plots for 2.5 mM Boc-Ala-Gly-NHMe in $CDCl_3$ are included for comparison.

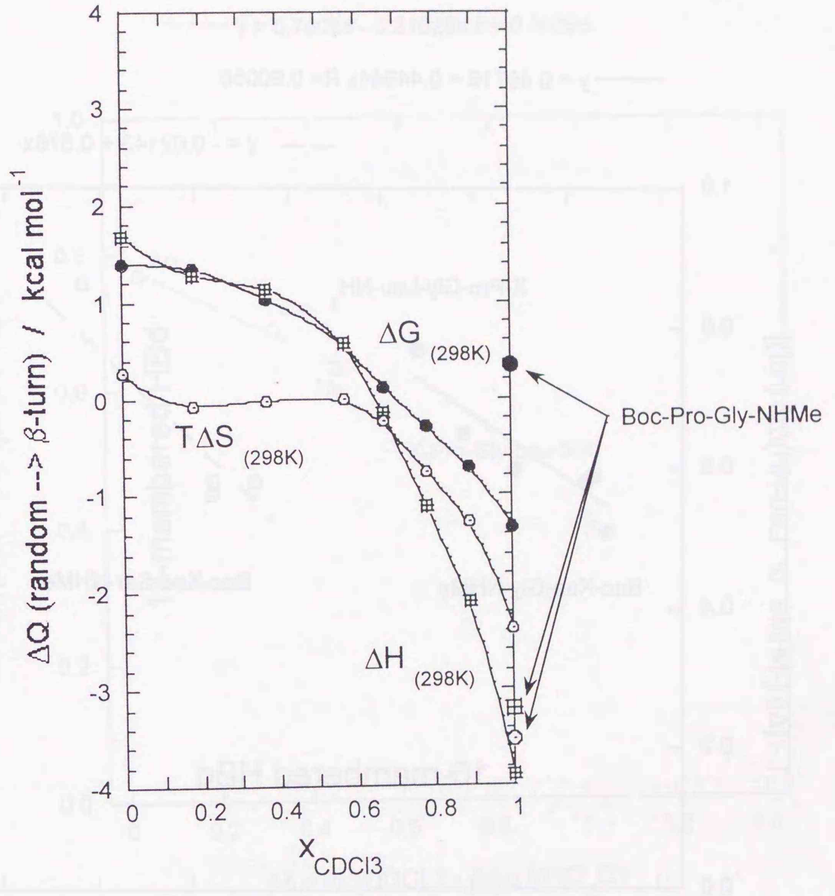

Figure 6.42. Plots of the thermodynamic properties, ΔG, ΔH, $T\Delta S$, for β–turn formation of Boc-Pro-Sar-NHMe against molar fraction of $CDCl_3$, x_{CDCl3}, in the $CDCl_3$/DMSO-d_6 mixed solvents at 25˚C. Plots for 2.5 mM Boc-Pro-Gly-NHMe in $CDCl_3$ are included for comparison.

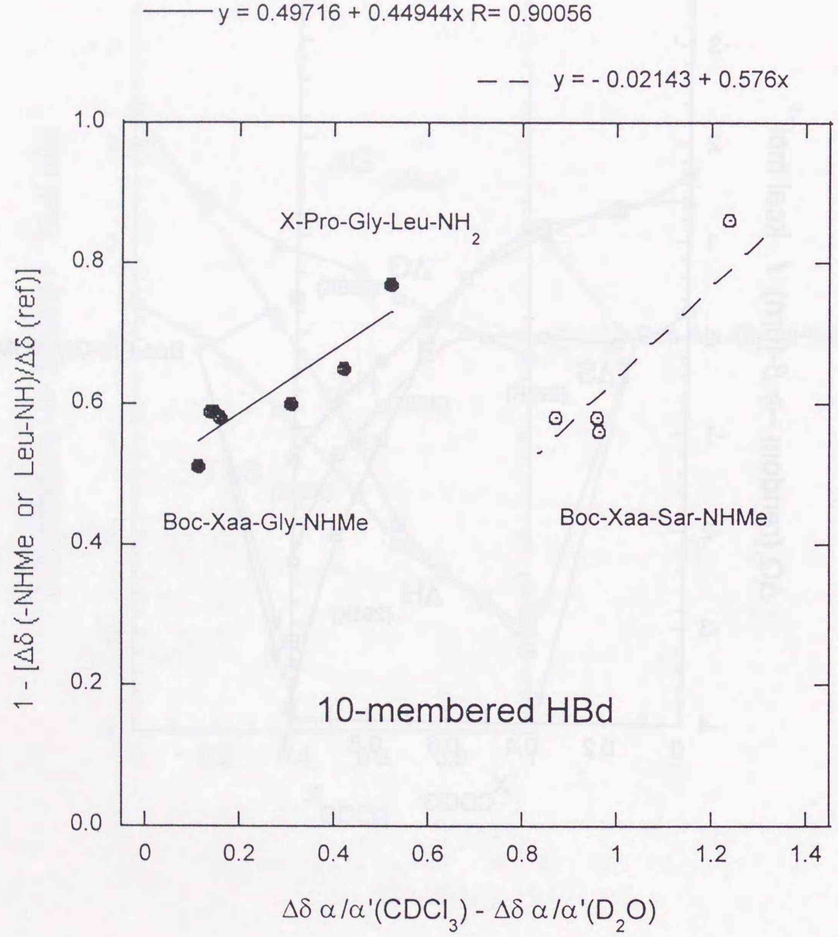

Figure 6.43. Relationships between the [1-$\Delta\delta/\Delta\delta$ ref]] values obtained in Chapter 5 and [$\Delta\delta_{\alpha/\alpha'}(CDCl_3)$- $\Delta\delta_{\alpha/\alpha'}(D_2O)$] values for the peptides with sequences of Boc-Xaa-Gly-NHMe, Boc-Xaa-Sar-NHMe, and X-Pro-Gly-Leu-NH_2. The [1-$\Delta\delta$ /$\Delta\delta$(ref)] values are for amide protons involved in the 10-membered HBd rings.

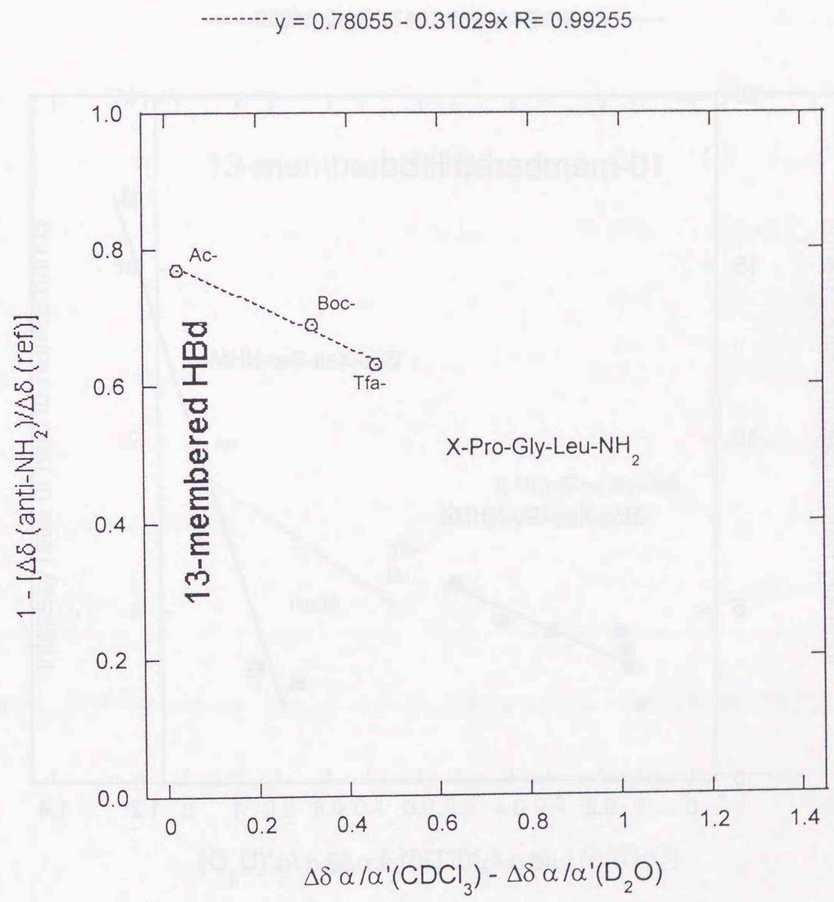

Figure 6.44. Relationships between the [1-$\Delta\delta/\Delta\delta$(ref)] values obtained in Chapter 5 and [$\Delta\delta_{\alpha/\alpha'}(CDCl_3)$- $\Delta\delta_{\alpha/\alpha'}(D_2O)$] values for Ac-Pro-Gly-Leu-NH_2, Boc-Pro-Gly-Leu-NH_2, and Tfa-Pro-Gly-Leu-NH_2. The [1-$\Delta\delta/\Delta\delta$ (ref)] values are for the anti amide protons of the NH_2 groups involved in the 13-membered HBd rings.

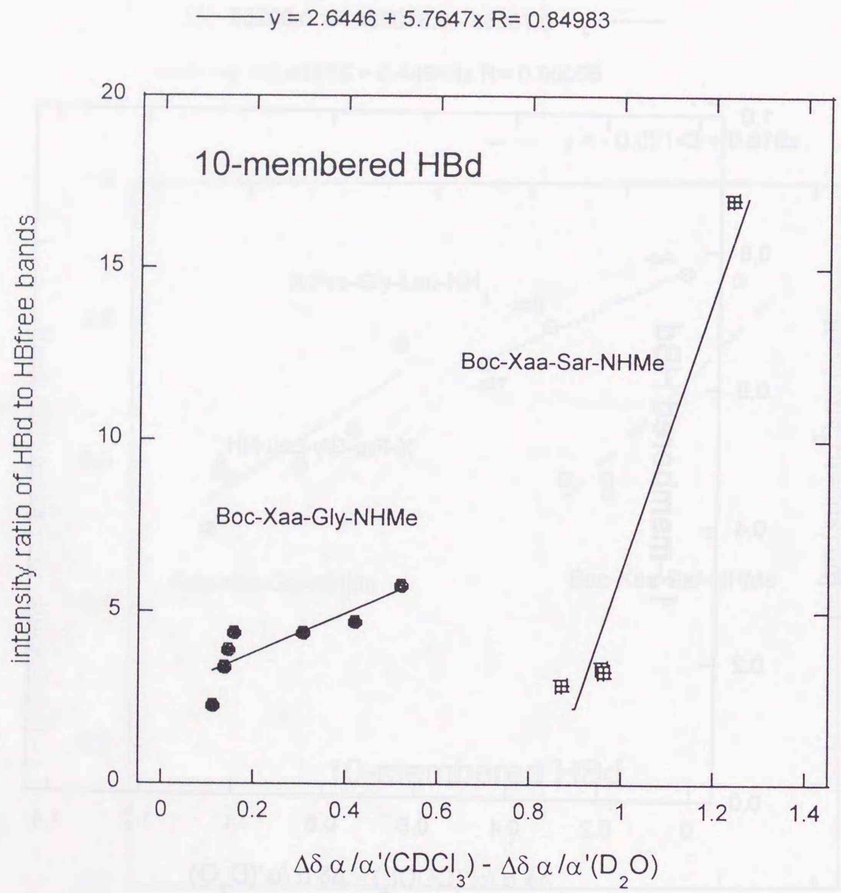

Figure 6.45. Relationships between intensity ratios of the HBd bands to the HBfree bands assigned to the NH stretchings of the terminal $NHCH_3$ groups, which are involved in the 10-membered HBd rings, and $[\Delta\delta_{\alpha/\alpha'}(CDCl_3)- \Delta\delta_{\alpha/\alpha'}(D_2O)]$ values for the peptides with sequences of Boc-Xaa-Gly-NHMe and Boc-Xaa-Sar-NHMe.

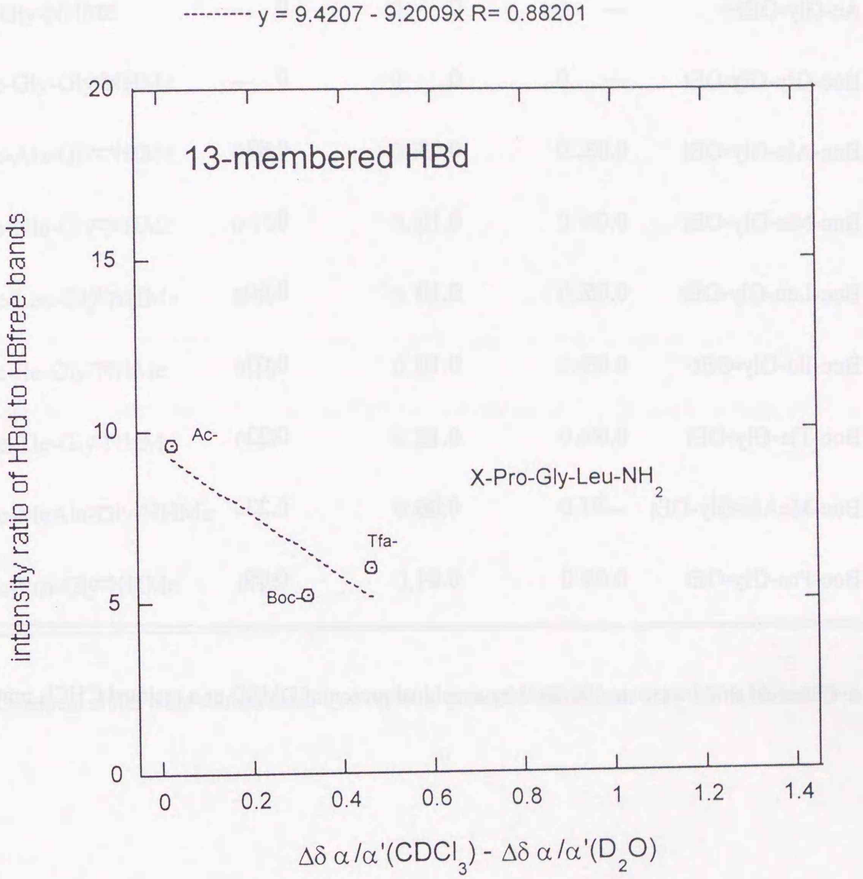

Figure 6.46. Relationships between intensity ratios of the HBd bands to the HBfree bands assigned to the NH stretchings of the terminal NH_2 groups, which are involved in the 13-membered HBd rings, and $[\Delta\delta_{\alpha/\alpha'}(CDCl_3)- \Delta\delta_{\alpha/\alpha'}(D_2O)]$ values for Ac-Pro-Gly-Leu-NH_2, Boc-Pro-Gly-Leu-NH_2, and Tfa-Pro-Gly-Leu-NH_2.

Table 15. Difference of chemical shifts between two α-protons of the Gly residues in peptides. [a]

compounds	$\Delta\delta_\alpha$ (D_2O)	$\Delta\delta_\alpha$ (DMSO)	$\Delta\delta_\alpha$ ($CDCl_3$)	$\Delta\delta_\alpha$ (CCl_4)
Ac-Gly-OEt	—	0	0	—
Boc-Gly-Gly-OEt	—	0	0	—
Boc-Ala-Gly-OEt	0.03	0.08	0.03	—
Boc-Nle-Gly-OEt	0.05	0.10	0	—
Boc-Leu-Gly-OEt	0.05	0.10	0.00_2	—
Boc-Ile-Gly-OEt	0.05	0.10	0.03	—
Boc-Tle-Gly-OEt	0.09	0.12	0.23	—
Boc-MeAla-Gly-OEt	—	0.06	0.23	—
Boc-Pro-Gly-OEt	0.05	0.04	0.09	—

a. Chemical shifts were standardized by a residual proton of DMSO or a residual $CHCl_3$ proton.

Table 16. Difference of chemical shifts between two α-protons of the Gly residues in peptides. [a]

compounds	$\Delta\delta_\alpha$ (D_2O)	$\Delta\delta_\alpha$ (DMSO)	$\Delta\delta_\alpha$ ($CDCl_3$)	$\Delta\delta_\alpha$ (CCl_4)
Ac-Gly-NHMe	—	0	0	—
Boc-Gly-Gly-NHMe	—	0	0	—
Boc-Ala-Gly-NHMe	0.09	0.11	0.25	—
Boc-Nle-Gly-NHMe	0.10	0.11	0.24	—
Boc-Leu-Gly-NHMe	0.09	0.11	0.22	—
Boc-Ile-Gly-NHMe	0.13	0.15	0.45	—
Boc-Tle-Gly-NHMe	0.17	0.28	0.69	—
Boc-MeAla-Gly-NHMe	—	0.05	0.19	—
Boc-Pro-Gly-NHMe	0.15	0.19	0.67	—

a. Chemical shifts were standardized by a residual proton of DMSO or a residual $CHCl_3$ proton.

Table 17. Difference of chemical shifts between two α-protons of the Sar residues in peptides. [a]

compounds	$\Delta\delta_\alpha$ (D_2O)	$\Delta\delta_\alpha$ (DMSO)	$\Delta\delta_\alpha$ ($CDCl_3$)	$\Delta\delta_\alpha$ (CCl_4)
Ac-Sar-OEt	—	0	0	—
Boc-Ala-Sar-OEt	0.12	0.20	0.42	0.63
Boc-Leu-Sar-OEt	0.20	0.38	0.67	0.89
Boc-MeAla-Sar-OEt	0.16	0.23	0.41	—
Boc-Pro-Sar-OEt	0.31	0.45	1.24	0.99

a. Chemical shifts were standardized by a residual proton of DMSO or a residual $CHCl_3$ proton.

Table 18. Difference of chemical shifts between two α-protons of the Sar residues in peptides. [a]

compounds	$\Delta\delta_\alpha$ (D_2O)	$\Delta\delta_\alpha$ (DMSO)	$\Delta\delta_\alpha$ ($CDCl_3$)	$\Delta\delta_\alpha$ (CCl_4)
Ac-Sar-NHMe	—	0	0	—
Boc-Ala-Sar-NHMe	0.08	0.10	0.96	0.89
Boc-Leu-Sar-NHMe	0.09	0.12	1.05	0.95
Boc-MeAla-Sar-NHMe	0.09	0.10	1.05	—
Boc-Pro-Sar-NHMe	0.26	0.35	1.50	1.59

a. Chemical shifts were standardized by a residual proton of DMSO or a residual $CHCl_3$ proton.

Table 19. Difference of chemical shifts between two α-protons of the Gly residues in peptides. [a]

compounds	$\Delta\delta_\alpha$ (D_2O)	$\Delta\delta_\alpha$ (DMSO)	$\Delta\delta_\alpha$ ($CDCl_3$)	$\Delta\delta_\alpha$ (CCl_4)
Boc-Pro-Gly-Leu-NH_2	0.102	0.127	0.425	—
Ac-Pro-Gly-Leu-NH_2	0.041	0.090	0.065	—
Tfa-Pro-Gly-Leu-NH_2	0.099	0.090	0.563	—

a. Chemical shifts were standardized by a residual proton of DMSO or a residual $CHCl_3$ proton.

Chart 10: Molecular Mechanics Calculation (MM2) for Boc-Pro-Sar-NHMe (*trans+trans*).

$\psi_{Pro} = -30^{o}$

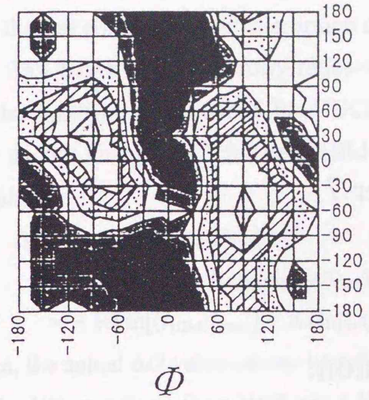

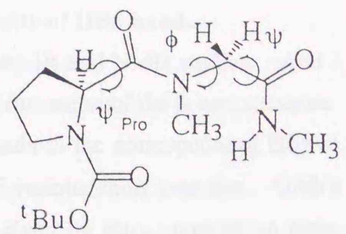

$\psi_{Pro} = 120^{o}$

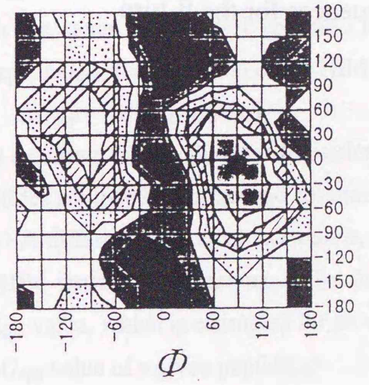

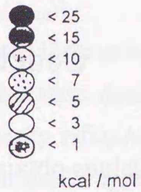

two α-protons

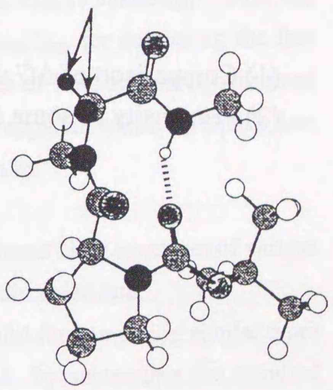

● type II β-turn

Chapter 7

Conclusion:

(1) Comparison of ΔG values obtained from the three indices
(2) Propensity of some amino acid sequences for the β-turn.

1. Comparison of ΔG values obtained from the three indices:

1.1. Estimation of ΔG value from relative intensity of HBd band.

In this chapter, I will summarize all of the present IR and NMR studies. And I will discuss contribution of each amino acid residue to formation of the β-turn structure.

In Chapter 3, the intensity ratios of the HBd bands to the corresponding HBfree bands, I_{HBd}/I_{free}, are obtained for $CDCl_3$ solutions of various short peptides. Gibb's free energy change, ΔG, for each HBd formation is given by actual population ratio, P_{HBd}/P_{free}.

$$\Delta G = -RT\ln[P_{HBd}/P_{free}]$$
$$= -RT\ln[(I_{HBd}/I_{free})/(A_{HBd}/A_{free})]$$
$$= -\mathrm{RT}\ln[(I_{HBd}/I_{free})] + \mathrm{RT}\ln[(A_{HBd}/A_{free})].$$

Then, the actual ΔG value cannot be estimated if the ratio of molar integrated intensities of the NH stretching for a HBd and a HBfree state, A_{HBd}/A_{free}, is unknown. However, it seems possible to use the observed intensity ratio, I_{HBd}/I_{free}, for comparing the free energy of HBd structure formation between similar types of HBd structures concerned with the same kind of NH groups. In this case, the apparent value of Gibb's free energy, ΔG_{app}, for formation of the HBd structure is given by

$$\Delta G_{app} = -RT\ln[I_{HBd}/I_{free}].$$

The resulting ΔG_{app} values for formation of the 10-membered HBd structures of various peptides are listed in the second column in Table 20 and discussed later.

A difference of actual ΔG values, $\Delta\Delta G$, is also useful for comparing similar types of HBd structure formations. The $\Delta\Delta G$ value is given by subtracting the standard ΔG_{app} value, which is estimated for an appropriate equilibrating HBd-HBfree pair, from a ΔG_{app} value of a given peptide, p:

$$\Delta\Delta G_{app} = -\Delta G(\mathrm{p}) - \Delta G(\mathrm{std})$$
$$= \{\Delta G_{app}(\mathrm{p}) - \Delta G_{app}(\mathrm{std})\} + RT\ln[\{A_{HBd}(\mathrm{p})/A_{HBd}(\mathrm{std})\}/\{A_{free}(\mathrm{p})/A_{free}(\mathrm{std})\}]$$
$$\sim \Delta G_{app}(\mathrm{p}) - \Delta G_{app}(\mathrm{std}).$$

This is because molar integrated intensities for both the HBd and HBfree states can be assumed to be the same for the peptides with the same NH groups and with the same type of HBd formation. In this view, the $\Delta\Delta G$ value is taken as a contribution from each amino acid residue at a certain position in a peptide sequence to formation of some

secondary structure. The $\Delta\Delta G$ values are listed in the second columns in Tables 21 to 23, and discussed later.

1.2. Estimation of DG value from chemical shift change of amide proton.

As discussed in Chapter 5, chemical shift variation of an amide proton in the mixed solvents from pure DMSO to pure $CDCl_3$, $\Delta\delta_{NH}$, provides a good information about intramolecular hydrogen-bonding in $CDCl_3$. Through these analyses, I have discussed the value, $[1 - \Delta\delta_{NH}/\Delta\delta_{NH}(ref)]$, as a measure of the extent to which each NH proton of the peptide participates in formation of a HBd structure. In this case, populations of the HBd and HBfree states, respectively, are given as follows,

$$P_{HBd} = 1 - \Delta\delta_{NH}/\Delta\delta_{NH}(ref)$$

$$P_{free} = \Delta\delta_{NH}/\Delta\delta_{NH}(ref).$$

Then, the ΔG value for the HBd formation is given by

$$\Delta G = - RT\ln[\{1 - \Delta\delta_{NH}/\Delta\delta_{NH}(ref)\}/(\Delta\delta_{NH}/\Delta\delta_{NH}(ref))]$$

$$= - RT\ln[\{\Delta\delta_{NH}(ref) - \Delta\delta_{NH}\}/\Delta\delta_{NH}].$$

Resulting ΔG values are listed in the third column in Table 20. Differences in ΔG value, $\Delta\Delta G$, are also listed in the third columns in Tables 21 to 23.

1.3. Estimation of ΔG value from chemical shift difference between two α-protons.

Estimation of ΔG values using chemical shift differences between two glycyl α-protons, $\Delta\delta_{\alpha/\alpha'}$, has been described in Chapter 6, and the results are listed in the fourth columns in Tables 20 to 23.

1.4. Comparison of ΔG values obtained from three indices.

In Table 20, the ΔG values for the 10-membered HBd structure formation, estimated from the IR and two kinds of NMR indices, are compared for some peptides. For all examples, the ΔG_{app} values from the IR results are found to be by 0.2-0.7 kcal/mol lower than the ΔG values from the chemical shift analyses of amide protons. Moreover, the corresponding ΔG values, each of which is obtained by subtracting an appropriate standard from each ΔG, are in a better agreement with one another among the three indices through not satisfactory yet.

Contribution of N-CH_3 moiety of the Sar residue to β-turn stabilization is estimated as shown in Table 23. Results from the three indices are different from one another, especially the $\Delta\Delta G$ values from the $\Delta\delta_{\alpha/\alpha'}$ indices are a little smaller for the Sar-peptides series and much larger for the Gly-peptides series. However, as can be seen in the following three tables, $\Delta\Delta G$ values from the $\Delta\delta_{\alpha/\alpha'}$ indices are deviated from other two. This is probably because the $\Delta\delta_{\alpha/\alpha'}$ indices inform us of the rigidity just around the Gly and Sar residues of the peptides, while other two indices are based on the state of the terminal $NHCH_3$ group of the peptides.

2. Propensity of some amino acid sequences for the β-turn.

As described above, contribution of each amino acid residue is estimated by a free energy change by the replacement of an Ala residue at the $(i + 1)$-th with other residues. The order of stabilizing the β-turn structure, which is called the propensity for β-turn, is found to be in the following: Pro (−1.3 ~ −0.9 kcal/mol) > Leu (−0.1 ~ 0 kcal/mol) > [Ala] > MeAla (−0.1 ~ +0.1 kcal/mol) > Gly (+0.6 kcal/mol) for Xaa in Boc-Xaa-Sar-NHMe, and Gly (−0.5 ~ −0.1 kcal/mol) > Phe (−0.4 ~ 0 kcal/mol) > [Ala] > Leu (+0.1 ~ +0.3 kcal/mol) > Val (+0.2 ~ +0.6 kcal/mol) for Yaa in Boc-Pro-Yaa-NHMe. From these results, order of the overall propensities for the two sequential Xaa-Yaa position in the β-turn of the Boc-Xaa-Yaa-NHMe peptides in $CDCl_3$ solutions are roughly suggested as follows: Pro-Gly (−1.8 ~ −1.0 kcal/mol) > Pro-Phe (−1.7 ~ −0.9 kcal/mol) > Pro-Ala(−1.3 ~ −0.9 kcal/mol) > Pro-Leu (−1.2 ~ −0.6 kcal/mol) > Pro-Val (−1.1 ~ −0.3 kcal/mol) > Leu-Gly (−0.6 ~ −0.1 kcal/mol) > Ala-Gly (−0.5 ~ −0.1 kcal/mol) > MeAla-Gly (−0.6 ~ 0 kcal/mol) > [Ala-Ala] > Leu-Leu (0 ~ +0.3 kcal/mol) > Gly-Gly (+0.1 ~ +0.5 kcal/mol) > Gly-Leu (+0.7 ~ +0.9 kcal/mol) > Gly-Val (+0.8 ~ +1.2 kcal/mol).

These observed propensities for the $(i + 1)$-th and $(i + 2)$-th positions of the β-turn for some amino acid residues in $CDCl_3$ solutions can be compared with statistical propensity data which are based on a probability of occurring in several secondary structures in various proteins for each of the 20 kinds of amino acid residues. According to the parameters in the Chou-Fasman secondary structure prediction

methods,[4-5] the statistical propensity, P_k, with which each amino acid occurs in a certain secondary structure (k), is calculated by dividing each probability, f_k, by the averaged probability, $< f_k >$, for such occupation over total 4741 residues in 29 kinds of different proteins, $P_k = f_k / < f_k >$. The statistical propensities of a few amino acids for the (i + 1)-th positions of the β-turns in proteins, P_{i+1}, are given as follows: Pro (3.59) > Gly (1.01) > Ala (0.907) > Val (0.572) > Phe (0.489) > Ile (0.406) > Leu (0.298), while the propensities for the (i + 2)-th positions, P_{i+2}, are as follows: Gly (2.27) > Phe (0.776) > Leu (0.430) > Ala (0.418) > Val (0.334). The overall propensities for the two sequential position in the turns, P_{i+1} x P_{i+2}, are in the following order: Pro-Gly (8.15) > Pro-Phe (2.79) > Gly-Gly (2.29) > Ala-Gly (2.06) > Pro-Leu (1.54) > Pro-Ala (1.50) > Pro-Val (1.20) > Leu-Gly (0.676) > Gly-Leu (0.434) > Ala-Leu (0.390) > [Ala-Ala (0.379)] > Val-Leu (0.223) > Phe-Leu (0.210) > Leu-Leu (0.128).

The β-turn propensities obtained in the present study for small peptides in $CDCl_3$ solution are consistent with those from the statistical analysis of protein molecules, except for the Gly-Gly sequence. This fact means that the β-turn forming tendencies of the individual local sequences, which are estimated from IR and NMR measurements in $CDCl_3$, survive in environments in protein molecules. This is probably because the environments of protein molecules in which β-turns embedded are somewhat similar to a solvent condition of $CDCl_3$.

Table 20. Comparison of ΔG values estimated by the three different methods for 10-membered HBd structure formation in $CDCl_3$ solutions.

compounds	ΔG (HBd formation in $CDCl_3$) / kcal mol^{-1}		
	[IR intensity][a]	[NMR:$\Delta\delta_{NH}$][b]	[NMR:$\Delta\delta_{\alpha/\alpha'}$]
Boc-Pro-Gly-NHMe	-0.96(9)	-0.7(1)	+0.34(5)
Boc-Pro-Ala-NHMe	-0.88(9)	-0.23(2)	—
Boc-Pro-Leu-NHMe	-0.61(9)	-0.22(2)	—
Boc-Pro-Val-NHMe	-0.28(9)	+0.10(4)	—
Boc-Pro-Phe-NHMe	-0.92(9)	-0.30(1)	—
Ac-Pro-Gly-NHMe	-1.02(4)	-0.60(1)	—
Tfa-Pro-Gly-NHMe	-0.57(4)	—	—
Boc-MeAla-Gly-NHMe	-0.49(4)	-0.03(3)	—
Boc-Tle-Gly-NHMe	-0.85(9)	-0.37(1)	+0.32(6)
Boc-Ile-Gly-NHMe	-0.92(9)	-0.22(2)	+0.73(7)
Boc-Leu-Gly-NHMe	-0.72(9)	-0.21(2)	+1.3(2)
Boc-Nle-Gly-NHMe	-0.82(9)	-0.21(2)	+1.3(2)
Boc-Ala-Gly-NHMe	-0.87(9)	-0.18(2)	+1.3(2)
Boc-Gly-Gly-NHMe	-0.59(9)	—	—
Boc-Pro-Sar-NHMe	-1.68(2)	-1.1(1)	-1.5(2)
Boc-MeAla-Sar-NHMe	-0.71(4)	-0.13(3)	-0.30(5)
Boc-Leu-Sar-NHMe	-0.72(7)	-0,19(2)	-0.32(3)
Boc-Ala-Sar-NHMe	-0.63(7)	-0.18(2)	-0.19(5)
Boc-Gly-Sar-NHMe	-0.08(7)	—	—

a. Values in parentheses are the standard deviations estimated by an error propagation law.

b. Values in parentheses are errors estimated from chemical shift uncertainty (0.02 ppm).

Table 21. Contribution of individual amino acid residue to ΔG values of β-turn formation in $CDCl_3$ solutions estimated as a difference from that of an Ala residue, $\Delta\Delta G$.[a]

compounds	$\Delta\Delta G$ (β-turn formation in $CDCl_3$) / kcal mol^{-1}		
	[IR intensity]	[NMR:$\Delta\delta_{NH}$]	[NMR:$\Delta\delta_{\alpha/\alpha'}$]
Boc-Xaa-Gly-NHMe			
Xaa/Ala	[0]	[0]	[0]
Xaa/Ala → Gly	+0.28(13)	—	—
Xaa/Ala → Nle	+0.05(13)	-0.03(3)	0.0 (3)
Xaa/Ala → Leu	+0.15(13)	-0.03(3)	0.0 (3)
Xaa/Ala → Ile	-0.05(13)	-0.04(3)	-0.6(2)
Xaa/Ala → Tle	+0.02(13)	-0.19(3)	-1.0(2)
Xaa/Ala → MeAla	+0.38(10)	+0.15(3)	—
Xaa/Ala → Pro	-0.09(16)	-0.5(1)	-1.0(2)
Boc-Pro-Yaa-NHMe			
Yaa/Ala	[0]	[0]	—
Yaa/Ala → Gly	-0.08(13)	-0.47(3)	—
Yaa/Ala → Leu	+0.27(13)	+0.01(3)	—
Yaa/Ala → Val	+0.60(13)	+0.17(3)	—
Yaa/Ala → Phe	-0.04(13)	-0.37(2)	—

a. Values in parentheses are the standard deviations estimated by an error propagation law.

Table 22. Contribution of individual amino acid residue to ΔG values of β-turn formation in $CDCl_3$ solutions estimated as a difference from that of an Ala residue, $\Delta\Delta G$.[a]

compounds	$\Delta\Delta G$ (β-turn formation in $CDCl_3$) / kcal mol^{-1}		
	[IR intensity]	[NMR:$\Delta\delta_{NH}$]	[NMR:$\Delta\delta_{\alpha/\alpha'}$]
Boc-Xaa-Sar-NHMe			
Xaa/Ala	[0]	[0]	[0]
Xaa/Ala → Gly	+0.55(10)	—	—
Xaa/Ala → Leu	-0.09(10)	-0.01(3)	-0.13(3)
Xaa/Ala → MeAla	-0.08(8)	+0.05(4)	-0.11(7)
Xaa/Ala → Pro	-1.05(7)	-0.92(2)	-1.3(2)

a. Values in parentheses are the standard deviations estimated by an error propagation law.

Table 23. Differences of ΔG values between Boc-Xaa-Sar-NHMe and Boc-Xaa-Gly-NHMe, $\Delta\Delta G = \Delta G$(Boc-Xaa-Sar-NHMe) - ΔG(Boc-Xaa-Gly-NHMe), for Xaa = Ala, Gly, Leu, MeAla, Pro, respectively.[a]

compounds	$\Delta\Delta G$ (β-turn formation in $CDCl_3$) / kcal mol^{-1}		
	[IR intensity]	[NMR:$\Delta\delta_{NH}$]	[NMR:$\Delta\delta_{\alpha/\alpha'}$]
Xaa/ Ala	+0.24(12)	0.00(3)	-1.49(21)
Xaa/ Gly	+0.51(11)	—	—
Xaa/ Leu	0.00(12)	-0.02(3)	-1.6(2)
Xaa/ MeAla	-0.22(6)	-0.10(4)	—
Xaa/ Pro	-0.75(9)	-0.38(1)	-1.8(2)

a. Values in parentheses are the standard deviations estimated by an error propagation law.

References:

1. In *Mechanisms of Protein Folding*; Pain R.H., Ed.; Oxford University Press: Oxford, 1994; Chapter 1-4.
2. Creigton, T.E. *Proteins: Structure and Molecular Properties*, 2nd ed.; Freeman: New York, 1993.
3. Dill, K. A. *Biochemistry* **1990**, 29, 7133.
4. Chou, P. Y.; Fasman, G. D. *Biochemistry*, **1974**, 13, 222.
5. Chou, P. Y.; Fasman, G. D. *Ann. Rev. Biochem.* **1978**, 47, 251.
6. Robson, B.; Suzuki, E. *J. Mol. Biol.* **1976**, 107, 327.
7. Garnier, J.; Osguthorpe, D. J. *J. Mol. Biol.* **1978**, 120, 97.
8. Arnez, J. G.; Haarris, D. C.; Mistscler, A.; Rees, B.; Francklyn, C. S.; Moras, D. *EMBO J.* **1995**, 14, 4143.
9. Hogar, T. H.; Krohne, G.; Franke, W.W.; Moras, D. *J. Cell. Biol.* **1988**, 47, 283.
10. Rieger, M.; Jorcano, J. L.; Franke, W. W.; Moras, D. *EMBO J.* **1985**, 4, 2261.
11. Shoemaker, K. R.; Kim, P. S.; York, E. J.; Stewart, J. M.; Baldwin, R. L. *Nature* **1987**, 326, 563.
12. Goodman, E. M.; Kim, P. S. *Biochemistry* **1989**, 28, 4343.
13. Tonan, K.; Kawata, Y.; Hamaguchi, K. *Biochemistry* **1990**, 29, 4424.
14. Higashijima, T.; Tasumi, M.; Miyazawa, T.; Miyoshi, M. *Eur. J. Biochem.* **1978**, 89, 543.
15. Wang, Y. S.; Kempe, T. G.; Raina, A. K.; Mazzocchi, P. H. *Int. J. Peptide Protein Res.* **1994**, 43, 277.
16. Pimentel, G. C.; McClellan, A. L.; *The Hydrogen Bond*; Freeman: San Fransisco, 1960.
17. Aaron, H. S. *Top. Stereochem.* **1980**, 11, 1.
18. Tsuboi, M.; Shimanouchi, T.; Mizushima, S. *J. Am. Chem. Soc.* **1959**, 81, 1406.
19. Rose, G. D.; Gierasch, L. M.; Smith, J. A. *Adv. Protein Chem.* **1985**, 37, 1.
20. Boussard, G.; Marraud, M.; Neel, J. *J. Chim. Phys. Phys.-Chim.* **1974**, 71, 1081.
21. Boussard, G.; Marraud, M. *J. Am. Chem. Soc.* **1985**, 107, 1825.
22. Aubry, A.; Cung, M. T.; Marraud, M. *J. Am. Chem. Soc.* **1985**, 107, 7640.
23. Pietzynski, G. ; Rzeszotarska, B.; Kubica, Z. *Int. J. Peptide Protein Res.* **1992**, 40,

524.
24. Han, S. J.; Kang, Y. K. *Int. J. Peptide Protein Res.* **1993**, 42, 518.
25. Gellman, S. H.; Dado, G. P.; Liang, G. B.; Adams, B. R. *J. Am. Chem. Soc.* **1991**, 113, 1164.
26. Liang, G. B.; Rito, C. J.; Gellman, S. H. *J. Am. Chem. Soc.* **1992**, 114, 4440.
27. Gallo, E. A.; Gellman, S. H. *J. Am. Chem. Soc.* **1993**, 115, 9774.
28. Dado, G. P.; Gellman, S. H. *J. Am. Chem. Soc.* **1994**, 116, 1173.
29. Schnck, H. L.; Gellman, S. H. *J. Am. Chem. Soc.* **1998**, 120, 4869.
30. Gardner, R.R.; Liang, G. B.; Gellamn, S. H. *J. Am. Chem. Soc.* **1999**, 121, 1806.
31. Kline, A. D.; Braun, W.; Wüthrich, K. *J. Mol. Biol.* **1986**, 189, 377.
32. Karplus, M. *J. Phys. Chem.* **1959**, 30, 11.
33. Bystrov, V. F. *Prog. NMR Spectrosc.* **1976**, 10, 41.
34. Pardi, A.; Billeter, M.; Wüthrich, K. *J. Mol. Biol.* **1984**, 180, 741.
35. Milburn, P. J.; Konishi, Y.; Meinwald, Y. C.; Scheraga, H. A. *J. Am. Chem. Soc.* **1987**, 109, 4486.
36. Milburn, P. J.; Meinwald, Y. C.; Takahashi, S.; Ooi, T.; Scheraga, H. A. *Int. J. Peptide Protein Res.* **1988**, 31, 311.
37. Scholtz, J. M.; Marqusee, S.; Baldwin, R. L.; York, E. J.; Stewart, J. M.; Santoro, M.; Bolen, D. W. *Proc. Natl. Acad. Sci. U. S. A.* **1991**, 88, 2854.
38. O'Neil, K. T.; DeGrado, W. F. *Science* **1990**, 250, 646.
39. Miick, S. M.; Martinez, G. V.; Flori, W. R.; Todd, A. P.; Milhauser, G. L. *Nature* **1992**, 359, 653.
40. Lovejoy, B.; Choe, S.; Cascio, D.; McRorie, D. K.; Degrado, W. F.; Eisenberg, D. *Science* **1993**, 259, 1288.
41. Chothia, C. *Nature* **1975**, 254, 305.
42. Konig, W.; Geiger, R. *Chem. Ber.* **1970**, 103, 708.
43. Konig, W.; Geiger, R. *Chem. Ber.* **1970**, 103, 2024.
44. Konig, W.; Geiger, R. *Chem. Ber.* **1970**, 103, 2034.
45. Sheehan, J. C.; Hlavka, J. J. *J. Org. Chem.* **1956**, 21, 439.
46. Sheehan, J. C.; Preston, J.; Cruikshank, P. A. *J. Am. Chem. Soc.* **1965**, 87, 2492.
47. Sheehan, J. C.; Bose, A. K. *J. Am. Chem. Soc.* **1951**, 73, 1761.
48. Guttman, S.; Boissnnas, R. A. *Helv. Chim. Acta.* **1958**, 41, 1852.

49. Tarbell, D. S.; Yamamoto, Y.; Pope, B. M. *Proc. Natl. Acad. Sci. U. S. A.* **1972**, 69, 730.
50. Moroder, L.; Hallett, S.; Wünisch, E.; Keller, O.; Wersin, G. *Hoppe Seyler's Z. Physiol. Chem.* **1976**, 357, 1651.
51. Schallenberg, E. E.; Calvin, M. *J. Am. Chem. Soc.* **1955**, 77, 2779.
52. Pauling, L.; Coley, R. B.; Branson, H. R. *Proc. Natl. Acad. Sci. U. S. A.* **1951**, 37, 205.
53. Kendrew, J. C.; Dickinson, R. E.; Strandberg, B. E.; Hart, R. G.; Davies, D. R.; Philips, D. C.; Shore, V. C. *Nature* **1960**, 185, 422.
54. Leung, Y. C.; Marsh, R. E. *Acta Crystallogr.* **1958**, 11, 17.
55. Marsh, R. E.; Donohue, J. *Adv. Protein Chem.* **1967**, 22, 235.
56. Zimmerman, S. S.; Pottle, M. S.; Nemethy, G.; Scheraga, H. A. *Macromolecules* **1977**, 10, 1.
57. Brandts, J. F.; Halvorson, H. R.; Brennan, M. *Biochemistry* **1975**, 14, 4953.
58. Schmid, F. X.; Baldwin, R. L. *J. Mol. Biol.* **1979**, 135, 199.
59. Kim, P. S.; Baldwin, R. L. *Annu. Rev. Biochem.* **1982**, 51, 459.
60. Lin, L. N.; Brandts, J. F. *Biochemistry* **1982**, 22, 559.
61. Kiefhaber, T.; Quaas, R.; Hahn, U.; Schmid, F. X. *Biochemistry* **1990**, 29, 3053.
62. Müller, G.; Gurrath, M.; Kessler, H. *Proteins Struct. Funct. Genet.* **1993**, 15, 235.
63. Lin, X.; Siegel, D. L.; Fan, P.; Brodsky, B.; Baum, J. *Biochemistry* **1996**, 35, 4306.
64. Nall, B. T. in [Ref.1], Chapter 4.
65. Wüthrich, K.; Billeter, M.; Braun, W. *J. Mol. Biol.* **1984**, 180, 715.
66. Zuiderweg, E.; Kaptein, R.; Wüthrich, K. *Eur. J. Biochem.* **1983**, 137, 279.
67. Pardi, A.; Wagner, G.; Wüthrich, K. *Eur. J. Biochem.* **1983**, 137, 445.
68. Wennerberg, A.; Cooke, R. M.; Carlquest, M.; Riger, R.; Campbell, I. D. *Biochem. Biophys. Res. Comm.* **1990**, 166, 1102.
69. Liu, X.; Otter, A.; Scott, P. G.; Cann, J. R.; Kotovych, G. *J. Biomol. Struct. Dyn.* **1993**, 11, 541.
70. Sternlicht, W.; Wilson, H. *Biochemistry* **1988**, 27, 7620.
71. Giessner-Prettre, C.; Cung, M. T.; Marraud, M. *Eur. J. Biochem.* **1987**, 163, 79.
72. Gresh, N.; Giessner-Prettre, C. *Biochem. Biophys. Res. Comm.* **1990**, 171, 1211.
73. Wüthrich, K. *NMR in Biological Research: Peptides and Proteins*, North-Holland

Publishing Company: Amsterdam, 1976; Chapter 2.
74. Sprague, J. T.; Tai, J. C.; Yuh, Y.; Allinger, N. L. *J. Comput. Chem.* **1987**, 7, 581.